



UNIVERSIDADE D
COIMBRA

Madson Ricardo Everton Santos

**ATOM TRANSFER RADICAL POLYMERIZATION:
STUDY OF LIGANDS AND PREPARATION OF BLOCK
COPOLYMERS WITH CONTROLLED STRUCTURES FOR
APPLICATION IN HIGH-PERFORMANCE COATINGS**

Tese no âmbito do doutoramento em Engenharia Química orientada pelo Professor Doutor Arménio Coimbra Serra, Professor Doutor Jorge Fernando Jordão Coelho e Doutora Patrícia Vitorino Mendonça e apresentada ao Departamento de Engenharia Química da Faculdade de Ciências e Tecnologia da Universidade de Coimbra

Julho 2020

Madson Ricardo Everton Santos

Atom transfer radical polymerization: study of ligands and
preparation of block copolymers with controlled structures
for application in high-performance coatings

Doctoral thesis submitted to the Faculty of Sciences and Technology of the University of
Coimbra, to obtain the Degree of Doctor in Chemical Engineering

Coimbra 2020



UNIVERSIDADE DE
COIMBRA

Madson Ricardo Everton Santos

Atom transfer radical polymerization: study of ligands and preparation of block copolymers with controlled structures for application in high-performance coatings

Thesis submitted to the Faculty of Sciences and Technology of the University of Coimbra, to obtain the Degree of Doctor in Chemical Engineering

Advisors

Professor Dr. Jorge Fernando Jordão Coelho

Professor Dr. Arménio Coimbra Serra

Dr. Patrícia Vitorino Mendonça

Host institution

University of Coimbra

Financing

Conselho Nacional de Desenvolvimento Científico e Tecnológico (CNPq)

Doctoral degree grant: 202484/2015-7



Ao meu pai Manoel Santos e
minha à minha mãe Maria José.

“A tarefa não é tanto ver aquilo
que ninguém viu, mas pensar o
que ninguém ainda pensou sobre
aquilo que todo mundo vê.”

Arthur Schopenhauer

Acknowledgments

Agradeço imensamente a todos que fizeram parte e contribuíram para o resultado deste trabalho.

Ao Professor Jorge Coelho por me ter recebido e me acolhido no grupo de pesquisa Polysyc. Sem dúvida, foi um período muito importante para meu desenvolvimento profissional e pessoal.

Ao Professor Arménio Serra pelos conselhos e pela sua disponibilidade para ajudar, com certeza de muito valor para o bom desenvolvimento deste trabalho.

À Dr^a Patrícia Mendonça pela dedicação conjunta a todos projetos desenvolvido ao longo deste doutoramento e por estar sempre disposta a orientar e a motivar

Ao CNPq e ao programa ciências sem fronteiras, este resultado somente foi possível graças aos investimentos em educação.

Aos amigos do grupo Polysyc por todo suporte emocional que muito me ajudou até aqui chegar.

Aos amigos que fiz em Coimbra, Eduardo, Halisson, McSorley e à família Knoche por toda a motivação e afeto.

À família por mim escolhida Lice, Fernando, Janás, Isaque e Valery, por representarem a minha idealização de amizade.

À minha família, por todo apoio, suporte e afeto.

Abstract

This work aimed to develop a new antimicrobial system using supplemental activator and reducing agent atom transfer radical polymerization (SARA ATRP) with potential to be applied in coating formulations and to prepare innovative antimicrobial surfaces. It was also a goal to study a new ligand for metal-catalyzed ATRP as a cost-effective alternative for other ligands commonly used in ATRP.

ATRP, at the scientific level, is one of the most used reversible deactivation radical polymerization (RDRP) processes for the preparation of complex and well-defined polymeric structures. However, one of the issues related to the scale-up of such technique to an industrial scenario is the high cost of the *N*-based ligands, which are indispensable to conduct the polymerizations. Thus, the development of new ATRP systems using economically affordable ligands is a key-step that can contribute to the feasible preparation of controlled polymers at large scale. In this project, for the first time, *N,N,N',N'*-tetramethyl guanidine (TMG), an inexpensive compound, was successfully used as ligand for the SARA ATRP of several methacrylates, namely methyl methacrylate (MMA), glycidyl methacrylate (GMA), ethyl methacrylate (EMA), butyl methacrylate (BMA) and 2-(diisopropylamino)ethyl methacrylate (DPA). Reproducible kinetics could be only obtained after careful adaptation of the setup and degassing procedures to avoid interaction between initiator and TMG. After the optimization of the synthetic procedure, the control over the polymerizations was similar to that obtained using other ligands often employed in ATRP ($M_w/M_n \approx 1.2$). The influence of DP and initiator/TMG ratio on the polymerization was investigated and showed that the rate of polymerization decreased with increasing DP. Also, cyclic voltammetry studies were conducted to prove the formation and stability of Cu^{I} /TMG complexes. The high chain-end functionality of PMMA-Br was proved by self-chain extension and block copolymerization with BMA, with a remarkable agreement between M_n^{th} and M_n^{SEC} and low dispersity ($M_w/M_n < 1.2$). In addition, experiments conducted in the absence of Cu^0 (SARA agent) showed that TMG can act simultaneously as the ligand for the metal coordination and as reducing agent, affording well-defined PMMA-Br ($M_w/M_n \approx 1.2$).

Healthcare-acquired microbial infections are recognized as the most frequent adverse event in hospitals with dramatic associated consequences. This fact is even more serious, considering the current increase rate of microbial resistance development and the

declining discovery of new antibiotics. In this regard, there is an urgent need to develop innovative approaches able to prevent or reduce the rate of acquisition of infections. One promising approach for the efficient elimination of bacteria is based on the use of antimicrobial polymers that present several advantages over conventional treatments, which include broad-spectrum antimicrobial activity and a microbial inactivating mechanism that is not prone to resistance development. In this work, SARA ATRP was used for the preparation of new linear and star-shaped amphiphilic cationic copolymers, based on poly(butyl acrylate) (PBA) and poly((3-acrylamidopropyl)trimethylammonium chloride) (PAMPTMA) with well-defined composition, topology and molecular weight (MW). The antimicrobial efficacy of the novel polymeric systems was evaluated against three different strains of bacteria causing nosocomial infections (*Staphylococcus aureus*, *Escherichia coli* and *Pseudomonas aeruginosa*) and two *Bacillus* strains (*Bacillus cereus* and *Bacillus subtilis*). The systematic study relating polymer features with antimicrobial efficacy was conducted and it was found that antimicrobial activity increased with increasing MW. To understand the inactivating mechanism of the novel antimicrobial system, membrane cell integrity assays using *E. coli* were performed and the results revealed a bactericidal behavior by the polymers through bacterial cell membrane disruption.

Antimicrobial photodynamic inactivation (aPDI) uses photosensitizers (PS), which are activated upon visible light absorption, to produce reactive oxygen species (ROS) that can cause several irreversible damages to the bacteria cells. The methodology has been explored in the biomedical field, mostly for the treatment of localized infections and more recently, to produce light-activated polymeric materials aiming to prevent bacterial infections. In this project, three different PS molecules, namely curcumin, proflavine and toluidine blue O (TBO) had their PDI activity evaluated against five different bacteria (the same subjected to the study of the antimicrobial polymers). In the first part of the study, light-assisted assays in liquid medium were performed to determine the minimum inhibitory concentration (MIC) of the PS molecules, using three LED light sources (white, blue and red) and varying both the light intensity and the exposure time aiming to evaluate the influence of these parameters on the antimicrobial activity of the PS. This allowed to establish experimental conditions for further analysis of the polymers containing PS in their structure or polymer/PS mixtures. In general, the results revealed that Gram-positive bacteria were more susceptible to the action of the PS molecules, presenting lower MIC

values than the ones obtained against Gram-negative under similar conditions. Also, an improvement on the antimicrobial activity was observed for tests using light with specific wavelengths (blue light or red light), according to the maximum absorption of each PS, and at high-mode intensity energy. Next, the synergistic effects of simple mixtures of polymers (PAMPTMA-Br or PAMPTMA-*co*-PBA-Br) and PS molecules (curcumin, proflavine and TBO) were investigated against *E. coli*. Each antimicrobial agent was used below its MIC value, and it was found that at certain polymer/PS ratios, the mixture could inhibit the *E. coli* growth.

Another strategy to evaluate the synergistic antimicrobial effect of polymer/PS concerned the preparation of polymers containing one PS molecule covalently bonded to the polymeric structure. To achieve this, derivatives based on curcumin and proflavine were synthesized and used as ATRP initiators. Here, a library of non-functionalized and PS-initiated cationic PAMPTMA-Br homopolymers and amphiphilic PAMPTMA-*co*-PBA-Br copolymers were prepared, and the samples were tested against the five microorganisms selected for this project. To investigate if PS-polymers could exhibit light-mediated activity, the assays were performed under dark and light (blue and white) conditions, but no significant differences on the MIC values were observed. The quantity of PS molecule present in the material was very low (one PS molecule per polymeric chain) and probably the quantity of ROS generated was not enough to cause lethal toxicity for the bacteria.

The last part of the light-assisted study was dedicated to the evaluation of the potential of the polymeric system developed during this PhD project to be used as an additive for varnish formulations to produce surfaces with antimicrobial activity. Several glass surfaces coated with varnishes containing non-functionalized polymers, PS-polymers and polymers/PS mixtures in different amounts were prepared and the antimicrobial activity against *E. coli* was evaluated under dark and under light (blue and white). The results revealed that the surfaces displayed a photoantimicrobial action, achieving the highest activity for surfaces prepared with the PAMPTMA/curcumin mixture and exposed to blue light.

Resumo

Este trabalho visou desenvolver um novo sistema antimicrobiano utilizando activador suplementar e agente redutor da polimerização por radicais de transferência de átomo (SARA ATRP) com potencial para ser aplicado em formulações de revestimento e para preparar superfícies antimicrobianas inovadoras. Era também um objectivo estudar um novo ligante para ATRP catalisado por metal como alternativa mais acessível para outros ligantes normalmente utilizados em ATRP.

A nível científico, ATRP é uma das técnicas de polimerização radicalar por desactivação reversível (RDRP) mais utilizada para a preparação de polímeros com estruturas complexas e bem definidas. No entanto, um dos problemas associados à expansão desta técnica para um cenário industrial é o alto custo dos ligantes à base de azoto, que são indispensáveis nestas polimerizações. Assim, o desenvolvimento de novos sistemas ATRP usando ligantes economicamente acessíveis é um passo-chave que pode contribuir para a preparação viável de polímeros controlados em larga escala. Neste projeto, pela primeira vez, *N,N,N',N'*-tetrametil guanidina (TMG) foi usada como ligante para o SARA ATRP de vários metacrilatos, como metacrilato de metilo (MMA), metacrilato de glicidilo (GMA), metacrilato de etilo (EMA), metacrilato de butilo (BMA) e metacrilato de 2-(diisopropilamino)etilo (DPA). Resultados cinéticos reproduzíveis foram somente obtidos após a adaptação dos procedimentos de preparação e degaseificação da reacção, a fim de evitar a interação entre iniciador e TMG. Após a otimização do procedimento, o controlo sobre as polimerizações observado foi semelhante ao obtido com outros ligantes frequentemente empregados em ATRP ($M_w/M_n \approx 1.2$). A influência do grau de polimerização (DP) e do rácio iniciador/TMG na polimerização foi investigada e os resultados mostraram que a velocidade de polimerização diminuiu com o aumento do DP e que a eficiência de iniciação aumentou com a diminuição do rácio iniciador/TMG. Estudos de voltametria cíclica foram realizados para comprovar a formação e a estabilidade dos complexos Cu^I/TMG . A alta funcionalidade de final de cadeia de PMMA-Br foi comprovada por auto-extensão de cadeia e através da copolimerização em bloco usando BMA como monómero do segundo segmento, com notável concordância entre M_n^{th} e M_n^{SEC} e baixa dispersividade ($M_w/M_n \approx 1.2$). Além disso, polimerizações conduzidas na ausência de Cu^0 (agente SARA) mostraram que a TMG é capaz de atuar

simultaneamente como ligante para a coordenação do metal e como agente redutor, produzindo PMMA-Br bem definido ($M_w/M_n \approx 1.2$).

As infecções microbianas adquiridas em casas de saúde são reconhecidas como um evento adverso muito frequente, associado a diversas consequências dramáticas. Este facto torna-se ainda mais preocupante, tendo em conta a actual crescente taxa de desenvolvimento de resistência microbiana e a descoberta declinante de novos antibióticos. Neste sentido, há uma séria urgência para desenvolver abordagens inovadoras capazes de prevenir ou reduzir a taxa de aquisição de infecções nosocomiais. Uma estratégia promissora para a eliminação eficiente de bactérias baseia-se no uso de polímeros antimicrobianos que apresentam várias vantagens comparativamente com tratamentos convencionais, incluindo atividade antimicrobiana de amplo espectro e um mecanismo de inativação microbiana que não é propenso ao desenvolvimento de resistência. Neste trabalho, a técnica de SARA ATRP foi utilizada para a preparação de novos copolímeros catiónicos anfifílicos lineares e em forma de estrela, baseados em poli(acrilato de butilo) (PBA) e cloreto de poli((3-acrilamidopropil trimetilamónio) (AMPTMA) com composição, topologia e peso molecular (MW) bem definidos. A eficácia antimicrobiana do novo sistema polimérico foi avaliada contra três estirpes de bactérias comumente associadas a infecções nosocomiais (*Staphylococcus aureus*, *Escherichia coli* e *Pseudomonas aeruginosas*) e duas espécies de *Bacillus* (*Bacillus cereus* e *Bacillus subtilis*). Foi realizado um estudo sistemático que permitiu relacionar as características do polímero com a eficácia antimicrobiana, verificando-se que a mesma aumentou com o aumento do MW. Para entender o mecanismo de inativação microbiano, foram realizados ensaios de integridade da membrana celular bacteriana, com bactérias *E. coli*, tendo os resultados revelado um comportamento bactericida por rompimento da membrana bacteriana.

A inativação fotodinâmica antimicrobiana (aPDI) utiliza fotossensibilizadores (PS), que são activados na absorção de luz visível, para produzir espécies reactivas de oxigénio (ROS) e que podem causar vários danos irreversíveis às células bacterianas. A metodologia tem sido explorada no campo biomédico, principalmente para o tratamento de infecções localizadas e, mais recentemente, para produzir materiais poliméricos activados à luz com o objectivo de prevenir infecções bacterianas. Neste projecto, três moléculas diferentes de PS, nomeadamente curcumina, proflavina e azul de toluidina O (TBO) tiveram a sua actividade de PDI avaliada contra cinco bactérias diferentes (as

mesmas submetidas ao estudo dos polímeros antimicrobianos). Na primeira parte do estudo, foram efectuados ensaios com luz assistida em meio líquido para determinar a concentração inibitória mínima (MIC) das moléculas PS, utilizando três fontes de luz LED (branca, azul e vermelha) e variando tanto a intensidade da luz como o tempo de exposição com o objectivo de avaliar a influência destes parâmetros na actividade antimicrobiana dos PS. Isto permitiu estabelecer condições experimentais para uma análise mais aprofundada dos polímeros que contêm PS na sua estrutura ou das misturas de polímeros/PS. Em geral, os resultados revelaram que as bactérias Gram-positivas eram mais susceptíveis à acção das moléculas de PS, apresentando valores MIC inferiores aos obtidos contra as Gram-negativas, em condições semelhantes. Também se observou uma melhoria da actividade antimicrobiana nos testes que utilizaram luz com comprimentos de onda específicos (luz azul ou vermelha), de acordo com a absorção máxima de cada PS, e utilizando energia de alta intensidade. Em seguida, foram investigados os efeitos sinérgicos das misturas simples de polímeros (PAMPTMA-Br ou PAMPTMA-co-PBA-Br) e moléculas de PS (curcumina, proflavina e TBO) contra a *E. coli*. Cada agente antimicrobiano foi utilizado abaixo do seu valor de MIC, tendo-se constatado que, em certos rácios polímero/PS, a mistura poderia inibir o crescimento da *E. coli*.

Outra estratégia para avaliar o efeito antimicrobiano sinérgico do polímero/PS dizia respeito à preparação de polímeros contendo uma molécula de PS ligada de forma covalente à estrutura polimérica. Para tal, foram sintetizados derivados à base de curcumina e proflavina, que foram utilizados como iniciadores de ATRP. Aqui foi preparada uma biblioteca de homopolímeros PAMPTMA-Br catiónicos não funcionalizados e iniciados por PS e copolímeros anfifílicos PAMPTMA-co-PBA-Br, tendo as amostras sido testadas contra os cinco microrganismos seleccionados para este projecto. Para investigar se os polímeros PS podiam exhibir actividade mediada pela luz, os ensaios foram realizados em condições em escuro e com luz (azul e branco), mas não foram observadas diferenças significativas nos valores do MIC. A quantidade de molécula de PS presente no material foi muito baixa (uma molécula de PS por cadeia polimérica) e provavelmente a quantidade de ROS gerada não foi suficiente para causar toxicidade letal para as bactérias.

A última parte do estudo realizado na presença de luz foi dedicada à avaliação do potencial do sistema polimérico desenvolvido durante este projecto de doutoramento para

ser utilizado como aditivo em formulações de verniz e para produzir superfícies com actividade antimicrobiana. Foram preparadas várias superfícies de vidro revestidas com vernizes contendo polímeros não funcionalizados, PS-polímeros e misturas de polímeros/PS em diferentes quantidades e a actividade antimicrobiana contra *E. coli* foi avaliada em escuro e com luz (azul e branco). Os resultados revelaram que as superfícies apresentavam uma acção fotoantimicrobiana, obtendo a maior actividade para superfícies preparadas com a mistura PAMPTMA/curcumina e expostas à luz azul.

List of publications

Papers published from the research work presented in this thesis:

Santos M. R. E., Fonseca A. C., Mendonça P. V., Branco R., Serra A. C., Morais P. V., Coelho J. F. J., Recent Developments in Antimicrobial Polymers: A Review, *Materials*, 2016, 9, (7), 599.

Madson R.E. Santos, Patrícia V. Mendonça, Mariana C. Almeida, Rita Branco, Armenio C. Serra, Paula V. Morais and Jorge F J Coelho, Increasing the antimicrobial activity of amphiphilic cationic copolymers by the facile synthesis of high molecular weight stars by SARA ATRP, *Biomacromolecules*, 2019, 20, 3, 1146-1156.

Madson R. E. Santos, Sílvia M. Ferreira, Patrícia V. Mendonça, Francesco De Bon, Armenio C. Serra and Jorge F. J. Coelho. Guanidine as inexpensive dual function ligand and reducing agent for ATRP of methacrylates, *Polym. Chem.*, 2019, 10, 4944-4953.

Papers published from the collaboration in other projects during the PhD program:

Pedro Maximiano, Patricia V. Mendonça, Madson R. E. Santos, Joao R. C. Costa, Tamaz Guliashvili, Armenio C. Serra, Jorge F. J. Coelho, Eutectic Mixtures as a Green Alternative for Efficient Catalyst Recycling in Atom Transfer Radical Polymerizations, *J. Polym. Sci., Part A: Polym. Chem.*, 2017, 55, 371–381.

Thesis outline

This project was designed to develop a novel antimicrobial polymeric system with the potential to be incorporated into varnish formulations for the preparation of surfaces with antimicrobial activity. In this study, cationic homopolymers and amphiphilic copolymers were prepared *via* SARA ATRP. At the same time, *N,N,N',N'*-tetramethyl guanidine (TMG) was used as ligand in SARA ATRP experiments, with the aim to find out an inexpensive and commercially available alternative ligand for ATRP.

Considering the goals mentioned, Chapter 1 is dedicated to a literature review involving RDRP methods, with a detailed description of the ATRP techniques, the approaches of microorganism's inactivation/killing, either by polymers or by a light-mediated mechanism.

Chapter 2 presents the materials, the characterization techniques and the synthetic procedures used during this PhD work.

Chapter 3 is dedicated to the results and discussion of the studies developed during this PhD project. In the first part of the chapter, the results concerning the use of TMG as ligand for the ATRP of selected methacrylates, namely MMA, EMA, GMA, BMA and DPA, are presented. Results showed the efficiency of TMG as ligand to afford polymethacrylates with low dispersity. The second part is dedicated to the development of cationic amphiphilic polymers prepared by SARA ATRP. An extensive library consisting of polymers with different composition (homopolymers, random and block copolymers) and architecture (linear and star-shaped) was prepared and the antimicrobial activity of the materials was evaluated against both Gram-positive and Gram-negative bacteria. Also, preliminary membrane integrity assays showed that the (co)polymers exhibited a bactericidal behavior through membrane disruption of *E. coli* bacteria. In sequence, the results concerning the antimicrobial tests performed in the presence of light using three different PS molecules, namely TBO, curcumin and proflavine, are presented. ATRP initiators were prepared from both curcumin and proflavine and used for the preparation of PS-containing polymers. Their antimicrobial activity was also evaluated in the presence and absence of light (white and blue) irradiation. The last part of this chapter presents the antimicrobial results obtained for the glass surfaces coated with varnishes containing polymer, PS-initiated polymer or polymer/curcumin mixtures.

Finally, Chapter 4 presents the most relevant conclusions of the PhD work as well as further recommendations for future research.

List of acronyms

AMP	Antimicrobial peptide
AMPTMA	(3-Acrylamidopropyl)trimethylammonium chloride
aPDI	Antimicrobial photodynamic inactivation
ARGET	Activators regenerated by electron transfer
ATRP	Atom transfer radical polymerization
BAAm	<i>N,N'</i> -methylene bis(acrylamide)
BiB	α -bromoisobutyryl bromide
BMA	Butyl methacrylate
CCS	Core cross-linked
CFU	Colony-forming units
CL	Crosslinker
CLSI	Clinical laboratory standard institute
CV	Crystal violet
DETA	Diethylenetriamine
DLS	Dynamic light scattering
DMAEMA	2-(<i>N,N</i> -dimethylamino)ethyl methacrylate
DMEG _{2e}	<i>N',N''</i> -bis(1,3-dimethylimidazolin-2-ylidene)ethane-1,2-diamine
DMSO	Dimethyl sulfoxide
DP	Degree of polymerization
DPA	2-(Diisopropylamino)ethyl methacrylate
EBiB	Ethyl α -bromoisobutyrate
EBPA	Ethyl α -bromophenylacetate
ECP	Ethyl 2-chloropropionate
EMA	Ethyl methacrylate
ESBL	Extended spectrum β -lactamase
FRP	Free radical polymerization
GMA	Glycidyl methacrylate

HEAA	<i>N</i> -Hydroxyethyl acrylamide
HEMA	2-Hydroxyethyl methacrylate
ICAR	Initiators for continuous activator regeneration
ITP	Iodine transfer polymerization
LED	Light emitting diode
LPS	Lipopolysaccharides
MA	Methyl acrylate
MALDI-TOF	Matrix-assisted laser desorption ionization-time of flight
MBC	Minimum bactericidal concentration
MDS	Molecular dynamics simulations
Me ₆ TREN	Tris(2-(dimethylamino)ethyl)amine
MFC	Minimum fungicidal concentration
MI	Macroinitiator
MIC	Minimum inhibitory concentration
MMA	Methyl methacrylate
MRSA	Methicillin-resistant <i>S. Aureus</i>
<i>n</i> -BA	<i>n</i> -Butyl acrylate
NI	Nosocomial infections
NMP	Nitroxide-mediated polymerization
NMR	Nuclear magnetic resonance
NPs	Nanoparticles
OD	Optical density
PAMPTMA	Poly((3-acrylamidopropyl) trimethylammonium chloride))
PBA	Poly(butyl acrylate)
PBMA	Poly(butyl methacrylate)
PDPA	Poly(2-(diisopropylamino)ethyl methacrylate)
PEMA	Poly(ethyl acrylate)
PGMA	Poly(glycidyl methacrylate)
PMDETA	<i>N,N,N',N'',N'''</i> -pentamethyldiethylenetriamine

PMMA	Poly(methyl methacrylate)
PRE	Persistent radical effect
PTFE	Polytetrafluoroethylene
QAS	Quaternary ammonium salts
QPS	Quaternary phosphonium salts
RAFT	Reversible addition-fragmentation chain transfer
RBC	Red blood cells
RDRP	Reversible deactivation radical polymerization
ROS	Reactive oxygen species
SARA	Supplemental activator and reducing agent
SEC	Size exclusion chromatography
SEM	Scanning electron microscopy
SMAMP	Synthetic mimics of antimicrobial peptide
TBO	Toluidine blue O
TMG	<i>N,N,N',N'</i> -Tetramethyl guanidine
TREN	Tris(2-aminoethyl)amine
VREF	Vancomycin-resistant <i>E. faecium</i>
WHO	World health organization

Nomenclature

D	Dispersity
M_n^{th}	Theoretical number-average molecular weight
M_n^{SEC}	Number-average molecular weight determined by SEC
M_w	Weight-average molecular weight
k_p^{app}	Apparent rate constant of propagation
k_a	Activation rate constant
k_d	Deactivation rate constant
K_{ATRP}	ATRP equilibrium constant
T	Temperature
I_{eff}	Initiation efficiency
CI	Curcumin initiator
PF	Proflavine initiator

Contents

Acknowledgments.....	vii
Abstract	ix
Resumo.....	xiii
List of publications.....	xvii
Thesis outline	xix
List of acronyms.....	xxi
Nomenclature	xxv
List of Figure.....	xxxii
List of Scheme.....	xxxix
List of Tables.....	xli
Motivation, targets and research significance	xliii
Chapter 1 – Introduction.....	45
1.1. Reversible deactivation radical polymerization	3
1.2. Atom transfer radical polymerization	6
1.2.1. Development of new ligands for ATRP	9
1.2.2. Tailoring polymeric structures by ATRP	10
1.3. Most relevant microbial threats to health and units on antimicrobial and hemolytic activity	13
1.4. From natural antimicrobial peptides to synthetic antimicrobial polymers.....	16
1.5. Mechanisms of microbial cell death induced by antimicrobial macromolecules and molecular basis of selectivity	18
1.6. Polymer properties influencing their antimicrobial activity.....	20
1.6.1. Random copolymers.....	21
1.6.2. Block copolymers.....	25
1.6.3. Branched polymers.....	27
1.6.4. Hydrophilic/hydrophobic balance	29
1.6.5. The effect of the molecular weight.....	29
1.6.6. Bioactive polymers containing ammonium or phosphonium salts.....	31
1.7. Antimicrobial photodynamic inactivation.....	33
1.7.1. Photobiological processes	34
1.7.2. Reactive oxygen species (ROS)-induced cytotoxicity	35
1.7.3. Photosensitizer	36
Toluidine blue O.....	37

Proflavine	38
Curcumin	39
1.7.4. Light-activated polymeric antimicrobial surfaces	40
Chapter 2 - Materials and methods	43
2.1. Materials.....	45
2.2. Procedures.....	46
2.2.1. Typical synthesis of PMMA-Br by Cu ⁰ -mediated SARA ATRP.....	46
2.2.2. Typical synthesis of PGMA-Br by Fe ⁰ -mediated SARA ATRP.....	46
2.2.3. Typical synthesis of PEMA-Br by Cu ⁰ -mediated SARA ATRP.....	47
2.2.4. Typical synthesis of PEG- <i>b</i> -PDPA-Br by Cu ⁰ -mediated SARA ATRP	47
2.2.5. “One-pot” chain extension of PMMA-Br with MMA or BMA by Cu ⁰ -mediated SARA ATRP	47
2.2.6. ARGET ATRP of MMA using TMG as reducing agent.....	48
2.2.7. Typical homopolymerization of AMPTMA by Cu ⁰ -mediated SARA ATRP.....	48
2.2.8. Typical homopolymerization of <i>n</i> -BA by SARA ATRP	49
2.2.9. Typical “one-pot” block copolymerization of AMPTMA and <i>n</i> -BA.....	49
2.2.10. Typical synthesis of random PAMPTMA- <i>co</i> -PBA copolymer.....	50
2.2.11. Typical synthesis of star-shaped polymers via core-first and arm-first.....	50
2.2.12. Synthesis of proflavine ATRP initiator (PF) - <i>N,N'</i> -(acridine-3,6-diyl)bis(2-bromo-2-methylpropanamide).	50
2.2.13. Synthesis of curcumin ATRP initiator (CI) - ((1E,3Z,6E)-3-hydroxy-5-oxohepta-1,3,6-triene-1,7-diyl)bis(2-methoxy-4,1-phenylene) bis(2-bromo-2-methylpropanoate)).	51
2.2.14. Synthesis of photosensitizer-functionalized antimicrobial polymers.....	51
2.2.15. Synthesis of curcumin acrylate 4-((1E,3Z,6E)-3-hydroxy-7-(4-hydroxy-3-methoxyphenyl)-5-oxohepta-1,3,6-trien-1-yl)-2-methoxyphenyl acrylate.....	51
2.2.16. MIC determination in solution	52
2.2.17. Assessment of antimicrobial activity of the surfaces	52
2.3. Techniques	53
2.3.1. Determination of molecular weight parameters SEC.....	53
2.3.2. Determination of the <i>dn/dc</i> of the polymers.....	54
2.3.3. Nuclear magnetic resonance.....	54
2.3.4. Matrix assisted laser desorption ionization-time of flight.....	54

2.3.5.	UV/Vis spectroscopy.....	55
2.3.6.	Voltammetry.....	55
2.3.7.	Dynamic light scattering (DLS).....	56
2.3.8.	Scanning electron microscopy (SEM).....	56
2.3.9.	Live/dead membrane integrity assay.....	56
Chapter 3 – Results and discussion		57
3.1.	Guanidine as inexpensive dual function ligand and reducing agent for ATRP of methacrylates.....	59
3.1.1.	Influence of the targeted degree of polymerization.....	61
3.1.2.	Evaluation of the polymer chemical structure and chain-end functionality.....	62
3.1.3.	Polymerization of other methacrylates.....	64
3.1.4.	Dual behavior of TMG: ligand and reducing agent.....	65
3.1.5.	Electrochemical characterizations.....	67
3.1.6.	Conclusions.....	70
3.2.	Development of cationic amphiphilic antimicrobial polymers by SARA ATRP	71
3.2.1.	Influence of MW and hydrophobicity on polymers' antimicrobial activity.....	73
3.2.2.	Influence of architecture on polymers' antimicrobial activity	77
3.2.3.	Influence of the structure of copolymers on their antimicrobial activity	79
3.2.4.	Preliminary studies on cell-polymer interactions.....	80
3.2.5.	Synthesis and evaluation of the antimicrobial activity of the high-branched core cross-linked star-shaped (CCS) PAMPTMA prepared via arm-first.....	82
3.2.6.	Conclusions.....	86
3.3.	Antimicrobial photodynamic inactivation.....	86
3.3.1.	Photodynamic activity of TBO.....	87
3.3.2.	Photodynamic activity of proflavine	89
3.3.3.	Photodynamic activity of curcumin	90
3.3.4.	Photodynamic activity of photosensitizer/polymer mixtures	93
3.3.5.	Combination of polymers and toluidine blue O towards <i>E. coli</i>	94
3.3.6.	Combination of polymers and curcumin over <i>E. coli</i>	95
3.3.7.	Combination of polymers and proflavine towards <i>E. coli</i>	96
3.3.8.	PS-functionalized antimicrobial polymers	97
3.3.9.	Photodynamic antimicrobial activity of PS-functionalized polymers.....	104

3.3.10. Light-activated antimicrobial surfaces	107
3.3.11. Conclusions	111
Chapter 4 - Final remarks	113
4.1. Overall conclusions	115
4.2. Future work	117
Appendices	119
Appendix A: Guanidine as inexpensive dual function ligand and reducing agent for ATRP of methacrylates.....	121
Appendix B: Increasing the antimicrobial activity of amphiphilic cationic copolymers by the facile. synthesis of high molecular weight stars by SARA ATRP	127
Appendix C: Antimicrobial photodynamic inactivation.....	133
References	133

List of Figure

Figure 1.1 Chemical structures of representative ligands, initiators and monomers commonly used in ATRP.	9
Figure 1.2. Schematic representation of the different types of antimicrobial polymeric systems	17
Figure 1.3. Basis of the selectivity of antimicrobial macromolecules. (a) Illustration of the cross sections of mammalian cells (left) and bacterial cell envelop (right). (b) Selective interactions between cell membranes and amphiphilic antimicrobial polymer.	20
Figure 1.4 Representative polymeric architectures and composition employed as antimicrobial polymers	21
Figure 1.5 Chemical structure of PABMA- <i>co</i> -PEMA and MIC values for <i>S. aureus</i> . .	22
Figure 1.6 Chemical structure and MIC values of the amine/guanidine-functionalized amphiphilic polymethacrylates.....	23
Figure 1.7. Chemical structure and MIC values of PAEMA- <i>co</i> -PHEMA- <i>co</i> -PEMA...	24
Figure 1.8. Chemical structure of poly- β -peptide and MIC values towards Gram-positive and Gram-negative bacteria.....	25
Figure 1.9. Chemical structure and MIC values of (a) PBMA- <i>b</i> -PDMAEMA and (b) poly(IBVE- <i>b</i> -PIVE)	26
Figure 1.10. Chemical structure of lysine-valine-based SNAPPs	27
Figure 1.11. Chemical structure and MIC values of the antimicrobial hyperbranched emulsifiers	28
Figure 1.12. Chemical structure and MIC values of (a) PMAGH- <i>b</i> -PS- <i>b</i> -PMAGH and (b) PDMAEMA- <i>g</i> -rosin.	30
Figure 1.13. Chemical structure of (a) sugar-functionalized polymers and (b) chitosan derivatives bearing quaternary phosphonium salts.....	32
Figure 1.14. Jablonsky diagram and ROS formation by photodynamic process.....	35

Figure 1.15. Chemical structures of representative photosensitizers.	36
Figure 3.1. Chemical structures of the EBPA initiator, MMA monomer and the ligand TMG.	59
Figure 3.2. Kinetic plots of (a) $\ln([M]_0/[M])$ vs. time and (b) M_n^{SEC} and M_w/M_n vs. monomer conversion for the SARA ATRP of MMA at 30 °C in DMSO using different molar ratios of ligand (0.5; 0.7, 1.0 and 2.0). Conditions: $[MMA]_0/[DMSO] = 2/1$ (v/v); $[MMA]_0/[EBPA]_0/[CuBr_2]_0/[TMG]_0 = 100/1/0.1/x$; Cu^0 wire: $l = 5.0$ cm, $d = 1$ mm. .	60
Figure 3.3. Kinetic plots of (a) $\ln([M]_0/[M])$ vs. time and (b) M_n^{SEC} and M_w/M_n vs. monomer conversion for the SARA ATRP of MMA at 30 °C in DMSO using different molar ratios of ligand. Conditions: $[MMA]_0/[DMSO] = 2/1$ (v/v); $[MMA]_0/[EBPA]_0/[CuBr_2]_0/[TMG]_0 = DP/0.1/1$; Cu^0 wire: $l = 5.0$ cm, $d = 1$ mm.	61
Figure 3.4. Enlargement of the MALDI from m/z 4700 to 5350 of PMMA-Br ($M_n^{SEC} = 7000$, $M_w/M_n = 1.14$), obtained by Cu^0 -mediated SARA ATRP using TMG as ligand.	62
Figure 3.5. 1H NMR spectrum in $CDCl_3$ of PMMA-Br prepared by SARA ATRP ($M_n^{SEC} = 7000$, $M_w/M_n = 1.14$), obtained by Cu^0 -mediated SARA ATRP using TMG as ligand.	63
Figure 3.6. SEC traces of the PMMA-Br macroinitiator (red line) and the extended PMMA-Br (black line) prepared by “one pot” SARA ATRP in DMSO at 30 °C. Conditions: first block – $[MMA]_0/[EBPA]_0/[CuBr_2]_0/[TMG]_0 = 50/1/0.1/1$; Cu^0 wire: $l = 50$ mm, $d = 1$ mm; $[MMA]_0/[DMSO] = 2/1$ (v/v), $conv_{MMA} = 93\%$; second block – $[BMA]_0/[EBPA]_0 = 350$, $conv_{MMA} = 53\%$	63
Figure 3.7. Chemical structures of the methacrylates polymerized by SARA ATRP using TMG as the ligand.	64
Figure 3.8. Kinetic plots of (a) $\ln([M]_0/[M])$ vs. time and (b) M_n^{SEC} and M_w/M_n vs. monomer conversion for the SARA ATRP of MMA at 30°C in DMSO using different molar ratios of TMG. Conditions: $[MMA]_0/[DMSO] = 2/1$ (v/v); $[MMA]_0/[EBPA]_0/[CuBr_2]_0/[TMG]_0 = 100/1/0.1/x$	65

- Figure 3.9.** UV-vis spectra recorded at different times ($T = 30\text{ }^{\circ}\text{C}$) of (a) CuBr_2/TMG in DMSO; $[\text{CuBr}_2]_0/[\text{TMG}]_0 = 0.1/1.0\text{ mmol/mL}$ and (b) $\text{CuBr}_2/\text{Me}_6\text{TREN}/\text{TMG}$ in DMSO; $[\text{TMG}]_0/[\text{CuBr}_2]_0/[\text{Me}_6\text{TREN}]_0 = 1.0/0.1/0.15\text{ mmol/mL}$ 66
- Figure 3.10.** (a) Cyclic voltammetry of $1.1\text{ mM Cu}^{\text{I}}(\text{CH}_3\text{CN})\text{BF}_4$ in the presence of 0 (—), 1 (—), 2 (—) and 3 (—) equivalents of TMG; (b) cyclic voltammetry of $1.0\text{ mM Cu}^{\text{II}}(\text{OTf})_2$ in the presence of 0 (—) and 1 (—) equivalents of TMG. CV are recorded in DMSO + $0.1\text{ M Et}_4\text{NBF}_4$ at $25\text{ }^{\circ}\text{C}$, on a GC electrode at 0.2 V/s . The arrow shows the scan direction. 68
- Figure 3.11.** (a) Cyclic voltammetry of $1.05\text{ mM Cu}^{\text{II}}(\text{OTf})_2$ in the presence of 1 (—), 2 (—), 3 (—) equivalents of TMG and 3 equivalents of TMG + 1 equivalent of TEABr (—); (b) cyclic voltammetry of $1.05\text{ mM Cu}^{\text{II}}(\text{OTf})_2$ in the presence of 3 (—) and 0 (—) equivalents of TMG. Sharp oxidation peak corresponds to Cu stripping from electrode surface. CV are recorded in DMSO + $0.1\text{ M Et}_4\text{NBF}_4$ at $25\text{ }^{\circ}\text{C}$, on a GC electrode at 0.2 V/s 69
- Figure 3.12.** General structures of the monomers (AMPTMA and n -BA), initiators (EBiB, 4-EBiB and 6-EBiB), and representation of linear and star-shaped (PAMPTMA-Br, PAMPTMA-*co*-PBA or PAMPTMA-*b*-PBA) (co)polymers prepared by SARA ATRP. 72
- Figure 3.13.** $400\text{ MHz } ^1\text{H NMR}$ spectrum in d_6 -EtOD of purified PAMPTMA₅₀-*co*-PBA₁₅ copolymer ($M_n^{\text{th}} = 12.4 \times 10^3$) obtained by SARA ATRP. 72
- Figure 3.14.** SEM and fluorescence microscopy images of *E. coli* cells before and after treatment with 6-arm, 4-arm star-shaped and linear PAMPTMA homopolymers and PAMPTMA-*co*-PBA copolymers. Conditions: 5 h incubation at concentration of MIC. Live/dead staining shows live (SYTO 09 labeled) green cells and dead (propidium iodide labeled) in red. Percentage of death by membrane damage for untreated, 6SA114B0, 6SA69B41, 4SA84B20, 4SA93B0, LA115B0 and LA98B29-treated *E. coli* cells. At least 100 cells were counted in triplicates for at least two independent experiments. *** $p = 0.0001$; **** $p < 0.0001$ 81
- Figure 3.15** Reaction scheme of the reparation of CCS-PAMPTMA via “one-pot” arm-first approach. 83

- Figure 3.16.** SEC traces obtained during the synthesis of CCS-PAMPTMA prepared by SARA ATRP. Conditions: $[AMPTMA]_0/[EBiB]_0/[CuBr_2]_0/[Me_6TREN]_0/Cu^0$ wire = 30/1/0.5/1.0; $[MI]/[CL] = 12$; $[AMPTMA]_0 = 1.45$ M; solvent: $[EtOH]/[H_2O] = 40/60$ (v/v) Cu^0 wire: $l = 5$ cm; $d = 1$ mm. 84
- Figure 3.17.** Absorbance spectrum of TBO in LB medium and emission spectrum of the LED emitting red light ($\lambda = 635$ nm) and the LED emitting white light ($\lambda = 400 - 750$ nm)..... 88
- Figure 3.18.** Absorbance spectrum of proflavine in LB medium ($\lambda_{max} = 440$ nm) and emission spectra of the blue-light LED ($\lambda = 450$ nm) and white-light LED. 89
- Figure 3.19.** Absorbance spectrum of curcumin in LB medium and emission spectra of the blue-light LED ($\lambda = 450$ nm) and white-light LED. 91
- Figure 3.20.** 400 MHz 1H NMR spectrum of the curcumin-based initiator (CI) in $CDCl_3$ 98
- Figure 3.21.** 400 MHz 1H NMR spectrum of the proflavine-based initiator (PF) in $DMSO-d_6$ 98
- Figure 3.22.** 400 MHz 1H NMR spectrum in d_6 -EtOD of the curcumin-initiated PAMPTMA₂₀₀-Br (CA200B0) prepared by SARA ATRP ($M_n^{th} = 44100$). Conditions: $[AMPTMA]_0/[CI]_0/[CuBr]_0/[Me_6TREN]_0 = 740/1/0.5/1$; Cu^0 wire $l = 5$ cm, $d = 1$ mm; $[AMPTMA]_0 = 3.0$ M in $EtOH/DMF = 85/15$ at 30 °C (v/v)..... 101
- Figure 3.23.** 400 MHz 1H NMR spectrum in d_6 -EtOD of the curcumin-initiated PAMPTMA_{200-co}-PBA₂₅-Br (CA200B25) prepared by SARA ATRP ($M_n^{th} = 45500$). Conditions: $[AMPTMA]_0/[n-BA]_0/[CI]_0/[CuBr_2]_0/[Me_6TREN]_0 = 370/37/1/2/1$; Cu^0 wire $l = 5$ cm, $d = 1$ mm at 30 °C; $[AMPTMA]_0 = 3.0$ M $EtOH/DMF = 85/15$ (v/v)..... 101
- Figure 3.24.** UV-vis spectra in LB growth medium of curcumin ($\lambda_{max} = 431$ nm), CI-PAMPTMA CA200B0 homopolymer ($\lambda_{max} = 353$ nm) and CI-PAMPTMA-co-PBA CA200B25 copolymer ($\lambda_{max} = 351$ nm). 102
- Figure 3.25.** 400 MHz 1H NMR spectrum in D_2O of the proflavine-initiated PAMPTMA₁₉₃-Br (PA193B0) prepared by SARA ATRP ($M_n^{th} = 42500$). Conditions:

[AMPTMA]₀/[PF]₀/[CuBr₂]₀/[Me₆TREN]₀ = 222/1/0.5/1; Cu⁰ wire $l = 5$ cm, $d = 1$ mm; [AMPTMA]₀ = 3.0 M, solvent: [EtOH]₀/[H₂O]₀/[DMF] = 0.65 /0.2/0.15 (v/v/v)..... 102

Figure 3.26. 400 MHz ¹H NMR spectrum in *d*6-EtOD of the proflavine-initiated PAMPTMA_{191-co}-PBA₁₉-Br (PA191B19) prepared by SARA ATRP ($M_n^{\text{th}} = 42400$). Conditions [AMPTMA]₀/[*n*-BA]₀/[PF]₀/[CuBr₂]₀/[Me₆TREN]₀ = 210/21/1/0.5/1; Cu⁰ wire $l = 5$ cm, $d = 1$ mm; [AMPTMA]₀ = 3.0 M, solvent: EtOH/H₂O/DMF = 0.65 /0.2/0.15 (v/v/v). 103

Figure 3.27. UV-vis spectra in LB growth medium of the proflavine ($\lambda_{\text{max}} = 440$ nm), proflavine initiator ($\lambda_{\text{max}} = 384$ nm), PF-PAMPTMA homopolymer PA193B0 ($\lambda_{\text{max}} = 379$ nm) and PF-PAMPTMA-*co*-PBA copolymer PA191B19 ($\lambda_{\text{max}} = 381$ nm)..... 103

Figure 3.28. Antimicrobial activity of non-functionalized and PS-initiated polymers in dark and in the presence of light for Gram-positive bacteria. 104

Figure 3.29. Antimicrobial activity of PS-initiated polymers in dark and in the presence of light for Gram-negative bacteria (*) MIC higher than 200 μM in solution..... 106

Figure 3.30 Antimicrobial activity of light-activated surfaces towards *E. coli*. (SF) surface with no antimicrobial agent; (SF+AX) surface containing CA200B0 homopolymer at the corresponding quantity, where X = 35 mg, 60 mg or 85 mg; (SF+CAX) surface containing CA200B0; (SF+CX) surface containing curcumin; (SF+AX+CX) surface containing CA200B0 + curcumin mixture..... 109

Figure A1. 400 MHz ¹H NMR, in CHCl₃, of ethyl α -bromophenyl acetate (EBPA). 121

Figure A2. 400 MHz ¹H NMR, in CHCl₃, of 1,1,3,3-tetramethylguanidine (TMG)... 122

Figure A3. 400 MHz ¹H NMR, in CHCl₃, of a [EBPA]₀/[TMG]₀ = 1/1 (molar)..... 122

Figure A4. SEC traces of a PMMA-Br ($M_n^{\text{SEC}} = 10 \times 10^3$; $M_w/M_n = 1.12$) prepared by SARA ATRP using TMG as the ligand (black line) and a PMMA standard (blue line). 123

Figure A5. MALDI-TOF MS spectrum of PMMA-Br ($M_n^{\text{SEC}} = 7000$, $M_w/M_n = 1.14$) from m/z 500 to 7500, using DCTB matrix. 123

Figure A6. SEC traces of the polymethacrylates obtained by SARA ATRP. 124

- Figure A7.** 400 MHz ^1H NMR spectrum, in CHCl_3 , of PGMA-Br homopolymer ($M_n^{\text{th}} = 22600$, $M_n^{\text{SEC}} = 37300$, $M_w/M_n = 1.31$)..... 124
- Figure A8.** 400 MHz ^1H NMR spectrum, in CHCl_3 , of PEMA-Br homopolymer ($M_n^{\text{th}} = 8340$, $M_n^{\text{SEC}} = 1070$, $M_w/M_n = 1.26$)..... 125
- Figure A9.** 400 MHz ^1H NMR spectrum in CHCl_3 of PMMA-*b*-PBMA-Br copolymer ($M_n^{\text{th}} = 27900$, $M_n^{\text{SEC}} = 35200$, $M_w/M_n = 1.06$). 125
- Figure A10.** 400 MHz ^1H NMR spectrum in CHCl_3 of PEG-*b*-PDPA-Br block copolymer ($M_n^{\text{th}} = 20100$, $M_n^{\text{SEC}} = 20900$, $M_w/M_n = 1.24$). 126
- Figure A11.** Kinetic plots of (a) $\ln([M]_0/[M])$ vs. time and (b) M_n^{SEC} and M_w/M_n vs. monomer conversion for SARA ATRP of MMA at 30 °C in DMSO in the presence and absence of light. Conditions: $[\text{MMA}]_0/[\text{DMSO}] = 2/1$ (v/v); $[\text{MMA}]_0/[\text{EBPA}]_0/[\text{CuBr}_2]_0/[\text{TMG}]_0 = 100/1/0.1/2$; Cu^0 wire: $l = 5.0$ cm, $d = 1$ mm.A126
- Figure B1.** Kinetic plots of (a) $\ln([M]_0/[M])$ vs. time and (b) plot of number-average molecular weights (M_n^{SEC}) and M_w/M_n vs. conversion for the SARA ATRP of AMPTMA in EtOH. $[\text{AMPTMA}]_0/[\text{EBiB}]_0/[\text{CuBr}_2]_0/[\text{Me}_6\text{TREN}]_0/\text{Cu}^0$ wire = 100/1/0.5/1.0/ Cu^0 wire; $[\text{AMPTMA}]_0 = 2.0$ M; Cu^0 wire: $l = 5$ cm; $d = 1$ mm; $V_{\text{solvent}} = 4.8$ mL. 127
- Figure B2.** Kinetic plots of (a) $\ln([M]_0/[M])$ vs. time and (b) plot of number-average molecular weights (M_n^{SEC}) and M_w/M_n vs. conversion for the SARA ATRP of *n*-BA in EtOH. $[\textit{n}\text{-BA}]_0/[\text{EBiB}]_0/[\text{CuBr}_2]_0/[\text{Me}_6\text{TREN}]_0/\text{Cu}^0$ wire = 100/1/0.5/1.0/ $\text{Cu}(0)$ wire; $[\textit{n}\text{-BA}]_0 = 6.9$ M; Cu^0 wire: $l = 5$ cm; $d = 1$ mm; $V_{\text{solvent}} = 2.0$ mL..... 127
- Figure B3.** SEC traces of star-shaped (a) 6-arm and (b) 4-arm PAMPTMA homopolymers prepared by SARA ATRP in EtOH..... 128
- Figure B4.** Dynamic light scattering volume distributions of representatives PAMPTMA-*co(b)*-PBA in LB bacterial cell culture media at their respective MIC values (25 °C). 128
- Figure B5.** SEC traces of the (black) 6-arm PAMPTMA and (red) CCS03 131
- Figure C1.** TCL of the curcumin (right stains) and the resulting product of the acetylation reaction (left stains) 133

Figure C2. 400 MHz ^1H NMR spectrum 400 Hz, CHCl_3 of the curcumin monoacrylate	134
Figure C3. LED systems for the antimicrobial assays in liquid medium.....	134

List of Scheme

Scheme 1.1. Dynamic equilibrium between the active and dormant species.	4
Scheme 1.2 Types of deactivation mechanisms in RDRP (I) degenerative chain transfer, (II) reversible deactivation and (III) reversible deactivation atom transfer.....	5
Scheme 1.3 Generic mechanism of copper-catalyzed ATRP.	6
Scheme 1.4 General mechanisms of the ATRP-related techniques.....	8
Scheme 1.5. Approaches for star-shaped polymer synthesis.	11
Scheme 3.7. Synthesis of the PS-based ATRP initiators (a) curcumin (CI) and (b) proflavine (PF).....	97
Scheme 3.8. Scheme reaction of the synthesis of curcumin-based monomer	107

List of Tables

Table 3.1. Reaction conditions and results of the polymerization of several methacrylates by SARA ATRP using TMG as the ligand at T = 30 °C.....	64
Table 3.2. Reaction conditions and results for the activation model experiments in DMSO at 30 °C, using TMG.	67
Table 3.3. Characteristics of the antimicrobial polymers prepared by SARA ATRP. ...	74
Table 3.4. Characteristics of linear PAMPTMA- <i>co</i> -PBA copolymers with different MW values and hydrophobic characters and respective MIC values obtained in liquid medium.	75
Table 3.5. Characteristic of linear and star-shaped PAMPTMA- <i>co</i> -PBA-Br copolymers, PAMPTMA-Br homopolymer and MIC values obtained in liquid medium.....	78
Table 3.6. Characteristics of PAMPTMA- <i>co</i> -PBA and PAMPTMA- <i>b</i> -PBA copolymers and MIC values obtained in liquid medium.	80
Table 3.7. MIC values in mass base of the star-shaped homopolymers prepared by SARA ATRP via arm-first and core-first approach.....	85
Table 3.8. Values of fluences and the respective light dose for 30 minutes of radiation	87
Table 3.9. MIC values for toluidine blue (TBO)	88
Table 3.10. MIC values for proflavine.....	90
Table 3.11. MIC values for curcumin.....	92
Table 3.12. Antimicrobial synergetic effect of polymers + toluidine blue O (TBO) mixtures over <i>E. coli</i>	95
Table 3.13. Antimicrobial synergetic effect of polymers and curcumin mixtures towards <i>E. coli</i>	96
Table 3.14. Antimicrobial synergetic effect of polymers and proflavine mixtures towards <i>E. coli</i>	96

Table 3.15. Characteristics of the non-functionalized and PS-functionalized polymers obtained by SARA ATRP.	99
Table A1. Results of the Cu ⁰ -mediated ATRP of MMA using TMG as the ligand and freeze-thaw degassing procedure (replicate experiments). Conditions: [MMA] ₀ /[EBPA] ₀ /[TMG] ₀ /[CuB ₂] ₀ ; 222/1/0.5/0.1, [MMA] ₀ /[DMSO] = 1/0.5 (v/v); t = 6.5 h; T = 30 °C; Cu ⁰ _{wire} : l = 5 cm, d = 1 mm.	A121
Table B1. Characteristics and of the antimicrobial polymers and the respective MIC values in weight-based concentration.	B129
Table B2. Characterization of the polymers prepared by SARA ATRP.	B130
Table C1. Molar ratio and kinetics data of polymers prepared via Cu ⁰ -mediated SARA ATRP.	C133

Motivation, targets and research significance

RDRP methods are essential for the preparation of polymers with high structural complexity, well-controlled microstructure and architecture. ATRP is one of the most used RDRP methods due to the compatibility with a wide range of monomers with different functionalities, the possibility to efficiently conduct the polymerizations in organic or aqueous media, and relatively mild reaction conditions needed. These interesting attributes have attracted the interest of the industry, and, at the same time, they have motivated scientists to develop cost-effective ATRP systems aiming to improve the production of well-controlled polymers at large-scale, which is already a reality. However, there is still a current demand for less expensive ligands, a critical component of the ATRP process. In this regard, this project aimed the development of a new complex catalytic system for ATRP using a commercially available compound as the ligand, able to provide a control over the polymerization similar to the one obtained for other ATRP systems that use more expensive ligands. It was expected to decrease the cost/production ratio of polymers prepared by ATRP for future industrial implementation.

Due to the ability to afford well-controlled and complex polymeric structures, ATRP is an important tool to produce macromolecules with tailored properties. The increasing bacterial resistance development, along with the decreasing rate of the discovery of new antibiotics, exposes the necessity for alternative and efficient antimicrobial treatments. Nowadays, infection diseases caused by resistant microbes is considered one of the most serious public health problems. The proliferation of pathogens on hospital surfaces is the main vector of transmission of infections in the healthcare environment, being responsible for a substantial burden in acute care hospitals, with serious public health and economic consequences. Therefore, there is a clear demand not only for the development of new antimicrobials directed for *in vivo* treatment but also to mitigate or stop the occurrence of the entire infection. However, due to the diverse nature of the pathogenic microorganisms, it is very challenging to develop a universal approach that could prevent microbial infections by viruses, bacteria and fungi. In this context, this PhD project also aimed to develop a new bioactive polymeric system by ATRP, and to study their antimicrobial properties towards diverse bacteria strains. Aiming to obtain a bioactive system with enhanced properties, a combination of antimicrobial polymers and light-mediated antimicrobial inactivation was also explored. In addition, as a proof-of-concept, this

project intended to evaluate the potential of the novel antimicrobial materials to be used as additives for varnish coating formulations, which could be used to prepare self-decontaminating surfaces.

Chapter 1 – Introduction

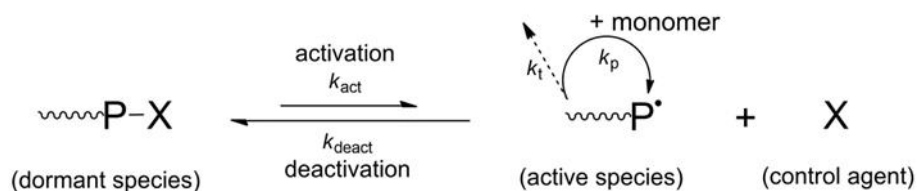
1.1. Reversible deactivation radical polymerization

Synthetic polymers display significant importance in modern Human life since they are used from basic household wares to high-performance materials. To supply the substantial demand of such materials, free radical polymerization (FRP) has been one of the preferred methods to produce polymers (about 50 % of the world production).^{1, 2} However, this method presents a critical limitation for the preparation of advanced polymeric materials because it does not provide control over the polymer's molecular weight (MW) as well it does not allow the preparation of complex structures (e.g. block copolymers).^{3, 4}

For decades, the access to the control over the polymer's structure was considered unattained but the advent of living anionic polymerization allowed, for the first time, to obtain well-defined polymeric structures as well the possibility to prepare block copolymers.^{5, 6} These advances were achieved by developing conditions to extend the growing chain lifetime, affording a continuous growth throughout the polymerization. Indeed, the concept of anionic polymerization opened the way for the fabrication of specific macromolecules composed of block segments. However, disadvantages as the limited choice of monomers, the need for compounds with a high degree of purity, and the extremely stringent reaction conditions (e.g. high vacuum) limited the widespread of this polymerization technique.⁷

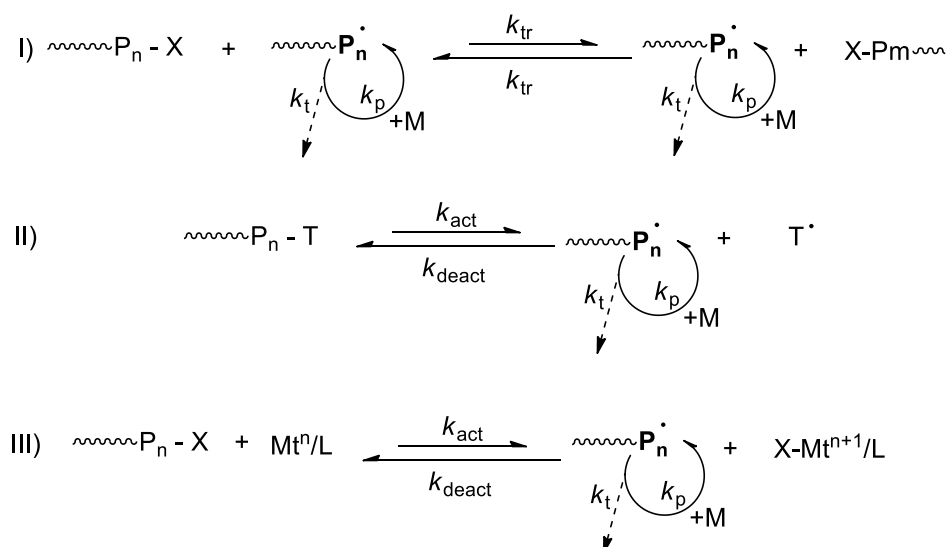
The difficulty to control the polymerization which proceeds via radical processes is due to the inherent high reactivity of the radicals and the very short lifetime before the irreversible termination (ca. 1s). Then, it was realized that to attain control at a level similar to the living ionic systems, it would be necessary to extend the lifetime of the propagating radicals and minimize the terminations reactions. This understanding led to the development of the reversible deactivation radical polymerization (RDRP) methods, in which selected compounds are used in order to reversibly react with the propagating radicals (active), putting them momentarily into a dormant state, with no activity. At any time, the majority of the growing chains are inactive but not irreversibly (dead), only a small quantity of the radicals is in the active state (propagating) and the polymerization proceeds through a dynamic equilibrium between the active and dormant species (Scheme 1.1).⁷ As the rate of deactivation of the active radicals is higher than the rate of activation

of the dormant species, the concentration of radicals is always very low, which makes termination reactions by radical coupling unlikely to occur and ensures the continuous and uniform growth of all chains. Consequently, the MW of the polymers prepared by RDRP is controlled and the dispersity low ($M_w/M_n < 1.5$).⁸



Scheme 1.1. Scheme of the dynamic equilibrium between the active and dormant species.

The establishment of the dynamic equilibrium between active and dormant species, while maintaining the concentration of propagating radical very low along the polymerization is mandatory for all RDRP methods.⁹ Over the years, different approaches on how to regulate this dynamic equilibrium have been developed leading to the creation of several RDRP techniques, which can be grouped in three classes according to the type of the deactivation process: (i) degenerative chain transfer, as it is in reversible addition-fragmentation chain transfer polymerization (RAFT) (Scheme 1.2 I) and iodine transfer polymerization (ITP),¹⁰ (ii) reversible termination as it is in nitroxide-mediated radical polymerization (NMP)¹¹, (Scheme 1.2 II) and (iii) reversible deactivation atom transfer as it is in atom transfer radical polymerization (ATRP), (Scheme 1.2 III). In both to NMP and ATRP systems, the deactivation process is governed by the persistent radical effect (PRE) which is a self-regulating phenomenon that describes the very selective formation of the dormant species ($P_n\text{-X}$) as a result of the interaction between propagating chains (P_n^\bullet , transient radical) and the persistent radicals (X or T^\bullet in Scheme 1.2 II and III). At the beginning of the polymerization, self-termination of some propagating radicals (or species) can take place, leading to an increase of the persistent radical (or species) which do not react between each other but can reversibly react with the propagating radicals (deactivation, k_{deact}).¹² As a consequence, there will be an excess of persistent radicals that shift the dynamic equilibrium towards the dormant species allowing the polymer chains to grow uniformly.¹³



Scheme 1.2 Types of deactivation mechanisms in RDRP (I) degenerative chain transfer, (II) reversible deactivation and (III) reversible deactivation atom transfer.

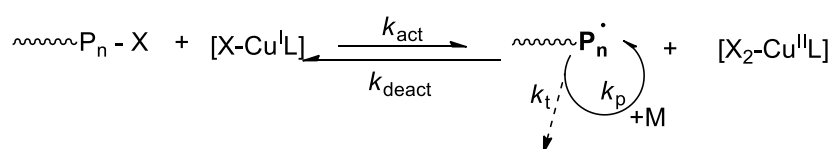
Comparatively, FRP and RDRP follow the same propagation mechanism and possess similar chemoselectivities, regioselectivities and stereoselectivities. However, contrarily to FRP, the initiation in RDRP is very fast and all the chains start to grow nearly at the same time. In RDRP systems, the lifetime of propagating radicals is extended to hours through the dynamic equilibrium between the dormant and active species, whereas in FRP the lifetime is $\sim 1\text{s}$.¹⁴ In FRP, nearly all chains are irreversibly dead whereas, in RDRP, termination reactions can also take place but in much lower proportions as the concentration of the propagating chains are very low. Additionally, since the rate of termination and the rate of chain transfer to monomer per chain is much lower, they do not affect the final properties of the polymer.¹⁵ Hence, in RDRP, it is expected a linear evolution of the molecular weight with respect to monomer conversion. Also, polymers prepared by RDRP methods present active chain-ends (“living” character), which can be further reinitiated (extended) or functionalized to afford specific structures, such as block copolymers.^{16, 17}

This methodology has provided unprecedented access to the preparation of polymers with well-defined structures. Also, the interest on RDRP comes with the fact that this technique, as in FRP, does not require rigorous reaction conditions, but can provide control over the polymer composition, as anionic polymerization does. Moreover, the high tolerance to several functional groups, the possibility to conduct the reactions in diverse conditions (solution, bulk, suspension and emulsion) were decisive to turn RDRP

one of the most promising polymerization technologies, from the academic and industrial standpoints. Therefore, materials prepared through RDRP can be used in diverse commercial applications such as lubricants, dispersants, coatings, adhesives, membranes, surfactants, electronic devices, drug delivery, gene delivery and antimicrobials agents, among others.¹²

1.2. Atom transfer radical polymerization

Atom transfer radical polymerization was introduced in 1995 by Matyjaszewski and Sawamoto research groups and it has become one of the most applied RDRP technique for the preparation of tailor-made polymers due to its versatility, compatibility with a wide range of monomers, solvents and mild operation conditions.¹⁸ The mechanism involves a reversible equilibrium between dormant species (P_n-X) and propagating radicals (P_n^\bullet) mediated by a transition metal/ligand catalytic complex. Due to the appropriate activity, efficiency and low price, copper-amine complexes are the most used catalyst in ATRP systems rather than other transition metal-based complexes. The activation proceeds via abstraction of the halogen atom ($X = Br$ or Cl) from an alkyl halide initiator or the dormant polymer chain (P_n-X , in the case of a polymer chain extension), by the activator $[X-Cu^I L]$ ($L =$ nitrogen-based complexing ligand), forming the propagating radicals (P_n^\bullet) and the catalytic complex in the higher oxidation state $[X_2-Cu^{II} L]$. Then, the active species (P_n^\bullet) propagating by adding only a few monomers units before being deactivated back to the dormant chain by the catalyst in its high oxidation state form $[X_2-Cu^{II} L]$ (Scheme 1.3).¹⁹



Scheme 1.3 Generic mechanism of copper-catalyzed ATRP.

Usually, the amount of deactivator is predominant in comparison to the activator which shifts the equilibrium towards dormant species (PRE), as previously mentioned. After the polymerization, the polymer presents a “living” character due to the presence of a halogen

atom (active chain), ideally, at the end of all-polymer chains. Due to this feature, polymers can be further used as macroinitiators to produce block copolymers or other complex architectures.⁹

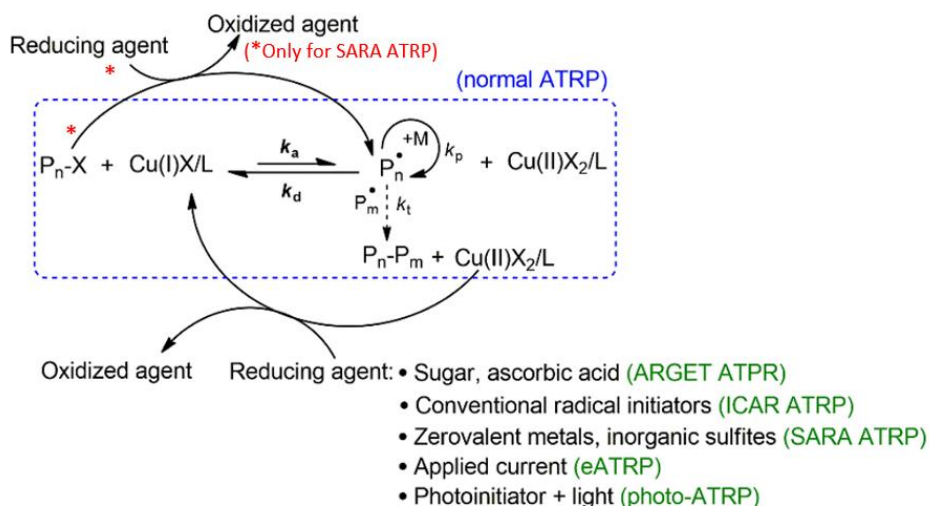
The rate of polymerization in ATRP (R_p) is a function of the rate constant of propagation, the monomer concentration and concentration of growing chains (Eq. 1.1), which depends on the ATRP equilibrium constant ($K_{\text{ATRP}} = k_{\text{act}}/k_{\text{deact}}$). Thus, the rate of polymerization as well the polymer dispersity are strongly influenced by the activity of the catalytic complex, which depends on the type of the complexing ligand,²⁰ the transition metal used, reaction temperature and nature of the solvent (Eq. 1.1 and 1.2). Also, R_p is influenced by the monomer structure and reaction conditions (temperature, pressure and solvent), as they contribute to the overall value of K_{ATRP} .^{21, 22}

$$R_p = k_p[M][P_n^*] = k_p K_{\text{ATRP}}[M][P_nX] \left(\frac{[X - \text{Cu}^{\text{I}}\text{L}]}{[X_2 - \text{Cu}^{\text{II}}\text{L}]} \right) \quad \text{Eq. 1.1}$$

$$D = \frac{M_w}{M_n} = 1 + \left(\frac{[P_nX]_0 k_p}{k_d [X_2 - \text{Cu}^{\text{II}}\text{L}]} \right) \left(\frac{2}{\text{conv.}} - 1 \right) \quad \text{Eq. 1.2}$$

One important drawback of the original ATRP was the high quantity of metal catalyst necessary for the polymerizations (>10000 ppm) which imply²³ for example, extensive purification procedures. Yet, the final product may still contain relatively high quantities of metals which compromise the use in electronics, biomedical among other applications. Modifications on the original ATRP technique led to the development of diverse ATRP variations requiring low catalyst loadings (<1000 ppm), making ATRP more eco-friendly and cost-effective.²⁴ These techniques are based on the central idea of *in situ* and continuous regeneration of the activator species $[X - \text{Cu}^{\text{I}}\text{L}]$ through the reaction between several reducing agents and the deactivator species $[X_2 - \text{Cu}^{\text{II}}\text{L}]$ (Scheme 1.4). Through this concept, it was possible to reduce the catalyst amount from ≥ 10000 ppm to less than 50 ppm, still affording good control over the polymerization.¹⁹ For example, activators regenerated by electron transfer (ARGET) ATRP,²⁵ is a method where Cu^{I} species can be regenerated from Cu^{II} by diverse reducing agents such as triphenylphosphine, ascorbic

acid or phenol hydrazine.²⁶⁻²⁹ In initiator for continuous activator regeneration (ICAR) ATRP, a source of free radicals (*e.g.*, thermal initiators) is used as reducing agent.³⁰ In electrochemically mediated ATRP (*e*ATRP), the ratio between Cu^I and Cu^{II} is regulated according to the given applied potential or current which allow the modulation the overall rate of polymerization.³¹ Studies have also reported well-controlled polymers obtained via ATRP mediated by light in presence or absence of metal catalyst.³²⁻³⁴



Scheme 1.4 General mechanisms of the ATRP-related techniques.

Supplemental activator and reducing agent (SARA) ATRP is widely applied for the preparation of a variety of polymers with precise structure. In this technique, certain components (SARA agents) are used to react with the deactivator [$X_2-Cu^{II}L$] to generate the activator species [$X_2-Cu^{II}L$]. However, the SARA agents present a particularity of acting as supplemental activator by reacting with dormant chains (P_n-X). Nevertheless, the supplemental activator behavior has a minimal contribution to the activation process, in which Cu^I species still act as the primary activator, similarly to the other ATRP techniques. Diverse metals in their zero oxidation state such as iron, zinc and magnesium and especially copper have been used as SARA agents.³⁵ Nevertheless, studies have also reported the preparation of diverse well-controlled polymers in the presence of inorganic sulfites as SARA agents at mild reaction conditions.^{36, 37}

As previously mentioned, the rate of polymerization and polymer dispersity is influenced by the reagents used, namely the transition metal, complexing ligand, initiator and

solvent. Therefore, the judicious selection of each reaction component is critical to attain polymers with low dispersity and high chain-end functionality. Several studies have been dedicated to elucidate the individual and global contribution of each ATRP component to both R_p and D . Figure 1.1 illustrates the chemical structure of the components often used in ATRP procedures.

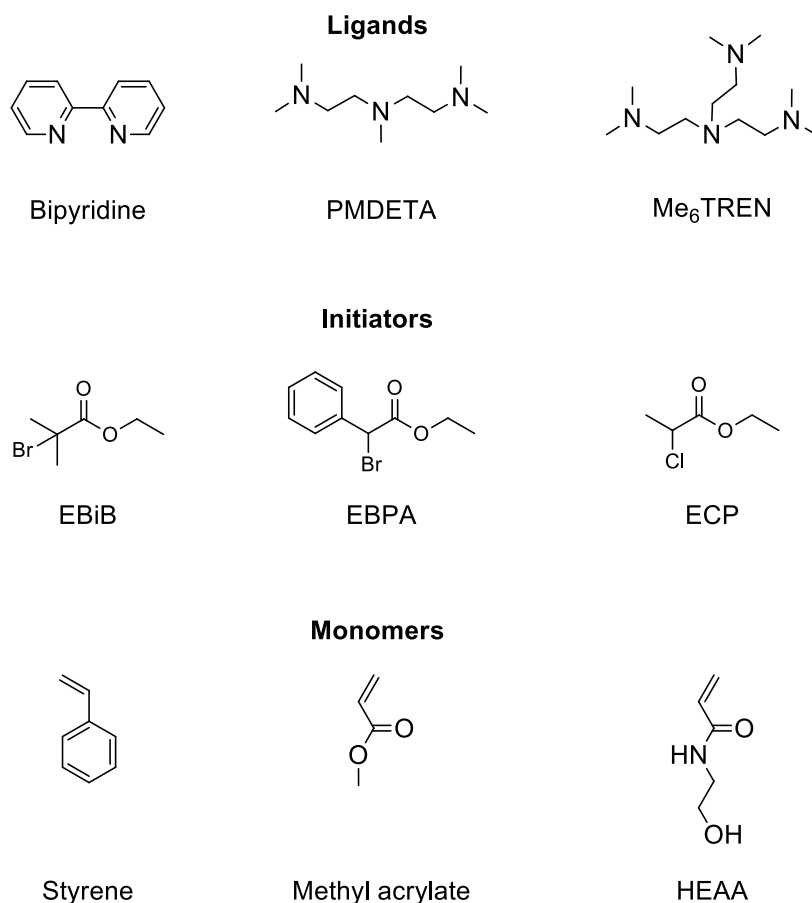


Figure 1.1 Chemical structures of representative ligands, initiators and monomers commonly used in ATRP.

1.2.1. Development of new ligands for ATRP

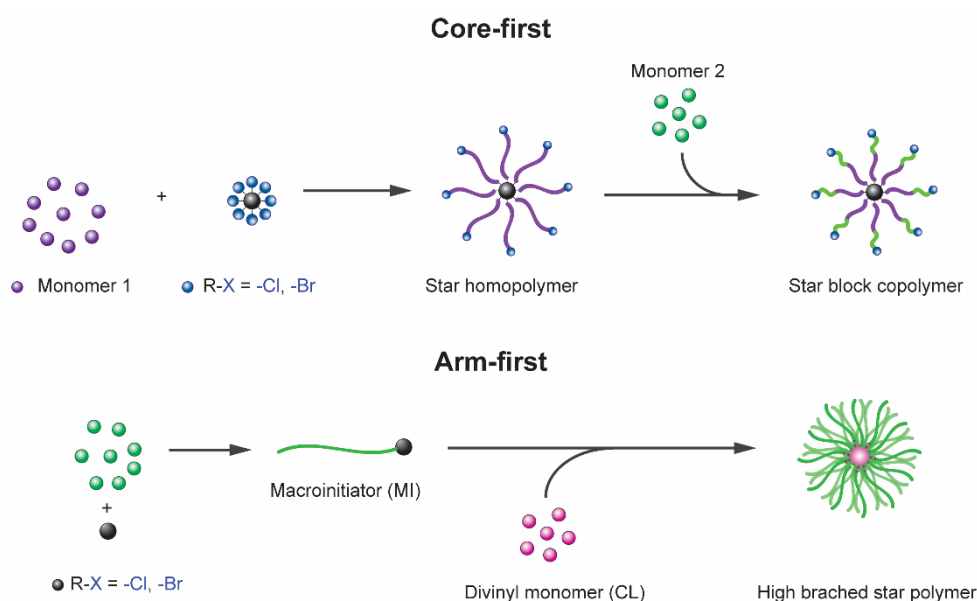
Along with the decrease of the concentration of metal catalyst, the use of eco-friendly solvents, such as water, water/alcohol mixtures and deep eutectic solvents have contributed for the development of more industrially-feasible ATRP procedures.³⁸⁻⁴⁰ Unfortunately, these systems still require the use of complexing ligands that can be extremely expensive and consequently present prohibitive costs for large scale production.

Ligands are essential for ATRP as their main function is to solubilize the transition metal in reaction media and to regulate the redox potential for appropriate atom transfer.²³ The need for active catalytic complexes using affordable ligands constitutes an important key-step for the sustainability of ATRP systems. To date, very few reports with inexpensive ligands can be found in the literature. Magenau *et. al.*,²⁵ reported the use of the *N,N,N',N'',N'''*-pentamethyldiethylenetriamine (PMDETA) and 4,4'-dinonyl-2,2'-dipyridyl (dNbpy) as ligands for the SARA ATRP of methacrylic monomers. Well-controlled polymers ($M_w/M_n < 1.2$) were obtained using both ligands. Moreover, poly(methyl methacrylate) (PMMA-Br) macroinitiator was extended with methyl acrylate (MA) showing that such systems are effective for the preparation of block copolymers. Commercial diethylenetriamine (DETA) and tris(2-aminoethyl)amine (TREN) ligands were also employed for the ARGET ATRP and *e*ATRP of MA and their performance was compared with that of other ligands typically used for ATRP, such as Me₆TREN and PMDETA.⁴¹ By decreasing the amount of deactivator species CuBr₂/L, the authors found that the activity of the ligands decreased in this order: Me₆TREN > TREN > PMDETA > DETA. The polymers showed excellent chain-end functionality since a PMA-Br macroinitiator was successfully extended.²⁵ Several studies have also reported the use of guanidine-based compounds as *N*-donor ligands for copper-mediated ATRP. (*N*¹,*N*²-bis(1,3-dimethylimidazolin-2-ylidene)ethane-1,2-diamine) (DMEG_{2e}) and a TMG derivative (bis(*N,N,N',N'*-tetramethylguanidino)ethane) (TMG_{2e}) were synthesized and tested as ligands, coordinated with CuCl, for the ATRP of styrene. However, the polymerizations were poorly controlled giving polymers with $M_w/M_n \approx 1.5$. In the mentioned studies, the compounds were mostly formed by the modification of the guanidine with other guanidine or amine-containing compounds, which requires previous synthetic steps.^{42, 43}

1.2.2. Tailoring polymeric structures by ATRP

Substantial advances in macromolecular engineering have been achieved employing RDRP methods which allow to accurately design polymers to present desired properties for targeted applications. Particularly, ATRP has enabled the preparation of specific polymers presenting controlled topologies (stars, combs, brush), compositions (block, graft, gradient, periodic) and functionalities (side chains, telechelic, multifunctional)

directed to areas as diverse as environment, adhesives, microbiology and several others.³ Regarding the topology, star-shaped polymers are a type of branched macromolecules with a structure consisting on linear arms radiating from a central core.⁴⁴ This polymeric architecture has gained increased attention due to their unique characteristics as this structure combines the features of the linear arms, compact structure and three-dimensional shape into one entity. Regardless of the RDRP method used, well-established approaches namely core-first and arm-first can be used to prepare star-shaped-polymers (Scheme 1.5).⁴⁵



Scheme 1.5. Approaches for star-shaped polymer synthesis.

The preparation of star polymers via core-first consists of the polymerization of monomers using multifunctional initiators (core), from which the arms can grow (Scheme 1.5). To obtain well-defined structures, the initiating functional sites must have identical reactivity to enable high initiating efficiency. Additionally, the polymerization method must ensure a rate of initiation greater than the rate of propagation and exhibit negligible terminations reactions to afford stars with equal arm's length. Since ATRP fulfil these mechanistic requirements, this technique is suitable to prepare stars via core-first with high level of control over the polymer microstructure using a combination of monomers with different natures and multifunctional initiators. Last, the final product retains the living character at the periphery of each arm which can be used for chain extension with a second monomer to form star block copolymers (Scheme 5.1).⁴⁴ Star polymers prepared via core-first generally present low number of arms, typically ranging from three to eight

arms and a small core domain with negligible effect over the properties of the macromolecule. This is because multifunctional small size molecules are generally used as the core, which will define the number of arms according to the number of initiating sites presenting in the molecular structure.⁴⁶

Different from core-first, in the arm-first procedure, linear arms (macroinitiator, MI) are prepared in a first stage via typical ATRP procedure and then, they react with a cross-linker (CL) to form the core by convergent cross-linking reactions.⁴⁷ This technique produces stars polymers with a highly condensed cross-linked core and a statistical distribution of the numbers of arms. Although this procedure produces highly branched stars in a facile manner, there are also other important factors to consider. According to Flory-Stockmayer's theory,⁴⁸ when the molar concentration of the cross-linker is higher than the primary polymer chain, the critical gel point is achieved giving an interconnected polymer matrix (gelation).⁴⁹ To prevent such macroscopic gelation and also star-star intermolecular coupling, it is mandatory to promote the intramolecular cyclization reactions of the cross-linker rather than intermolecular cross-linking reactions.⁵⁰ This goal can be achieved by using appropriate [MI/[CL] molar ratio and by conducting the polymerization in a diluted system. By this means, individual hyper-branched star polymers are generated in a homogenous media.⁵¹ Unlike the core-first approach, the arm-first gives star polymers with high molecular weight and large number of arms (>100). Therefore, the number of incorporated arms is influenced by diverse factors, such as the DP of the MI, the [MI/[CL] molar ratio, nature of cross-linker and the timing of cross-linker addition, in the case of the one-pot approach.⁵² Also, star prepared via arm-first exhibit a core consisting of a very high cross-linked network, normally representing 30 wt% relative to the overall molecular weight of the polymer. Reports often mention star-shaped prepared via arm-first as core cross-linked stars (CCS) polymers, since this term highlights the unique core characteristics and distinguishes them from other star-shaped macromolecules.⁴⁴

Impressive scientific advances have been achieved during the last years concerning the development of innovative polymeric materials and have brought unprecedented benefits to diverse fields including human health-related areas. For example, the insurgence of resistant bacteria along with the decreasing of the conventional treatment efficiency is found as one of the most serious issues in modern medicine considering the exponentially

growing number of cases of death caused by bacterial infections worldwide. On this matter, antimicrobial polymers tend to have a decisive role in this global effort to find effective solutions for this problem due to their intrinsic features. At the same time, the RDRP methods will be extremely important to design tailor-made functionalized polymers with outstanding outcomes concern the fight against microbial infections.

1.3. Most relevant microbial threats to health and standard units on antimicrobial and hemolytic activity evaluation

Microbial infections are a great concern because they are one of the main primary causes of death worldwide. A concern is given to healthcare facilities due to the high rate of occurrence of bacterial infection. These places represent a serious threat since most of the patients are in a vulnerable health condition, and therefore, more sensitives to the infection-associated disorders.⁵³ Hospital-acquired infection or nosocomial infection (NI) is a systemic or localized infection resulting from an adverse reaction to bacterial infectious agents or toxins that develops after the admission. As reported, the most common type of NI is primary bloodstream infections (normally associated with the use of intravascular devices), urinary tract infection (normally associated with the use of catheters), surgical site infections and pneumonia (normally associated with the ventilation system).⁵⁴ More worrisome, the increasing number of antimicrobial-resistant pathogens display a relevant burden on healthcare systems which include increased treatment costs and high morbidity and mortality rates.⁵⁴

Since the discovered in the middle of the 19th century, low molecular weight antibiotics have been used as the primary source of the treatment of infectious diseases and successfully reduced the mortality caused by infectious disorders. However, as soon as these agents were used, it was identified that some bacterial strains could respond to the treatment by exhibiting mechanism of resistance. It is important to point out that some species of bacteria are naturally resistant to one or more classes of antibiotics. On the other hand, as a consequence of chromosomal mutations, some initially susceptible species can acquire resistance to the antimicrobial agent and transmit these genes to other microorganisms, spreading the resistance traits to the entire bacterial colony.^{55,56} The Infectious Diseases Society of America grouped a fraction of antibiotic-resistant bacteria,

namely *Enterococci* species, *Staphylococcus aureus* (*S. aureus*), *Klebsiella pneumoniae* (*K. pneumoniae*), *Acinetobacter baumannii* (*A. baumannii*), *Pseudomonas aeruginosa* (*P. aeruginosa*) and *Enterobacter* species, as the ESKAPE pathogens, due to their ability of “escaping” the biocidal action of antibiotics and mutually represent new paradigms in pathogenesis, transmission and treatment.⁵⁷ Recently, the World Health Organization (WHO) classified several bacteria in three categories namely critical, high and medium priority to the urgency of need of new antibiotics. According to WHO, the ESKAPE pathogens were classified as critical or high priority.⁵⁸ The list of critical priority of pathogens involves carbapenem-resistant *A. baumannii* and *P. aeruginosa* along with extended-spectrum β -lactamase (ESBL) or carbapenem-resistant *K. pneumoniae* *E. coli*, *Enterobacter* spp., whereas vancomycin-resistant *E. faecium* (VREF), methicillin-resistant *S. aureus* (MRSA) and vancomycin-resistant *S. aureus* (VRSA) are listed in the high priority subgroup.^{59, 60} These mentioned microbes are often associated to a substantial percentage of NI and represent the vast majority of isolates whose resistance to antimicrobial agents presents serious therapeutic dilemmas for physicians.^{61, 62} In this regard, there is an urgent need to create and employ unconventional strategies for the development of antimicrobial products to tackle the rising of global threats imposed by the spread of antimicrobial resistance, which can be exhibited not only by bacteria but also by virus, parasites and fungi.^{63,64}

Methodologies for evaluating the antimicrobial activity are necessary to test the microbial susceptibility upon a drug discovery, epidemiology or prediction of therapeutic outcome regime. Testing antimicrobial properties means testing the microorganisms’ ability to survive in the presence of a given antimicrobial agent at a determined concentration and/or time of exposition.^{65,66} There are a variety of antimicrobial susceptibility testing guidelines recognized by the clinical laboratory standard institute (CLSI) which are routinely adopted for the evaluation of potential therapeutics including antimicrobial polymers, which are mostly carried out using disk-diffusion and broth or agar dilution methods.⁶⁵ The agar diffusion test or the Kirby-Bauer disk diffusion method are often used for testing microorganisms’ growth. The procedure consists in impregnating filter paper disks with the antimicrobial agent and place them on the surface of a solid growth medium. The antimicrobial potency, therefore, is measured according to the size of the inhibition zone produced around the disks after the period of incubation. Assessing the antimicrobial activity by agar plates provides semi-quantitative information

about the antimicrobial efficiency and the diffusivity of the antimicrobial agent through the growth medium.⁶⁷ The broth dilution assay is used to measure the *in vitro* activity of an antimicrobial agent against a bacterial isolate in the planktonic form (free-floating) or fungi. In this procedure, a stock solution of the testing antimicrobial is prepared and dispensed, usually in doubling dilutions (*e.g.*, 1, 2, 4, 8... $\mu\text{g. mL}^{-1}$), to the test tubes containing standardized bacterial suspensions. After an overnight of incubation under standardized conditions, the minimum inhibition concentration (MIC) is determined. The MIC is the lowest concentration of an antimicrobial agent necessary to completely inhibit the bacterial growth.⁶⁸ OD of the bacterial culture media is often used to determine MIC values, which is normally carried out by UV-vis spectroscopy analysis. However, as the OD is strongly influenced by the amount of the cells present in the culture medium (turbidity), the accuracy of the results can be compromised because the technique does not differentiate living cells from the dead cells with the undamaged membrane.

The MIC gives insights about the antimicrobial activity of a certain agent, but it does not provide information if the antimicrobial agent is bacteriostatic or bactericidal. A biologically active agent is bacteriostatic when it stops bacteria from reproducing, but it does not necessarily kill them. In contrast, bactericidal agents can truly kill bacteria and normally present higher antimicrobial activity than the bacteriostatic ones. On this matter, the bactericidal character of a certain antimicrobial agent can be identified by determining the minimum bacterial concentration (MBC), described as the lowest concentration needed to reduce the viability of the cell inoculum by $\geq 99,9\%$. The protocol to determine MBC is similar to the MIC and the concept can be also applied to assays using fungi, in this case, to determine the minimum fungicidal concentration (MFC).⁶⁹

Additional tests can be used to study inhibitory behavior in depth. Time-kill assay is a significant tool to assess the pharmacokinetic behavior of a given antimicrobial agent as the test reveals the time-dependence, the concentration-dependence and it also provides information about the microbial inhibitory nature (bactericidal or bacteriostatic).⁷⁰ Also, live/dead and flow cytometric assays are also recommended to study mechanistic aspects of the antimicrobial behavior as they provide insights of the cell integrity.⁷¹ Scanning electron microscopy (SEM) is also a useful technique widely employed in microbiology to measure cell attachment and evaluate changes in the bacteria's morphology upon damages inflicted to the cell membrane.⁷²

As important as measuring the antimicrobial performance of new potential antimicrobial agents, is assessing their biocompatibility. Preliminary information of the biocompatibility can be obtained by hemolytic activity assays against red blood cells (RBCs) and the 50% hemolytic concentration (HC_{50}), determined *in vitro*. HC_{50} is defined as the lowest concentration of a giving agent that causes lysis in 50% of the RBCs within a standardized incubation period. The half-maximal inhibitory concentration (IC_{50}) is defined as the lowest concentration that inhibits the biological function or biological component (*e.g.*, enzyme, bacteria, cell) by 50%. Therapeutic index (TI) is defined as the safety window of a given therapeutic agent and can be calculated, for example, as the ratio between HC_{50}/MIC or IC_{50}/MIC .⁷³

1.4. From natural antimicrobial peptides to synthetic antimicrobial polymers

Natural antimicrobial peptide (AMP) represent an important class of antimicrobial macromolecules occurring in diverse immune systems of multicellular organisms, acting as the first line of defense against invading pathogens. With the rise of bacterial resistance along with the declining discovery rate of novel antibiotics, AMPs have found considerable significance as models for new therapeutics mainly because of their broad-spectrum activity and low bacterial resistance development. These advantages have directed researchers toward the development of synthetic AMPs able to reproduce their biophysical characteristics inside the bacterial environment.⁷⁴ On this matter, synthetic mimics of AMPs (SMAMPs) have gained increased attention since they have shown higher antimicrobial efficiency than those of the natural counterparts.⁷⁵ However, despite of attractive attributes, laborious and high manufacturing costs, lack of long-term stability and relatively low biocompatibility have limited the application of the SMAMPs on the clinical scenario.^{76, 77} On the other hand, advances on the modulation of the chemical structure and functional properties, affordable synthetic procedures, increased stability and biological selectivity give to antimicrobial polymers favorable advantages over SMAMP. In addition, antimicrobial polymers also present advantages over conventional antibiotics such as reduced residual cytotoxicity, non-volatilization, low skin permeation and pronounced bioactivity, which address significant potential to antimicrobial polymers to be the next generation of therapeutics for topical and systemic applications.⁷⁸ At the same time, there is a particular need to develop strategies also to prevent bacterial

adherence onto a surface (biofilm formation) considering that contaminated surfaces with pathogens represent an important vector of transmission of nosocomial infections.⁵⁴ In this regard, antimicrobial polymers found a significant advantage over several types of antimicrobials due to their versatility and the possibility to precisely modulate their physical and chemical properties.

According to the type of polymeric system, antimicrobial polymers can be classified into three categories⁷⁹ (Figure 1.2): (i) biocidal polymers, which are polymers with intrinsic antimicrobial activity; (ii) polymeric biocides, which are based on polymer backbones with biocide molecules attached and (iii) biocide-releasing polymers, which consist in polymers loaded with biocide molecules.

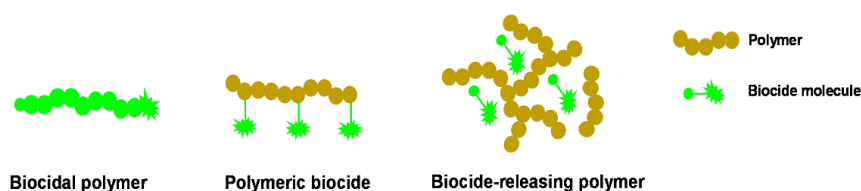


Figure 1.2. Schematic representation of the different types of antimicrobial polymeric systems.⁷⁹

Polymers with intrinsic antimicrobial activity are usually based on polycations, which can kill microbes due to their interaction with negatively charged cell's membrane.⁸⁰ Common cationic groups found in these polymers are quaternary ammonium salts (QAS), quaternary phosphonium salts (QPS), guanidinium or tertiary sulfonium.⁸⁰⁻⁸² The use of biocidal polymers is very advantageous considering the design of antimicrobial surfaces since no harmful biocides will be released to the environment. Concerning polymeric biocides, these are prepared by the attachment of several known biocide molecules to a polymer. Usually, these materials present lower efficacy than the free biocide molecules, due to the steric hindrance created by the polymer backbone.⁷⁹ Finally, biocide-releasing polymers are based on polymeric matrices loaded with biocide molecules, which can be entrapped using different methods, or polymers containing biocides attached by cleavable linkages.^{83, 84} This antimicrobial approach presents an excellent efficacy due to the high concentration of biocide achieved during the releasing and closeness to the target cells. However, the toxicity associated with the biocide molecules is a serious disadvantage associated with this strategy, and their efficiency reduces significantly with the time.

1.5. Mechanisms of microbial cell death induced by antimicrobial macromolecules and molecular basis of selectivity

The bacterial cell envelope, cell wall and plasma membrane are responsible for the diverse fundamental functions such as providing protection against the surrounding environment, promoting cell integrity, regulation of the cell reproduction, osmoregulation and metabolic processes. Therefore, it is well accepted that one efficient strategy to kill such microorganisms is by directly attacking and disrupting the plasma membrane, promoting irreversible disturbs to their vital functioning. The unique antimicrobial activity of AMPs comes with the fact that AMPs are structurally composed of cationic and hydrophobic amino acid residues, which permit a strong interaction with both the anionic and hydrophobic components present in the bacterial cell envelope. At the plasma membrane, the microbicidal activity is driven by irreversible physical changes as reorganization, pore formation or membrane disruption.⁸⁵ Also, antimicrobial polymers display similar antimicrobial activity mechanism of that AMPs,⁸⁶ following distinct sequential process: (i) it starts by the adsorption on the microbial cell surface; (ii) the polymer diffuses through the cell wall towards the cell cytoplasmic membrane; (iii) it interacts with the cell membrane inflicting irreversible damages to membrane integrity; (iv) subsequent release of the cytoplasmic contents as K^+ ions, DNA/RNA; (v) Cell death.⁸⁷

Recent studies have been focused to understand polymer-membrane interactions in-depth.⁸⁸ Koruda *et al.*, studied the mechanistic aspects of the interactions between model bacterial membranes and random polymethacrylates.^{89, 90} Supported by molecular dynamics simulations (MDS), it was observed that the polymers assemble into micellar aggregates in aqueous media presenting extended cationic side chains out and the hydrophobic groups oriented towards the centre. The polymers reached the membrane surface through interactions between the cationic groups on the polymer and the negatively charged lipid head of the membrane. Afterwards, the polymers assumed an extended structure increasing the contact surface, which enhances interactions polymer-membrane. Later, the polymers partitioned onto the membrane surface and acquired a facially amphiphilic confirmation with the hydrophobic and cationic groups completely separated, as showed by the MDS results. As indicated by the authors and in concordance

with several other studies,^{91,92} the fact of polymers assembling into a facially amphiphilic conformation affect the membrane thickness, inducing cellular leakage and bacterial death.⁵⁰ In essence, amphiphilic antimicrobial polymers are considered a non-natural peptide mimics, since both present an amphiphilic nature (hydrophilic and hydrophobic domains) and because they display similar mode of action.⁹⁰

As previously mentioned, the mechanism of the biocidal activity of AMPs is mostly governed by pore-forming effects. However, it is also reported that AMPs can directly enter into the cytoplasm membrane and cause cell death without causing significant membrane disturbs.⁹³ Studies have shown that translocated AMPs can inactivate nucleic acids, cytoplasmic proteins, alters cytoplasmic membrane septum formation,⁹⁴ inhibit cell-wall synthesis and enzymatic activity.⁹⁵ On this matter, polymers can also present similar behavior. For instance, it was demonstrated that a polymer belonging to the nylon-3 family can permeate the bacterial membrane, bind to intracellular DNA and induce cell death without causing membrane lyse.⁹⁶ A study was conducted to elucidate the mechanism of its antimicrobial action using polyhexanide which is typically used as a biocide against a variety of microorganism. The results obtained by confocal imaging revealed that the polymer does not cause membrane lysis. Indeed, it accumulates inside the cytoplasmic region of the bacteria. Additionally, the authors suggested that the polyhexanide induced cell death by interfering on the cell division and condensing bacterial chromosomes.⁹⁷

Polymers have demonstrated that are capable of inactivating bacteria by causing destabilization on the outer region of the cell wall. Poly(acrylic acid)/poly(vinyl alcohol) electrospun nanofibers showed strong antimicrobial activity against *S. aureus* and *E. coli* as their growth was drastically impaired upon in contact with nanofibers. In this case, the antimicrobial mechanism was addressed to the abstraction of divalent Ca^{2+} from bacterial cell wall which directly affected the metabolic activity and the bacterial growth.⁹⁸

An efficient antimicrobial agent must exhibit not only high antimicrobial activity but also high selectivity to bacteria over mammalian cells, like most of AMPs. The essence of the selectivity of AMPs, SMAMPs and antimicrobial polymers towards microorganisms relies on the differences of the lipid composition and surface.⁹⁹ Typically, the mammalian cell membrane displays asymmetry on the charge distribution. For instance, the outer leaflet of the red blood cell membrane is mostly composed of zwitterionic lipids (overall

neutral charge character) while the inner leaflet is composed of phospholipids bearing negatively charged groups.¹⁰⁰ In contrast, the outer leaflet of the cell membrane of bacteria and fungi present diverse phosphate-containing lipids which give an overall negative charge to the outer surface of the bacterial membrane (Figure 1.3 (a)). Also, bacteria and fungi cell envelop possess essential components that provide mechanical strength to withstand the osmotic pressure exerted by the surrounding environment. In Gram-positive organisms, the presence of teichoic acids which are anchored to the glycan cell wall and cell membrane, impart net negative charges to the cell wall due to the presence of phosphate groups in the teichoic acid structure. Gram-negative bacteria present an additional outer membrane which overlaps a thin layer of peptidoglycans and present lipopolysaccharides (LPS) in the outer side (Figure 1.3 (a)). These LPSs are regarded to impart a strong negative charge to the cell surface.^{101, 102} Therefore, improvements on the antimicrobial activity along with the biocompatibility are key-points to establish the topical or systemic clinical use of synthetic antimicrobial macromolecules.

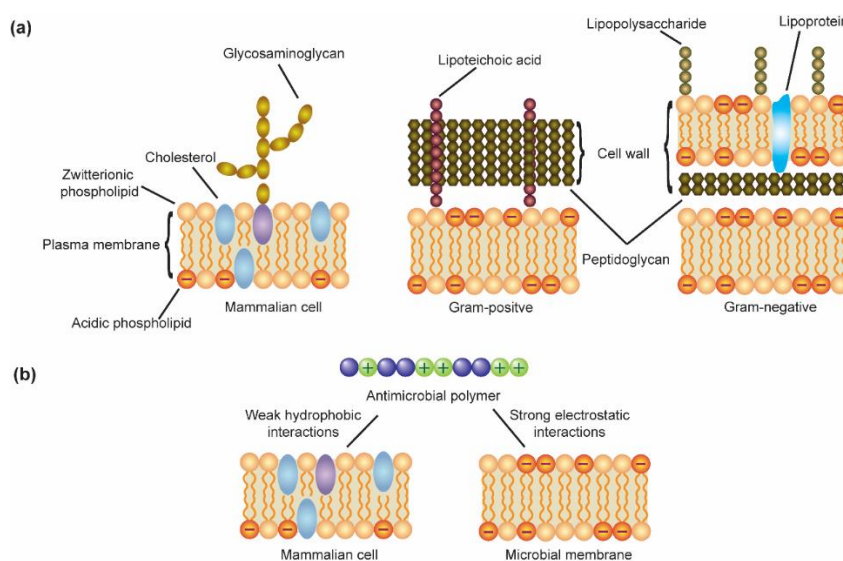


Figure 1.3. Basis of the selectivity of antimicrobial macromolecules. (a) Illustration of the cross-sections of mammalian cells (left) and bacterial cell envelop (right). (b) Selective interactions between cell membranes and amphiphilic antimicrobial polymer.^{99, 103}

1.6. Polymer properties influencing their antimicrobial activity

Concerning the development of new antimicrobial macromolecular systems, there are relevant considerations that must be taken into account when designing a polymer aiming high antimicrobial activity and with good selectivity towards bacteria over mammalian cells.¹⁰⁴ Generally, cationic amphiphilic copolymers are the most used structures since

they mimic the mode of action of the natural AMPs (see section 1.5). Unlike small antimicrobial molecules, the advantage of antimicrobial polymeric systems is that different architectures can be designed from unique chemical composition. For instance, using the same monomers in conjunction with RDRP methods, it is possible to prepare random copolymers, block copolymers or stars-like polymers, and therefore evaluate the impact of the different structures on the antimicrobial activity (Figure 1.4).

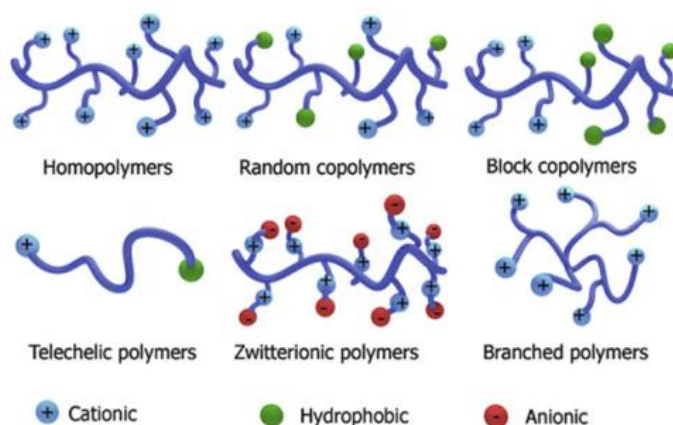


Figure 1.4 Representative polymeric architectures and composition employed as antimicrobial polymers.⁸²

Besides these characteristics, other properties as MW, hydrophilic/hydrophobic balance nature of the cationic group and branching degree strongly influence the antimicrobial activity, and judicious evaluation of these parameters is essentially required to attain relevant antimicrobial/selectivity outcomes. The following sections are dedicated to detail the properties of the polymers that have a higher influence in the antimicrobial activity.

1.6.1. Random copolymers

Random copolymers are probably the most studied amphiphilic systems devoted to antimicrobial applications. Such polymeric composition can be prepared by either FRP or RDRP methods through the combination, for example, of cationic and non-polar monomers. The final structure can be obtained by a one-pot strategy (both monomers are polymerized at the same time) or by a post-polymerization modification of the polymer's structure. The advantage of the one-pot strategy along with RDRP is that the polymers are obtained in a one-step procedure and the amphiphilicity can be finely modulated by controlling the feeding ratios of each monomer. On the other hand, the advantage of the

post-polymerization modification is that different functional groups can be introduced into the structure of the polymers to generate polymer derivatives from a common polymer backbone and chain length. Regardless of the strategy adopted, it is possible to vary the degree of amphiphilicity and thus, assess the influence of this factor over the antimicrobial activity.¹⁰⁵

Hong *et al.*,¹⁰⁶ used the one-pot strategy to prepare a pH-responsive random copolymer consisting of aminobutyl methacrylate (ABMA) and ethyl methacrylate (EMA) by reversible RAFT polymerization. The new PABMA-*co*-PEMA (Figure 1.5) copolymer was evaluated against clinical isolates of MRSA. Results showed that the polymer was effective in killing *S. aureus* only under neutral conditions, while it was inactive under acidic pH (pH = 5.5). In addition, the copolymer did not present any significant activity against red blood cells or human dermal fibroblasts over a range of pH values (pH = 5.5-7.4), indicating the potentiality of the polymer for the treatment of infections at pH-neutral wound sites with no effect over the surrounding acidic healthy skin.¹⁰⁶

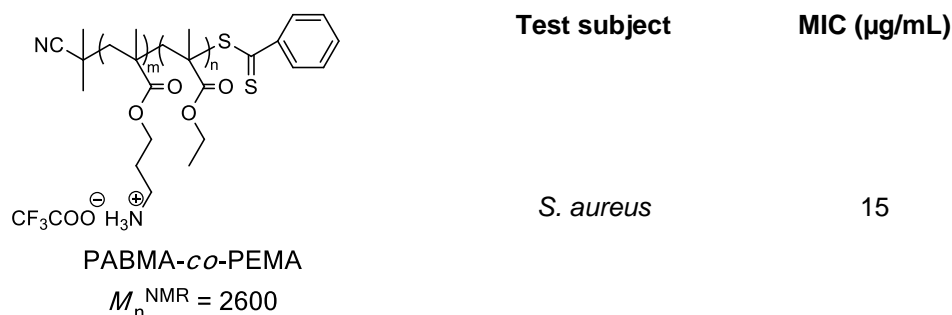


Figure 1.5 Chemical structure of PABMA-*co*-PEMA and MIC values for *S. aureus*.

Locock and co-workers¹⁰⁷ prepared a series of amine-containing polymethacrylates by RAFT varying the MW and mole percentage of the methyl side chains ($\text{MP}_{\text{methyl}} = 0 - 70\%$). In this study, the authors used the post-polymerization modification procedure to convert the amine groups into guanidine groups, enabling the direct comparison of the effectiveness between the library of polymers containing amine or guanidine groups with the same DP and $\text{MP}_{\text{methyl}}$ (Figure 1.6). The antimicrobial activity was measured in solution against significant microorganisms commonly involved in nosocomial infections namely *S. epidermidis*, *S. aureus*, *E. coli* and the fungal often associated with

opportunistic *C. albicans*. The selectivity of the polymers was assessed in terms of % hemolysis. For *S. aureus*, two strains were used, MRSA and methicillin-sensitive *S. aureus* (MSSA), and all the polymers showed identical MIC values for the two bacteria. Concerning the Gram-positives, the polymers showed higher activity towards *S. epidermidis* in comparison to *S. aureus*. On the other hand, for the Gram-negative *E. coli*, none of the polymers showed activity as all MIC value obtained were superior to 500 $\mu\text{g/mL}$. The results also revealed that increasing the $\text{MP}_{\text{methyl}}$ and the DP negatively influenced the activity and selectivity of the polymers as the MIC values and % hemolysis increased. Moreover, the guanidine-functionalized polymers showed higher activity towards the Gram-positive strains and *C. albicans* in comparison to the group containing amine with similar MW.

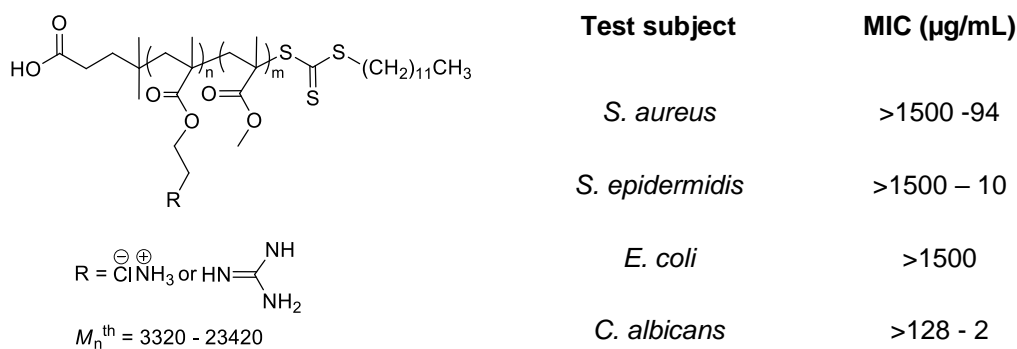


Figure 1.6 Chemical structure and MIC values of the amine/guanidine-functionalized amphiphilic polymethacrylates.

The presence of a cationic segment and some level of hydrophobicity is the minimum requirement to achieve antimicrobial activity with high selectivity indices. The use of binary systems composed of a positively charged monomer and a hydrophobic one is typically chosen to prepare selective and efficient antimicrobial copolymers, as such composition mimics one of AMPS (which also is composed of cationic and hydrophobic domains) and presents a similar mode of action.^{77, 108, 109} Even though, this type of copolymers can be easily prepared by RDRP, the optimization of the polymer composition to achieve high levels of activity and selectivity might be difficult. This is because both the electrostatic binding between polymer and bacteria, and the diffusion of the polymer through the bacterial membrane cannot be controlled separately for a system

in which, both the cationic and hydrophobic domains are coupled. For instance, for the same MW, increasing the hydrophobicity of the copolymer will simultaneously decreasing the content of the cationic groups. This change would improve the diffusion of the polymer and the microbial cell envelop disruption but, at the same time, the electrostatic action could be compromised due to the reduction of the overall content of positively charged groups.⁷⁷ In an approach to independently evaluate the variation of the hydrophilic/hydrophobic contents over the bioactivity of the copolymer, Mortazavian *et al.*, designed a library of ternary methacrylate-based statistical copolymers. The polymer structure was composed by cationic ammonium (amino-ethyl methacrylate: AEMA), hydrophobic alkyl (ethyl methacrylate: EMA), and neutral hydroxyl (hydroxyethyl methacrylate: HEMA) moieties and evaluated their activity against *S. aureus*, *S. mutans* and *E. coli* (Figure 1.7).

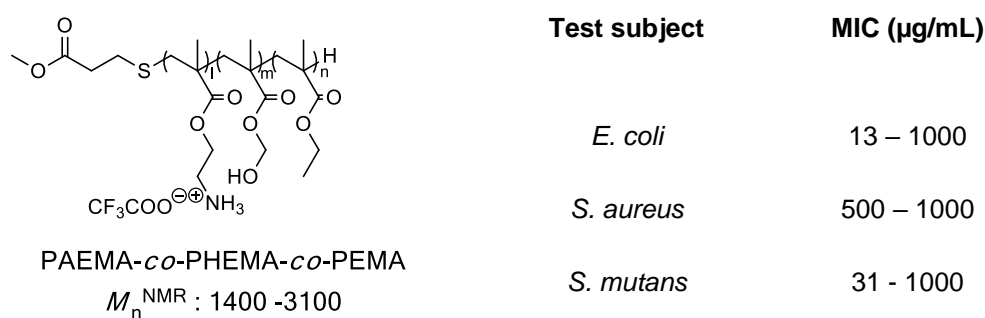
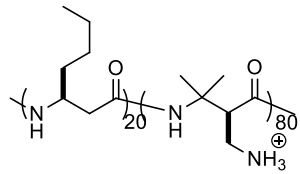


Figure 1.7. Chemical structure and MIC values of PAEMA-*co*-PHEMA-*co*-PEMA.

Data showed that this ternary system was more active than the binary PAEMA-*co*-PEMA analogues. Moreover, the antimicrobial activity towards *E. coli* as a function of the electrostatic interactions achieved a plateau for copolymers having 30 mol % of the cationic monomer and, in this case, the increment on the efficiency observed was determined by hydrophobic interactions. Besides, the presence of the HEMA moiety could have a particular role of acting as a spacer to distribute the hydrophobic and cationic groups along the polymer chain.¹¹⁰

As mentioned, the used of SMAMPs can be compromised due to some innate drawbacks as moderate activity and tendency to undergo proteolysis (long-term chemical stability).¹¹¹ To solve these limitations, SMAMPs based on poly- β -peptides containing a

similar backbone to natural AMPs were designed and synthesized *via* ring-opening polymerization of β -lactams (Figure 1.8).¹¹²



poly- β -peptide (Bu : DM)
 M_n^{SEC} : 3700 - 3900

Test subject	MIC ($\mu\text{g/mL}$)
<i>S. epidermidis</i>	6.25 - 12.5
<i>E. coli</i>	12.5 - 50
<i>P. aeruginosa</i>	3.13 - 12.5
<i>K. pneumoniae</i>	25 - 100
<i>A. Baumannii</i>	12.5 - 50
<i>K. pneumoniae</i>	6.25 - 12.5
<i>A. baumannii</i>	6.25 - 12.5
<i>S. aureus</i>	6.25 – 12.5

Figure 1.8. Chemical structure of poly- β -peptide and MIC values to Gram-positive and Gram-negative bacteria.

The structure of the random poly- β -peptides copolymers was composed of a cationic segment, containing primary amine side chains (named DM), and a hydrophobic segment, containing an alkyl side chain (named Bu), combined in different molar ratios. Interesting, the proposed poly- β -peptides presented excellent antimicrobial activity against a wide range of bacteria including *E. coli*, *P. aeruginosa*, *K. pneumoniae*, *Acinetobacter baumannii*, methicillin-resistant *S. epidermidis* and *S. aureus*. Among the variety of polymers prepared, the composition 20: 80 (Bu: DM), showed the greatest overall activity with lower MIC values ($3.13\text{-}25 \mu\text{g mL}^{-1}$) and high selectivity indices ($\text{HC}_{50} = 200 \mu\text{g mL}^{-1}$, $\text{IC}_{50} = 100 \mu\text{g mL}^{-1}$). Also, the non-susceptibility to proteolysis and the facile synthetic procedure suggest the great potential of these poly- β -peptides to face the enormous challenge of the microbial resistance.¹¹²

1.6.2. Block copolymers

Block copolymers are formed by distinct polymeric segment derived from different monomers, for instance, hydrophilic and hydrophobic ones. Unlike random copolymers, block copolymers are generally prepared by RDRP methods by direct chain extension or coupling of RDRP-derived homopolymer with a complementary functionality (*e.g.*, click

chemistry).¹¹³ There are relatively few studies dealing with antimicrobial block copolymers in the literature, probably because they generally show higher cytotoxicity for mammalian cells than that of random polymers analogues having similar antimicrobial activity. Moreover, as block copolymers show a high tendency to form nano aggregates, most of these architectures are employed for the preparation of micelles, antimicrobial fibres and coatings.¹¹⁴⁻¹¹⁶

Random and block copolymers of 2-(*N,N*-dimethylamino)ethyl methacrylate (DMAEMA) and butyl methacrylate (BMA) were prepared *via* ATRP by Liu *et al.*,¹⁰⁹ (Figure 1.9a). Results showed similar antibacterial activity against *S. aureus* and *E. coli* but the diblock structures exhibited much lower hemolytic activity in comparison to that of random copolymers.

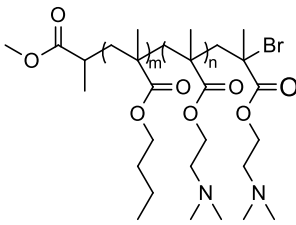
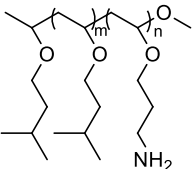
	Test subject	MIC ($\mu\text{g/mL}$)
(a)		<i>S. aureus</i> 34 - 67 <i>E. coli</i> 54 - 97
	PBMA- <i>b</i> -PDMAEMA $M_n^{\text{NMR}} = 4,000 - 5,000$	
(b)		<i>E. coli</i> 1.6 - 2.4
	poly(IBVE- <i>b</i> -PIVE) $M_n^{\text{NMR}} = 7,100 - 25,000$	

Figure 1.9. Chemical structure and MIC values of (a) PBMA-*b*-PDMAEMA and (b) poly(IBVE-*b*-PIVE)

These results demonstrated that by partitioning the functionalities of bioactive copolymers it is possible to have a strong influence on their hemolytic activity; however, with no significant changes in their antimicrobial activity.^{117, 118} Similarly, Kuroda and coworkers.¹¹⁷ have also prepared several amphiphilic block copolymers based on poly(vinyl ether) derivatives *via* base-assisting living cationic polymerization.¹¹⁷ In this

study, the authors observed comparable antimicrobial activity against *E. coli* for both random and block copolymers with similar molecular weight and composition (Figure 1.9 (b)). Surprisingly, random copolymers showed significant hemolytic activity while block copolymers did not present hemolytic activity even at 1000 $\mu\text{g. mL}^{-1}$. The authors proposed that block copolymer might assemble into a nanostructure in which the cationic shell prevented the hydrophobic core of interacting with the red blood cell membrane.

1.6.3. Branched polymers

While linear polymeric chains have a unique spatial orientation, branched polymers such as stars present multi-direction orientation forming a globular structure in solution. These polymers have been explored in several areas, including the use for therapeutic purposes.⁴⁴ In this vein, Shirbin and coworkers synthesized a library of star-shaped antimicrobial peptides named as structurally nanoengineered antimicrobial peptide polymers (SNAPPs, Figure 1.10).¹¹⁹

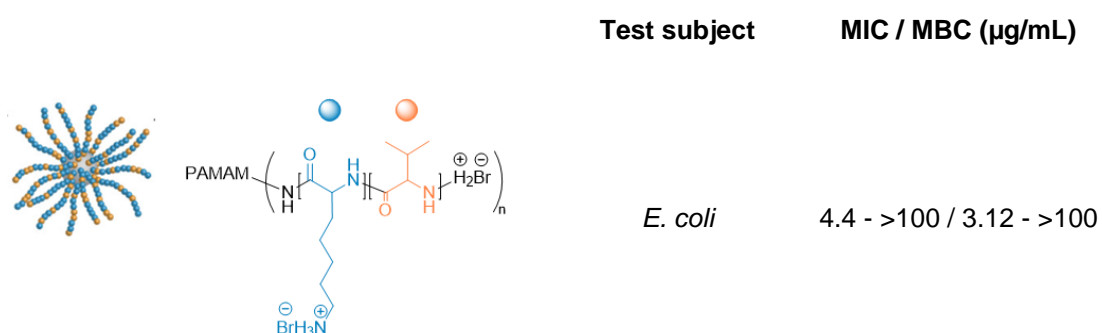


Figure 1.10 Chemical structure of lysine-valine-based SNAPPs

These nanoparticles were prepared using two types of amino acids residues, the cationic lysine and the hydrophobic valine (Figure 1.10). In this study, a systematic investigation was made to understand the SNAPPs structure-activity relationship, by focusing on two key parameters: (i) the number of arms (4, 8 and 16 arms) and (ii) the arm-length (small, medium and long/very long). *In vitro* results showed that although the antimicrobial activity increased against *E. coli* for SNAPPs with more and longer arms, a similar trend was also observed for the cytotoxicity of stars with up to 8 arms. In addition, it was figured

out that the 4-long-arm SNAPP showed similar therapeutic index ($TI = IC_{50}/MIC$) to that of the 16-medium-arm SNAPP (8.0 vs 8.6), being also easier to synthesize.

Zhao *et al.*, reported the evaluation of amphiphilic hyperbranched polyurea-based antimicrobial emulsifiers prepared using a one-step synthetic pathway by simple reacting primary amines with biscaprolactam.¹²⁰ A library of monomers containing different alkyl chains length (C2, C3, C4 and C6) was prepared by reacting triamines with carbonyl biscaprolactam which rendered monomers with various spacer groups. The polymerization proceeded in a facile manner by only submitting the blocked isocyanate monomers at 145 °C under an inert atmosphere in DMF. Afterwards, the isocyanate-blocked polymers (HBP-NH₂B) were functionalized with QAS groups also having varied alkyl chains length to obtain structures (HBP-NH-N⁺(C8-C12)) with varied amphiphilicity degree and MW (Figure 1.11).

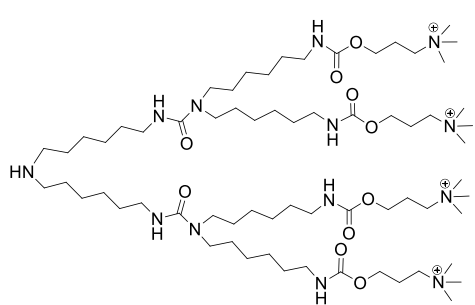
	Test subject	MIC (µg/mL)
	<i>S. epidermidis</i>	>2560 - 5
	<i>S. aureus</i>	>2560 - 5
	<i>A. baumannii</i>	>2560 - 5
	<i>K. pneumoniae</i>	>2560 - 10
	<i>E. coli</i>	>2560 - 20
	<i>C. albicans</i>	>2560 - 5
	<i>C. parapsilosis</i>	>2560 - 5

Figure 1.11. Chemical structure and MIC values of the antimicrobial hyperbranched emulsifiers

The authors evaluated the influence of the length of the alkyl moiety (C₂ to C₁₂) over the antimicrobial activity of the polymers, which was measured in terms of MIC, MBC and MFC for several microorganisms including Gram-positive, Gram-negative bacterial strains and fungi. Results showed a higher biocidal behavior against cells for structures having longer alkyl chains (HBP-NH₂-N⁺(C8-C12)). The study aimed to present new amphiphilic antimicrobial macromolecule as an alternative for the commercially available surfactants to be employed as emulsifiers. In this line, two aqueous suspensions

were prepared, and the antimicrobial activity against *S. epidermidis* was assessed. One suspension was prepared with the emulsifier (HBP-NH-N⁺C8, 0.10 wt%) and PMMA (0.25wt%) whereas a suspension containing polyvinyl alcohol (PVA, 0.10 wt%) and PMMA (0.25wt%) was used as control. The suspension containing HBP-NH-N⁺C8 showed much higher antimicrobial activity (MIC = 4 ± 8 µg/mL) in comparison of that PVA-containing suspension (MIC > 640 µg/mL), indicating the potential of the novel emulsifier for the preparation of waterborne antimicrobial coatings.

1.6.4. Hydrophilic/hydrophobic balance

With no doubt, one of the most important parameters on the design of bioactive polymers is the amphiphilicity, also named as hydrophilic/hydrophobic balance. This factor is closely related to the antimicrobial activity and selectivity of these macromolecules.⁵⁰ Only the naturally occurring AMPs possess the optimal amphiphilicity, as a consequence of years of improvement of living organisms to create an efficient defense mechanism against pathogens.¹²¹ The progress in polymer chemistry has also enabled scientists to acquire the essence of these compounds to prepare synthetic antimicrobial polymers able to play similar mode of action to that of the AMPs. For instance, highly dense polycations may have enhanced ability to electrostatically bind to the anionic bacterial surfaces. On the other hand, with no hydrophobicity, they may not diffuse into the lipid bilayer which is significantly important to cause membrane destabilization and inner cell compounds leakage.¹²² Concurrently, structures with high hydrophobicity may present equal toxicity for both, bacterial and mammalian cells.^{123, 124} Finally, it is important mentioning that there is no universal degree of amphiphilicity for synthetic compounds once this factor is strongly influenced by the intrinsic chemical and physical features of the polymers. Therefore, it is reasonable to state that each antimicrobial polymeric system will present its own optimal hydrophilic/hydrophobic ratio, depending on the nature of the monomers and the bacterial strain to kill/treat.

1.6.5. The effect of the molecular weight

Controlled polymerization techniques (RDRP) provide the possibility to prepare polymers with pre-defined molecular weight. This advantage allows to methodically evaluate the effect of this factor over the polymer's bioactivity. Studies suggest that

higher molecular weights lead to higher antimicrobial activity as the interaction between polymers and bacteria depend on the polycation charges density.¹²² Additionally, the increment on the MW might mean the increase of both cationic and hydrophobic moieties thus, favoring simultaneously both electrostatic interactions between polymer and bacteria, and the penetration of the polymer into the cell wall. Notwithstanding, parameters such as aggregation, solubility and diffusion can become important with increasing MW and they should be also considered.

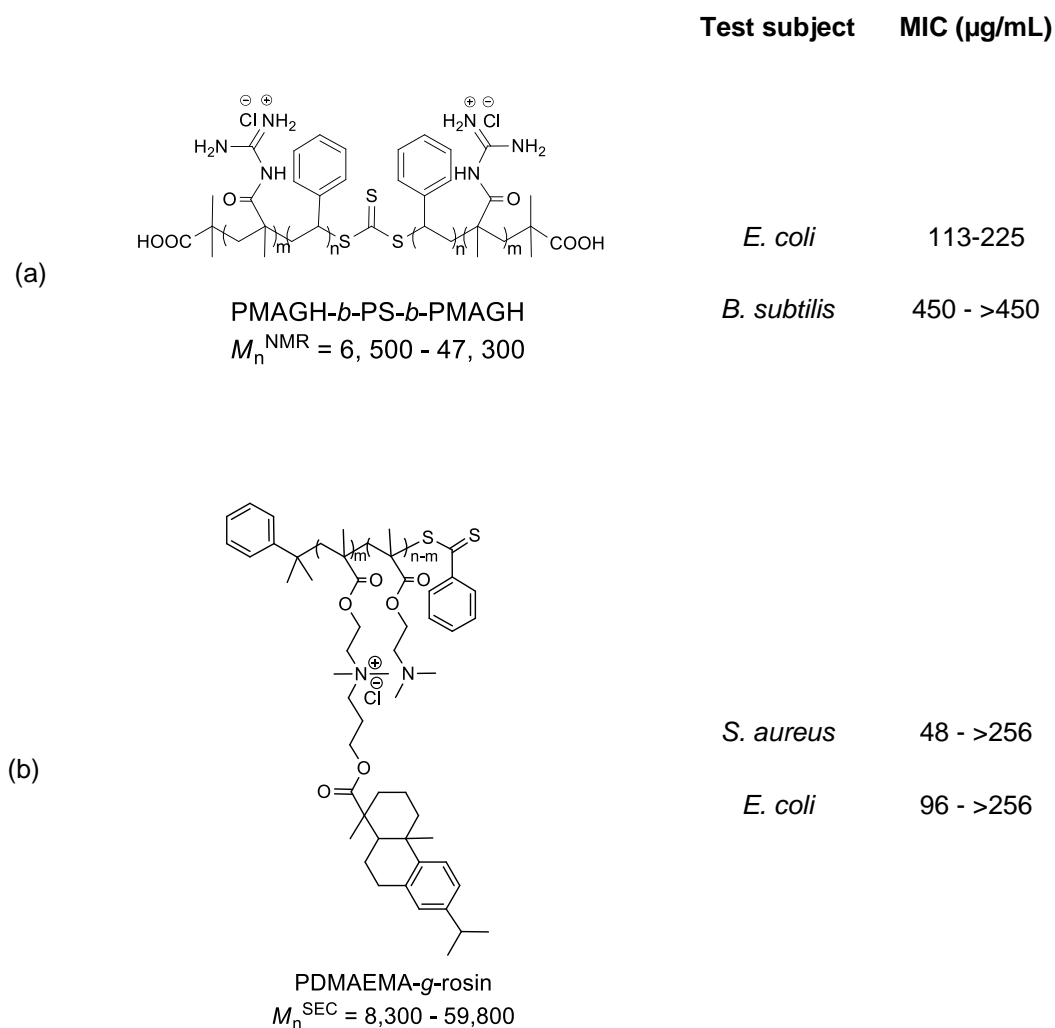


Figure 1.12. Chemical structure and MIC values of (a) PMAGH-*b*-PS-*b*-PMAGH and (b) PDMAEMA-*g*-rosin.

Zhang *et al.*,¹²⁵ prepared a library of guanidine-based poly(methacryl guanidine hydrochloride)-*b*-polystyrene-*b*-poly(methacryl guanidine hydrochloride) (PMAGH-*b*-PS-*b*-PMAGH), *via* sequential RAFT varying the MW from 6,500 to 46,000 (Figure 1.12a).¹²⁵ The authors tested the biological activity of the polymers against two bacterial strains, *E. coli* and *B. subtilis*. The results showed better overall activity towards *E. coli*

with lower MIC values than those against *B. subtilis*, for same MW. Still for *E. coli*, MICs decreased from 225 to 113 $\mu\text{g mL}^{-1}$ as the MW of the polymer increased. However, the polymers did not show pronounced activity to *B. subtilis* and no significant changing on the MIC values was observed by varying the MW. A novel class of cationic antimicrobial polymer based on PDMAEMA containing rosin as pendant group (PDMAEMA-*g*-rosin) and hydrophenanthrene as the hydrophobic head with different MW, were prepared. Results showed that low MW polymers presented higher antimicrobial activity in comparison to the high MW counterparts (Figure 1.12 (b)). The authors argued that increasing the MW influenced strongly on the solubility of the polymers resulting in partial aggregation. In addition, polyion-polyion complexation between the negatively charged compounds of bacteria and the positive charges of the polymer might become irreversible as the MW increased, thus affecting the efficacy of the polymers.¹²⁶

1.6.6. Bioactive polymers containing ammonium or phosphonium salts

To reproduce a similar antimicrobial mechanism of that natural AMPs, the synthetic antimicrobial macromolecules must present a net positive charge, as AMPs. Indeed, the electrostatic interactions are the driving force at the initial process of killing/inactivating bacteria. Generally, the cationic segment of synthetic antimicrobial macromolecules is composed of amine-containing monomers, including primary amine, tertiary amine or quaternary ammonium groups. Others cationic groups such as phosphonium, sulphonium¹²⁷ or metal particles¹²⁸ have been also employed in studies regarding antimicrobial materials. However, the most efficient one is based on ammonium and phosphonium cations.

The ammonium cation is the most used species for the preparation of antimicrobial materials, possibly because it is the same group present in natural AMPs. While in AMPs the positive charge is pH-dependent, comes upon the protonation of primary amines or guanidine in lysine or guanidine moieties respectively, most of the synthetic antimicrobial polymers employ quaternary ammonium salts (QAS), as it gives a permanent positive charge. Judzewitsch *et al.*,¹²⁹ evaluated the influence of the cation structure of different amphiphilic copolymers bearing primary amine, tertiary amine or quaternary ammonium

on the antibacterial activity. In this study, the authors used photo-induced electron transfer RAFT for the polymer synthesis and tested the materials against three distinct bacteria: *P. aeruginosa*, *S. aureus* and *Mycobacterium smegmatis*. The results showed a broad-spectrum activity for all polymers and indicated that primary amine worked better for Gram-negative (*P. aeruginosa*), while quaternary ammonium was more effective towards the Gram-positive *Mycobacterium smegmatis*, for the polymer with similar MW.

Polymers containing phosphonium groups are widely studied concerning ionic liquids¹³⁰ and acid nucleic delivery¹³¹. However, their antimicrobial efficiency is not so explored as the ammonium cation. Cuthbert *et al.*,¹³² reported the antimicrobial activity and hemolytic concentrations of a novel phosphonium polymers functionalized with two types of sugar (Figure 1.13a), mannose and glucose. Interestingly, these polymers showed comparable activity being more efficient against *S. aureus* than *E. coli*. In addition, the insertion of sugars to the more hydrophilic polymers increased the HC₅₀ values leading to better selectivity indices in comparison to the lipophilic conventional antibiotic. In another study, Inta *et al.*,¹³³ prepared a series of water-soluble chitosan derivatives bearing quaternary phosphonium salts (Figure 1.13 (b)).

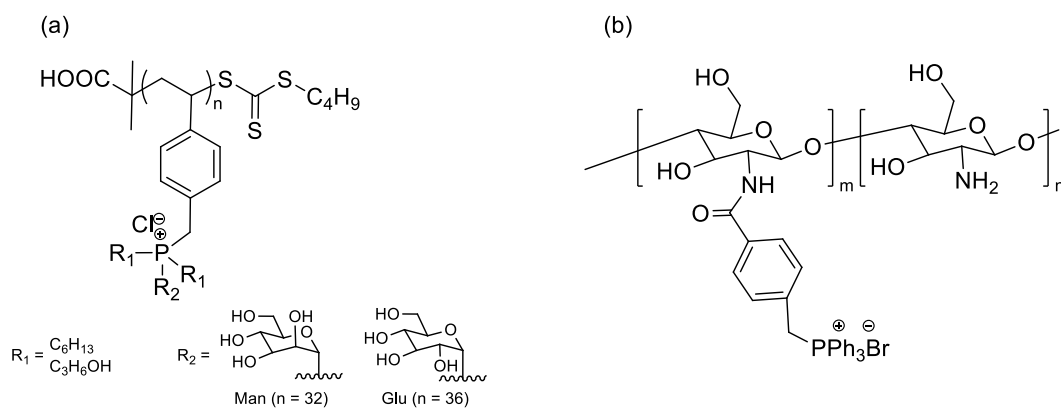


Figure 1.13. Chemical structure of (a) sugar-functionalized polymers and (b) chitosan derivatives bearing quaternary phosphonium salts.

The different derivatives were shown to have antimicrobial activity towards two different bacterial strains (*E. coli* and *S. aureus*). The results have also demonstrated that the antibacterial activity is higher for the derivatives with a higher degree of substitution (DS) (viz., 26.7% and 41.4%). The antibacterial efficacy determined by the LB-agar plate methods for the chitosan derivative with a DS of 41.4% was capable to eliminate 99.9%

of *E. coli* and 99% of *S. aureus*. For neat chitosan, the antibacterial efficacy did not surpass 40%. The chitosan derivative with a DS of 41.4% was shown to have low cytotoxicity towards a human skin fibroblast cell line, making it an interesting candidate to be used in the biomedical field.

As previously mentioned, polymers are versatile and suitable materials to be used as antimicrobial agents. There are several synthetic techniques available to prepare these materials (*e. g.*, RDRP methods) and the wide range of applications such as antifouling surfaces, antimicrobial textiles or antimicrobial polymers for oral treatment, making them the most promising alternative to prevent or treat microbial infections. Notwithstanding, considering the growing emergence of MDR bacteria, which today is seen as a serious issue to the health area, it is mandatory to develop new approaches to efficiently defeat this imminent threat. Antimicrobial photodynamic inactivation (aPDI) is a methodology that uses the combination of light, photosensitizers and molecular oxygen to generate ROS, which also represents an attractive alternative to inhibit bacterial growth. The technique has shown enormous potential, but it still challenging to accomplish acceptable antimicrobial therapy in humans, for example, the total eradication of bacteria at the site of infection with no recurrence of a new infection post-treatment. Moreover, other limitations of aPDI such as the ineffectiveness in eradicating microorganism in biofilms, and the fact that the results obtained *in vitro* are rarely transposed to animal models, difficult its establishment at a clinical practice .¹³⁴

The combination of multiple mechanisms of bactericidal action could be an alternative strategy to overcome such limitations. In this regard, polymeric materials, for example, can be easily used to widen the application of aPDI allowing the construction of effective and advanced approaches to benefit human health. The following section will present the general aspects of aPDI including the challenges and perspectives of this technology.

1.7. Antimicrobial photodynamic inactivation

The use of a photodynamic mechanism to produce ROS is a therapeutic methodology largely studied for the treatment of infectious diseases and cancer.¹³⁵ The death of microorganisms upon exposure to photo-sensitive compounds and visible light was discovered over 100 years ago.¹³⁶ Shortly after, it was found out that molecular oxygen

also played a fundamental in the process and the term “photodynamic action” was conceived.¹³⁷ Although the photodynamic action was firstly devoted for bacterial eradication, its application during the last century was most directed for cancer treatment, mainly because antibiotics have been in the front line of bacterial infectious diseases treatment. It was only during the 1900s, that aPDI has gained increased attention, especially due to the important discoveries that showed that cationic photosensitizers belonging the family of the porphyrins,¹³⁸ phenothiazines¹³⁹ and phthalocyanines¹⁴⁰ could induce a fast killing of Gram-negative bacteria such as *E. coli* and *P. aeruginosa*, in addition to Gram-positive bacteria and fungi.

Even though the light-mediate treatments are still in development, these technologies are likely to become an important therapeutic option considering some important particularities as:¹⁴¹⁻¹⁴³

- The possibility to develop efficient treatment regimens for a wide range of pathogens like yeasts, fungi, Gram-positive, Gram-negative, parasitic and protozoa;
- The selectivity for microbial cells over the host tissues;
- The possibility to develop protocols of minimal invasiveness treatment by using non-hazardous visible light sources;
- The non-propensity of the microorganisms to acquire resistant against aPDI.

1.7.1. Photobiological processes

The photodynamic process occurs with the application of a photosensitizer (PS), which is photoactivated by light at an appropriate wavelength in the presence of molecular oxygen to generate ROS that includes singlet oxygen and free radicals (e.g., OH[•]).^{144, 145} The mechanism of the process can be illustrated in the Jablonsky diagram shown in Figure 1.14. It starts when the PS in its ground state (PS⁰) absorbs light and it is converted into a short-lived excited state, called singlet state (PS¹). In this higher level of energy, the molecule can decay back to its ground state, releasing the energy in the form of fluorescence emission or heat. Some molecules can further transit to a long-lived level of excitation, the triplet state (PS³). In its PS³ form, the molecule can follow two distinct pathways to produce ROS. In the first pathway (termed type I reaction), it can generate

ROS from PS radical ions upon an electron transfer reaction, which will react with oxygen to produce cytotoxic species such as hydroxyl radicals and/or hydrogen peroxide and superoxide. In the type II reaction, the PS^3 transfers its energy to molecular oxygen reaching the singlet oxygen state (O_2^1). All forms of ROS possess potent toxicity to microorganisms and they can react with a wide range of cellular macromolecules, inducing the oxidation of lipids, amino acids in proteins, cross-linking of proteins and oxidative damage of the nucleic acids, which will disturb the normal functioning of the pathogens.^{146, 147}

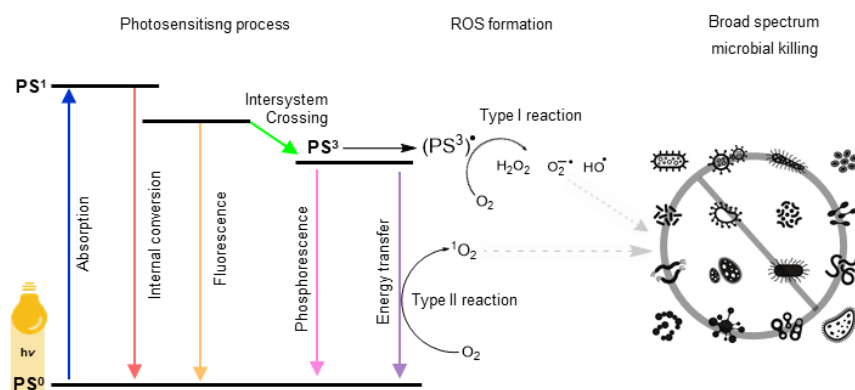


Figure 1.14. Jablonsky diagram and ROS formation by the photodynamic process.

1.7.2. Reactive oxygen species (ROS)-induced cytotoxicity

The general knowledge of the potential mechanisms of damage by ROS comes from studies that superoxide radicals ($O_2^{\bullet-}$) and hydrogen peroxide (H_2O_2) are produced in the cytoplasm of *E. coli* when oxygen randomly collides with flavin moieties presented in flavoenzymes.¹⁴⁸ The iron-sulphur (4Fe-4S) clusters of many proteins are the main targets of ROS damage, but other enzymes can be also often affected. Protein damages frequently result in metabolic defects that could compromise cell survival. When 4Fe-4S clusters are injured, the iron ion is released and can react with H_2O_2 , in a Fenton reaction, resulting in the production of hydroxyl radicals (OH^{\bullet}). All ROS enforce harsh damage to several biomolecules, mostly nucleic acids, proteins and lipids.^{148, 149} In the case of DNA, the ROS attack the sugar group, pyrimidine and purine bases yielding single and double-strand breaks, several adducts and cross-linkers molecules.¹⁵⁰ The main damages in protein involve oxidation of sulfhydryl groups, modification of prosthetic groups or metal clusters, protein-protein cross-linking and protein carbonylation causing inactivation of

crucial enzymes^{151, 152}, therefore, compromising the cell viability. Lipids are also important targets of ROS. The reactive species can easily attack polyunsaturated fatty acids in membranes leading to lipid peroxidation.¹⁵³ This event has a deleterious effect on the cells due to a decrease in membrane fluidity. Recently, the emphasis has been put in the study of stimuli-responsive polymers as precursors for ROS generator. Different materials, such as metal and metal oxide nanoparticles combined, can generate ROS as a consequence of external stimuli and consequently induce cytotoxicity to microbes.^{154, 155}

1.7.3. Photosensitizer

Since the discovery of aPDI, several synthetic and natural PS have been used in microbiology. Today, they represent a large group of photoantimicrobial agents, which have been extensively investigated for areas as dentistry,¹⁵⁶ wound healing,¹⁵⁷ infection diseases¹⁵⁸ and light-responsive antimicrobial surfaces.¹⁵⁹ PS may be grouped as porphyrins and non-porphyrins. Porphyrins-derived compounds represent the largest class of PS, which are composed of interconnected pyrroles groups, forming a macrocyclic structure (Figure 1.15).

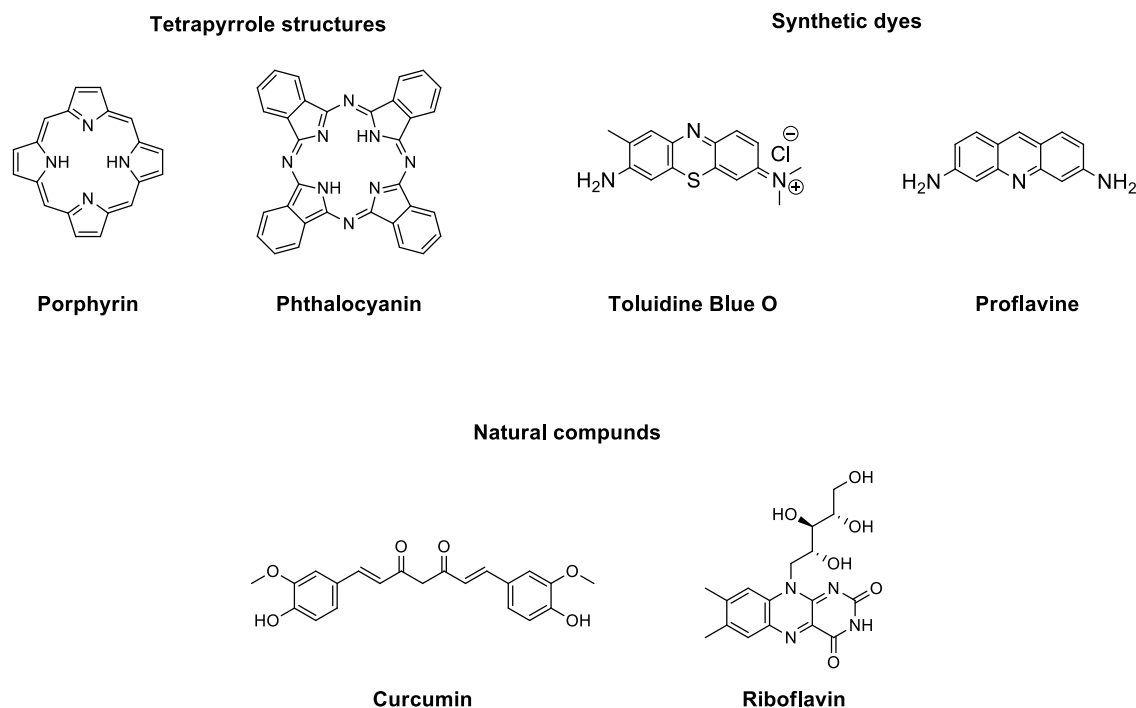


Figure 1.15. Chemical structures of representative photosensitizers.

The family termed synthetic dyes, is the second main group of PS, which englobes a vast number of compounds such as phenothiazines salts (*e.g.*, toluidine blue O) and acridines (*e.g.*, proflavine), Figure 1.15. Finally, the third main group includes the naturally occurring compounds, which are represented by curcumin and riboflavin in Figure 1.15.¹⁶⁰ In general, all photo-sensitive compounds have proved to be very active against a broad-spectrum of microorganism showing inhibition activity at micromolar concentrations in addition to the high selective indices to the mammalian cells. The most accepted mechanism of the bacterial death is due to the cytoplasmic membrane damages, with exception to acridines (*e.g.*, proflavine) that strongly interact with DNA bases.¹⁶¹

Toluidine blue O

An important compound belonging to the phenothiazine family is toluidine blue O (TBO), a cationic PS which absorbs light in the red region of the visible spectrum ($\lambda_{\max} \approx 760$ nm). This molecule presents an enormous potential for application in several forms of treatment of bacterial-related infections due to its hydrophilic nature, high water solubility and efficacy of singlet oxygen generation.¹⁶² Moreover, several studies have also reported its photoinactivation activity. For example, TBO was tested in the *in vivo* treatment of *Vibrio vulnificus* wound in mice.¹⁵⁸ A lethal infection was systematically induced by 30 min incubation with the bacteria inoculum in a dose 100 times superior to the lethal dose. Surprisingly, 53% of the animals survived after being treated with 100 $\mu\text{g/mL}$ of TBO and 150 J/cm^2 of light ($\lambda = 560 - 780$ nm). On the other hand, most of the animals submitted only to irradiation or only to TBO died after 24-36 h. The tests performed *in vitro* showed that complete inhibition of the bacteria was achieved using 0.1 $\mu\text{g/mL}$ of TBO and providing 100 J/cm^2 of light. Additionally, TBO showed antimicrobial activity in the absence of light, *in vitro* results revealed the complete inhibition of bacterial growth after 24 h of 5×10^5 CFU of *V. vulnificus* exposed to 1 or 10 $\mu\text{g/mL}$ of TBO. The same effect was observed at a concentration of 100 $\mu\text{g/mL}$ of TBO but in a period of 2 h.

The photosensitizing features of TBO have been also evaluated on the eradication not only planktonic bacteria but also formed biofilms. Rout *et al.*,¹⁶³ used different microemulsion formulations with tween 80, eucalyptus oil, glycerol and EDTA to encapsulate TBO and to test against biofilms formed by *Staphylococcus* species. The total energy delivered was 0.607 J/cm^2 using a cluster of LED lamps emitting light in the range

of 610-630 nm. The results showed that all the formulations were more effective than the free PS dissolved in water, and the prevention of further formation of biofilms was also observed. In another study, the efficacy of TBO was compared with other PSs, such as methylene blue and malachite green, against biofilms of *E. coli* and *S. aureus*.¹⁶⁴ A light dose of 20 J/cm² was delivered over the biofilms with a 660 nm laser. The results showed that methylene blue and TBO promoted the reduction of both microorganisms counts around 1 log at 300 and 150 μM. The malachite green exhibited a bacterial reduction of 1.6 logs for *S. aureus* and 4.1 logs for *E. coli*, but it was required a concentration of 3000 μM to achieve such effect.

Proflavine

Proflavine is a synthetic dye belonging to the acridine family, a group of compounds with significant pharmacological interest. They were extensively used as antiseptic and antimicrobials before the advent of antibiotics when their usage was set aside. Recently, acridines have gained increased attention mainly because of their ability to intercalate with DNA bases, which is considered to be the major mode of toxicity, and, the major feature of this group of PS.¹⁶⁵⁻¹⁶⁷ Acridine-based drugs are known to have antifungal, antibacterial and antimalarial properties, which make them an important class of therapeutics. However, only a few studies report their photo-inducible activity in bacterial inactivation therapies.¹⁶⁸ In the late '90s, Wainwright *et al.*,¹⁶⁹ prepared a library of acridine derivatives and compared their efficiency with commercially available compounds, namely acridine orange and proflavine. Several bacteria including *S. aureus*, *E. faecalis*, *B. cereus*, *E. coli* and *P. aeruginosa* were subjected in the study. For the photosensitization, an external light source ($\lambda = 400 - 450$ nm) with 1.7 mW/cm² of energy fluence was used for a period of 1 h, delivering a total of 6.3 J/cm² of light dose. The authors observed a substantial increment on the antibacterial activity of all acridines under lighting condition, especially towards the Gram-positives. Surprisingly, proflavine was found to be the most active PS for the Gram-negative bacteria. For *E. coli*, the MIC value decreased from 100 to 10 μM and for *P. aeruginosa*, the MICs decreased from 250 to 10 μM.

Curcumin

Curcumin, a yellow natural dye derived from the rhizome of *Curcuma longa* has been widely used for therapeutic purposes with applications including photoinactivation of planktonic bacteria and eradication of biofilms.¹⁷⁰ Due to its bioactive features, curcumin has been also used as an anti-inflammatory and antiseptic agent, in addition to other properties such as anti-tumour effects.¹⁷¹ The molecule absorbs light in a region border of UV to visible with maximum absorption at 420 nm.¹⁷² Even though, it is considered as a poor singlet oxygen generator (quantum yield lower than 0.10), curcumin has found a significant contribution for human health in several aspects *e.g.*, as bactericidal agent.¹⁷³ However, one of the major disadvantages of curcumin it is the lack of solubility in water which difficult its application in biological media. Nonetheless, efforts have been made to improve the solubility, increase the bioavailability and enlarge its pharmacological employment. For instance, Suzuki *et al.*,¹⁷³ developed a nanoparticle system using poly(lactide-*co*-glycolide) as the polymeric matrix to encapsulate curcumin, therefore, improving its solubility in aqueous media and providing protection against hydrolysis. Free curcumin and the new nanosystems were tested against *S. aureus*, *E. coli* and *Candida albicans* under 21 and 42 J/cm² of light dose and their efficiencies were compared. Results revealed a significant enhancement of the aPDI activity of the encapsulated curcumin in comparison to that of its free form, showing 6 logs reduction for *S. aureus* in the first 10 minutes. All the microorganisms tested were more susceptible to the curcumin-loaded nanoparticles with pronounced activity against the Gram-positive strains. Nonetheless, *E. coli* and *Candida albicans* were more resistant and the inactivation only occurred for higher concentrations of the nanoparticles were used. In another study, the photoinactivation potential of curcumin was also tested against MRSA biofilms located in cavities of bovine bones.¹⁷⁰ The experiments were carried out in dark and under 450 nm illumination and with 20.1 J/cm².¹⁷⁰ The approach promoted 3.67 log reduction, showing that curcumin can be also effective against strains with resistance profiles to the antibiotic.

In summary, photodynamic inactivation has proved to be suitable for several protocols regarding bacteria inactivation. Indeed, the approach can pave new possibilities to be used in diverse pharmacological sectors and minimize the need for conventional antibiotics during the treatment. In addition to this, the concept of aPDI has been also used in the

development of light-responsive antimicrobial surfaces as an alternative to prevent the acquisition of infections, especially in hospital environments. This technology presents a significant interest as the infections acquired in healthcare facilities are mainly caused by touching in surfaces contaminated with pathogens.

1.7.4. Light-activated polymeric antimicrobial surfaces

Researchers reported the development of light-activated polymeric antimicrobial surfaces.^{174,175} For instance, a white light-activated self-sterilizing surface was developed using ZnO nanoparticles (NPs), the photosensitizer crystal violet (CV) and poly(dimethylsiloxane) (PDMS) as the polymeric matrix.¹⁵⁹ The main objective was to investigate the photoantimicrobial effect of novel surfaces upon low-intensity white light exposure (6500 - 300 lux). The surfaces were obtained by incorporating varied content, of ZnO NPs (0.5, 1 and 5 wt%) into the PDMS matrix. In sequence, the resultant mixture was degassed and cast on glass substrates and then brought to cure in a preheated oven at 100 °C. Bare PDMS and ZnO-containing samples were immersed in a solution of CV in acetone for 24 h, from which they were removed and dried for 24 h. The photobactericidal properties of the samples were assessed against *S. aureus* and *E. coli* under dark and light conditions during 45 min of incubation. The results showed that the surfaces covered with only polymer or polymer-ZnO NPs did not present a significant reduction on the bacterial number, whereas the surfaces containing ZnO (1-5 wt%)-CV remarkably reduced *S. aureus* counts within 45 minutes of light. For *E. coli*, 90 minutes of exposure was required to achieve expressive effects and among the surfaces evaluated, only that containing CV with higher quantities of ZnO NPs could reduce the bacterial counts to below the detection limit.

Walker and co-workers¹⁷⁶ developed white light-activated silicone-based surfaces doped with methylene blue, CV and gold NPs. The samples were prepared by immersing the medical-grade silicone in a 9:1 acetone/gold NPs solution saturated with methylene blue for 72 h. Then, the solvent was removed by an air-drying process during 24 h and the samples were washed with distilled water. After that, the resulting samples were immersed in an aqueous solution of crystal CV 24 h, being subsequently washed. The photobactericidal properties were assessed against *S. epidermidis*, *Saccharomyces*

cerevisiae and MS2 Bacteriophage as the microorganism models of bacteria, yeasts and virus, respectively. Results showed a reduction of 2.92 log of the *S. epidermidis* counts to below the detection limit of 400 CFU/mL. For the bacteriophage, a 4.61 log reduction after 8h was achieved, while 1.5 log reduction of *S. cerevisiae* population was observed after 7.5h. Furthermore, the authors indicated the mechanism of action of the exogenous ROS. Following another report,¹⁷⁷ it is suggested that during the early stages of exposure, most of the produced ROS are quenched by the peptidoglycans, hindering these oxygen species to achieve the cytoplasmic membrane of the bacteria. However, over time, as the ROS concentration increases, they are more likely to achieve the cytoplasmic membrane and consequently, causing its peroxidization.

Chapter 2 - Materials and methods

2.1. Materials

1,1,3,3-Tetramethylguanidine (TMG, 99%, TCI), aluminum oxide (basic, Fisher Scientific), copper^{II}bromide (CuBr₂, +99% extra pure, anhydrous; Acros), dimethylformamide (DMF HPLC, 99.8%, Fisher Scientific), ethyl α -bromoisobutyrate (EBiB 98%, Sigma-aldrich), ethyl α -bromophenylacetate (EBPA, 97% Sigma-Aldrich), hexane (98% José Manuel dos Santos, Lda), methanol (chemically pure, José Manuel dos Santos, Lda), and zerovalent iron powder (Fe⁰, 99%, ~70 mesh, Acros) deuterium oxide (D₂O) (Sigma-Aldrich, 99.9% atom D), deuterated (D₆) ethanol (*d*₆-EtOD) (Euriso-top, 99+%), DMF (Sigma-Aldrich, 99,8+%), tetrahydrofuran (THF) (HPLC grade) and *N,N'*-Methylenebis(acrylamide), (BAAm, Sigma Aldrich 99.8 %), proflavine hemisulphate hydrate (97.0% TCI chemicals), natural curcumin (TCI chemicals), Dichloromethane (JMS 99%+) toluidine blue O (99,0% TCI chemicals) and α -bromoisobutyryl bromide (BiB, 97% Sigma Aldrich). ethyl α -bromoisobutyrate (EBiB, 98% Sigma Aldrich) were used as received.

Metallic copper (Cu⁰ wire, *d* = 1 mm, Sigma-Aldrich) was washed with HCl in methanol and subsequently rinsed with methanol and dried under an air steam.

PEG-Br macroinitiator was synthesized as reported in the literature.¹⁷⁸ Deionized purified water (Milli-Q®, Millipore, resistivity >18 MΩ.cm) was obtained by reverse osmosis. Dimethyl sulfoxide (DMSO, analytical grade, Fisher Scientific) was dried over calcium hydride, distilled under reduced pressure and stored over molecular sieves.

2-(diisopropylamino) ethyl methacrylate (DPA, 97%, Sigma-Aldrich), butyl methacrylate (BMA, 99%, Sigma-Aldrich), ethyl methacrylate (EMA, 99% Sigma-Aldrich), glycidyl methacrylate (GMA, 97%, Sigma-Aldrich), *n*-Butyl acrylate (*n*-BA) (Sigma-Aldrich, 99+%) and methyl methacrylate (MMA, 99%, Acros) were passed over a sand/alumina column before use to remove the radical inhibitor.

Ethanol (JMS, 96%) was passed though rotatory evaporator before use. Triethyl amine (Et₃N, Sigma Aldrich) was distilled before using.

(3-Acrylamidopropyl)trimethylammonium) chloride (AMPTMA) (TCI chemicals, solution 75% in H₂O) was washed with acetone to remove the water from the solution. The pure monomer was used in the polymerizations.

Tris(2-(dimethylamino)ethyl)amine (Me₆TREN)¹⁷⁹ was obtained using procedures described, pentaerythritol tetrakis(2-bromoisobutyrate) (4f-BiB) and dipentaerythritol hexakis(2-bromoisobutyrate) (6f-BiB) were synthesized according the procedure described in the literature.¹⁸⁰

2.2. Procedures

2.2.1. Typical synthesis of PMMA-Br by Cu⁰-mediated SARA ATRP

A mixture of MMA (3.8 g, 37.1 mmol) and EBPA (93.2 mg, 371.8 μmol) was prepared separately from a mixture of TMG (42.8 mg, 371.8 μmol), CuBr₂ (8.3 mg, 37.2 μmol) and DMSO (2.0 mL). Both mixtures and a 10 mL Schlenk flask equipped with a magnetic stirring bar and Cu⁰ wire (*l* = 5 cm; *d* = 1 mm) were purged with nitrogen for 20 minutes. After this time, both mixtures were added to the Schlenk flask (under nitrogen flow), which was placed in a water bath at 30 °C. The polymerization was allowed to proceed, and different samples of the reaction mixture were collected over time. The samples were analyzed by ¹H NMR spectroscopy, to determine the monomer conversion and by SEC, to determine the molecular weight and dispersity of the polymers. The final reaction mixture was diluted with THF and passed through an alumina column to remove copper catalyst. Pure PMMA-Br was recovered after precipitation in cold methanol, followed by drying under reduced pressure.

2.2.2. Typical synthesis of PGMA-Br by Fe⁰-mediated SARA ATRP

A mixture of GMA (4.3 g, 29.3 mmol) and EBPA (36.8 mg, 146.7 μmol) was prepared separately from a mixture of TMG (16.9 mg, 146.7 μmol), CuBr₂ (3.3 mg, 14.7 μmol) and DMSO (4.0 mL). Both mixtures and a 10 mL Schlenk flask equipped with a magnetic stirring bar and Fe⁰ powder (8.3 mg, 146.7 μmol) were purged with nitrogen for 20 minutes. After this time, both mixtures were added to the Schlenk flask (under nitrogen flow), which was placed in a water bath at 30 °C. The polymerization was allowed to proceed, and different reaction mixture samples were collected over time. The samples were analyzed by ¹H NMR spectroscopy, to determine the monomer conversion and by SEC, to determine the molecular weight and dispersity of the polymers. The final reaction mixture was diluted with THF and passed through an alumina column to remove copper catalyst. The pure PGMA-Br was recovered after precipitation in cold hexane, followed by drying under reduced pressure.

2.2.3. Typical synthesis of PEMA-Br by Cu⁰-mediated SARA ATRP

A mixture of EMA (3.7 g, 31.8 mmol) and EBPA (79.7 mg, 318.1 μ mol) was prepared separately from a mixture of TMG (36.6 mg, 318.1 μ mol), CuBr₂ (7.1 mg, 31.8 μ mol) and DMSO (2.0 mL). Both mixtures and a 10 mL Schlenk flask equipped with a magnetic stirring bar and Cu⁰ wire ($l = 5$ cm; $d = 1$ mm) were purged with nitrogen for 20 minutes. After this time, both mixtures were added to the Schlenk flask (under nitrogen flow), which was placed in a water bath at 30 °C. The polymerization was allowed to proceed, and different reaction mixture samples were collected over time. The samples were analyzed by ¹H NMR spectroscopy, to determine the monomer conversion and by SEC, to determine the molecular weight and dispersity of the polymers. The final reaction mixture was diluted with THF and passed through an alumina column to remove copper catalyst. The pure PEMA-Br was recovered after precipitation in cold methanol, followed by drying under reduced pressure.

2.2.4. Typical synthesis of PEG-*b*-PDPA-Br by Cu⁰-mediated SARA ATRP

A mixture of DPA (2.7 g, 12.3 mmol), PEG-Br (245.5 mg, 122.8 μ mol) and DMF (3.0 mL) was prepared separately from a mixture of TMG (14.1 mg, 122.8 μ mol), CuBr₂ (2.7 mg, 12.3 μ mol) and DMF (3.0 mL). Both mixtures and a 10 mL Schlenk flask equipped with a magnetic stirring bar and Cu⁰ wire ($l = 5$ cm; $d = 1$ mm) were purged with nitrogen for 20 minutes. After this time, both mixtures were added to the Schlenk flask (under nitrogen flow), which was placed in a water bath at 30 °C. The polymerization was allowed to proceed, and different reaction mixture samples were collected over time. The samples were analyzed by ¹H NMR spectroscopy, to determine the monomer conversion and by aqueous SEC, to determine the molecular weight and dispersity of the polymers. The final reaction mixture was dialyzed against deionized water with pH = 3.0 (cut off = 3500) and the polymer was obtained after freeze drying.

2.2.5. “One-pot” chain extension of PMMA-Br with MMA or BMA by Cu⁰-mediated SARA ATRP

A mixture of MMA (2.7 g, 23.2 mmol) and EBPA (116.5 mg, 464.7 μ mol) was prepared separately from a mixture of TMG (53.5 mg, 464.7 μ mol), CuBr₂ (10.4 mg, 46.5 μ mol) and DMSO (1.25 mL). Both mixtures and a 10 mL Schlenk flask equipped with a magnetic stirring bar and Cu⁰ wire ($l = 5$ cm; $d = 1$ mm) were purged with nitrogen for

20 minutes. Both mixtures were added to the Schlenk flask (under nitrogen flow), which was placed in a water bath at 30 °C. The reaction proceeded for 6 h until high MMA conversion ($\text{conv.}_{\text{MMA}} = 93\%$) and then, a desired amount of MMA (16 g, 162.7 mmol), previously bubbled with nitrogen for 20 minutes, was added into the polymerization mixture. The reaction was allowed to proceed for further 26 h ($\text{conv.}_{\text{MMA}} = 54\%$). The chemical structure of the copolymer was confirmed by ^1H NMR spectroscopy and the molecular weight and dispersity were determined by SEC.

In the synthesis of the PMMA-*b*-PBMA-Br block copolymer, the preparation of the PMMA-Br macroinitiator was conducted as previously described ($\text{conv.}_{\text{MMA}} = 91\%$). To form the second block, of nitrogen-bubbled BMA (15 mL, 92.9 mmol) was added into the Schlenk and the reaction proceeded for further 16 h ($\text{conv.}_{\text{BMA}} = 70\%$). The final reaction mixture was diluted with THF and passed through an alumina column to remove copper catalyst. The pure PMMA-*b*-PBMA-Br was recovered after precipitation in cold methanol, followed by drying under reduced pressure. The chemical structure of the copolymer was confirmed by ^1H NMR spectroscopy and the molecular weight and dispersity were determined by SEC.

2.2.6. ARGET ATRP of MMA using TMG as reducing agent

A mixture of MMA (3.94 g, 37.1 mmol) and EBPA (93.2 mg, 371.8 μmol) was prepared separately from a solution of TMG (42.8 mg, 371.8 μmol) in DMSO (1.0 mL) and a mixture of CuBr_2 (8.3 mg, 37.2 μmol), PMDETA (16.2 mg, 92.5 μmol) also in DMSO (1.0 mL). The mixtures and a 10 mL Schlenk flask equipped with a magnetic stirring bar were purged with nitrogen for 20 minutes. Afterwards, the mixtures were added to the Schlenk flask (under nitrogen flow), which was placed in a water bath at 30 °C. The polymerization was allowed to proceed for 24 h. The reaction mixture was analyzed by ^1H NMR spectroscopy, to determine the monomer conversion and by SEC, to determine the molecular weight and dispersity of the polymer.

2.2.7. Typical homopolymerization of AMPTMA by Cu^0 -mediated SARA ATRP

AMPTMA (2.5 mL, 4.8 mmol) and a solution of EBiB (9.6 mg, 48.3 μmol), CuBr_2 (5.4 mg, 24.2 μmol) and Me_6TREN (13.0 μL , 48.3 μmol) in ethanol (EtOH, 2.5 mL) were added to a 10 mL Schlenk flask equipped with a stirrer bar. Then, Cu^0 wire ($l = 5$ cm; $d = 1$ mm) was added to the reactor, which was sealed with a glass stopper, frozen with

liquid nitrogen, deoxygenated with three-freeze-vacuum-thaw cycles and purged with nitrogen. The reaction was allowed to proceed with stirring (360 rpm) at 30 °C during 24 h. The monomer conversion was determined by ^1H NMR in D_2O and the molecular weight parameters were determined by SEC analysis. The polymer was dialyzed against water (cut-off 3500) and the pure polymer was recovered after freeze drying.

2.2.8. Typical homopolymerization of *n*-BA by SARA ATRP

n-BA (2.5 mL, 17.4 mmol) and a solution of EBiB (36.9 mg, 174.0 μmol), CuBr_2 (19.4 mg, 86.7 μmol) and Me_6TREN (46.4 μL , 174.0 μmol) in EtOH (2.5 mL) were added to a 10 mL Schlenk flask equipped with a stirrer bar. Then, Cu^0 wire ($l = 5\text{cm}$; $d = 1\text{mm}$) was added to the reactor, which was sealed with a glass stopper, frozen with liquid nitrogen, deoxygenated with three-freeze-thaw cycles and purged with nitrogen. The reaction was allowed to proceed with stir (360 rpm) at 30 °C during 24 h. The monomer conversion was determined by ^1H NMR in CDCl_3 and the molecular weight parameters were determined by SEC analysis. The polymer was dissolved in THF and passed through a sand/alumina column to remove the catalyst. The pure polymer was obtained by precipitation in cold methanol.

2.2.9. Typical “one-pot” block copolymerization of AMPTMA and *n*-BA

AMPTMA (3.0 mL, 14.1 mmol) and a solution of CuBr_2 (15mg, 70.7 μmol) and Me_6TREN (37.8 μL , 142.0 μmol) in EtOH (3.0 mL) were added to a 25mL Schlenk flask equipped with a magnetic stirrer bar. Next, Cu^0 wire ($l = 5\text{cm}$; $d = 1\text{mm}$) was added to the reactor, which was sealed with a glass stopper, frozen with liquid nitrogen, deoxygenated with three freeze-vacuum-thaw cycles and purged with nitrogen. The reaction was allowed to proceed with stirring (360 rpm) at 30 °C. When the monomer reached more than 70 %, a degassed solution of *n*-BA (2.0 mL, 14.1 mmol) in EtOH (8.15 mL) was added to the Schlenk flask under nitrogen. The reaction was allowed to proceed until the maximum conversion of *n*-BA was achieved. The AMPTMA-*b*-PBA block copolymer was purified through dialysis (cut-off 3500) against water, followed by ethanol and then water and recovered after freeze drying. The conversion of both AMPTMA and *n*-BA and the theoretical molecular weight of the amphiphilic block copolymer were determined by ^1H NMR spectroscopy.

2.2.10. Typical synthesis of random PAMPTMA-*co*-PBA copolymer

AMPTMA (2.0 mL, 16.7 mmol), *n*-BA (1.5 mL, 10.4 mmol) and a solution of CuBr₂ (23.5 mg, 0.10 mmol) and Me₆TREN (55.0 μL, 0.21 mmol) in EtOH (2.0 mL) were added to a Schlenk flask equipped with a magnetic stirrer bar. Next, Cu⁰ wire (*l* = 5 cm; *d* = 1 mm) was added to the Schlenk flask, which was sealed with a glass stopper, frozen with liquid nitrogen deoxygenated with three freeze-vacuum-thaw cycles and purged with nitrogen. The reaction was allowed to proceed with stirring (360 rpm) at 30°C during 15 h. The conversion of both AMPTMA and *n*-BA and the theoretical molecular weight of the random copolymer were determined by ¹H NMR spectroscopy. The resulting mixture was dialyzed (cut-off 3500) against distilled water, followed by ethanol and then water and the purified copolymers were obtained after freeze-drying.

2.2.11. Typical synthesis of star-shaped polymers via core-first and arm-first

The star-shaped AMPTMA-Br homopolymer or PAMPTMA-*co*-PBA copolymers via core-first approach were synthesized using the procedures described in sections 2.2.7 or 2.2.10, but replacing the monofunctional EBiB initiator by either 4-EBiB or 6-EBiB for the preparation of 4-arm or 6-arm stars, respectively.

Star-shaped core-cross linked PAMPTMA homopolymers were synthesized via arm-first approach. A PAMAPTMA macroinitiator (MI) was synthesized via a typical SARA ATRP procedure in EtOH/H₂O 40/60 (v/v) (section 2.2.7) and the reaction was allowed to proceed during min, until 87% monomer conversion was achieved. Then, a degassed solution of the BAAM cross-linker in H₂O was injected under a N₂ purge into the flask containing the PAMPTMA-Br macroinitiator reaction mixture. The reaction was allowed to proceed for 24 h and samples were collected periodically to measure the BAAM conversion via ¹H NMR spectroscopy and molecular weight of the star-shaped PAMPTMA via SEC.

2.2.12. Synthesis of proflavine ATRP initiator (PF) - *N,N'*-(acridine-3,6-diyl)bis(2-bromo-2-methylpropanamide).

Proflavine hemisulphate hydrate (1.46 mmol) was put into a round bottom flask containing pyridine (10 mL) and equipped with a stirring bar. The mixture was allowed to stir for 30 min at 30 °C, after which Et₃N (5.9 mmol) was added. Finally, BiB was

added dropwise under inert atmosphere. The temperature was increased to 40 °C and the reaction was allowed to proceed for 5 h. The final product was obtained after precipitation into a concentrated NaOH solution followed filtration and removal of residual water by freeze-drying process. The recovered product was recrystallized from EtOH to render an orange colored powder (yield = 43%). The chemical structure was confirmed by ¹H NMR spectroscopy.

2.2.13. Synthesis of curcumin ATRP initiator (CI) - ((1E,3Z,6E)-3-hydroxy-5-oxohepta 1,3,6-triene-1,7-diyl)bis(2-methoxy-4,1-phenylene) bis(2-bromo-2-methylpropanoate)).

Curcumin (0.15 M, 4.0 mmol) was dissolved in the DMF HPLC grade (27 mL) and Et₃N (3.97 mmol) and the solution was stirred under inert atmosphere for 30 min at 0 °C. BiB (10 mmol) in THF was added dropwise to the reaction mixture at 0°C afterwards the temperature was increased to 30 °C. The mixture reacted for 5 h afterwards dichloromethane (100 mL) was added and the mixture was washed twice with NaOH solution (0.01 M) and HCl solution (0.01 M). The organic layer was recovered, removed under reduced pressure and the residual solvent was removed under vacuum at 40 °C. Finally, the yellow powder was dissolved in THF, precipitated in water, filtered, washed with excess of water and the residual water was removed by freeze-drying to obtain the purified product (yield = 80%). ¹H NMR spectroscopy confirmed the chemical structure of the pure product.

2.2.14. Synthesis of photosensitizer-functionalized antimicrobial polymers

The preparation of AMPTMA-Br homopolymer or random PAMPTMA-*co*-PBA copolymer functionalized with PS molecules were conducted following the procedures described in sections 2.2.10 and 2.2.7 but using either CI or PF as the ATRP initiator.

2.2.15. Synthesis of curcumin acrylate 4-((1E,3Z,6E)-3-hydroxy-7-(4-hydroxy-3-methoxyphenyl)-5-oxohepta-1,3,6-trien-1-yl)-2-methoxyphenyl acrylate.

Curcumin (0.014 mol), Et₃N (0.0134 mol) were placed in a round bottom flask and dissolved in THF HPLC grade (95 mL). The reaction mixture was purged with nitrogen while being stirred for 30 min at 0 °C. Afterwards, a solution of acryloyl chloride (0.014 mol) in THF HPLC grade (5 mL) was added dropwise. The reaction mixture was allowed

to stir for 5 h at room temperature. Next, THF was removed under reduced pressure and the crude product was dissolved in ethyl acetate and washed with a saturated aqueous solution of sodium carbonate. The organic layer was collected and dried using anhydrous sodium sulphate. The obtained product was concentrated under reduced pressure and purified by column chromatography (eluent: dichloromethane/ethyl acetate = 95:5 (v/v)) to obtain curcumin diacrylate as a primary product and curcumin acrylate as a secondary product. The chemical structure of the curcumin acrylate was confirmed by ^1H NMR spectroscopy.

2.2.16. MIC determination in solution

The assays to determine the antimicrobial activity and cell integrity were done by researchers at the Department of Life Science of the University of Coimbra, Portugal. Bacterial indicator strains (*Escherichia coli* ATCC25922, *Staphylococcus aureus* ATCC25923, *Bacillus subtilis* ATCC23857, *Bacillus cereus* 9843 and *Pseudomonas aeruginosa* HST244P) were grown at 37 °C. MIC determination was performed by agar diffusion test according to the Clinical & Laboratory Standards Institute (CLSI)¹⁸¹ by microdilution procedure in microplates in Luria–Bertani (LB) medium.

All polymer stock solutions (100 or 500 μM) were prepared in ultrapure sterile water. The MIC of the polymers was evaluated using the standard broth microdilution method. In this case, two-fold dilutions of the polymers were prepared in LB growth medium using 96-well microliter plate. Each well containing 150 μl of polymer solution was inoculated with 50 μl of bacterial suspensions prepared in LB medium (10^6 CFU. mL^{-1}) and further incubated at 37 °C for 24 h. Controls without polymer were performed for each bacterial strain. Each assay was repeated in triplicate to ensure reproducibility of the experiments. The MIC was the lowest concentration of polymer that completely inhibited bacterial growth.

2.2.17. Assessment of antimicrobial activity of the surfaces

The antimicrobial surfaces were prepared by researchers from the Department of the Chemical Engineering of the University of Porto and the antimicrobial activity assays were performed by researchers from the Department of Life Science of the University of Coimbra, Portugal.

2.3. Techniques

2.3.1. Determination of molecular weight parameters SEC

PAMPTMA-Br and PEG-*b*-PDPA-Br homopolymers were analyzed by SEC system with an online degasser, a refractive index (RI) detector and a set of columns: Shodex OHpak SB-G guard column, OHpak SB-804HQ and OHpak SB-802.5HQ columns. The polymers were eluted at a flow rate of 0.5 mL min⁻¹ with 0.1 M Na₂SO₄ (aq)/1 wt% acetic acid/0.02% NaN₃ at 40 °C. Before the injection (50 µL), the samples were filtered through a nylon membrane with 0.20 µm pore. The system was calibrated with five narrow poly(ethylene glycol) standards and the molecular weights (M_n^{SEC}) and D (M_w/M_n) were determined by conventional calibration using the Clarity software version 2.8.2.648.

The molecular weight parameters of PBA-Br, PEMA-Br, and PMMA-*b*-PBMA-Br were determined by high-performance (HP)SEC; Viscotek (Viscotek TDAmx) with a differential viscometer (DV), right-angle laser-light scattering (RALLS, Viscotek), low-angle laser-light scattering (LALLS, Viscotek) and RI detectors. The column set consisted of a PL 10 mm guard column (50 x 7.5 mm²) followed by one Viscotek T2000 column (6 µm), one Viscotek T3000 column (6 µm) and one Viscotek LT4000L column (7 µm). HPLC dual piston pump was set with a flow rate of 1 mL/min. The eluent (THF) was previously filtered through a 0.2 µm filter. The system was also equipped with an on-line degasser. The tests were done at 30 °C using an Elder CH-150 heater. Before the injection (100 µL), the samples were filtered through a PTFE membrane with 0.2 µm pore. The system was calibrated with narrow polystyrene standards. Molecular weight (M_n^{SEC}) and M_w/M_n of synthesized polymers were determined by Multidetectors calibration ($dn/dc_{\text{PMMA}} = 0.085 \text{ mL} \cdot \text{g}^{-1}$) using the OmniSEC software version: 4.6.1.354.

The chromatographic parameters of PMMA-Br and PGMA-Br SEC set-up from Viscotek (Viscotek TDAmx) equipped with differential viscometer (DV) and right-angle laser-light scattering (RALLS, Viscotek) and refractive index (RI) detectors. The column set consisted of a PLgel 5 µm guard column followed by one Viscotek T5000 column, one Viscotek T4000 column. A dual piston pump was set with a flow rate of 1 mL/min. The eluent (DMF with 0.03% LiBr) was previously filtered through a 0.2 µm filter. The system was also equipped with an on-line degasser. The tests were done at 60 °C using an Elder CH-150 heater. Before the injection (100 µL), the samples were filtered through

a polytetrafluoroethylene (PTFE) membrane with 0.2 μm pore. The system was calibrated with narrow PMMA standards. Molecular weight (M_n^{SEC}) and dispersity (M_w/M_n) of the synthesized polymers were determined by multidetectors calibration using the OmniSEC software version: 4.6.1.354.

The dn/dc of PMMA-*b*-PMBA was calculated following the equation: $dn/dc_{\text{PMMA-}b\text{-PMBA}} = dn/dc_{\text{PMMA}} \times m + dn/dc_{\text{PMBA}} \times n$; where m is the molar fraction of PMMA, and n is the molar fraction of PMBA in the block copolymer calculated from ^1H NMR.

2.3.2. Determination of the dn/dc of the polymers

The dn/dc of pure polymers were determined using a Rudolph J357 automatic refractometer and used for the determination of the M_n^{SEC} by multidetector calibration. Briefly, seven solutions with different concentrations (10, 8, 5, 3, 1, 0.5 and 0 $\text{mg}\cdot\text{mL}^{-1}$) were prepared from a 10 $\text{mg}\cdot\text{mL}^{-1}$ stock solution of pure polymer in the solvent. The RI of each solution was measured at the defined temperature (of Sec analysis) and the results were plotted *versus* the concentration. The dn/dc was given by the slope of the curve. $dn/dc_{\text{PMMA}} = 0.0676 \text{ mL}\cdot\text{g}^{-1}$ in DMF (with 0.03% LiBr) at 60 $^\circ\text{C}$ ($R^2 = 0.995$); $dn/dc_{\text{PGMA}} = 0.0785 \text{ mL}\cdot\text{g}^{-1}$ in DMF (with 0.03% LiBr) at 60 $^\circ\text{C}$ ($R^2 = 0.9964$); $dn/dc_{\text{PEMA}} = 0.0905$ in THF at 30 $^\circ\text{C}$ ($R^2 = 0.9957$); $dn/dc_{\text{PBMA}} = 0.0903$ in THF at 30 $^\circ\text{C}$ ($R^2 = 0.9948$).

2.3.3. Nuclear magnetic resonance

^1H NMR spectra of control experiment between TMG and EBPA were recorded on a Bruker Avance 200 MHz spectrometer. Reaction mixture samples, polymers and initiators spectra were recorded on a Bruker Avance III 400 MHz spectrometer, with a 5-mm TIX triple resonance detection probe. The characterization of the chemical structures of compounds and the determination of the monomer conversion were done by integration of the corresponding peaks using MestRenova software version: 6.0.2-5475.

2.3.4. Matrix assisted laser desorption ionization-time of flight

The PMMA-Br samples was dissolved in THF at a concentration of 5 mg/mL for the MALDI-TOF-MS analysis and *trans*-2-[3-(4-*tert*-Butylphenyl)-2-methyl-2-propenylidene]malononitrile (DCTB, 10 mg/ml in THF) was used as matrix. The dried-droplet sample preparation technique was used to obtain a 1:1 ratio (sample/matrix); an aliquot of 1 μL of each sample was directly spotted on the MTP AnchorChip TM 600/384

TF MALDI target, BrukerDaltonik (Bremen Germany) and, before the sample dried, 1 μL of matrix solution in THF was added and the mixture allowed to dry at room temperature, to allow matrix crystallization. External mass calibration was performed with a peptide calibration standard (PSCII) for the range 700-3000 (9 mass calibration points), 0.5 μL of the calibration solution and matrix previously mixed in an Eppendorf tube (1:2, v/v) were applied directly on the target and allowed to dry at room temperature. Mass spectra were recorded using an Autoflex III smartbeam1 MALDITOF-MS mass spectrometer BrukerDaltonik (Bremen, Germany) operating in the linear and reflectron positive ion mode. Ions were formed upon irradiation by a smart beam laser using a frequency of 200 Hz. Each mass spectrum was produced by averaging 2500 laser shots collected across the whole sample spot surface by screening in the range m/z 500-7500. The laser irradiance was set to 35-40 % (relative scale 0-100) arbitrary units according to the corresponding threshold required for the applied matrix systems

2.3.5. UV/Vis spectroscopy

The UV/Vis studies were performed with a Jasco V-530 spectrophotometer. The measurements were carried out in the 200 –1100 nm range at room temperature. A stock solution of TMG and TMG/ Me_6TREN in DMSO (2 mL) was prepared and added at volume of covets for analysis. The PSs (curcumin and proflavine), the curcumin initiator (CI) and proflavine initiator (PF) were dissolved in DMSO and added to the LB medium at a final concentration of (3.0 mg. mL^{-1}) for analysis. The PS-functionalized polymers (3.0 mg. mL^{-1}) were dissolved in LB medium and the solutions were analyzed.

2.3.6. Voltammetry

Voltammetric analysis was done by researcher from the Department of Chemical Science of the University of Padova, Italy. Electrochemical studies on the Cu catalyst were carried out in a 5-neck electrochemical cell, equipped with three electrodes and connected to an Autolab PGSTAT30 potentiostat/galvanostat (Metrohm AG, The Netherlands) run by a PC with GPES software. A glassy carbon (GC) disk electrode, fabricated from a 3 mm diameter rod (Tokai GC-20), was used as working electrode. Before each experiment, the disk was cleaned by polishing with a 0.25- μm diamond paste, followed by ultrasonic rinsing in ethanol for 5 min. The counter electrode was a Pt wire. The reference electrode was $\text{Ag}|\text{AgI}|\text{I}^-$ 0.1 M *n*- Bu_4NI in DMF. Ferrocene (Fc) was added at the end of each

experiment as internal standard, to refer all potentials to the ferrocenium/ferrocene ($\text{Fc}^+|\text{Fc}$) redox couple. The cell was thermostated at $T = 25\text{ }^\circ\text{C}$, and all experiments were performed under inert atmosphere (Ar).

2.3.7. Dynamic light scattering (DLS)

DLS measurements were performed on a Zetasizer Nano-ZS instrument (Malvern Instrument Ltd., UK). The measurements were made at $25\text{ }^\circ\text{C}$, $\lambda = 632.8\text{ nm}$, using backward scattering angle of 173° . All samples were dissolved in LB bacterial growth medium at their MIC.

2.3.8. Scanning electron microscopy (SEM)

An *E. coli* bacterial suspension of approximately $10^8\text{ cells mL}^{-1}$ in saline solution was incubated in the presence or absence of polymers for 5 h at $37\text{ }^\circ\text{C}$. Co-incubation of *E. coli* and polymers were tested at the MIC for each polymer. Cells were harvest by centrifugation and washed in phosphate buffered saline (PBS). Washed cells were adhered to steel slides and fixed twice with 2.5% glutaraldehyde for 10 min at room temperature. The slides were dehydrated using a series of graded ethanol solutions (70, 80, 90, 95 and 100%) for 15 min at room temperature before drying. The dehydrated samples were gold-coated for 20 sec and imaged under high vacuum using a Zeiss Merlin FEG-SEM microscope.

2.3.9. Live/dead membrane integrity assay

Similarly, to the SEM sample preparation, an *E. coli* bacterial suspension of $10^8\text{ cells mL}^{-1}$ in PBS was incubated in the presence or absence of polymer for 5 h at $37\text{ }^\circ\text{C}$. Co-gmincubation of *E. coli* and polymers was tested at the MIC for each polymer. Cells were harvest by centrifugation and washed in 1x PBS. Washed cells were stained with $3\text{ }\mu\text{L}$ of SYTO 9 and propidium iodine (PI) mixed solution (L7007 LIVE/DEAD BacLight Bacterial Viability Kit, Invitrogen) and incubated at room temperature for 15 min in dark conditions. $5\text{ }\mu\text{L}$ of dyed bacterial suspension was placed on a glass slide and covered with glass cover slip. Cells were visualized under a fluorescence Axioskop 2 Plus microscope using FITC and Rhodamine filters. SYTO 9 (green dye) stains both live and dead cells, while PI (red dye) stains only dead cells. At least 100 cells in triplicates were counted in each experiment.

Chapter 3 – Results and discussion

3.1. Guanidine as inexpensive dual function ligand and reducing agent for ATRP of methacrylates

TMG, an inexpensive and commercially available organic base, was used for the first time as ligand without any chemical modification for the ATRP of different methacrylates, namely MMA, DPA, BMA and GMA (Figure 3.7). Preliminary polymerizations of MMA using TMG as the ligand were conducted by loading the Schlenk reactor with monomer (MMA) and initiator (EBPA) (Figure 3.1), followed by a solution of solvent and catalyst (CuBr_2/TMG in DMSO).

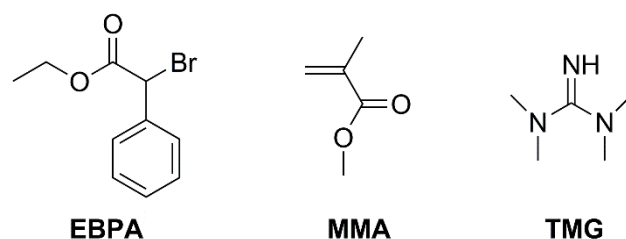


Figure 3.1. Chemical structures of the EBPA initiator, MMA monomer and the ligand TMG.

Then, Cu^0 was added to the reactor, which was immediately frozen in liquid nitrogen and degassed by freeze-thaw cycles. However, results showed a large deviation between experimental (M_n^{SEC}) and theoretical (M_n^{th}) molecular weights, suggesting a low initiation efficiency (Figure 3.2, $I_{\text{eff}} = M_n^{\text{th}}/M_n^{\text{SEC}} \times 100$). Also, the kinetic results were not reproducible (Table A.1). It was then hypothesized that unwanted interactions between TMG and EBPA could have been occurring during the preparation of the mixture and/or during the degassing process. To confirm this, a mixture of EBPA and TMG in deuterated chloroform was analyzed by ^1H NMR and the results showed that TMG could abstract Br from EBPA (Figures A.1-3), thus consuming part of the initiator before polymerization. Therefore, to avoid any unwanted interactions, the experimental procedure was modified. Solutions of the catalyst in DMSO and EBPA in MMA were separately degassed by nitrogen bubbling and subsequently added to a nitrogen flushed Schlenk reactor containing the activated Cu^0 wire, to decrease the contact time between ligand and initiator. Remarkably, reproducible kinetic results were achieved only due to the new procedure adopted. Also, the I_{eff} increased from 22% up to 78%, proved by the good agreement between M_n^{th} and M_n^{SEC} values (Figure 3.2 (b)). The results suggest that $[\text{Cu}^{\text{I}}\text{TMG}]^+$ active

species are readily formed at the beginning of the reaction. Also, considering the results obtained, the activation of EBPA by the $[\text{Cu}^{\text{I}}\text{TMG}]^+$ complex is faster than the reaction between TMG and EBPA. All polymerizations reported here were prepared with this new procedure, as described in the experimental section. Surprisingly, to the best of my knowledge, the use of TMG as ligand for ATRP has never been reported even on the publications dealing with TMG derivatives.

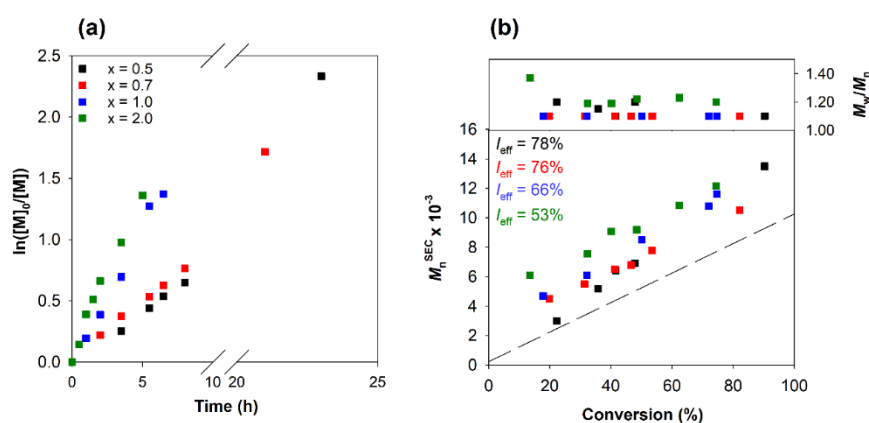


Figure 3.2. Kinetic plots of (a) $\ln([M]_0/[M])$ vs. time and (b) M_n^{SEC} and M_w/M_n vs. monomer conversion for the SARA ATRP of MMA at 30 °C in DMSO using different molar ratios of ligand (0.5; 0.7, 1.0 and 2.0). Conditions: $[\text{MMA}]_0/[\text{DMSO}] = 2/1$ (v/v); $[\text{MMA}]_0/[\text{EBPA}]_0/[\text{CuBr}_2]_0/[\text{TMG}]_0 = 100/1/0.1/x$; Cu^0 wire: $l = 5.0$ cm, $d = 1$ mm.

Kinetics studies were conducted using different molar ratios of the ligand in relation to the initiator and the effect over the polymerization was evaluated. The results expressed by the semilogarithmic kinetic plots of $\ln([M]_0/[M])$ versus time for the SARA ATRP of MMA (Figure 3.2 (a)), showed that the polymerization was first-order with respect to monomer conversion, which is typical of a RDRP process. In addition, increasing the molar ratio of ligand from 0.5 up to 1.0, not only increased the rate of polymerization, but also improved the control over the molecular weight, giving PMMA with low dispersity throughout the reaction ($M_w/M_n < 1.2$ in Figure 3.2 (b)). This behavior has been also observed in other SARA ATRP systems.³⁸ On the other hand, the initiation efficiency increased from 53% to 78%, with decreasing TMG ratio, possible due to the decrease of side reactions between EBPA and excess TMG (Figure 3.2 (b)).

3.1.1. Influence of the targeted degree of polymerization

The targeted degree of polymerization (DP) is one of the most critical factors on the polymerization kinetics since it determines the concentration of radicals. For high DP values, the maximum monomer conversion and the control over the polymerization could be compromised.¹⁸² In this study, the targeted DP of MMA was varied from 50 to 250 (Figure 3.3) and the molar ratio of Cu/ligand was maintained, so that the copper concentration relative to MMA decreased with increasing DP values. In agreement with previous reports,¹⁸³ results revealed that the rate of polymerization decreased with increasing target DP. However, in this DP range, the catalyst mediated the polymerization of MMA in an efficient manner, as evidenced by the good control observed ($M_w/M_n \sim 1.2$) and $I_{\text{eff}} = 92\%$. Another very important observation concerns the decrease of the amount of soluble copper from 2,000 ppm to 400 ppm when the value of the DP increased from 50 to 250, with no deleterious effect on the polymerization control (Figure 3.3 (b)).

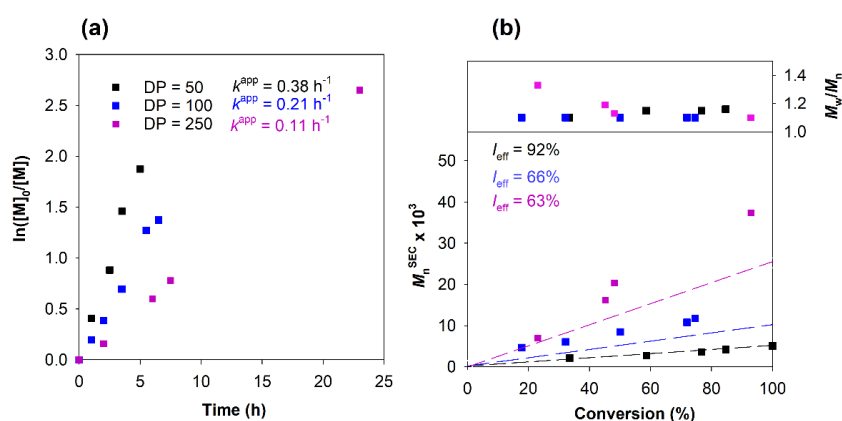


Figure 3.3. Kinetic plots of (a) $\ln([M]_0/[M])$ vs. time and (b) M_n^{SEC} and M_w/M_n vs. monomer conversion for the SARA ATRP of MMA at 30 °C in DMSO using different molar ratios of ligand. Conditions: $[MMA]_0/[DMSO] = 2/1$ (v/v); $[MMA]_0/[EBPA]_0/[CuBr_2]_0/[TMG]_0 = DP/0.1/1$; Cu^0 wire: $l = 5.0$ cm, $d = 1$ mm.

Furthermore, well-controlled high molecular weight PMMA-Br ($M_n^{\text{SEC}} = 1.0 \times 10^5$; $M_w/M_n = 1.2$) was prepared with only 100 ppm of $CuBr_2$, showing that TMG can efficiently promote the polymerization even using low catalyst loading. The I_{eff} decreased with increasing the DP (Figure 3.3 (b)) and the values presented here demonstrated to be lower than the ones reported for the SARA ATRP of MMA using either PMDETA ($I_{\text{eff}} = 96\%$) or dNbpy ($I_{\text{eff}} = 97\%$) as ligands. However, TMG showed comparable performance in terms of control ($1.2 > M_w/M_n > 1.1$), (representative SEC trace available in Figure A.4).¹⁸⁴

Therefore, this data associated with the much lower price of TMG compared with other ligands demonstrates the potential of this ligand to be used in large scale production of PMMA with well-defined structure *via* ATRP.

3.1.2. Evaluation of the polymer chemical structure and chain-end functionality

MALDI mass spectra of PMMA prepared *via* ATRP usually exhibit several isotopic peak distributions.¹⁸⁵ In Figure 3.4, the highest main series is attributed to a PMMA-Br polymer chain showing ion forms of single alkali metal adduct (structure (I) + K⁺), where R-Br is the EBPA initiator.

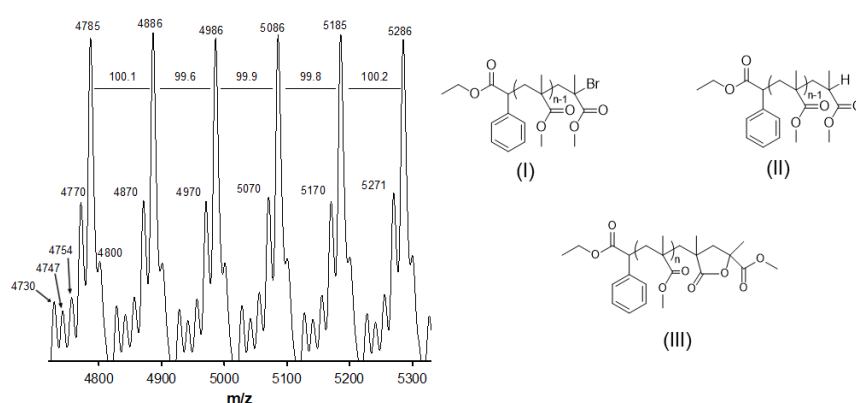


Figure 3.4. Enlargement of the MALDI from m/z 4700 to 5350 of PMMA-Br ($M_n^{SEC} = 7000$, $M_w/M_n = 1.14$), obtained by Cu⁰-mediated SARA ATRP using TMG as ligand.

The series of peaks at 4770 is assigned to a PMMA-Br polymer chain with ion forms of a single alkali metal adduct (structure (I) + Na⁺). Studies show that MALDI-ToF-MS may induce the loss of the methyl halide of PMMA prepared *via* ATRP leading to the formation of lactones (structure III).¹⁸⁶ This is evidenced in two series of peaks, the series attributed to these chains appear at 4800 (structure (III) + K⁺) and at 4754 (structure (IV), only). The signal appearing at 4747 is associated to PMMA-Br chains (structure (I), only). It was already reported the occurrence of PMMA with a H end-group (structure (II)) as minor species, the peak appearing at 4730 which was attributed to these chains. ¹H NMR analysis (Figure 3.5) also proved the chemical structure of the well-defined PMMA-Br, with the assignment of the proton's resonances in agreement with the ones published in the literature.¹⁸⁷

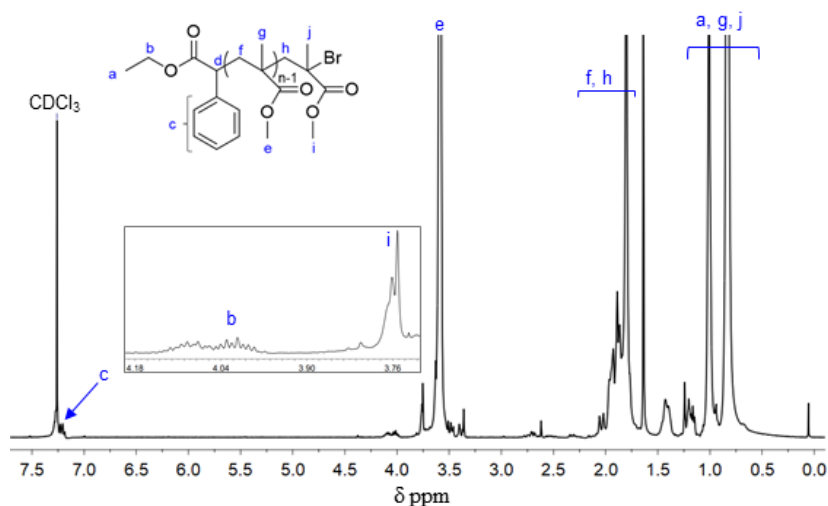


Figure 3.5. ^1H NMR spectrum in CDCl_3 of PMMA-Br prepared by SARA ATRP ($M_n^{\text{SEC}} = 7000$, $M_w/M_n = 1.14$), obtained by Cu^0 -mediated SARA ATRP using TMG as ligand.

The “livingness” of PMMA-Br prepared by SARA ATRP was confirmed by a chain extension experiment by “one-pot” polymerization. First, PMMA-Br macroinitiator was obtained at high MMA conversion (93%) following the previously described procedure. Next, the desired amount of degassed MMA was injected into the polymerization mixture, which reacted further until a substantial shift of the molecular weight distribution traces was observed (Figure 3.6). The complete shift towards high molecular weights, along with the absence of low molecular weight tailing, proves the high chain-end functionality of PMMA-Br prepared by the reported system. The good agreement between M_n^{th} and M_n^{SEC} shows high I_{eff} .

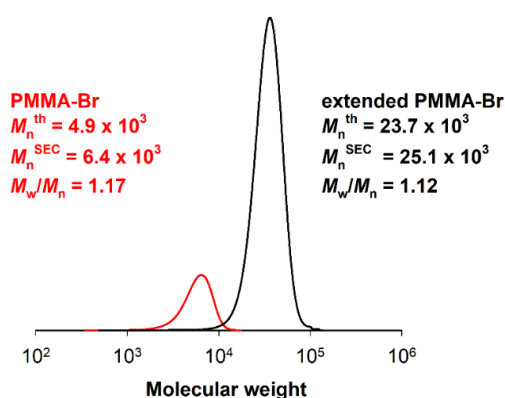


Figure 3.6. SEC traces of the PMMA-Br macroinitiator (red line) and the extended PMMA-Br (black line) prepared by “one pot” SARA ATRP in DMSO at 30 °C. Conditions: first block – $[\text{MMA}]_0/[\text{EBPA}]_0/[\text{CuBr}_2]_0/[\text{TMG}]_0 = 50/1/0.1/1$; Cu^0 wire: $l = 50$ mm, $d = 1$ mm; $[\text{MMA}]_0/[\text{DMSO}] = 2/1$ (v/v), $\text{conv.}_{\text{MMA}} = 93\%$; second block – $[\text{BMA}]_0/[\text{EBPA}]_0 = 350$, $\text{conv.}_{\text{MMA}} = 53\%$.

3.1.3. Polymerization of other methacrylates

Using optimized reaction conditions, the polymerization was extended to other methacrylates with different functional groups, such as GMA, EMA, BMA and DPA (Figure 3.7).

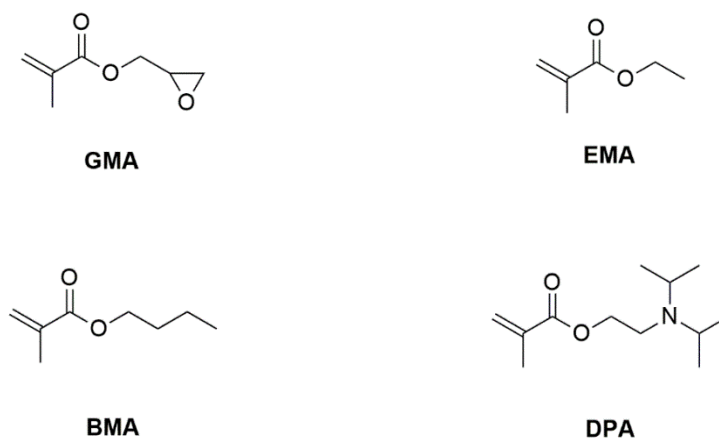


Figure 3.7. Chemical structures of the methacrylates polymerized by SARA ATRP using TMG as the ligand.

For each monomer, low dispersity ($M_w/M_n < 1.5$) and high conversion (Table 3.1) were obtained, showing again the versatility of TMG as an economically affordable and compatible ligand for the polymerization of diverse methacrylates.

Table 3.1. Reaction conditions and results of the polymerization of several methacrylates by SARA ATRP using TMG as the ligand at $T = 30\text{ }^\circ\text{C}$.

ATRP system	Time (h)	Conv. (%)	$M_n^{\text{th}} \times 10^{-3}$	$M_n^{\text{SEC}} \times 10^{-3}$	M_w/M_n
[MMA]/[EBPA] ₀ /[TMG] ₀ /[CuB ₂] ₀ = 200/1/1/0.1	48	79	22.6	37.3	1.31
^b [EMA] ₀ /[EBPA] ₀ /[TMG] ₀ /[CuB ₂] ₀ = 100/1/1/0.1	8.0	72	8.34	10.7	1.26
^b [BMA] ₀ /[PMMA-Br] ₀ /[TMG] ₀ /[CuB ₂] ₀ = 200/1/1/0.1	16	70	27.9	35.2	1.06
^b [DPA] ₀ /[PEG-Br] ₀ /[TMG] ₀ /[CuB ₂] ₀ = 100/1/1/0.1	25.5	86	20.1	20.9	1.24

[MMA]₀/[DMF] = 2/1, SARA agent: Fe⁰ powder; ^b[M]₀/[DMSO] = 2/1 (v/v), SARA agent: Cu⁰ wire.

It is worth mentioning that TMG showed similar performance in terms of control in comparison with other ligands commonly used in ATRP. For example, tris(2-pyridylmethyl)amine (TPMA) is an excellent ligand (Cu/TPMA) to afford PGMA with low dispersity ($M_w/M_n < 1.24$).¹⁸⁸ Likewise, dNbpy is a versatile and suitable ligand to prepare diverse polymethacrylates with good control, including PEMA and PBMA.¹⁸⁴ Comparatively, the dispersity of PDPA was in the same range of that obtained by SARA ATRP using Me₆TREN as the ligand ($M_w/M_n \sim 1.2$).¹⁸⁹ The chemical structure of the (co)polymers was confirmed by ¹H NMR spectroscopy (Figures A.6 to A.9).

3.1.4. Dual behavior of TMG: ligand and reducing agent

In the course of this work, it was observed that some preliminary polymerization mixtures lost their typical greenish color associated with CuBr₂. Based on such observations, it was hypothesized that TMG could act as ligand and reducing agent for copper simultaneously. This prompted a further investigation of the MMA polymerization in the absence of SARA agent copper wire. Three molar ratios of TMG (0.7, 1.0 and 2.0 in respect of the initiator) were used. The experiment at molar ratio 0.7 of TMG showed a limited monomer conversion (Figure 3.8 (a) and (b)).

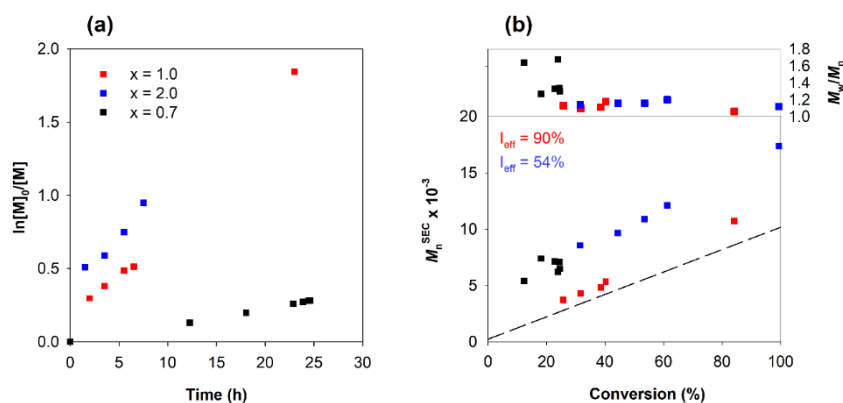


Figure 3.8. Kinetic plots of (a) $\ln([M]_0/[M])$ vs. time and (b) M_n^{SEC} and M_w/M_n vs. monomer conversion for the SARA ATRP of MMA at 30°C in DMSO using different molar ratios of TMG. Conditions: $[MMA]_0/[DMSO] = 2/1$ (v/v); $[MMA]_0/[EBPA]_0/[CuBr_2]_0/[TMG]_0 = 100/1/0.1/x$.

The kinetic plots illustrated in Figure 3.8a revealed a first-order kinetic relating to monomer conversion and the rate of polymerization increased with the increase of the TMG molar ratio from 0.7 to 2.0. On the other hand, the initiation efficiency was substantially affected when a TMG ratio of 2.0 was used, potentially due to the side reaction between the initiator

and excess of ligand Figure 3.8b. Surprisingly, $I_{\text{eff}} = 90\%$ was observed when TMG ratio was 1.0, being this value higher than the one obtained in similar conditions but in the presence of Cu^0 wire ($I_{\text{eff}} = 78\%$). The control of the molecular weight of PMMA-Br was very good throughout the reaction ($M_w/M_n \sim 1.2$), proving that TMG can act as both ligand and reducing agent. In this case, the polymerization could be ruled by either ARGET ATRP, if TMG only acts as reducing agent, or SARA ATRP, if this ligand can also activate dormant chains. To clarify the mechanism, UV-Vis spectra of the catalyst in DMSO were recorded over time to evaluate the formation of $[\text{Cu}^{\text{I}}\text{TMG}]^+$ and the possible reducing agent behavior of TMG. Surprisingly, UV spectra (Figure 3.9 (a)) did not show the typical profile of $[\text{CuLBr}]^+$ (see $\text{CuBr}_2/\text{Me}_6\text{TREN}$ example spectra in Figure 3.9 (b)).

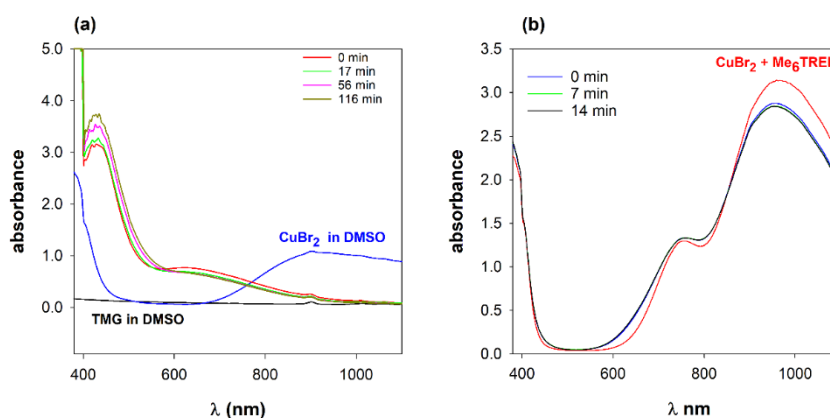


Figure 3.9. UV-vis spectra recorded at different times ($T = 30\text{ }^{\circ}\text{C}$) of (a) CuBr_2/TMG in DMSO; $[\text{CuBr}_2]_0/[\text{TMG}]_0 = 0.1/1.0\text{ mmol/mL}$ and (b) $\text{CuBr}_2/\text{Me}_6\text{TREN}/\text{TMG}$ in DMSO; $[\text{TMG}]_0/[\text{CuBr}_2]_0/[\text{Me}_6\text{TREN}]_0 = 1.0/0.1/0.15\text{ mmol/mL}$.

However, an increase in the absorbance arising at approximately $\lambda = 430\text{ nm}$ only for the catalyst in DMSO may suggest the formation of the lower state oxidation metal/ligand complex.¹⁹⁰ Contrarily, this absorbance at such wavelength was not observed in the profiles of the control solutions (CuBr_2 in DMSO and TMG in DMSO). It is interesting to note that the typical CuBr_2/TMG spectrum (Figure 3.9 (a)) also shows strong and saturated absorption in the blue/violet region leading to the hypothesis that some photo-mediated effect could be occurring during the polymerizations.^{191, 192} To exclude this hypothesis, MMA was polymerized also in the dark. Results revealed a remarkable agreement between both polymerization kinetics and control of the molecular weight of the polymer, excluding the influence of light on the results of this study (see Figure A.11). Yet, it was not possible to observe significant changes in the UV-Vis spectra (Figure 3.9 (a)). Alternatively, the

reduction of $[\text{Cu}^{\text{II}}\text{Me}_6\text{TRENBr}]^+$ by TMG in DMSO was estimated. The spectrum in Figure 3.9 (b) shows a reduction of the intensity of the peak around 980 nm assigned to the complex $[\text{Cu}^{\text{II}}\text{Me}_6\text{TRENBr}]^+$ over time.³⁷ Finally, PMMA-Br near to complete conversion (conv. > 98%, $M_n^{\text{SEC}} = 18.2 \times 10^3$, $M_w/M_n \approx 1.04$) was obtained using $\text{CuBr}_2/\text{PMDETA}$ as the catalyst and TMG as the reducing agent, proving that TMG regenerates Cu^{I} from Cu^{II} .

The potential supplemental activation of dormant species by TMG was evaluated with two model experiments. First, MMA was polymerized in the presence of TMG and EBPA (in copper-free system) to verify a possible activation of EBPA by TMG that would start the polymerization. Indeed, as shown in Table 3.2 entry 1, the polymerization occurred *via* free radical polymerization, leading to the formation of a polymer with high dispersity ($M_w/M_n > 1.5$) after 23 h, but with very low monomer conversion (7%). Moreover, the experiment triggered in the absence of EBPA initiator showed that no polymerization occurred after 24 h (Table 3.2 entry 2), showing that TMG itself is not able to initiate polymerization. The ability of TMG to activate copper-free PMMA-Br chains, which are in fact the dormant chains present during polymerization, was also evaluated. Results showed no monomer conversion after 24 h (Table 3.2 entry 2), thus suggesting that the mechanism of the polymerization is ruled by ARGET ATRP.

Table 3.2. Reaction conditions and results for the activation model experiments in DMSO at 30 °C, using TMG.

Entry	Conditions	Time (h)	Conv. (%)	M_n^{th}	M_n^{SEC}	M_w/M_n
1	$[\text{MMA}]/[\text{EBPA}]_0/[\text{TMG}]_0 = 100/1/1$	23	7	0.9	75.9	1.68
2	$[\text{MMA}]_0/[\text{TMG}]_0 = 100/1$	24	0	-	-	-
3	$[\text{MMA}]_0/[\text{PMMA-Br}]_0/[\text{TMG}]_0 = 400/1/1$	24	0	-*	-*	-*

*Same SEC trace as the one of the macroinitiator.

3.1.5. Electrochemical characterizations

Copper complexes with TMG derivatives are known in the literature and some of them were also previously used in ATRP.^{181, 193-196} To the best of my knowledge, TMG has never been used as ligand without structural modifications; for this reason, electrochemical characterization was done to collect more information about its behavior as ligand for ATRP. In DMSO, solvated Cu^+ ions exhibited a reversible peak couple with $E^{\circ} \approx E_{1/2} = -$

0.421 V vs. $\text{Fc}^+|\text{Fc}$, calculated as $E_{1/2} = (E_{\text{pa}} + E_{\text{pc}})/2$ where E_{pa} and E_{pc} are the anodic and cathodic peak potentials. The addition of 1 equivalent of TMG to Cu^+ ions changed the color of solution from very pale blue to pale green. The peak couple decreased in intensity becoming more stretched, the potential shifted to more positive value $E_{1/2}[\text{Cu}^{\text{I}}\text{TMG}] = -0.382$ V vs $\text{Fc}^+|\text{Fc}$, which indicates a better stabilization of Cu^{I} with respect to Cu^{II} . The addition of a second equivalent of ligand, reduced again the intensity of the peak couple while not affecting $E_{1/2}$. At the third equivalent, the peak couple disappeared in the electrochemical window, suggesting the quantitative formation of another electrochemical specie (Figure 3.10 (a) which is a redox couple in another electrochemical window. The decrease of current, at the first equivalent of TMG, was likewise observed starting from solvated Cu^{2+} ions (Figure 3.10 (b)).

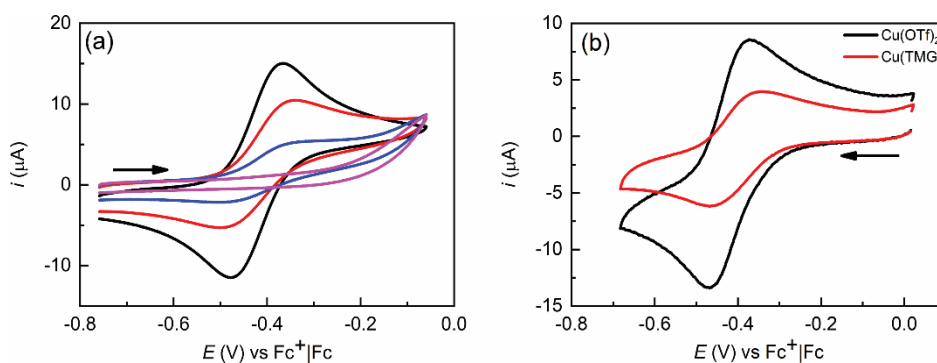


Figure 3.10. (a) Cyclic voltammetry of 1.1 mM $\text{Cu}^{\text{I}}(\text{CH}_3\text{CN})\text{BF}_4$ in the presence of 0 (—), 1 (—), 2 (—) and 3 (—) equivalents of TMG; (b) cyclic voltammetry of 1.0 mM $\text{Cu}^{\text{II}}(\text{OTf})_2$ in the presence of 0 (—) and 1 (—) equivalents of TMG. CV are recorded in DMSO + 0.1 M Et_4NBF_4 at 25 °C, on a GC electrode at 0.2 V/s. The arrow shows the scan direction.

Starting from solvated Cu^{2+} ions in the presence of 1 eq of TMG, the voltammetric response was analyzed more in detail. The addition of a second equivalent of TMG changed dramatically the shape of the voltammetry: the original $[\text{Cu}^{\text{II}}(\text{TMG})]^{2+}$ signal disappeared and a broad irreversible reduction wave was observed at $E_{\text{pc}} = -1.26$ V vs $\text{Fc}^+|\text{Fc}$. This is consistent with the quantitative formation of a new electroactive specie, possibly $[\text{Cu}^{\text{II}}(\text{TMG})_2]^{2+}$, markedly more stable than $[\text{Cu}^{\text{II}}(\text{TMG})]^{2+}$. The addition a third equivalent of TMG shifted the reduction peak to $E_{\text{pc}} = -1.33$ V vs $\text{Fc}^+|\text{Fc}$, possibly again more stable than $[\text{Cu}^{\text{II}}(\text{TMG})_2]^{2+}$.

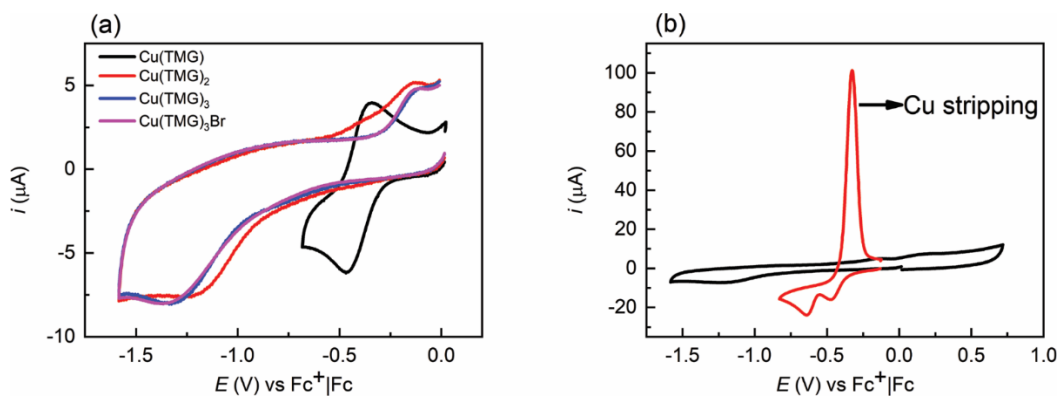


Figure 3.11. (a) Cyclic voltammetry of 1.05 mM $\text{Cu}^{\text{II}}(\text{OTf})_2$ in the presence of 1 (—), 2 (—), 3 (—) equivalents of TMG and 3 equivalents of TMG + 1 equivalent of TEABr (—); (b) cyclic voltammetry of 1.05 mM $\text{Cu}^{\text{II}}(\text{OTf})_2$ in the presence of 3 (—) and 0 (—) equivalents of TMG. Sharp oxidation peak corresponds to Cu stripping from electrode surface. CV are recorded in DMSO + 0.1 M Et_4NBF_4 at 25 °C, on a GC electrode at 0.2 V/s.

One equivalent of bromides changed only slightly the electrochemical pattern: the new reduction peak was recorded $E_{\text{pc}} = -1.38$ V vs $\text{Fc}^+|\text{Fc}$. The slight shift to more negative potentials is compatible with the stabilization of $[\text{Cu}^{\text{II}}(\text{TMG})_3\text{Br}]^+$ with respect to $[\text{Cu}^{\text{II}}(\text{TMG})_3]^{2+}$, suggesting also the coordination of the bromine atom to the metallic center. It is noteworthy to mention these CVs with a relatively negative inversion potential (-1.6 V vs $\text{Fc}^+|\text{Fc}$) did not show, on the anodic wave, the appearance of typical sharp peak of metallic copper stripping from electrode surface. This indicates that Cu^{I} species in solution are stable and not reduced to metallic copper in the electrochemical window of interest (Figure 3.11 (b)). Nevertheless, the electrochemical behavior so far described differs sensibly to that of the typical copper complexes with polydentate amine ligands (*e.g.* $[\text{Cu}^{\text{II}}\text{TPMA}]^{2+}$).

By analyzing this very complex electrochemical response and previous successful experimental evidence from polymerizations, the following assumptions are formulated: i) at least 3 molecules of TMG are needed to form a new Cu^+ complex; ii) the possibility of triggering the polymerization in a controlled manner ($M_w/M_n < 1.3$) clearly points out that hypothetical species such as $[\text{Cu}^{\text{I}}(\text{TMG})_3]^+$ and $[\text{Cu}^{\text{II}}(\text{TMG})_3\text{Br}]^+$ are relatively stable and act as activator and deactivator of propagating radicals, respectively; iii) comproportionation in presence of Cu^0 generates at least one Cu^{I} species, possibly $[\text{Cu}^{\text{I}}(\text{TMG})_3]^+$, that activates the dormant macromolecules and molecular initiators; iv) the polymerization proceeds *via* atom transfer mechanism; v) in presence of metallic iron also

at least one Cu^{I} species can be formed, probably the same of point ii), which is an active catalyst as. However, these results cannot rule out the presence of other Cu^{I} and Cu^{II} species in solution that can participate in ATRP equilibrium.

3.1.6. Conclusions

SARA ATRP of several methacrylates was studied using for the first time the inexpensive TMG as ligand without chemical modifications. The successful and reproducible polymerizations were only achieved after the development of an appropriate reaction setup and degassing procedures. Results showed that $[\text{Cu}^{\text{I}}\text{TMG}]^+$ can trigger controlled polymerizations even at low concentrations of copper (100 ppm). PMMA-Br maintained excellent chain end-functionality, as revealed by the preparation of a well-defined PMMA-Br self-extended homopolymer ($M_w/M_n < 1.15$). Diverse well-controlled polymethacrylates were also synthesized, showing the usefulness of this catalyst for methacrylic monomers. This inexpensive ligand exhibited similar performance in terms of control in comparison to the one obtained with ligands frequently used in SARA ATRP, showing the potential of the TMG as an economically affordable alternative ligand for methacrylates. Voltammetry results showed that Cu^{I} species in solution are stable. Polymerizations carried out in the absence of zero-valent metals show that TMG can have a dual function behavior, namely as ligand and reducing agent. Model experiments suggested that, in this case, the polymerization is ruled by the ARGET ATRP mechanism.

3.2. Development of cationic amphiphilic antimicrobial polymers by SARA ATRP

A novel antimicrobial polymeric system based on the QAS-containing AMPTMA and the hydrophobic monomer *n*-BA was developed by SARA ATRP. In this study, an extensive library consisting of polymers with different composition (homopolymers, random and block copolymers) and architecture (linear and star-shaped) was prepared and the antimicrobial activity was evaluated against both Gram-positive and Gram-negative bacteria. Furthermore, preliminary membrane integrity evaluation was performed to elucidate the mechanistic aspects of the antimicrobial action of the (co)polymers, which showed a bactericidal effect through membrane disruption.

It is known from the literature¹⁹⁷ that a proper balance of hydrophilic cationic segments and hydrophobic regions is a key factor for a polymer to achieve its maximum antimicrobial activity. Therefore, the control over the polymer composition is essential for the preparation of antimicrobial polymers with enhanced performance, which can be achieved by using RDRP techniques. In this work, SARA ATRP was explored for the preparation of cationic amphiphilic antimicrobial copolymers, based on PAMPTMA as the cationic segment and PBA as the hydrophobic domain. Prior work reported by the research group showed that star-shaped PMA-*b*-PAMPTMA block copolymers could be successfully prepared using an eco-friendly SARA ATRP system.¹⁹⁸ Here, the same catalytic system was used for the polymerization of both AMPTMA and *n*-BA. Due to the very different nature of the monomers (AMPTMA is a highly hydrophilic monomer whereas *n*-BA is hydrophobic), the first step was to select an appropriate solvent for the copolymerization. In this case, EtOH enabled homogeneous polymerization, dissolving all monomers and polymers. The successful polymerization of both AMPTMA and *n*-BA by ATRP techniques has already been reported.^{199, 200} However, to best of my knowledge, this is the first time that methods have been developed for the controlled one-pot synthesis of PAMPTMA-*b*-PBA block copolymers by SARA ATRP (Figure 3.12).

First experiments were dedicated to the homopolymerization of either AMPTMA (linear and star-shaped) or *n*-BA (linear) by SARA ATRP in EtOH aiming to define the reaction conditions for a controlled and compatible synthesis of both polymers (Appendix B, Figures B1 to B3). Then, the reaction conditions were optimized for the preparation of the PAMPTMA-*co(b)*-PBA copolymers. Figure 3.13 shows a typical ¹H NMR spectrum of a

PMAPTMA-*co*-PBA copolymer, successfully prepared by SARA ATRP in EtOH at 30 °C. The recorded spectrum shows the characteristic signals of the cationic segment appearing at 3.38 ppm, corresponding to the quaternary ammonium group, and an isolated signal of the PBA segment at 4.55 ppm, corresponding to the -OCH₂- protons of the ester group.²⁰¹

202

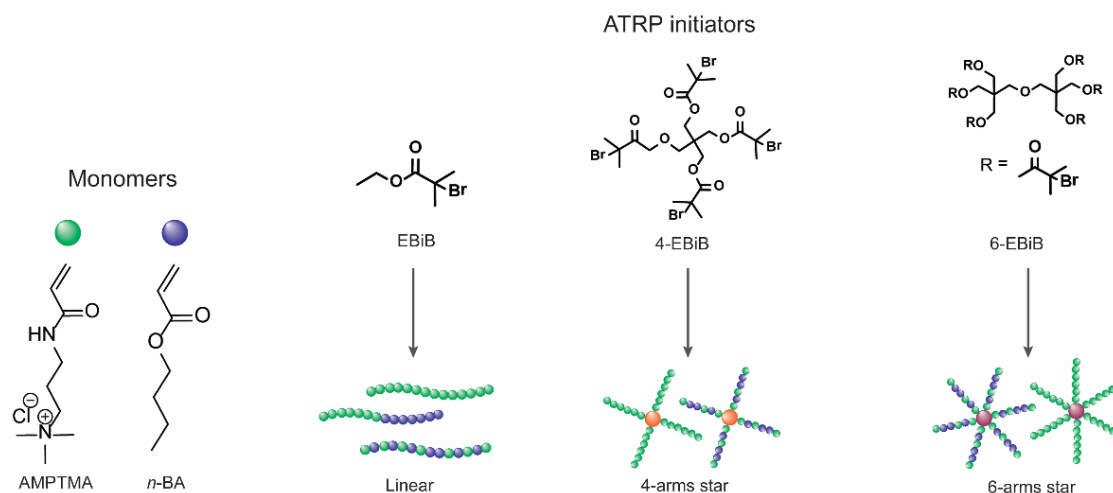


Figure 3.12. General structures of the monomers (AMPTMA and *n*-BA), initiators (EBiB, 4-EBiB and 6-EBiB), and representation of linear and star-shaped (PAMPTMA-Br, PAMPTMA-*co*-PBA or PAMPTMA-*b*-PBA) (co)polymers prepared by SARA ATRP.

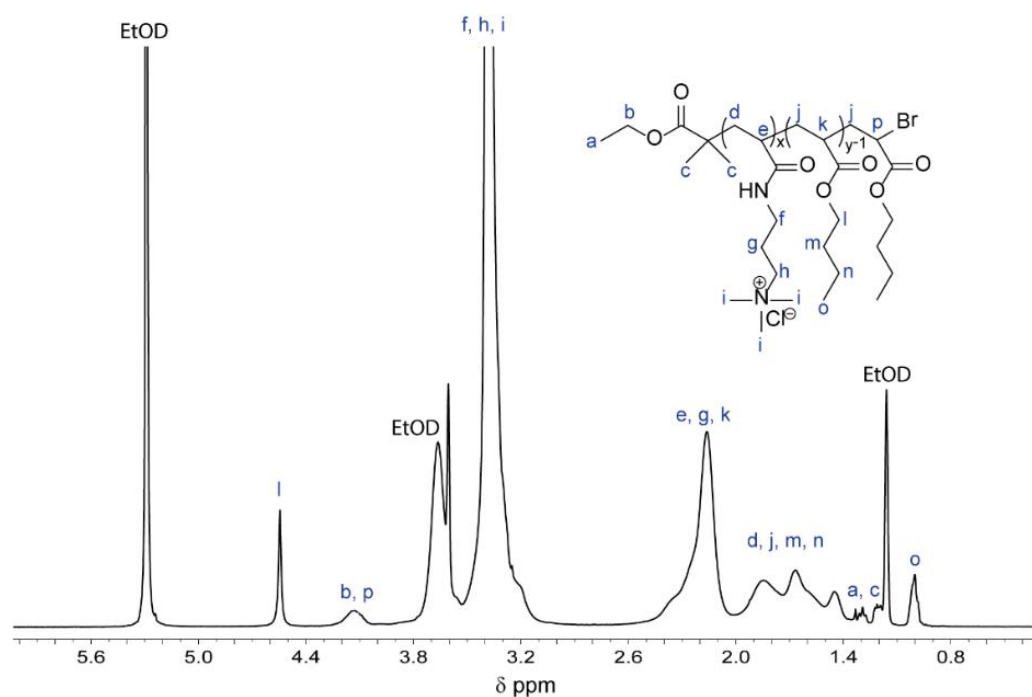


Figure 3.13. 400 MHz ¹H NMR spectrum in *d*₆-EtOD of purified PAMPTMA₅₀-*co*-PBA₁₅ copolymer ($M_n^{\text{th}} = 12.4 \times 10^3$) obtained by SARA ATRP.

Using the developed SARA ATRP method, a library of different amphiphilic (co)polymers was prepared by targeting several parameters: molecular weight (MW), the mole fraction of the hydrophobic segment (PBA), and architecture of the polymers (Table 3.3 and Appendix B, Table B2). PAMPTMA and PBA homopolymers were also synthesized and used as control samples. It is worth mentioning that the systematic study of the antimicrobial efficiency requires the preparation of polymers with diverse characteristics (*e.g.*, composition, architecture, etc.), which can only be achieved using advanced polymerization techniques, such as the SARA ATRP, ARGET, photo-ATRP, eATRP and sono-ATRP.²⁰³⁻²⁰⁷ The samples were labelled according to the architecture and composition of the (co)polymers to facilitate the interpretation of the results: L – linear random (co)polymer or homopolymer; Lb – linear block copolymer; 4S – 4-arm star; 6S – 6-arm star; A – PAMPTMA segment followed by the correspondent DP value; B – PBA segment followed by the correspondent DP value. As an example, the sample LA27B33 (Table 3.3, entry 12) is a linear random copolymer with 27 units of PAMPTMA and 33 units of PBA.

For the determination of the MW parameters of the copolymers, SEC analysis using a refractive index detector and EtOH as the eluent was carried out. However, unfortunately, it was found that the cationic segment (PAMPTMA) interacted with the column (Shodex Asahipak® 5 µm GF-510 HQ, LC Column 300 x 7.5 mm) either in the form of homopolymer or as a segment of the copolymers, which avoided the acquisition of chromatograms. Even with the addition of stabilizers (*e.g.*, amines, LiBr, etc.) to the eluent, there was no separation of the polymers. Only the PBA homopolymer eluted properly in the conditions described. Therefore, for this study, the molecular weight used for the characterization of the polymers was the M_n^{th} (Table 3.3), considering that the polymerization of both monomers is well-controlled and gives polymers with M_n^{SEC} close to the theoretical ones.

3.2.1. Influence of MW and hydrophobicity on polymers' antimicrobial activity

The MW of an antimicrobial polymer has been previously found to play an important role in bacterial death induction.²⁰⁸ Recent studies have demonstrated bacterial inactivation and/or death by low MW polymers,^{118, 209, 210} based on the fact that such structures can easily diffuse through the lipid membrane.

Table 3.3. Characteristics of the antimicrobial polymers prepared by SARA ATRP.

Entry	Polymer code	Topology	Composition	DP PAMPTMA*	DP PBA*	M_n^{thx} 10^{-3}	% PBA (molar)
1	6SA114B0	6-arm star	homopolymer	114	0	142.0	0
2	6SA69B41	6-arm star	random copolymer	69	41	117.4	37
3	6SA79B24	6-arm star	random copolymer	79	24	117.3	23
4	6SA95B0	6-arm star	homopolymer	95	0	117.0	0
5	6SA22B0	6-arm star	homopolymer	22	0	28.1	0
6	6SA9B0	6-arm star	homopolymer	9	0	12.7	0
7	4SA93B0	4-arm star	homopolymer	93	0	77.6	0
8	4SA84B20	4-arm star	random copolymer	84	20	80.5	20
9	LA38B2	linear	random copolymer	38	2	8.3	5
10	LA34B9	linear	random copolymer	34	9	8.4	20
11	LA23B23	linear	random copolymer	23	23	8.0	50
12	LA27B33	linear	random copolymer	27	33	10.0	56
13	LA50B4	linear	random copolymer	50	4	11.0	7
14	LA45B15	linear	random copolymer	45	15	11.5	24
15	LA39B47	linear	random copolymer	39	47	14.2	55
16	LA115B0	linear	homopolymer	115	0	24.0	0
17	LA98B29	linear	random copolymer	98	29	24.2	23
18	LA59B44	linear	random copolymer	59	44	18.2	42
19	LbA79B47	linear	block copolymer	79	47	22.5	37
20	LbA78B63	linear	block copolymer	78	63	24.4	44
21	LbA68B40	linear	block copolymer	68	40	19.4	37
22	LbA264B33	linear	block copolymer	264	33	59.0	10
23	LA335B0	linear	homopolymer	335	0	68.3	0
24	LA0B49	linear	homopolymer	0	49	6.4	100

* Degree of polymerization (DP) value per star arm

However, since the antibacterial activity largely depends on polycationic charges, high MW can provide a higher number of cationic units thus, increasing the electrostatic forces and simultaneously, the bactericidal effect.^{208, 82} On the other hand, solubility issues, aggregation and interaction with the cell wall barrier could become crucial with MW

increase. Nevertheless, these factors are dependent on both the polymeric system employed and the type of bacteria tested. Here, three series of PAMPTMA-*co*-PBA linear random copolymers with targeted MW values around 8000, 12000 and 24000 were synthesized (Table 3.3, entries 9-18, except entries 15 and 16). In each series, the content of PBA was varied from 0% to 50% intending to evaluate the influence of the hydrophobicity of the polymers on their antimicrobial activity. The efficiencies were investigated by determining the MIC of the polymers (Table 3.2) against a range of Gram-positive (*S. aureus*, *B. subtilis* and *B. cereus*) and Gram-negative (*E. coli* and *P. aeruginosa*) bacteria in liquid medium.

Table 3.4. Characteristics of linear PAMPTMA-*co*-PBA copolymers with different MW values and hydrophobic characters and respective MIC values obtained in liquid medium.

Polymer code	DP _{PAMPTMA} / DP _{n-BA}	% PBA (molar)	M _n th x 10 ⁻³	MIC (μM)**				
				<i>S. aureus</i>	<i>B. subtilis</i>	<i>B. cereus</i>	<i>E. coli</i>	<i>P. aeruginosa</i>
LA38B2	38 / 2	5	8.3	>200	3.1	200	>200	>200
LA34B9	34 / 9	20	8.4	>200	0.8	200	200	>200
LA23B23	23 / 23	50	8.0	>200	28.1	112.5	56.2	>200
LA50B4	50/4	7	11.0	25	0.8	50	200	200
LA45B15	46/ 15	24	11.5	>200	1.5	>200	200	>200
LA27B33	27 / 33	56	10.0	>200	200	200	100	200
LA39B47	39 / 47	55	14.2	200	6.2	25	200	200
LA98B29	100 / 28	21	24.4	200	0.8	200	200	3.1
LA59B44	59 / 44	42	18.2	>200	0.8	>200	100	100
LA115B0*	115 / 0	0	24.0	25	6.2	12.5	200	200
LA335B0*	335/0	0	68.0	2.5	1.2	10	> 40	40

* Homopolymer for control; **MIC values in weight-based concentration are provided in Appendix B, Table B1

For the copolymers with a low percentage of PBA (LA38B2 vs. LA50B4 in Table 3.4), the increase of the MW led to an enhancement of the antimicrobial activity for all Gram-positive and Gram-negative bacteria tested. The same behavior was observed for the PAMPTMA homopolymers used as control samples (LA115B0 and LA335B0 in Table 3.4), as well as for the copolymers with 20% PBA in a less pronounced variation of the MIC values (LA34B9 vs. LA45B15 vs. LA98B29 in Table 3.4). However, for the highest

contents of PBA studied (up to 50 %), the antimicrobial activity of the copolymers was dependent on the bacterial species tested (LA23B23 vs. LA27B33 vs. LA39B47 in Table 3.4). In general terms, the amphiphilic copolymers investigated were more active towards *B. subtilis* bacteria, as judged by the lower MIC values.

While the cationic segments of the polymers provide electrostatic interaction with the negatively-charged bacterial cell wall, the presence of hydrophobic domains within the copolymer structure is also important, since it can allow for a better permeation of the polymer through the bacteria lipid membrane.²¹¹ Several studies have shown that the antimicrobial activity of amphiphilic structures is higher than that of hydrophilic (cationic) analogues^{212, 213} and it increases with the hydrophobicity character of the amphiphilic structures.^{209, 214, 215} However, in this work, the percentage variation of the hydrophobic PBA segment in the copolymers did not influence their antimicrobial activity. Only a small improvement was observed for the samples with MW around 8000 (LA38B2 vs. LA34B9 vs. LA23B23 in Table 3.4), for *B. cereus* and *E. coli*, suggesting that only low MW polymers that could permeate the bacteria lipid membrane can benefit from having hydrophobic domains. Possibly, most of the polymers investigated in this work have high MW (> 10000), preventing them from penetrating the bacterial membrane. The PAMPTMA homopolymers (LA115B0 and LA335B0 in Table 3.4) used as control samples (no hydrophobic domains) showed the broadest spectrum of antimicrobial activity, along with some of the lowest MIC values, compared to the amphiphilic PAMPTMA-co-PBA copolymers. Besides the high MW of the samples, it was hypothesized that the behavior observed in this work might be attributed to the fact that the increase of the hydrophobicity could lead to different self-assembled polymeric structures in aqueous media, consequently reducing the availability of the cationic active polymeric segments, which are responsible for the interaction with the bacterial cell wall.²¹³ To investigate this, DLS analyses of three different representatives amphiphilic copolymers (highest content of PBA, LbA68B40 and LA39B47; lowest content of PBA, LbA264B33), at their respective MIC values in the growth medium used for the antimicrobial activity assays, were performed. The results (Appendix B, Figure B4) showed size distributions in the range of 1 nm up to 10 nm, which suggest that these polymers do not form aggregates but exist as single chains (unimers) at their MIC. Therefore, in this case the effect of polymer aggregation on the antimicrobial activity can be ruled out. The PBA homopolymer (LA0B49 in Table 3.3) did not show any antimicrobial activity against the bacteria strains

investigated. This result highlights the need for a cationic segment in the structure of a polymer in order to exhibit antimicrobial activity.

In summary, this set of results indicates that the antimicrobial activity of the studied copolymers does not show dependence with hydrophobicity, but it is positively influenced by the increase of the MW of the polymers.

3.2.2. Influence of architecture on polymers' antimicrobial activity

The SARA ATRP method is a very useful tool to prepare polymers with distinct architectures, which can result in materials with different antimicrobial performances. Star-shaped polymers have been pointed out as promising antimicrobial agents, with a considerably higher activity than their linear analogues.²¹² Here, new stars PAMPTMA homopolymer and PAMPTMA-*co*-PBA star copolymers were tailored via core-first method to have different number of arms, MW values and hydrophobic contents to investigate the influence of these parameters on their antimicrobial performance (Table 3.3, entries 1-8). The MIC values of the polymers were obtained in liquid medium and the results are shown in Table 3.5.

In general, the MIC values either increased or remained constant with PBA content increase, as previously observed for the linear copolymers. Compared to the star-shaped cationic PAMPTMA homopolymers, the amphiphilic star-shaped copolymer analogues were much less active against bacteria. This effect was highly visible for *S. aureus*, with MIC values at least 8-fold higher than those of the homopolymers (Table 3.5, 6SA114B0 vs. 6SA69B41 and 6SA79B24; 4SA93B0 vs. 4SA84B20). When compared to its star copolymer analogues (4SA84B20 and 6SA79B24 in Table 3.5), the linear copolymer (LA98B29 in Table 3.5) presented higher MIC values, except for *P. aeruginosa*. This decrease in antimicrobial efficacy might be associated with the initial adsorption/binding interaction between polymer and bacteria, which is stronger for star-shaped compared to linear polymers.²¹⁶ Moreover, it is expected that star-shaped polymers present high charge density which provides increased interactions between these polymeric structures and the anionic compounds of the bacterial cell wall.²¹⁷ This behavior has been previously observed by other authors for peptide stars²¹² or nanoparticles formed by self-assembly of linear peptides.²¹⁸ However, for this conclusion it is worth mentioning that the star-shaped polymers have higher molecular weight ($MW_{\text{star}} \approx MW_{\text{linear}} \times \text{number of arms}$) than their

linear analogues since the linear polymers studied are equivalent in MW to one arm of the star. This rationalization has been also used by other authors and could be argued due to the importance of the amounts of positive charges in polymer activity.²¹² The increase of antimicrobial activity from linear to star, in these cases, could be then associated with the increase of the MW of the polymers, as previously observed.

Table 3.5. Characteristic of linear and star-shaped PAMPTMA-*co*-PBA-Br copolymers, PAMPTMA-Br homopolymer and MIC values obtained in liquid medium.

Polymer code	DP _{PAMPTMA} / DP _{n-BA} *	% PBA (molar)	M _n th x 10 ⁻³	MIC (μM)**				
				<i>S. aureus</i>	<i>B. subtilis</i>	<i>B. cereus</i>	<i>E. coli</i>	<i>P. aeruginosa</i>
6-arms star								
6SA114B0	114 / 0	0	142.0	2.5	1.2	10	40	10
6SA22B0	22 / 0	0	28.1	40	5	10	> 40	> 40
6SA9B0	9 / 0	0	12.7	> 40	40	> 40	> 40	> 40
6SA79B24	79 / 24	23	117.3	20	1.2	> 40	> 40	10
6SA69B41	69 / 41	37	117.4	20	0.6	> 40	40	10
4-arms star								
4SA93B0	93 / 0	0	77.6	2.5	1.2	10	40	20
4SA84B20	84 / 20	20	80.5	20	1.2	> 40	40	40
Linear								
LA115B0	115/0	0	24.0	25	6.2	12.5	200	200
LA335B0	335/0	0	68.0	2.5	1.2	10	> 40	40
LA98B29	98/29	23	24.2	200	0.8	200	200	3.1

*DP value per star arm; **MIC values in weight-based concentration are provided in Appendix B, Table B1

The real influence of the architecture could be then evaluated by comparing linear and star-shaped polymers with similar MW values. The results presented in Table 3.5 show that the MIC values of linear and star-shaped PAMPTMA homopolymers (6SA22B0 vs. LA115B0 and 4SA93B0 vs. LA335B0) are in the same range for the bacteria investigated, suggesting that in fact, the architecture itself might not play a key role in the antimicrobial activity. In this case, it seems that the MW of the polymers has a greater influence on their

performance, than the particular shape. The results obtained with star-shaped polymers seem to be only related to the increase in the molecular weight of the polymer (considering the same DP for the star arm). On this matter, the preparation of stars by SARA ATRP is still an advantageous strategy since it is a straightforward route for the synthesis of very high MW polymers, under controlled conditions ($D < 1.5$). The most effective polymers prepared in this work (e.g., 6SA114B0 and 4SA93B0) were active for all the bacteria strains investigated and presented lower MIC values, in particular for Gram-positive, than amphiphilic peptide nanoparticles reported in the literature,²¹⁸ making them excellent candidates for antimicrobial applications. Besides the good performance of the polymers presented in this work, the synthesis via SARA ATRP is much more affordable than the chemistry involving the preparation of polypeptides.

3.2.3. Influence of the structure of copolymers on their antimicrobial activity

As previously mentioned, several studies investigated the role of key factors that control the bactericidal activity of polymers.^{117, 118, 216} Structural parameters such as amphiphilicity,²¹⁹ MW, type and density of cationic charges,²¹⁶ have been shown to influence the biological activity of different polymers. However, there are relatively few reports investigating amphiphilic block copolymers.^{117, 220} Here, the MIC values of amphiphilic PAMPTMA-*co(b)*-PBA random and block copolymers with similar MW and molar ratio of *n*-BA were evaluated to understand if the distribution of the hydrophobic domains within the copolymers affects their antimicrobial activity.

The antimicrobial activity of block copolymers was higher against Gram-positive bacteria when compared to that of random copolymers with similar MW and composition (LA59B44 and LbA68B40 in Table 3.6). Nonetheless, for *E. coli*, the random copolymer presented a better performance, showing a lower MIC value than the analogue block copolymer. These results are in sharp contrast with previous data reported in the literature, showing that the bactericidal activity of random and block amphiphilic poly(vinyl ether)s copolymers was similar against *E. coli*.¹¹⁷ Based on these observations, it seems that the structure of the copolymers could influence their antimicrobial activity depending on the bacterial strain considered and the nature of the monomers. It is then important to investigate the performance of antimicrobial polymers in conditions mimicking those of the targeted application of the materials (e.g., target bacteria strains, *in vivo* or *ex vivo* application, etc.).

Similarly, to what was observed for the random copolymers, the decrease of the hydrophobic content in the block copolymers and the increase in the MW led to an increase of the antimicrobial activity (LbA264B33 sample in Table 3.6 exhibited the lowest MIC values). Overall, block copolymers showed the broadest spectrum of activity and lower MIC values.

Table 3.6. Characteristics of PAMPTMA-*co*-PBA and PAMPTMA-*b*-PBA copolymers and MIC values obtained in liquid medium.

Polymer code	DP _{PAMPTMA} / DP _{n-BA} *	% PBA (molar)	M _n th x 10 ⁻³	MIC (μM)**				
				<i>S. aureus</i>	<i>B. subtilis</i>	<i>B. cereus</i>	<i>E. coli</i>	<i>P. aeruginosa</i>
Block copolymers								
LbA264B33	264 / 33	10	59.0	20	1.2	> 40	> 40	40
LbA68B40	68 / 40	37	19.4	225	0.8	28.1	225	112.5
LbA78B63	78 / 63	44	24.4	200	50	200	200	200
Random copolymers								
LA59B44	59 / 44	42	18.2	> 200	1.5	> 200	100	100
LA98B29	98/29	23	24.2	200	0.8	200	200	3.1

* Calculated from ¹H NMR; **MIC values in weight-based concentration are provided in Appendix B, Table B1

3.2.4. Preliminary studies on cell-polymer interactions

In order to evaluate whether the antimicrobial effect of the polymers was due to loss of bacterial membrane integrity, two distinct approaches to assess membrane damage were used: SEM and fluorescence microscopy, as described in Chapter 2 (Sections 2.3.8 and 2.3.9). For this study, representative PAMPTMA homopolymers and PAMPTMA-*co*-PBA copolymers of each architecture (linear and star-shaped) were selected based on their antimicrobial performance. In both techniques, *E. coli* cells were incubated for 5 h with 4-arm star (4SA84B20 and 4SA93B0, Table 3.3), 6-arm star (6SA114B0 and 6SA69B41, Table 3.3) or linear (LA115B0 and LA98B29, Table 3.3) polymers at a concentration of MIC.

As shown in Figure 3.14, untreated *E. coli* cells exhibited rod-shaped morphology and smooth surface. Treatment of the cells with the star-shaped polymers (4SA84B20, 4SA93B0, 6SA114B0 and 6SA69B41, Table 3.3) caused increased granules at the cell surface (cell debris) and lysed cell morphologies, regardless the number of arms of the stars. Treatment with linear polymers (LA115B0 and LA98B29, Table 3.3) also cause increased cell debris granules at the cell surface, but to a less extent than the star-shaped polymers.

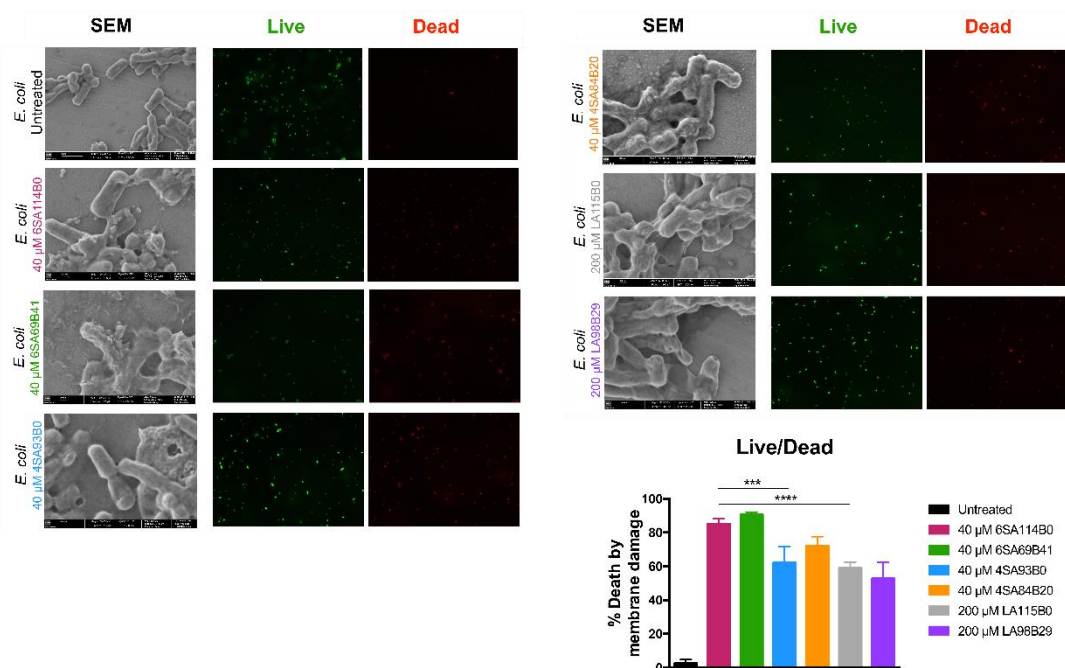


Figure 3.14. SEM and fluorescence microscopy images of *E. coli* cells before and after treatment with 6-arm, 4-arm star-shaped and linear PAMPTMA homopolymers and PAMPTMA-*co*-PBA copolymers. Conditions: 5 h incubation at a concentration of MIC. Live/dead staining shows live (SYTO 09 labelled) green cells and dead (propidium iodide labelled) in red. Percentage of death by membrane damage for untreated, 6SA114B0, 6SA69B41, 4SA84B20, 4SA93B0, LA115B0 and LA98B29-treated *E. coli* cells. At least 100 cells were counted in triplicates for at least two independent experiments. *** $p = 0.0001$; **** $p < 0.0001$.

To further investigate whether the antimicrobial activity of these polymers is in fact due to direct damage of the bacterial membrane, a second approach using live (Syto 09)/dead (propidium iodide) staining was used to assess membrane damage after polymer treatment. In agreement with the SEM results, all tested polymers displayed a significant increase in cell death by membrane damage compared with untreated cells ($p < 0.0001$) (Figure 3.14). In particular, the 6-arm star polymers with the highest MW values (6SA114B0 and 6SA69B41, Table 3.3), exhibited the highest death by membrane damage (85.1 % and 90.5

%, respectively) compared with 2.5 % death in *E. coli* untreated cells. 4SA84B20 and 4SA93B0 (4-arm star polymers, Table 3.3) also showed increased of cell death by membrane damage (72.0 % and 62.1 %, respectively). Linear polymers (LA115B0 and LA98B29, Table 3.3) showed the lowest cell death among all polymer architecture types, but still as high as 58.9 % and 52.7 % for the homopolymer and random copolymer, respectively. When comparing bacterial membrane damage by different amphiphilic polymers, cell damage was higher for copolymers, except in linear ones. This result suggests that polymers with amphiphilic character and high MW increase membrane damage leading to cell death.

3.2.5. Synthesis and evaluation of the antimicrobial activity of the high-branched core cross-linked star-shaped (CCS) PAMPTMA prepared via arm-first

The systematic evaluation of the antimicrobial activity showed that the MW was the most influencing factor on the antimicrobial activity amongst the factors analyzed. Then, to obtain high MW PAMPTMA homopolymers to investigate whether the antimicrobial activity would increase with increasing MW, the arm-first procedure was used for the preparation of a new set of star-shaped polymers named core cross-linked CCS-PAMPTMA. This method, unlike core-first one, allows the preparation of star-shaped polymers with high number of arms by the reaction of a polymer (ATRP initiator) and a divinyl compound (crosslinker, CL). The “one-pot” synthetic procedure was done by preparing a linear Br-terminated PAMPTMA macroinitiator (MI) by SARA ATRP at 30 °C. Then, a degassed solution containing divinyl BAAM (CL) in water was added for the cross-linking reaction and subsequent formation of the star polymers (Figure 3.15). The monomer conversion, as well as the star formation, was closely monitored by both SEC and ¹H NMR.

The MW of the MI precursor was targeted to be 12 000 considering that longer MI chains may present lower mobility and could sterically hinder the incorporation of other MI precursors during the cross-linking reaction, leading to stars with low number of arms and/or unreacted MI chains in the final product.⁵¹ Moreover, as previously mentioned, the [MI]/[CL] molar ratio must be appropriate to prevent macroscopic gelation and guarantee the total incorporation of the MI.²²¹ In this work, several experiments were carried out varying AMPTMA conversion at which the crosslinker was added attaining to obtain fully

formed star polymers. However, none of the experiments performed led to the complete incorporation of the MI and consequently, a mixture of star polymer and linear MI was obtained in all experiments. As an example, Figure 3.16 (a) shows the appearance of a peak on the SEC trace corresponding to the formation of the star polymer and a slight decrease of the MI peak intensity, suggesting that most of the MI chains were already dead by the time the CL was added. This could be probably due to the loss of the bromine chain-end functionality of PAMPTMA-Br during the first step of the synthesis as the CL was injected at very high AMPTMA conversion (98%).

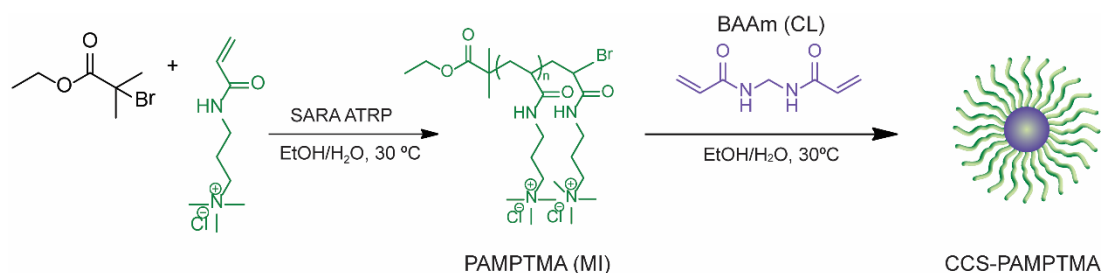


Figure 3.15 Reaction scheme of the preparation of CCS-PAMPTMA via “one-pot” arm-first approach.

To test this hypothesis, the CL was injected at lower AMPTMA conversion (87%). In this case, there was more incorporation of the MI during the cross-linking reaction, as evidenced by the decrease of MI peak intensity and the shift of the SEC curves corresponding of the CSS-PAMPTMA towards lower retention times (higher MW) during the reaction (Figure 3.16 (b)). Nonetheless, much of the MI precursor did not react despite the total conversion of the CL ($\text{Conv.}_{\text{CL}} > 99\%$). These results suggest the loss of the MI chain-end functionality.

Considerable incorporation of MI precursors was achieved by further diminishing the MI conversion at which CL was added to the reaction mixture. SEC traces (Figure 3.16 (c) and (d)) of these attempts show that even when the CL was added at AMPTMA conversion of 81% and 75%, there was always the presence of unreacted MI chains in the final product. However, in a much lower percentage when compared to the previous experiments in which the MI conversion was higher.

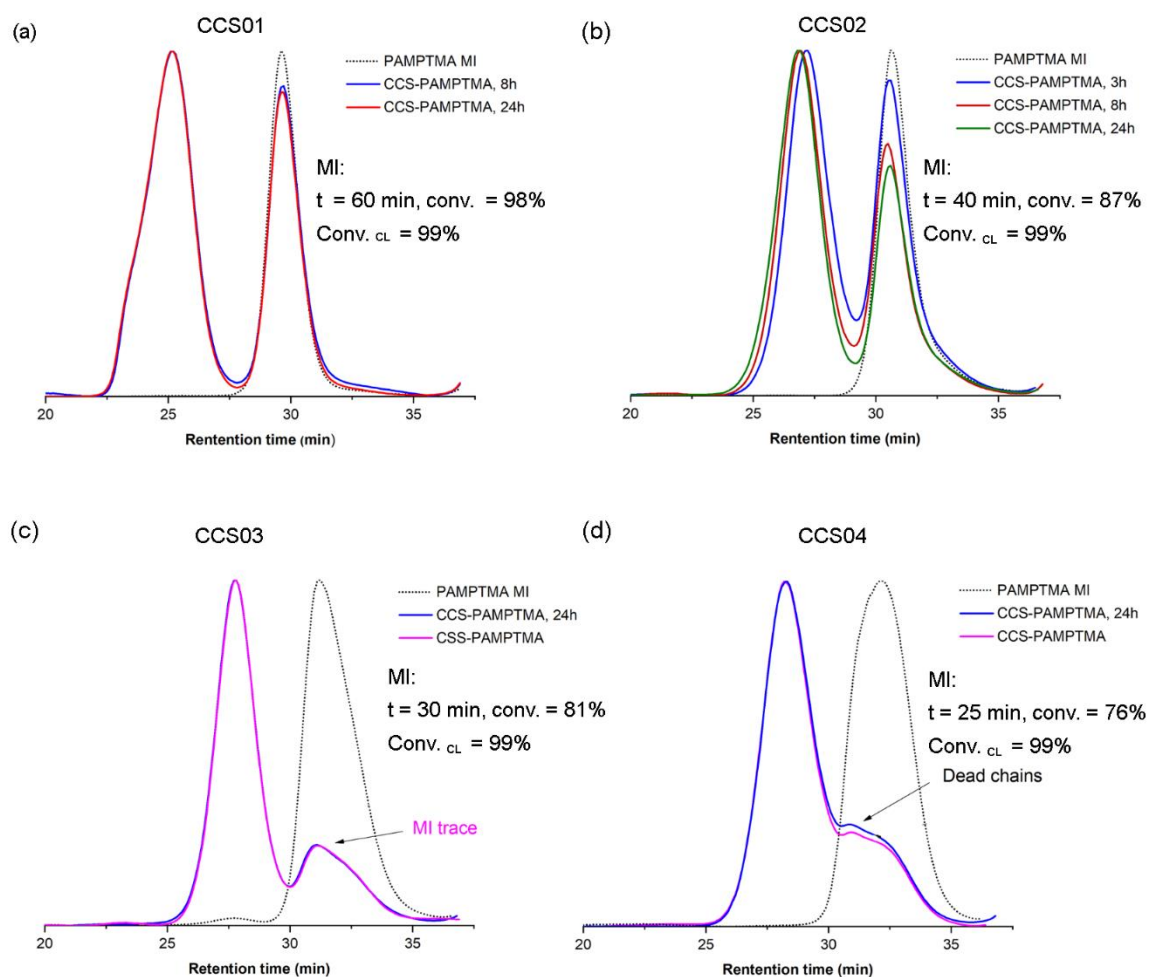


Figure 3.16. SEC traces obtained during the synthesis of CCS-PAMPTMA prepared by SARA ATRP. Conditions: $[AMPTMA]_0/[EBiB]_0/[CuBr_2]_0/[Me_6TREN]_0/Cu^0$ wire = 30/1/0.5/1.0; $[MI]/[CL]$ = 12; $[AMPTMA]_0$ = 1.45 M; solvent: $[EtOH]/[H_2O]$ = 40/60 (v/v) Cu^0 wire: l = 5 cm; d = 1 mm.

This suggests that in fact, the chain-end functionality of the MI is the main factor that affects the cross-linking step of the reaction. To achieve a full star formation, it is critically important to ensure a high end-functionality of the MI (“living” character), which can be challenging for the polymerizations carried out in aqueous media as the solvent can promote the hydrolysis of the halogen chain-end, leading to the formation of irreversibly deactivated chains.²²² Alternatively, the polymerizations could be conducted in water at low temperatures or using organic solvents to diminish the hydrolysis reactions and improve the star formation.⁵² Aiming to isolate the star polymers from the remaining MI, dialysis procedure of the CCS03 and CCS04 was performed using a membrane with cut-off 25000 (much higher than the MW of the MI). However, all the unreacted MIs were still present after the purification procedure.

Nonetheless, considering the high yield of star formation, the samples CCS03 and CCS04 were selected for antimicrobial activity evaluation in solution since most of the molecules should be star polymers rather than linear MIs. The MIC values obtained were expressed in weight-based as the absolute MW of star-shaped polymers produced by arm-first cannot be directly determined by ^1H NMR spectroscopy or by SEC equipped only with refractive index (conventional calibration). For this type of polymers, the MW as well the number of arms can be determined only with light scattering analysis, which was not available. Nevertheless, the MW of the star polymers should be high (SEC trace of CCS03 and 6-arm PAMPTMA available in Figure B5) considering the retention volume observed during the SEC analysis.

Preliminary results showed that the CCS-PAMPTMA polymers exhibited antimicrobial activity for all five bacteria tested presenting MIC values slightly higher than those of star-shaped polymers obtained via core-first approach (6-arm PAMPTMA and 4-arm PAMPTMA, Table 3.7).

Table 3.7. MIC values in mass base of the star-shaped homopolymers prepared by SARA ATRP via arm-first and core-first approach

Polymer	MW $\times 10^{-3}$	MIC (mg/mL)**				
		<i>S. aureus</i>	<i>B. Subtilis</i>	<i>B. Cereus</i>	<i>E. Coli</i>	<i>P. aeruginosa</i>
CCS03	*	3.75	3.75	1.87	3.75	3.75
CCS04	*	3.75	3.75	0.93	3.75	3.75
6-arm PAMPTMA	142	0.36	0.17	1.42	5.68	1.42
4-arm PAMPTMA	77.6	0.19	0.09	0.78	3.10	1.55

(*) MW not determined

Nonetheless, it is worth mentioning that these outcomes are not conclusive since the samples CCS03 and CCS04 present mixtures of linear and star-shaped polymers which can somehow affect the precision of the results. On this matter, optimization of the polymerization conditions must be done to achieve the total incorporation of the MI and consequently to obtain fully formed star polymers. Also, proper MW determination should be conducted.

3.2.6. Conclusions

A library of effective well-defined PAMPTMA-*co*-PBA-based antimicrobial polymers, with different architectures, MW and compositions, was prepared by SARA ATRP at near room temperature. Taking into account the several properties of the polymers that impact their antimicrobial activity, it was shown that increased MW led to increased antimicrobial performance regardless of the polymer shape. In contrast, increased hydrophobicity (PBA content), for the MW range investigated, resulting in higher MIC values (lower antimicrobial activity). Both cationic homopolymers and amphiphilic copolymers proved to be able to kill *E. coli* bacteria by membrane damage. Arm-first was a suitable approach for the straightforward synthesis of high-branched cationic star polymers which can be explored for the preparation of bioactive macromolecules. Despite controlled structures obtained using arm-first, none of the experiment led to the full incorporation of the MI precursors, possibly due to the loss of the chain-end functionality by hydrolysis of the bromine presenting in the MI chains (aqueous media). These hydrolysis reactions may be reduced by conducting the reactions in water at low temperature or using an organic solvent. By these means, the star formation could be possibly be maximized.

3.3. Antimicrobial photodynamic inactivation

Toluidine blue O, curcumin and proflavine have been effective in inactivating a wide range of microorganisms upon light irradiation. This section is dedicated to the results obtained from the light-assisted antimicrobial assays using these three photosensitizers in their free form or conjugated with polymers.

This section includes the results of the antimicrobial assays in the presence of light and PS. The first part is dedicated to the tests using only PS as the antimicrobial agent, in which the influence of the quantity of light emitted was made. Next, the synergistic effect of the presence of both PS and antimicrobial polymers on the antimicrobial activity of the system (PS + polymer) will be discussed. The last part of the section is devoted to the study of the PS-functionalized polymers. Derivatives of curcumin and proflavine were prepared and used as ATRP initiators to obtain these polymeric structures with one PS molecule covalently bounded, therefore, their photoantimicrobial activity were assessed. The experimental setup included the light system (Figure C3) and 96-well microtiter plates

(Figure C3). The light source consisted of three distinct light-emitting diode (LED) array systems: white light, blue light ($\lambda_{\max} = 450$ nm) red light ($\lambda_{\max} = 635$ nm). All lighting sources are composed with adjustable light intensity modulus which low and high mode (Table 3.8) were used in the first aPDI tests to evaluate the light strength effect over of the antimicrobial activity. Preliminary antimicrobial assays (MIC determined in liquid medium) were conducted using the three light sources and varying both the light intensity and the exposure time to evaluate the influence of these parameters on the antimicrobial activity of the PS and to be able to establish experimental setup for further analysis of the polymer and the PS-functionalized polymers.

Table 3.8. Values of fluences and the respective light dose for 30 minutes of radiation

Type of light	High mode (mW.cm ⁻² /J.cm ⁻²)	Low mode (mW.cm ⁻² /J.cm ⁻²)
White light (WL)	688 / 1239	69 / 124
Red light (RL)	314 / 566	31 / 56
Blue light (BL)	634 / 1142	63 / 142

3.3.1. Photodynamic activity of TBO

As previously mentioned, TBO is a cationic photosensitizer belonging to the phenothiazine group, which absorbs light in the higher wavelength regions of the visible spectrum ($\lambda = 635$ nm). The absorption spectrum of the PS dissolved in LB growth medium (used in the antimicrobial assays) was recorded and compared with the emission spectrum of the red light and white light systems. Figure 3.17 shows maximum absorption at 632 nm for TBO, which is coherent to the λ_{\max} emission of the red light. However, only a fraction of the white light emission spectrum overlays with the TBO's absorption wavelength.

The photodynamic effect of TBO was measured in terms of MIC values (liquid medium) over a broad microbial spectrum including both Gram-positive and Gram-negative strains and using the two modes of energy (high and low). The results depicted in Table 3.9 show that TBO exhibited toxicity to all bacteria in the absence of light (NL) with the lowest MIC values for the genus *Bacillus* (*B. subtilis* and *B. cereus*). Studies have shown that, at certain concentrations, PS belonging to the phenothiazine salts family might display dark toxicity towards bacteria through mechanisms comprising destabilization of plasm membrane by

electron transfers, effects over the efflux pump activity, energy sources and the energy-providing enzymes (ATPases).²²³⁻²²⁵ Nevertheless, the phenothiazine-related antimicrobial activity with no external light stimulus only occur at high concentrations and thus, being disadvantageous from the clinical standpoint.

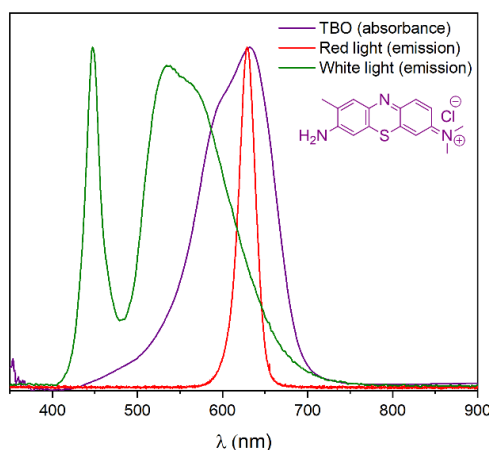


Figure 3.17. Absorbance spectrum of TBO in LB medium and emission spectrum of the LED emitting red light ($\lambda = 635$ nm) and the LED emitting white light ($\lambda = 400 - 750$ nm).

Table 3.9. MIC values for toluidine blue (TBO)

Light dose ($\text{J}\cdot\text{cm}^{-2}$)		MICs (μM)				
		<i>S. aureus</i>	<i>B. subtilis</i>	<i>B. cereus</i>	<i>E. coli</i>	<i>P. aeruginosa</i>
	NL	200	25	25	>200	200
High-power mode						
1239	WL	50	25	25	200	100
566	RL	25	25	25	100	100
Low-power mode						
	NL	200	50	50	200	>200
124	WL	100	50	50	200	>200
56	RL	100	25	50	100	>200

In the presence of light, the bacteria were exposed for 30 minutes under low-power mode and high-power mode irradiation. By this means, it was possible to evaluate the influence of the quantity of light on the aPDI efficacy of the PS. The results showed that the MICs for *S. aureus* decreased from 200 μM (NL) to 100 μM under 56 $\text{J}\cdot\text{cm}^{-2}$, reaching 25 μM under 566 $\text{J}\cdot\text{cm}^{-2}$ of red light (Table 3.9). A reduction on the MIC values was also observed for the Gram-negative; however, less significant than that observed for the Gram-positive.

The aPDI activity of TBO against four clinically isolated *P. aeruginosa* strains with different resistance profiles has been reported.²²⁶ Results have shown that the treatment with 20 μM of TBO and 90 $\text{J}\cdot\text{cm}^{-2}$ of red light, led to a 7-log reduction of all strains. Moreover, additional tests confirmed DNA fragmentation into small species and protein carbonylation as responses for the ROS attack.²²⁶

For the genus *Bacillus* (*B. subtilis* and *B. cereus*), no difference was observed among the MICs in the presence of light or dark conditions, suggesting that the microorganisms might be highly susceptible to the intrinsic antimicrobial character of the TBO (Table 3.9). The photobactericidal effects of TBO were evaluated by Demidova *et al.*, using *B. cereus* and *B. subtilis* as the subjects.²²⁷ The authors observed that, under appropriate wavelength and 40 $\text{J}\cdot\text{cm}^{-2}$ of irradiation, both bacteria strains were efficiently inactivated at concentrations up to 8 μM of TBO. In this work, it was observed that the aPDI was more effective using light with appropriate wavelength (close to the one of maximum absorption for TBO) since lower or equal MIC values were achieved using less energy (566 $\text{J}\cdot\text{cm}^{-2}$ vs 1239 $\text{J}\cdot\text{cm}^{-2}$) thus, agreeing with the aPDI concept which describes more efficiency under coherent illumination.

3.3.2. Photodynamic activity of proflavine

Figure 3.18 shows the absorbance spectrum of proflavine presenting the maximum absorption at 440 nm, being coherent with the blue-light LED emission spectrum and part of the white-light LED emission spectrum.

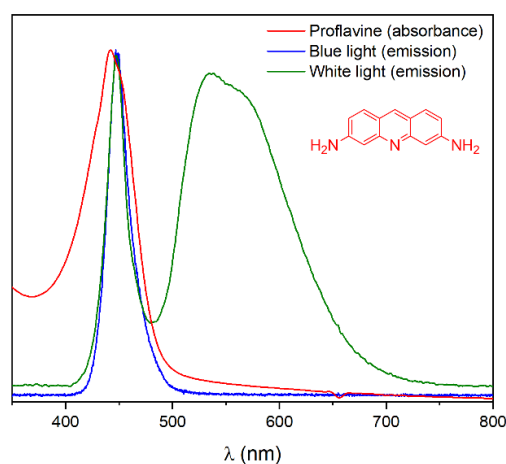


Figure 3.18. Absorbance spectrum of proflavine in LB medium ($\lambda_{\text{max}} = 440 \text{ nm}$) and emission spectra of the blue-light LED ($\lambda = 450 \text{ nm}$) and white-light LED.

The aPDI assays were conducted the LED emitting white light and the LED emitting blue light. Both systems present similar fluences rate, thereby, delivering a similar quantity of light during the 30 minutes of exposure (*e.g.*, 1239 J.cm⁻² white light and 1142 J.cm⁻² for the blue light). Table 3.10 shows the MIC values obtained in the presence of proflavine as the PS, which varied according to the type of light source and the power mode.

Table 3.10. MIC values for proflavine

Light dose (J.cm ⁻²)		MICs (μM)				
		<i>S. aureus</i>	<i>B. subtilis</i>	<i>B. cereus</i>	<i>E. coli</i>	<i>P. aeruginosa</i>
	NL	>200	50	100	>200	200
High-power mode						
1239	WL	200	25	100	100	200
1142	BL	25	12,5	100	50	200
Low-power mode						
124	WL	200	50	100	200	200
142	BL	50	25	100	50	200

Finally, to what was observed for TBO, the use of a light source with a wavelength similar to one of the max absorptions of the PS (*i.e.*, blue light for proflavine) led to an enhancement of the antimicrobial activity. For instance, for *S. aureus* under white light, the MIC was 200 μM for both energy modes, whereas, under blue light, the MIC values decreased to 25 and 50 μM, for the high-power mode and low-power mode respectively (Table 3.10). The same trend was also observed for *B. subtilis*, with lower MICs in the presence of blue light. Interestingly, proflavine showed good photoactivity against *E. coli* (better than TBO), presenting MIC of 50 μM under blue light regardless of the energy mode. For *B. cereus* and *P. aeruginosa*, the MIC values were similar in dark and under light conditions.

3.3.3. Photodynamic activity of curcumin

Curcumin is a PS that also absorbs light in the blue region as shown in Figure 3.19. It is worth mentioning that, the absorption spectrum was recorded by firstly preparing a stock solution of curcumin (10 mg. mL⁻¹) in dimethyl sulfoxide (DMSO) and add the proper amount to the LB growth medium as pure curcumin is not soluble in this medium. The UV-

vis spectrum presented in Figure 3.19 the maximum absorption wavelength of curcumin centered at 430 nm but with a broad peak. This could be due to the poor solubility of curcumin aqueous media, which might induce the aggregation of this PS.

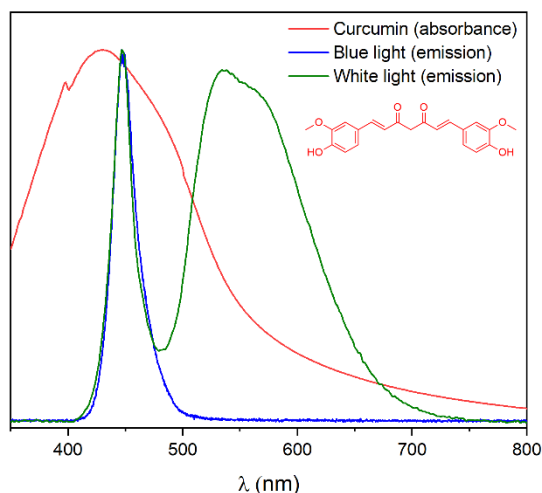


Figure 3.19. Absorbance spectrum of curcumin in LB medium and emission spectra of the blue-light LED ($\lambda = 450$ nm) and white-light LED.

The photoactivity of curcumin was also measured in different conditions of light irradiation and energy intensity (Table 3.8) against the five bacteria strains investigated in this work. The PS quantity and light intensity are two key factors ruling photoinactivation efficiency. As observed in a study dealing photoactivity of curcumin,²²⁸ high quantity of ROS will be generated after exposure, then, causing damage on bacteria. The reactive species may absorb hydrogen presented on the cell wall components and thereby provoking disturbances to the cell structure which will later be unable to resist the turgor pressure. The results presented in Table 3.11 show that the curcumin-mediated aPDI was more effective for the genus *Bacillus*, especially for *B. cereus* under 1142 J.cm^{-2} blue-light LED (lowest MIC). Similarly, to what was observed for both TBO and proflavine, using coherent light and delivering more energy led to a slight increment on the aPDI efficacy against both *S. aureus* and *E. coli*. On the other hand, for *P. aeruginosa*, no light-mediated toxicity was observed as judged by the similar MIC values obtained under dark and light conditions. Results suggest that the antimicrobial activity observed ($\text{MIC} \geq 200 \mu\text{M}$) could be to the intrinsic toxicity of curcumin.

Table 3.11. MIC values for curcumin

Light dose (J.cm ⁻²)		MICs (μM)				
		<i>S. aureus</i>	<i>B. subtilis</i>	<i>B. cereus</i>	<i>E. coli</i>	<i>P. aeruginosa</i>
	NL	>200	100	100	200	200
High-power mode						
1239	WL	>200	50	50	200	200
1142	BL	100	25	100	100	200
Low-power mode						
	NL	200	100	200	200	>200
124	WL	200	100	200	200	>200
142	BL	100	50	200	200	>200

Tyag *et al.*,²²⁹ evaluated the toxicity of curcumin against four bacteria strains *S. aureus*, *E. faecalis*, *E. coli* and *P. aeruginosa*, using three different concentrations (25 μM, 50 μM and 100 μM) and the percentage of survival was examined after different times of incubation in dark conditions. Results revealed a strong killing effect of curcumin against all microorganism tested and the effect increased with increasing both the time of exposure and curcumin concentration. In this study, it was verified that 100 μM of curcumin within 30 min of contact was efficient to kill ≈100% of *S. aureus*, *E. faecalis*, *E. coli* and 57±11.5% of *P. aeruginosa*. Moreover, aiming to address the process behind the antimicrobial activity of curcumin, the authors performed several examinations including membrane permeabilization, propidium iodide uptake, calcein leakage, scanning electron microscopy and membrane integrity, and conclude that membrane damage is the ruling mechanism of bacterial death.²²⁹ Studies have also reported the influence of curcumin on the cytokinesis in *Bacillus* and *Coccus* species by inhibiting the cell division process.²³⁰ Here, it was observed inactivation of the two *Bacillus* species at 100 μM in dark condition, whereas with blue-light, MIC achieved the lowest value in the high-power mode.

PS have proven to be effective agents against several types of microorganisms in either the absence of light or under illumination. Indeed, these compounds are of great interest for several pharmacological areas due to their versatility and selectivity towards pathogens. Recent research efforts have been focused on improving the efficacy of the treatment

against microbial infections by developing strategies with multiple modes of antimicrobial actions. As an example, strategies combining aPDI with conventional antimicrobials or with synthetic macromolecules have been proposed and presented promising results regarding the combat against bacterial infections.^{231, 232}

3.3.4. Photodynamic activity of photosensitizer/polymer mixtures

aPDI of bacteria has been recurrently presented in the literature as having several advantages over individual routinely antibiotics administration. ROS are the species responsible for the damage to the bacteria cell wall at diverse levels, which reduces the propensity of bacteria to develop resistance. The success of aPDI is also due to the ability to reduce several virulence factors by lessening the activity of proteases, lipases, secreted toxins.²³³⁻²³⁵ In most studies, aPDI has been proposed as an alternative treatment to successfully act over an infection. However, this technology still presents challenging issues, including efficient elimination of microorganisms growing biofilms and the fact that the results obtained *in vitro* rarely translate to animal models. Moreover, the regrowth of microorganisms and the development of new infection has been already observed even after an efficient elimination of microorganisms. Nonetheless, recent studies dealing with aPDI have demonstrated that it can improve the susceptibility of microbes to conventional treatments thus, lowering the demand for antibiotics. These reports have suggested that a synergistic approach can be a promising alternative to significantly reduce the emergence of resistance from the bacteria. For instance, the synergistic effect between light, PS and antimicrobial therapy on planktonic bacteria and bacterial biofilms was presented by Iluz *et al.*,²³⁶ In this study, cultures of planktonic *S. aureus* were incubated with deuteroporphyrin IX (DPIX) and oxacillin and exposed to a light dose of 46 J. cm⁻². A diverse synergistic effect was observed combining the two antimicrobials with the strongest effect when the cell cultures were exposed to 17 μM of DPIX and 1 μg. mL⁻¹ of the conventional antibiotic. In 2017, the first evidence that combined aPDI/antibiotics therapy could be efficient against multidrug-resistant *A. baumannii*.²³⁶ The presented study also aimed at the evaluation of the possible influence of aPDI on the expression of genes, which are responsible for *A. baumannii* resistance to colistin. Results showed that TBO (18.5 μM) and LED light exposure during 60 or 90 s improved the bacterial drug susceptibility, evidenced by a disk-diffusion assay using colistin, ceftazidime, piperacillin

and doripenem as model drugs. The aPDI treatment also affected the expression of the two genes responsible for the resistance to colistin. The results showed that the expression of these two genes was respectively 6.1-fold and 4.9-fold lower to the cells treated with TBO (14 mM) and light (180 J. cm⁻²) in comparison to the untreated cells. Diverse researchers have used several PS in combination with low molecular weight antibiotics and have examined the combined effect towards microbes *in vitro* and in animal models.²³⁷⁻²³⁹ However, to the best of our knowledge, the conjugation of antimicrobial polymers with aPDI has not been explored.

In this PhD project, preliminary experiments were performed to evaluate the effects of simple mixtures of antimicrobial polymers and PS against *E. coli*. For these tests, two representative antimicrobial polymers, from the library of ones prepared in this work, have been selected based on their antimicrobial activity: a cationic homopolymer (PAMPTMA) and a cationic amphiphilic random copolymer (PAMPTMA-*co*-PBA). The mixtures were prepared by using TBO, or curcumin or proflavine in conjunction with PAMPTMA₂₁₂-Br (A212B0, $M_n^{\text{th}} \approx 4400$) homopolymer or PAMPTMA₂₁₇-*co*-PBA₂₁-Br copolymer (A2017B21, $M_n^{\text{th}} \approx 47700$) prepared via SARA ATRP as representative polymers. Three LED systems were used in the assays, the red-light LED (irradiance = 314 mW. cm⁻², light density = 566 J.cm⁻²), blue-light LED (634 mW.cm⁻², 1142 J.cm⁻²) and white-light LED (688 mW.cm⁻², 1239 J.cm⁻²). Control experiments were done in the absence of light with bacterial suspensions being incubated for the same time with the antimicrobials. Polymers/PS were combined in different molar ratios (at sub-inhibitory concentration (MIC)) and were added to the bacterial suspension, which was submitted to light exposure for 30 minutes.

3.3.5. Combination of polymers and toluidine blue O towards *E. coli*

Table 3.12 shows that *E. coli* was able to grow at 100 μM, 200 μM or 100 μM of TBO, polymer A212B0 and polymer A217B21, respectively (entries 1-3). For the mixtures, a synergistic (polymer/PS) effect was observed for the case A212B0 200 μM + TBO 100 μM, in both dark and light conditions (entry 4) as judged by the growth inhibition. The same result was observed for the mixture A200B0 100 μM + TBO 100 μM (entry 6). For the homopolymer (A200B0), it was observed no effect over the *E. coli* growth using 50 μM of TBO (entries 5 and 7) when in combination.

Table 3.12. Antimicrobial synergetic effect of polymers + toluidine blue O (TBO) mixtures over *E. coli*.

Entry		Dark	White light	Red light
1*	TBO 100 μM	+	+	+
2*	A212B0 200 μM	+	+	+
3*	A217B21 100 μM	+	+	+
4	A212B0 200 μM + TBO 100 μM	-	-	-
5	A212B0 200 μM + TBO 50 μM	+	+	+
6	A212B0 100 μM + TBO 100 μM	-	-	-
7	A212B0 100 μM + TBO 50 μM	+	+	+
8	A217B21 100 μM + TBO 100 μM	+	+	+
9	A217B21 100 μM + TBO 50 μM	+	+	+
10	A217B21 50 μM + TBO 100 μM	+	+	+
11	A217B21 50 μM + TBO 50 μM	+	+	+

*control experiments, (+) bacterial growth (-) bacterial inhibition

3.3.6. Combination of polymers and curcumin towards *E. coli*

Preliminary antimicrobial tests using mixtures of polymer and curcumin were also performed. The assays were conducted in dark and exposure to white-light LED and blue-light LED. For 30 minutes of irradiation, a total of 1239 J. cm^{-2} and 1142 J. cm^{-2} of light were delivery by the white-light LED and blue-light LED respectively. In Table 3.16, no effect over the bacterium growth was observed for the control experiments (entries 1-3), which was expected as the antimicrobial agents were used below their MIC. On the other hand, combining 200 μM or 100 μM of A212B0 with 100 μM of curcumin allowed the inactivation of the bacteria (entries 4 and 5). These results show that when using PS and antimicrobial polymers, below their MIC, there is efficient eradication of the planktonic bacteria with no need of light exposure. No effect was observed for the mixtures with lower amounts of curcumin thus, suggesting that the presence of the PS might display an important influence on the sensitization of *E. coli*. Again, the bacteria growth was more affected for the mixtures with higher quantities of curcumin (entries 4-6), while no effect was observed for those containing curcumin at 50 μM (entries 5 and 7). The results for the mixtures using the copolymer A217B21 showed bacterial growth in all concentrations tested (entries 8-11), except for that with 100 μM of the copolymer and 100 μM of curcumin under white light (entry 8). In this case, the bacteria were inactivated through a combining effect of the copolymer and aPDI.

Table 3.13. Antimicrobial synergetic effect of polymers and curcumin mixtures towards *E. coli*.

Entry		Dark	Blue light	White light
1	Curcumin 100 μM	+	+	+
2	A200B0 200 μM	+	+	+
3	A217B21 100 μM	+	+	+
4	A200B0 200 μM + curcumin 100 μM	-	-	-
5	A200B0 200 μM + curcumin 50 μM	+	+	+
6	A200B0 100 μM + curcumin 100 μM	-	-	-
7	A200B0 100 μM + curcumin 50 μM	+	+	+
8	A217B21 100 μM + curcumin 100 μM	+	+	-
9	A217B21 100 μM + curcumin 50 μM	+	+	+
10	A217B21 50 μM + curcumin 100 μM	+	+	+
11	A217B21 50 μM + curcumin 50 μM	+	+	+

*control experiments, (+) bacterial growth (-) bacterial inhibition

3.3.7. Combination of polymers and proflavine towards *E. coli*

The combined effect polymer and proflavine were also tested using white and blue light irradiation. Interesting, lower quantities of the PS need to induce microbial growth inhibition, in comparison to mixtures containing TBO or curcumin, indicating higher activity of proflavine against *E. coli*. Concerning the results for the mixtures, it was observed an inhibition for the mixture containing 200 μM of the homopolymer and 50 μM of the PS, regardless the absence or presence of light (Table 3.14 entry 4).

Table 3.14. Antimicrobial synergetic effect of polymers and proflavine mixtures towards *E. coli*.

Entry		Dark	Blue light	White light
1	Proflavine 50 μM	+	+	+
2	A200B0 200 μM	+	+	+
3	A217B21 100 μM	+	+	+
4	A200B0 200 μM + proflavine 50 μM	-	-	-
5	A200B0 200 μM + proflavine 25 μM	+	-	+
6	A200B0 100 μM + proflavine 50 μM	+	-	+
7	A200B0 100 μM + proflavine 25 μM	+	+	+
8	A217B21 100 μM + proflavine 50 μM	+	-	+
9	A217B21 100 μM + proflavine 25 μM	+	-	+
10	A217B21 50 μM + proflavine 50 μM	+	-	+
11	A217B21 50 μM + proflavine 25 μM	+	+	+

*control experiments, (+) bacterial growth (-) bacterial inhibition

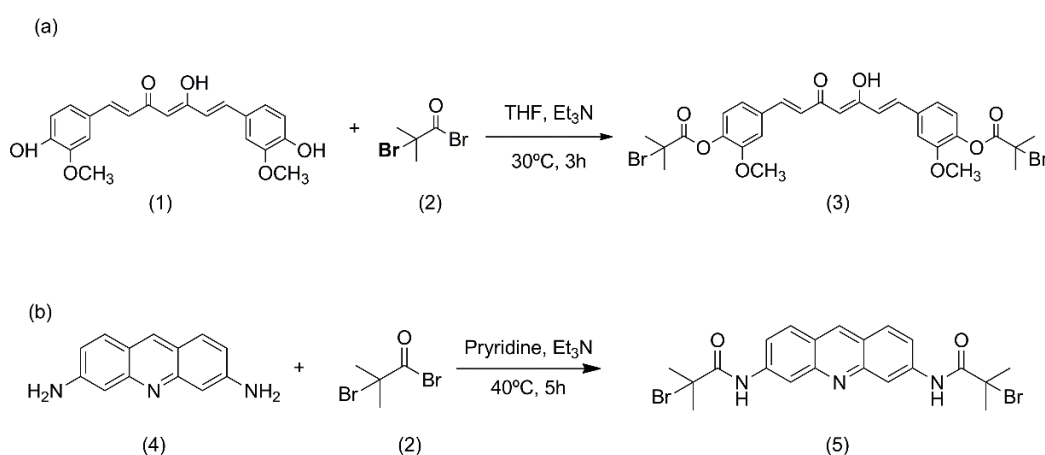
However, maintaining the concentration of the polymer at 200 μM , decreasing the quantity of the PS (entry 5) and using with blue light, a photoinduced effect was observed. A typical aPDI action was also observed with 100 μM of polymer and 50 μM of proflavine, again in the presence of blue light (entry 6). The same trend was also observed for the mixtures containing the copolymer (entries 8-10) suggesting that the photoactivity is strongly influenced according to the type of light. According to these results, proflavine seems to be the most appropriate PS to use against *E. coli*, from all the PS investigated in this work.

3.3.8. PS-functionalized antimicrobial polymers

Synthesis of the photosensitizer based ATRP initiator

For that novel ATRP initiators based on two PS namely curcumin and proflavine have been designed and synthesized (Scheme 3.2).

In this work synthetic procedures to obtain novel compounds based on curcumin or proflavine to be used as ATRP initiators were developed (Scheme 5.1). Figure 3.20 depicts the ^1H NMR spectrum of the curcumin-based initiator (3, CI) recorded in CHCl_3 . The signals appearing between 6.90 and 7.20 ppm were assigned to the aromatic protons of curcumin and the chemical shifts related to the methoxy groups appear at 3.88 and 3.73 ppm. Furthermore, the chemical shifts appearing at 2.88 ppm, related to the methyl groups belonging to the modifying agent (BiB (2), Scheme 5.1), confirm the success of the synthesis.



Scheme 3.6. Synthesis of the PS-based ATRP initiators (a) curcumin (CI) and (b) proflavine (PF).

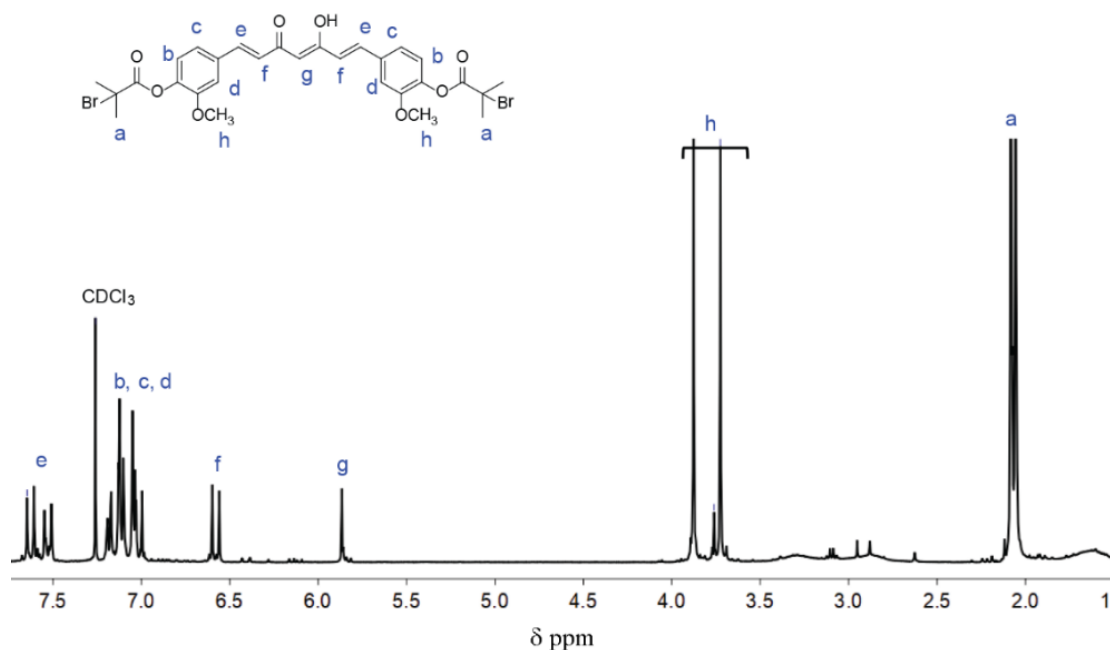


Figure 3.20. 400 MHz ^1H NMR spectrum of the curcumin-based initiator (CI) in CDCl_3

Similarly, the proflavine-based initiator (PF) was also obtained upon reacting 3-diamino acridine (4) with BiB (2), rendering a bifunctional compound (a detailed experimental procedure in section 2.2.12). The chemical structure was confirmed by the presence of the signals belonging to the acridine skeleton (c, d, e and f signals from 9.0 ppm to 7.5 ppm), the presence of the two protons belonging to amine (b signal at 10.2 ppm) and the presence of the methyl groups (signals at 2.1 ppm), as shown in the spectrum in Figure 3.21

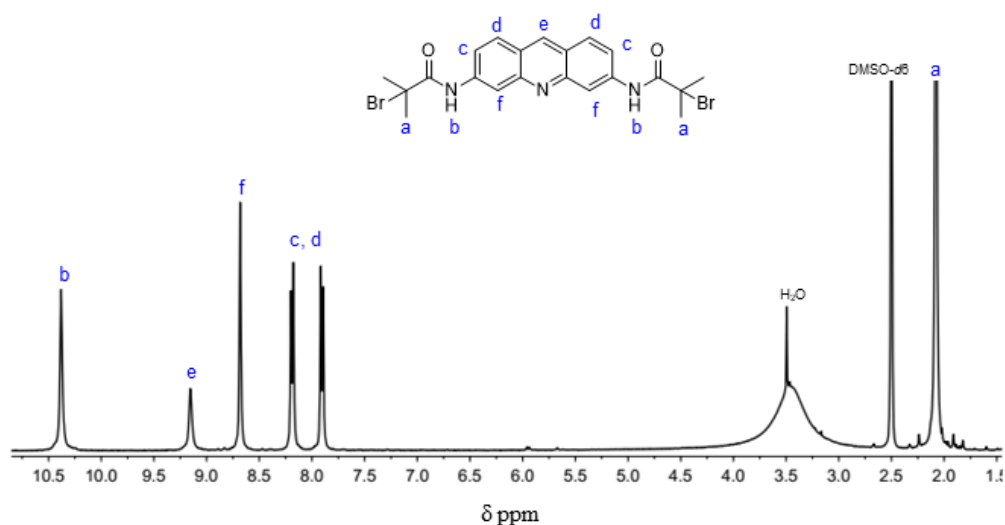


Figure 3.21. 400 MHz ^1H NMR spectrum of the proflavine-based initiator (PF) in $\text{DMSO}-d_6$.

Synthesis and characterization of the PS-functionalized polymers

The prepared initiators (CI and PF) were then used to synthesize cationic PAMPTMA homopolymers and amphiphilic PAMPTMA-*co*-PBA copolymers with similar molecular weight *via* SARA ATRP at 30 °C (Table 3.15). The objective of this study was to investigate whether the insertion of one PS molecule per polymer chain could exhibit aPDI in conjunction with the intrinsic antimicrobial activity of the polymers. For this new set, the polymers were designed to have a MW similar to that of LA335B0 (MW = 68000, DP_{PAMPTMA} = 335), as this polymer exhibited the highest antimicrobial activity among the linear ones (Table 3.4).

Table 3.15. Characteristics of the non-functionalized and PS-functionalized polymers obtained by SARA ATRP.

Sample	Time (h)	Conv. (%)		$M_n^{\text{th}} \times 10^{-3}$ *	DP _(PAMPTMA/PBA) *	% PBA*
		AMPTMA	<i>n</i> -BA*			
A212B0	24	95	-	44.1	212	0
A200B20	24	93	93	42.4	200 / 20	10
CA200B0	72	31	-	47.4	220	0
CA200B25	72	55	69	45.5	200 / 25	11
PA193B0	18	86	-	40.5	193 / 0	0
PA191B19	24	89	90	42.4	191 / 19	9

*Determined from ¹H NMR spectra.

Unfortunately, it was not possible to achieve this targeted MW using the CI initiator, as the rate of polymerization and maximum monomer conversion achieved were severely affected (conv._{AMPTMA} = 50% after 72h, Appendix C, Table C1 entry 3) in comparison with the polymerizations using EBiB as the initiator (conv._{AMPTMA} = 89% after 24h, Table C1 entry 1). Such behavior could be attributed to the ability of curcumin to chelate metals, in this case forming curcumin-Cu^{II} complexes^{240, 241} which are not able to mediate ATRP. Also, curcumin-Cu^{II} interactions could decrease the concentration of active catalytic complex (Cu^{II}/Me₆TREN) during the polymerization, slowing down the rate of monomer conversion. To test this hypothesis, higher concentration of catalyst (Cu^{II}/Me₆TREN) was

used, leading to a slight increase of the monomer conversion from 50% to 60% (Table C1, entry 4), but still low in comparison to the one obtained using EBiB as the initiator. Considering this conversion, the DP of the AMPTMA was increased to 740 aiming to obtain a polymer with $MW \approx 68000$. However, the rate of polymerization was much lower and only 30% of monomer conversion was achieved after 72h, leading to a final theoretical molecular weight (M_n^{th}) = 47400 (CA200B0). Due to time constrains, it was decided to proceed with the study using polymers with $MW \approx 45000$ (Table 3.15), as the objective was to investigate the synergistic antimicrobial features of antimicrobial polymeric structures also presenting PS molecules on their chains. The proflavine initiator (PF) did not present any adverse issue to the polymerization rate and the polymers were prepared targeting a DP ≈ 200 to achieve a $MW \approx 45000$.

The samples were named following the same concept previously adopted: C is referred to the polymers initiated by curcumin; P refers to the polymers initiated by proflavine; A is the PAMPTMA segment followed by the respective DP and B is the PBA segment followed by the respective DP. The content of PBA in the final copolymer structure was determined by the normalized integrals of the 1H NMR spectrum of the pure polymers and following Eq. 3.1. Values of monomer conversion, time of reaction, parameters as the M_n^{th} and hydrophobicity content (%PBA) are summarized in Table 3.15.

The polymers were characterized by 1H NMR spectroscopy to confirm their chemical structure and by UV-vis spectroscopy to verify any possible changes on the maximum absorption wavelength of the PS moiety. For the pure curcumin-functionalized (co)polymers, the 1H NMR spectra showed the chemical shifts assigned to the curcumin skeleton from 9.5 ppm to 5.5 ppm as well as the methyl groups present in the PS structure at 3.0 ppm (Figures 3.22 and 3.23). The spectra also present the characteristic peaks corresponding to the protons present in the PAMPTMA segment. For the PAMPTMA-co-PBA copolymer (CA200B25), the presence of the PBA segment was also confirmed (Figure 3.23).

$$\% \text{ PBA} = \frac{\int \text{peak}_{PBA} / \frac{1}{n}H_{PBA}}{\int \text{peak}_{PBA} / \frac{1}{n}H_{PBA} + \int \text{peak}_{PAMPTMA} / \frac{1}{n}H_{PAMPTMA}} \quad \text{Eq. 3.1}$$

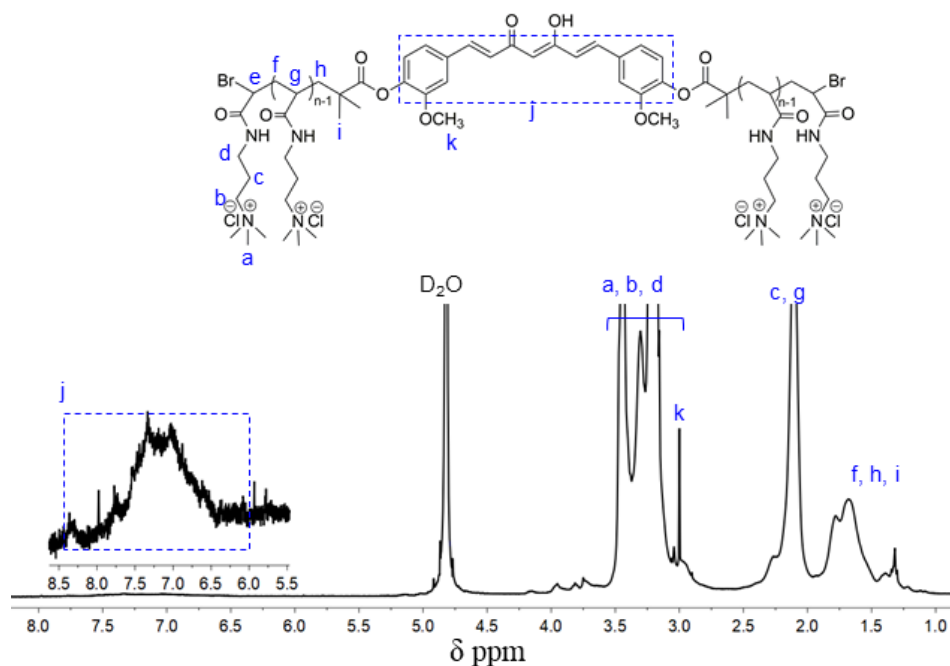


Figure 3.22. 400 MHz ^1H NMR spectrum in d_6 -EtOD of the CI-initiated PAMPTMA₂₀₀-Br (CA200B0) prepared by SARA ATRP ($M_n^{\text{th}} = 44100$). Conditions: $[\text{AMPTMA}]_0/[\text{CI}]_0/[\text{CuBr}_2]_0/[\text{Me}_6\text{TREN}]_0 = 740/1/0.5/1$; Cu^0 wire $l = 5$ cm, $d = 1$ mm; $[\text{AMPTMA}]_0 = 3.0$ M in EtOH/DMF = 85/15 (v/v) at 30 °C.

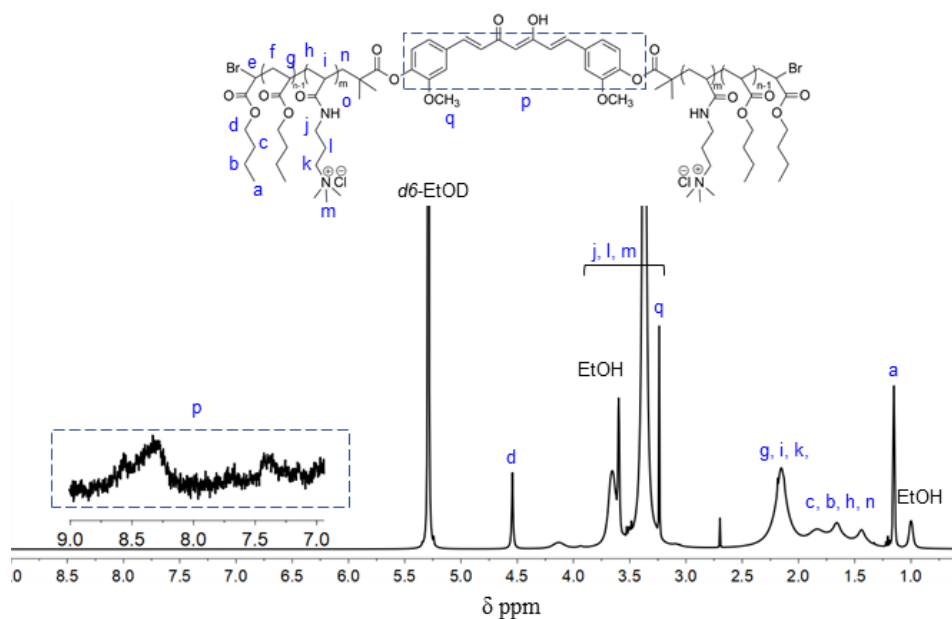


Figure 3.23. 400 MHz ^1H NMR spectrum in d_6 -EtOD of the CI-initiated PAMPTMA₂₀₀-co-PBA₂₅-Br (CA200B25) prepared by SARA ATRP ($M_n^{\text{th}} = 45500$). Conditions: $[\text{AMPTMA}]_0/[n\text{-BA}]_0/[\text{CI}]_0/[\text{CuBr}_2]_0/[\text{Me}_6\text{TREN}]_0 = 370/37/1/2/1$; Cu^0 wire $l = 5$ cm, $d = 1$ mm; $[\text{AMPTMA}]_0 = 3.0$ M in EtOH/DMF = 85/15 (v/v) at 30 °C.

The UV-vis spectra of the (co)polymers recorded in LB growth medium (Figure 3.24) show a shift of the maximum absorption peak in comparison with that of curcumin ($\lambda_{\text{max}} = 441$

nm). The spectrum of the CI shows the appearance of absorption peaks between 550 nm and 700 nm, a second one at 440 nm and the maximum peak absorption at 318 nm.

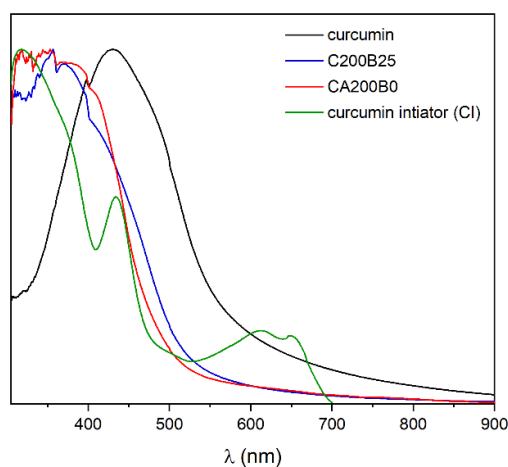


Figure 3.24. UV-vis spectra in LB growth medium of curcumin ($\lambda_{\max} = 431$ nm), CI ($\lambda_{\max} = 318$ nm), CI-PAMPTMA CA200B0 homopolymer ($\lambda_{\max} = 353$ nm) and CI-PAMPTMA-*co*-PBA CA200B25 copolymer ($\lambda_{\max} = 351$ nm).

The proflavine-functionalized (co)polymers ^1H NMR spectra, recorded in D_2O (Figure 3.25) or d_6 -EtOD (Figure 3.26) show the signals belonging to the protons of the proflavine molecule (chemical shifts from 9.2 ppm to 8.0 ppm) and the chemical shifts assigned to each polymeric segment, as previously mentioned for the case of curcumin.

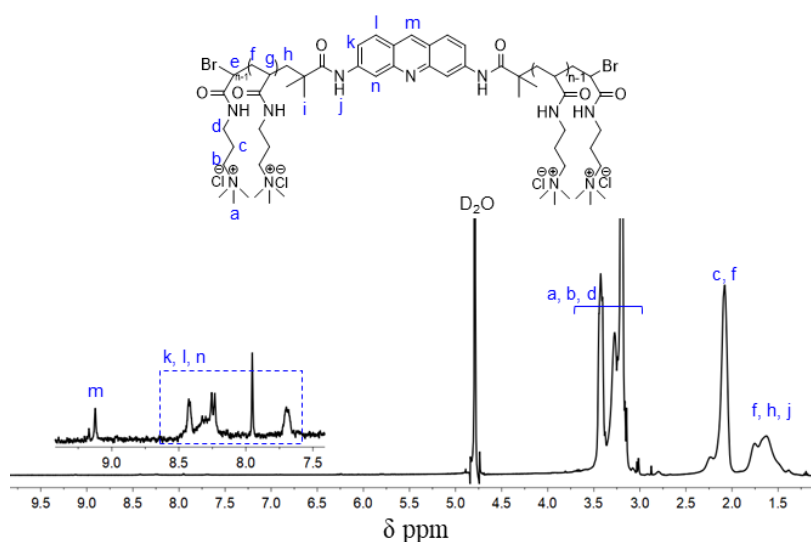


Figure 3.25. 400 MHz ^1H NMR spectrum in D_2O of the PF-initiated PAMPTMA₁₉₃-Br (PA193B0) prepared by SARA ATRP ($M_n^{\text{th}} = 42500$). Conditions: $[\text{AMPTMA}]_0/[\text{PF}]_0/[\text{CuBr}_2]_0/[\text{Me}_6\text{TREN}]_0 = 222/1/0.5/1$; Cu^0 wire $l = 5$ cm, $d = 1$ mm; $[\text{AMPTMA}]_0 = 3.0$ M in $\text{EtOH}/\text{H}_2\text{O}/\text{DMF} = 0.65/0.2/0.15$ (v/v/v) at 30°C .

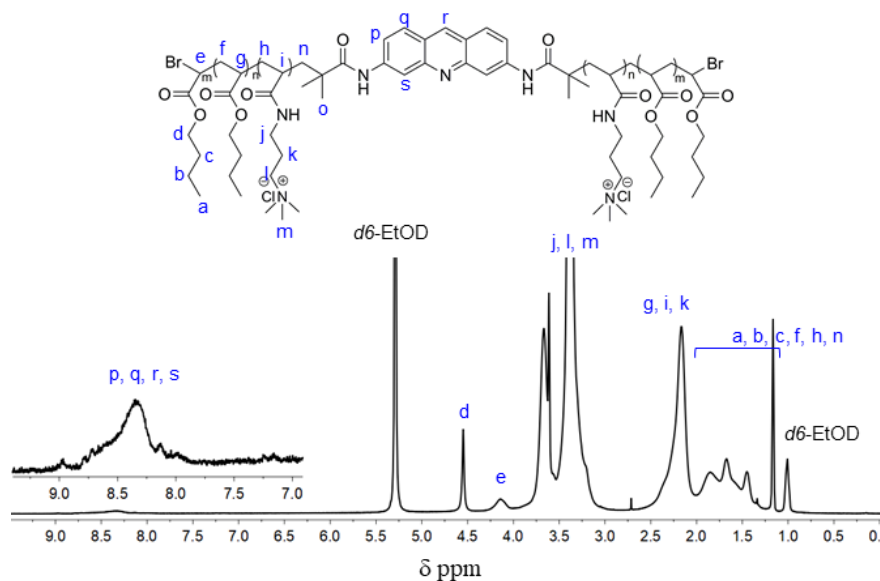


Figure 3.26. 400 MHz ^1H NMR spectrum in d_6 -EtOD of the PF-initiated PAMPTMA₁₉₁-*co*-PBA₁₉-Br (PA191B19) prepared by SARA ATRP ($M_n^{\text{th}} = 42400$). Conditions $[\text{AMPTMA}]_0/[\textit{n}\text{-BA}]_0/[\text{PF}]_0/[\text{CuBr}_2]_0/[\text{Me}_6\text{TREN}]_0 = 210/21/1/0.5/1$; Cu^0 wire $l = 5$ cm, $d = 1$ mm; $[\text{AMPTMA}]_0 = 3.0$ M, in $\text{EtOH}/\text{H}_2\text{O}/\text{DMF} = 0.65/0.2/0.15$ (v/v/v) at 30°C .

The UV-vis spectra recorded in LB growth medium (Figure 3.27) show a shift of the maximum absorption for the PF and PF-initiated polymers ($\lambda_{\text{max}} = 379 - 384$ nm) towards lower wavelength in comparison with the one of proflavine molecule ($\lambda_{\text{max}} = 340$ nm).

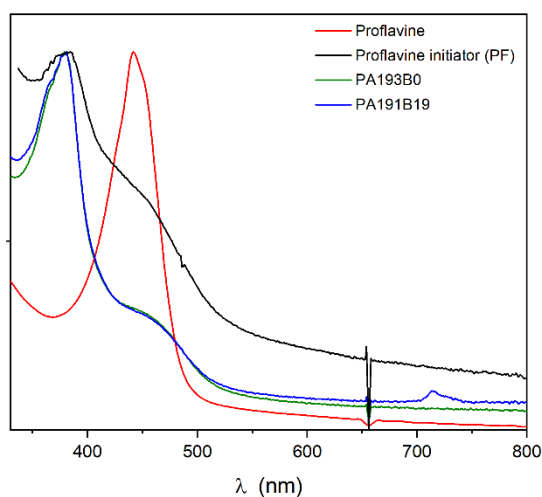


Figure 3.27. UV-vis spectra in LB growth medium of proflavine ($\lambda_{\text{max}} = 440$ nm), PF ($\lambda_{\text{max}} = 384$ nm), PF-PAMPTMA homopolymer PA193B0 ($\lambda_{\text{max}} = 379$ nm) and PF-PAMPTMA-*co*-PBA copolymer PA191B19 ($\lambda_{\text{max}} = 381$ nm).

3.3.9. Photodynamic antimicrobial activity of PS-functionalized polymers

It is known that for an efficient photodynamic inactivation of bacteria, most of the PS molecules should be very close to the cell membrane, as it is the targeted site of action. The use of a PS in its free form has proved to be effective against pathogens, showing activity at micromolar values, as demonstrated in this work. However, in an attempt to facilitate the PS reaching the cell membrane, thus potentially increasing aPDI action, the covalent conjugation with macromolecular materials has been explored.²⁴² Here, the aPDI activity of the polymers functionalized with either curcumin (CA200B0 and CA200B25) or proflavine (PA193B0 and PA191B19) was assessed in terms of MIC in solution and under dark or light (white and blue) irradiation Figure 3.28.

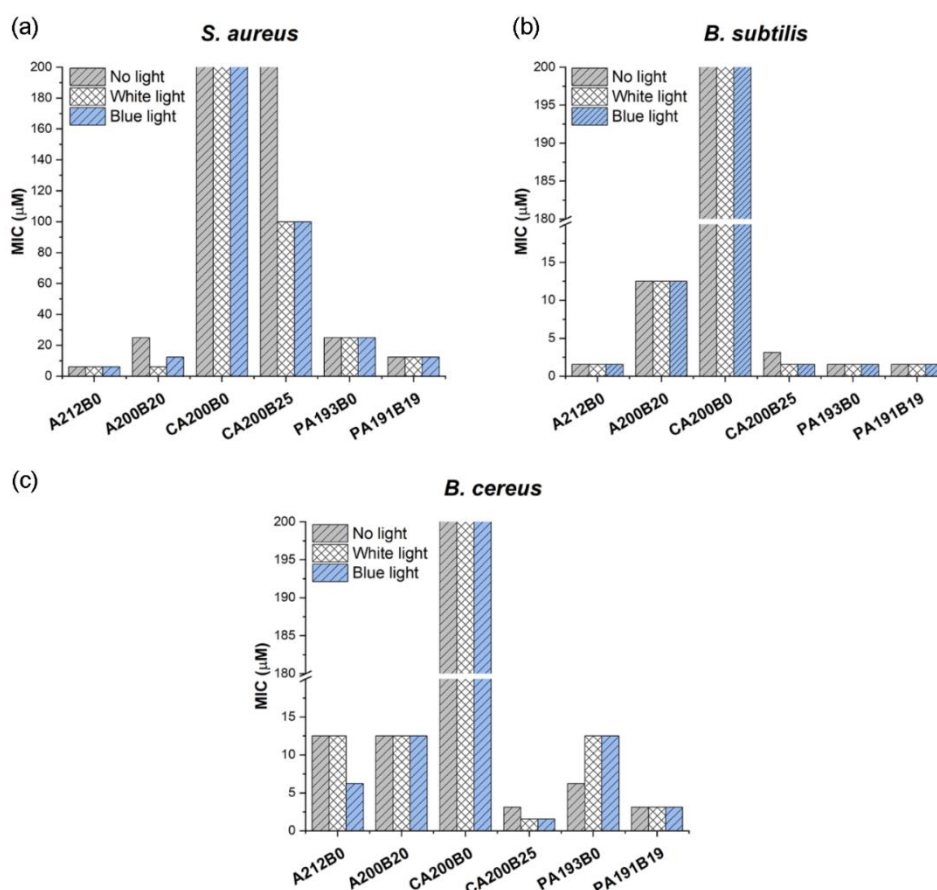


Figure 3.28. Antimicrobial activity of non-functionalized and PS-initiated polymers in dark and in the presence of light for Gram-positive bacteria.

As control samples, non-functionalized polymers with similar molecular weight of the one of PS-containing polymers were also tested under the same conditions. Figure 3.28 shows the results obtained against three Gram-positive bacteria, namely *S. aureus*, *B. subtilis* and *B. cereus*. For *S. aureus*, the homopolymer (A212B0) without PS in its structure showed a

strong antibacterial activity with MIC values of 6.25 μM for all conditions tested, whereas a slight increment on the MIC (12.5 μM) was observed for the copolymer A200B20 (Figure 3.28 (a)), which has a cationic (bactericidal) PAMPTMA segment with length similar to the one of the PAMPTMA homopolymer (DP around 200).

This behavior agrees with previous results (Table 3.4), which showed that the PAMPTMA homopolymer has higher antimicrobial efficacy than PAMTPMA-*co*-PBA copolymer with similar molecular weight. Unexpectedly, the homopolymer CA200B0 presented a MIC of 200 μM , being the highest value among the polymers tested. The MIC value of the disagree CA200B0 to what have been observed for a PAMPTMA-Br homopolymer with similar MW (*e.g.*, A212B0, MW \approx 44100) and an additional investigation with this polymer would be necessary. On the other hand, the correspondent copolymer CA200B25 exhibited a slight photodynamic action with MIC decreasing from 200 μM (under dark) to 100 μM (under light irradiation) (Figure 3.28 (a)). Although the polymers functionalized with proflavine (PA193B0 and PA191B19) could efficiently inactivate *S. aureus*, these did not show aPDI action as the MIC values were equal under dark and light conditions. As observed, the insertion of hydrophobicity (PBA) on the polymer structure favored the bioactivity, as the MIC values decreased from 25 μM (homopolymer) to 12.5 μM (Figure 3.28 (a)). Interestingly, the genus *Bacillus* (*B. subtilis* and *B. cereus*) showed a strong susceptibility to all polymers tested except to the homopolymer functionalized with curcumin (CA200B0), for which a MIC value of 200 μM was determined (Figure 3.28 (b) and (c)).

Unlike the Gram-positive bacteria, Gram-negative bacteria normally present higher resistance against biocidal agents, mainly because of the highly organized membrane which acts as a complex barrier for both low MW and macromolecular antimicrobials.¹⁰¹ The MIC values of most of the polymers tested against *E. coli* could not be determined, as they were higher than the upper concentration evaluated (200 μM) (Figure 3.29 (a)). Only the non-functionalized copolymer A200B20 showed a MIC value of 200 μM under blue light and a MIC of 100 μM in the presence of white light. *P. aeruginosa* (Figure 3.29 (b)) showed higher susceptibility for the polymers in comparison to *E. coli*, with the lowest MIC observed for those structures functionalized with proflavine (PA193B0 and PA191B19), even under dark conditions.

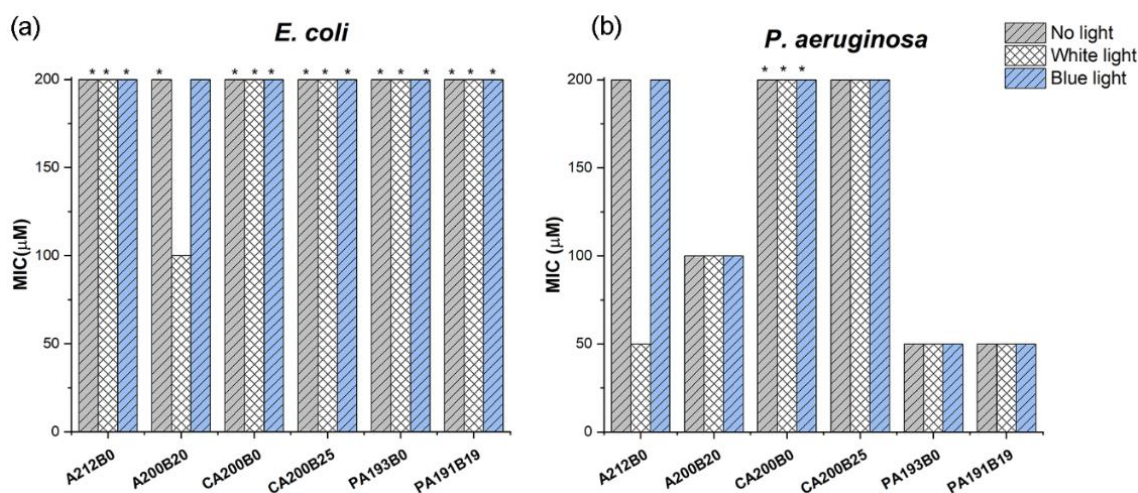
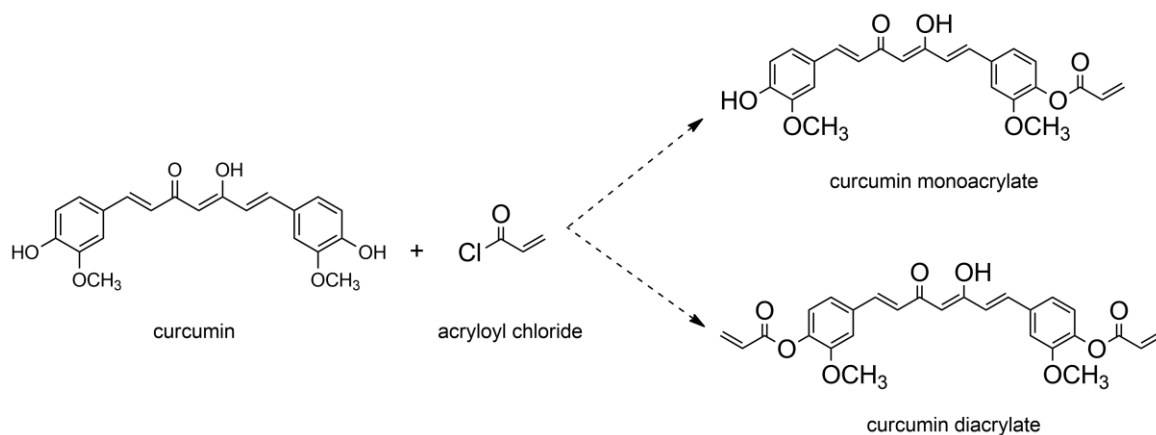


Figure 3.29. Antimicrobial activity of PS-initiated polymers in dark and in the presence of light for Gram-negative bacteria (*) MIC higher than 200 μM in solution.

Generically, no noticeable differences between the results in absence and presence of light were observed, for all bacteria tested, suggesting that the polymers *per se* are highly active for the bacteria and, most probably, the amount (in mass) of the PS present in the bacterial media is too low to produce enough quantity of ROS to exhibit toxicity to the bacteria (one molecule of PS per polymer chain). One alternative which could promote aPDI would be the incorporation of several PS molecules distributed along the polymeric chain to increase PS concentration and lead to the generation of a higher amount of ROS. During the course of this PhD work, a monomer based on curcumin was successfully synthesized (the ^1H NMR spectrum of the isolated curcumin monoacrylate is available in Figure C4). However, unfortunately, due to time constraints and several issues associated with the synthesis of the curcumin-based monomer, it was not possible to proceed with the polymerizations. From this, it is worth mentioning: (i) curcumin is a symmetric molecule presenting two methoxy groups on each side of the chemical structure, possibly with equal reactivity. Thus, all the synthesis procedures resulted in different products such as curcumin monoacrylate (the targeted one) and curcumin diacrylate (Scheme 3.7); (ii) the low yield of the final curcumin monoacrylate (c.a., 20%); (iii) as observed from the experiments using the CI initiator, the molecule seems to affect the catalytic complex ($\text{Me}_6\text{TREN}/\text{CuBr}_2$) activity used in SARA ATRP and this effect would be more significant using curcumin as a monomer as higher quantity is used in the polymerizations in comparison with that of initiator. This strategy is then suggested as future work.



Scheme 3.7. Reaction scheme of the synthesis of curcumin-based monomer.

3.3.10. Light-activated antimicrobial surfaces

As previously mentioned, there is an increasing interest to develop efficient strategies not only to treat infectious diseases but also to prevent them. Microbe contamination by touching hospital surfaces is extremely prevalent and originates widespread infections that can be reduced, for instance, using self-sterilizing surfaces. To date, several studies have been focused on the development of antimicrobial polymer surfaces using diverse strategies such as the incorporation of metals,²⁴³ covalent attachment of QAS,^{244, 245} microbicides releasing surfaces²⁴⁶ and nanoparticles-incorporated surfaces.²⁴⁷ Other studies have used aPDI as a strategy to reduce an environmental load of pathogens upon light exposure, which is particularly interesting due to the broad-spectrum activity and low risk of bacterial resistance development.²⁴⁸ However, most of these studies dealing with aPDI-mediated antimicrobial surfaces are devoted to developing materials for specific applications such as medical devices.^{248,249} Moreover, these reports normally use the combination of PS with inorganic compounds (metals or metals oxides) to achieve efficient antimicrobial activity, which can leach out from the surface to the environment.²⁴⁸ Here, a light-activated antimicrobial varnish, which can be applied to diverse surfaces in hospitals, was developed using the combination of polymer and curcumin. The objective of this study was to investigate as proof-of-concept the development of a varnish formulation able to produce surfaces with multiple mechanisms of antimicrobial activity, namely antimicrobial polymers and aPDI. The polymers selected for this study were the same used for the antimicrobial tests in liquid medium (Table 3.15).

The varnish formulation consisted of either bactericidal polymer or bactericidal polymer/curcumin mixtures and the surfaces were prepared by coating glass slides. It is worth mentioning that all the procedure for the preparation of the varnish formulation and development of surfaces was done by researchers from the Department of Chemical Engineering of the University of Porto and the antimicrobial assays were done by researchers from the Department of Life Sciences from the University of Coimbra.. To facilitate the identification of the samples, the surfaces were labeled according to the presence and quantity (35 mg, 60 mg and 85 mg) of antimicrobial agent: SF is referred to surface; C: curcumin; H: homopolymer A212B0; R: random copolymer A200B20; CH: CI-initiated homopolymer CA200B0; CR: CI-initiated random copolymer CA200B25. For instance, the sample SF+H85+C85 (Figure 3.30) is a surface that contains 85 mg of the homopolymer A212B0 and 85 mg of curcumin. The bactericidal properties of the surfaces were examined against the Gram-negative *E. coli*, a pathogen commonly associated to nosocomial infections.⁵⁵ The experiments were performed under dark and light conditions using white light (37.4 J.cm^{-2}) and blue light (49.0 J.cm^{-2}) for 15 min of exposure. A glass surface coated with varnish with no polymer or PS was also evaluated at the same conditions (control sample).

For these samples, it was observed higher reduction of the bacteria counts under light irradiation, in comparison to the test in dark. Such observation might be attributed to the fact that only light irradiation is able to exert toxicity to the bacteria, as already demonstrated in literature.^{250, 251} For all surfaces evaluated, a reduction of the number of viable bacteria was observed in the tests carried out in the presence of light, which evidences a typical aPDI properties (Figure 3.30 and 3.31). Moreover, the results revealed that the surfaces exhibited higher aPDI activity under blue light in comparison to that obtained under white light irradiation. Nonetheless, it is also important pointing out that the surfaces were irradiated with different light doses during the time of exposure (white light = 37.4 J.cm^{-2} and blue light = 49.0 J.cm^{-2}), which could also contribute for the differences on the reduction of the bacterial counts observed.

The surfaces were grouped in blocks according to the quantity of antimicrobial agents (polymer, curcumin, or polymer/curcumin mixtures), as follows: group 1 - 35 mg; group 2 - 60 mg and group 3 - 85 mg. The results revealed that surfaces containing polymer/curcumin mixture (SF+H+C) exhibited higher antimicrobial activity ($\text{CFU. mL}^{-1} \approx 10^2$) in comparison to those containing either only polymer or curcumin ($\text{CFU. mL}^{-1} \geq$

10^3), possibly due to the higher quantity of antimicrobial agent present in these surfaces (Figure 3.30). In addition, regardless the type of antimicrobial agent presents in the surface, it is evident a higher reduction in the bacterial number for those surfaces treated with blue light. These results indicate that, in fact, the intensity and the type of light have an important contribution for the overall efficiency of the aPDI.

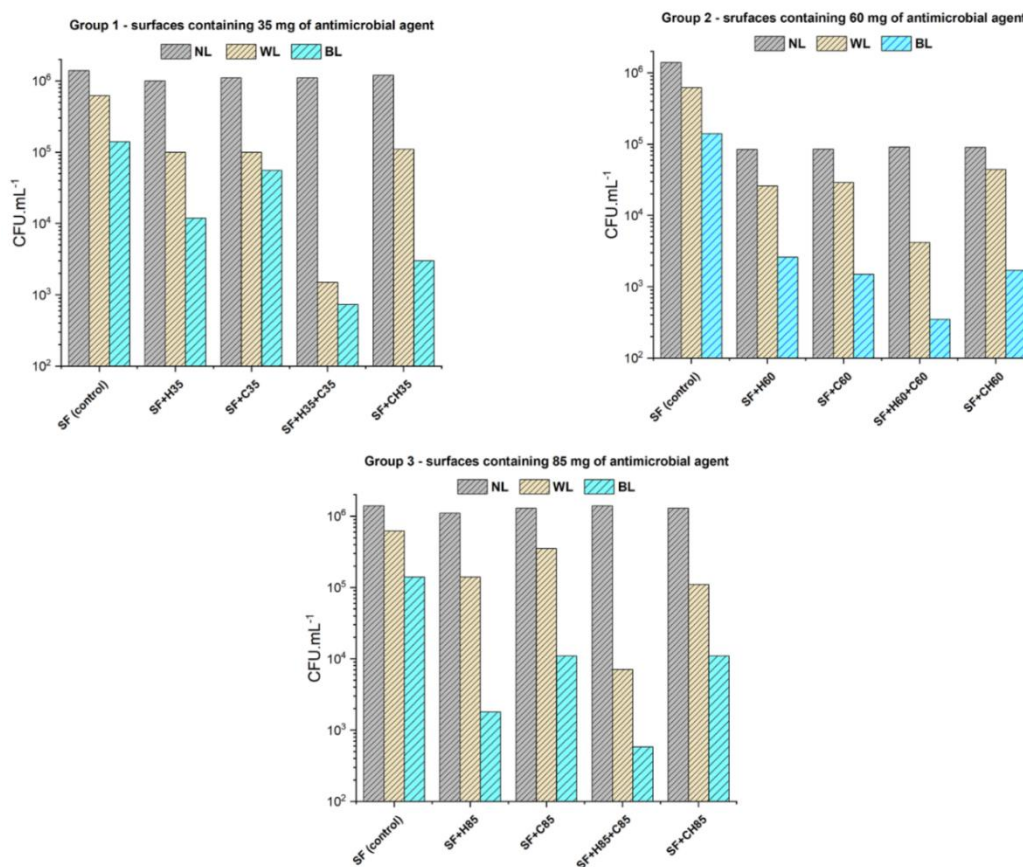


Figure 3.30. Antimicrobial activity of light-activated surfaces towards *E. coli*: (SF) surface with no antimicrobial agent; (SF+HX) surface containing A200B0 homopolymer at the corresponding quantity, where X = 35 mg, 60 mg or 85 mg; (SF+CHX) surface containing CA200B0; (SF+CX) surface containing curcumin at the corresponding quantity, where X = 35 mg, 60 mg or 85 mg; (SF+HX+CX) surface containing a mixture of A200B0 homopolymer and curcumin, each one at the corresponding quantity, where X = 35 mg, 60 mg or 85 mg.

Figure 3.31 shows the results for the surfaces containing the non-functionalized copolymer A200B20, the CA200B25 copolymer, and the A200B20 copolymer/curcumin mixtures. Similarly, to what was previously observed, the surfaces exposed to light irradiation showed a higher reduction in the number of viable bacteria than the one subjected to dark conditions, confirming the aPDI character of the surfaces. Interestingly, the samples containing the amphiphilic copolymers (A200B25 and CA200B25) and treated with blue

light, showed CFU. mL⁻¹ values in the order of 10⁴ - 10⁵ (Figure 3. 31), being equal or similar to those surfaces containing only curcumin also treated with blue light. These results indicated that, in the surfaces, the copolymers did not exert influence on the antimicrobial activity at the same extension of the PAMPTMA homopolymer has shown. As indicative, considering that the PAMPTMA-*co*-PBA present a degree of hydrophobicity (10% of PBA) and the varnish solution is water-based, it is speculated that the amphiphilic polymeric structure might behave differently from a cationic PAMPTMA homopolymer into the varnish formulation. Nonetheless, to confirm it, further studies of surfaces characterization should be performed. Lastly, the results obtained for surfaces containing A200B20 copolymer/curcumin mixtures were inconclusive. Therefore, these results were not included in this discussion and in-depth investigation of these surfaces is suggested as future work.

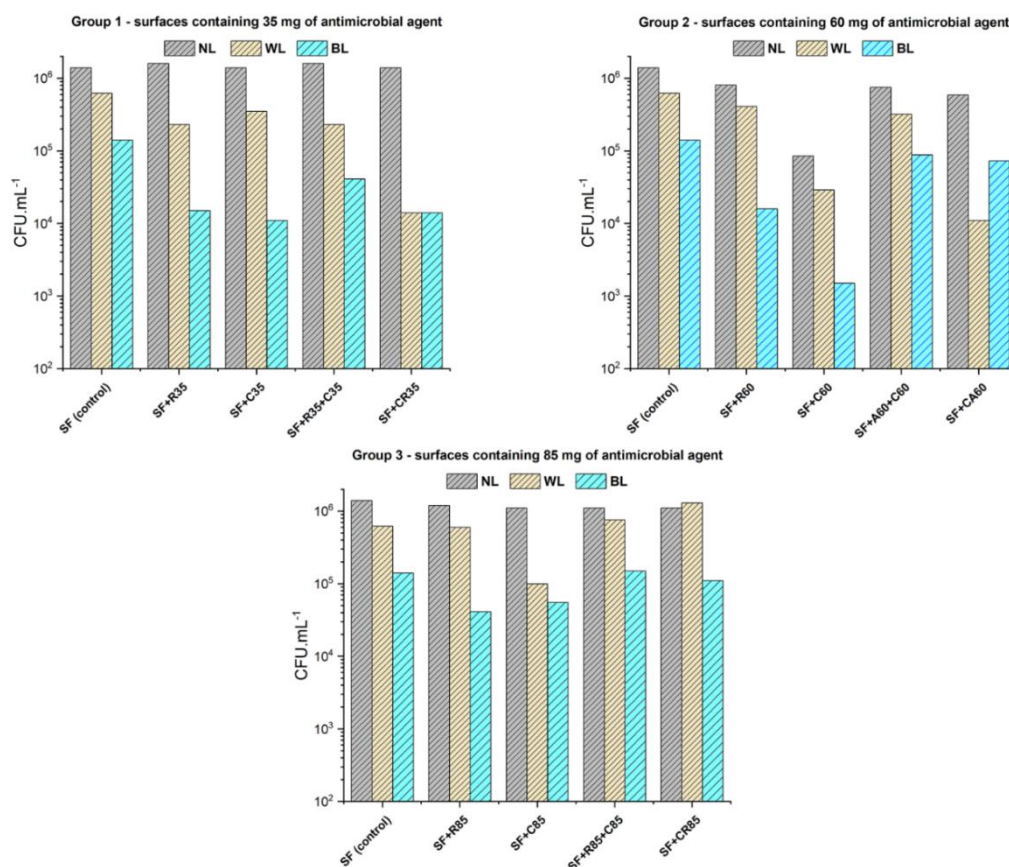


Figure 3.31 Antimicrobial activity of light-activated surfaces towards *E. coli*: (SF) surface with no antimicrobial agent; (SF+RX) surface containing A200B20 copolymer at the corresponding quantity, where X = 35 mg, 60 mg or 85 mg; (SF+CRX) surface containing CA200B25; (SF+CX) surface containing curcumin at the corresponding quantity, where X = 35 mg, 60 mg or 85 mg; (SF+RX+CX) surface containing a mixture of A200B20 copolymer and curcumin, each one at the corresponding quantity, where X = 35 mg, 60 mg or 85 mg.

3.3.11. Conclusions

TBO, curcumin and proflavine in their free form showed aPDI to a wide range of bacteria including three Gram-positive and two Gram-negative. Mixtures of polymers and photosensitizers were evaluated against *E. coli* and showed that at certain concentrations, the two agents exhibit synergistic antimicrobial effect in solution. The polymers functionalized with curcumin or proflavine also showed antimicrobial action but similar to the one of polymer with no PS in their structure. Also, these PS-functionalized polymers showed no significant difference in their antimicrobial activity under dark or light conditions, possibly due to the low quantity of PS present in the bacterial suspension, which did not produce ROS enough to exhibit lethal effect to the microorganisms. The novel antimicrobial polymeric system showed the potential to be used as additive in varnish formulations to produce antimicrobial surfaces. The aPDI assays of the surfaces revealed a photoantimicrobial property with higher activity under blue light than under white light, in the conditions investigated. The surfaces containing PAMPTMA/curcumin mixtures exhibited stronger activity in comparison to the one of other surfaces containing CA200B0 (CI-initiated PAMPTMA homopolymer) at the respective quantity. The surfaces doped with the amphiphilic random copolymers did not show a reduction in the number of viable cells in the same extension as the one observed for the surfaces containing the cationic homopolymers. These results suggest that the cationic PAMPTMA-Br homopolymer in conjunction with curcumin could be most appropriate for the use as antimicrobial additive for waterborne coating formulations to produce efficient light-responsive antimicrobial surfaces.

Chapter 4 - Final remarks

4.1. Overall conclusions

RDRP has brought countless advances to the macromolecular engineering field. One of the most used RDRP techniques is ATRP, which has enabled the expansion of the application of precisely designed polymers towards diverse fields including biomedical-related areas. Over the past decades, significant improvements of ATRP have been made, resulting on the development of more eco-friendly and industrially feasible systems using lower amounts of metal catalyst and benign solvents, such as water. However, there is still a current demand for the development of new catalytic complexes that could use commercially affordable ligands. The development of metal-catalyzed ATRP systems able to produce well-defined polymers using low amounts of copper (ppm levels) brought benefits for the application of these polymers in specific areas, such as the biomedical-related ones. On this matter, in the light of the increasing microbial resistance development and the urgent need for alternative therapeutic agents, ATRP has been one important tool for engineering macromolecules with improved features concerning pathogens inactivation. Polymers produced by ATRP, like those ones prepared in this PhD project, have demonstrated promising potential for the practical use as antimicrobial agents.

In the first part of chapter 3, it is described the use of the TMG as a new ligand for the SARA ATRP of diverse methacrylates including MMA, GMA, EMA, BMA and DPA. Using TMG as the ligand, it was possible to achieve similar control over the polymerizations ($M_w/M_n \approx 1.2$) to that obtained using other ligands often employed in ATRP (*e.g.*, PMDETA or Me₆TREN) for the investigated monomers. Also, TMG produced polymers with high end-functionality, as proved by self-extension and block copolymerization of PMMA-Br with BMA, resulting in polymer showing good agreement between theoretical (M_n^{th}) and experimental molecular weights (M_n^{SEC}) with low dispersity ($M_w/M_n \approx 1.2$). Additional experiments were conducted in absence of Cu⁰ (SARA agent) and it was demonstrated that TMG was able to simultaneously act as the ligand for metal coordination (catalytic complex formation) and as the reducing agent of Cu^{II} species. This work was a contribution to the development of more cost-effective ATRP systems using affordable commercial compounds, envisioning a future scale-up of the technique.

The second part of chapter 3 was dedicated to the development of a new polymeric system able to exhibit a broad range of antibacterial activity. In this study, several polymers with

different composition and architecture were prepared and evaluated against three bacteria commonly associated to the nosocomial infections (*S. aureus*, *E. coli*, and *P. aeruginosa*) and two species belonging the genus *Bacillus* (*B. cereus* and *B. subtilis*). The polymeric structures consisted of biocidal PAMPTMA homopolymer or (block)copolymers composed of biocidal PAMPTMA and hydrophobic PBA. Diverse polymeric compositions (homopolymers, block copolymers and random copolymers), architectures (linear and star-shaped) with varied MW were prepared using SARA ATRP. The MIC values of the polymers revealed a broad-spectrum antibacterial activity, with higher inactivation effect towards the Gram-positive (*S. aureus*, *B. cereus* and *B. subtilis*), being the most influencing factor the MW (antimicrobial activity increased with increasing MW). To address the mechanistic features of antimicrobial action of the novel polymeric system, live/dead assays and SEM microscopy imaging were used and it was proved that the polymers induced cell death (*E. coli*) by bacterial membrane disruption with subsequently leakage of the intramembrane cell compounds. Regarding the development of antimicrobial polymers, the arm-first procedure was used to prepare high-branched star-shaped PAMPTMA aimed to evaluate their antimicrobial behavior. Although well-defined star polymers were obtained, the complete incorporation of the linear PAMPTMA MI during the star formation was not achieved, resulting in a final product consisting of star polymers and unreacted linear PAMPTMA MI. Their MIC was determined but, it was not possible to properly measure the antimicrobial activity of these star polymers due to the presence of PAMPTMA MI in the samples analyzed.

The last part of chapter 3 was dedicated to exploring the aPDI effect of polymers combined with PS molecules. To do this, two strategies were used: (i) simple mixtures of biocidal polymer and PS and (ii) PS molecules were covalently bonded to the biocidal polymeric structure. Before the experiments using polymer/PS, the selected PS molecules, namely curcumin, TBO and proflavine were used as antimicrobial agents for the optimization of the aPDI assessment conditions. The results of the PS/polymer mixtures revealed that the combination produced a synergistic antimicrobial effect in solution towards *E. coli* with proflavine/polymer mixtures displaying the highest activity for this Gram-negative strain. As the second strategy, derivatives of curcumin or proflavine were synthesized and used as ATRP initiators to prepare biocidal polymeric structures presenting one PS molecule per polymeric chain. Their antimicrobial activity was evaluated and compared with that of the non-functionalized polymers (all polymers were designed to have similar MW). The results

obtained showed that the proflavine-initiated polymers exhibited similar antimicrobial activity to that of non-functionalized polymers, while the curcumin-initiated polymers were less active towards the microorganisms tested. Besides, no significant differences in the MIC values were obtained under dark or light conditions, possibly due to the low quantity of PS present in the bacterial media (one PS molecule per polymeric chain). In the final part of the chapter, the results regarding the aPDI properties of surfaces coated with varnishes containing non-functionalized polymers, curcumin-initiated polymers or polymers/curcumin mixtures in different contents were presented. The results revealed that the surfaces containing curcumin showed a higher reduction in the number of bacteria when exposed to light, indicating a typical aPDI character. Moreover, the mixtures PAMPTMA-Br/curcumin showed the lowest number of bacteria after the treatment with light, indicating that combining polymer and curcumin should be the most appropriate approach to create antimicrobial agents that could be used as additives for waterborne varnish formulations.

4.2. Future work

This work has contributed to the development of a more cost-effective ATRP system for the preparation of well-defined poly(methacrylates) using the commercially available TMG as the complexing ligand for copper species. This study presented an attractive perspective for the industrial scale-up production of well-controlled polymers. Although TMG produced well-defined polymers, the study was focused on the polymerization of methacrylate monomers. In this regard, there is still a demand for the development of non-expensive ligand-metal complexes to be used in the polymerization of diverse monomer families, such as acrylamides, acrylates and styrene.

This work also gave a significant contribution to the development of new antimicrobial agents with the potential to prevent microbial infections, namely the creation of antimicrobial surfaces. In this vein, the following topics are suggested to be further explored:

- ❖ Design of new antimicrobial polymeric systems using the arm-first approach. This methodology allows the straightforward preparation of high molecular weight polymers, which could be explored as potentials new antimicrobial agents. On the

matter, there is a vast range of cationic monomers which could be used for the preparation star-shaped polymeric structures *via* arm-first approach.

- ❖ Synthesis of a vinyl monomer from photosensitizer molecules and preparation an amphiphilic polymeric structure, presenting PS molecules distributed along the polymeric chain. Through this approach, it will be potentially possible to obtain an antimicrobial light-responsive polymer.

- ❖ Preparation of a coating formulation using light-responsive cationic polymers as antimicrobial agents. This approach will allow obtaining a self-decontaminated surface with dual-antimicrobial action: (i) contact-active antimicrobial action due to the presence of the cationic segment; (ii) aPDI due to the presence of PS molecules in the polymeric structure.

Appendices

Appendix A

Guanidine as inexpensive dual function ligand and reducing agent for ATRP of methacrylates.

Table A1. Results of the Cu⁰-mediated ATRP of MMA using TMG as the ligand and freeze-thaw degassing procedure (replicate experiments). Conditions: [MMA]₀/[EBPA]₀/[TMG]₀/[CuB₂]₀: 222/1/0.5/0.1, [MMA]₀/[DMSO] = 1/0.5 (v/v); t = 6.5 h; T = 30 °C; Cu⁰wire: l = 5 cm, d = 1 mm.

Entry	Conv. (%)	$M_n^{\text{th}} \times 10^{-3}$	$M_n^{\text{SEC}} \times 10^{-3}$	\bar{D}	I_{eff} (%)
1	64	15.0	21.4	1.29	70
2	66	15.0	48.8	2.32	30
3	71	16.9	74.6	1.49	22

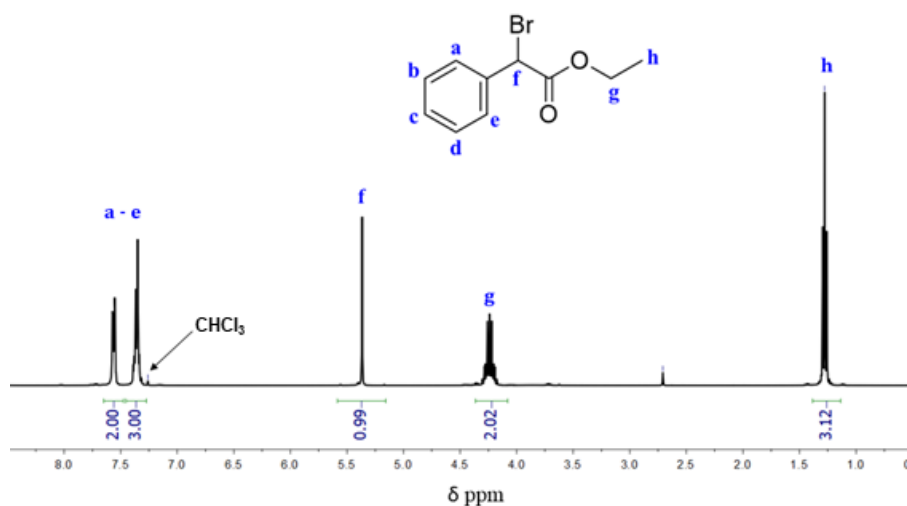


Figure A1. 400 MHz ¹H NMR, in CHCl₃, of ethyl α -bromophenyl acetate (EBPA).

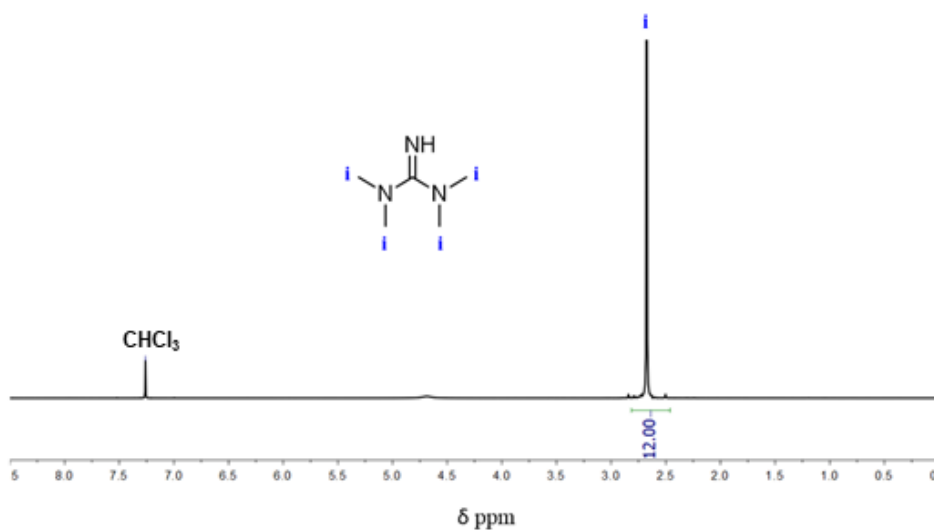


Figure A2. 400 MHz ^1H NMR, in CHCl_3 , of 1,1,3,3-tetramethylguanidine (TMG).

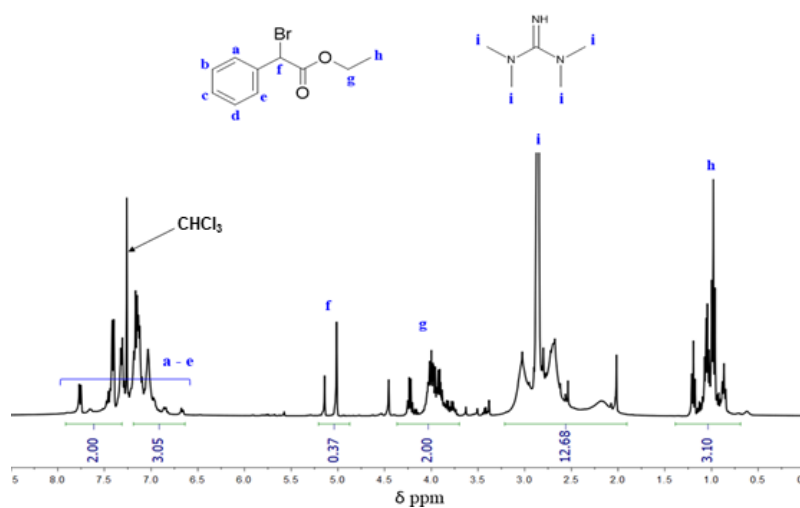


Figure A3. 400 MHz ^1H NMR, in CDCl_3 , of a $[\text{EBPA}]_0/[\text{TMG}]_0 = 1/1$ (molar)

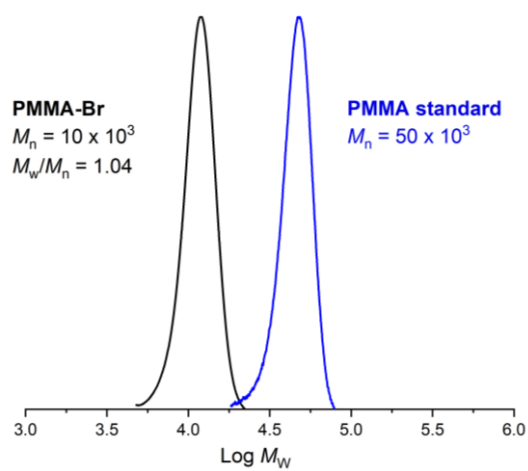


Figure A4. SEC traces of a PMMA-Br ($M_n^{\text{SEC}} = 10 \times 10^3$; $M_w/M_n = 1.12$) prepared by SARA ATRP using TMG as the ligand (black line) and a PMMA standard (blue line).

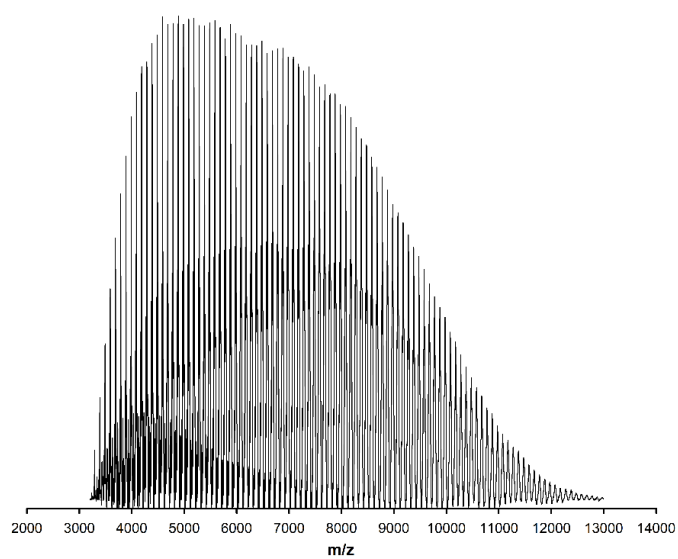


Figure A5. MALDI-TOF MS spectrum of PMMA-Br ($M_n^{\text{SEC}} = 7000$, $M_w/M_n = 1.14$) from m/z 500 to 7500, using DCTB matrix.

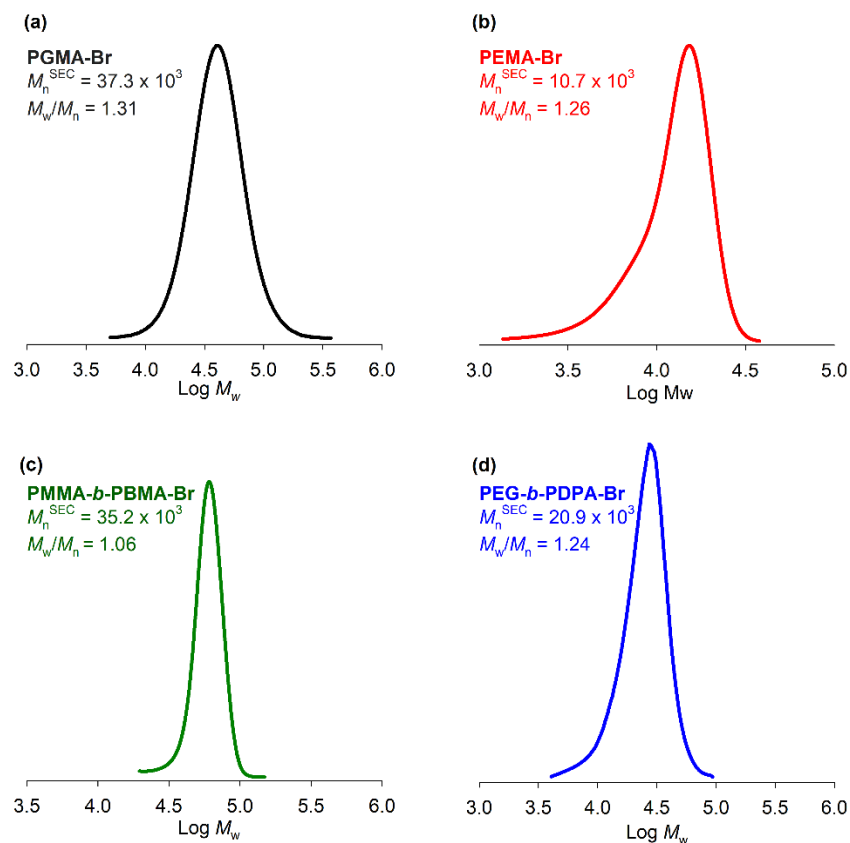


Figure A6. SEC traces of the polymethacrylates obtained by SARA ATRP.

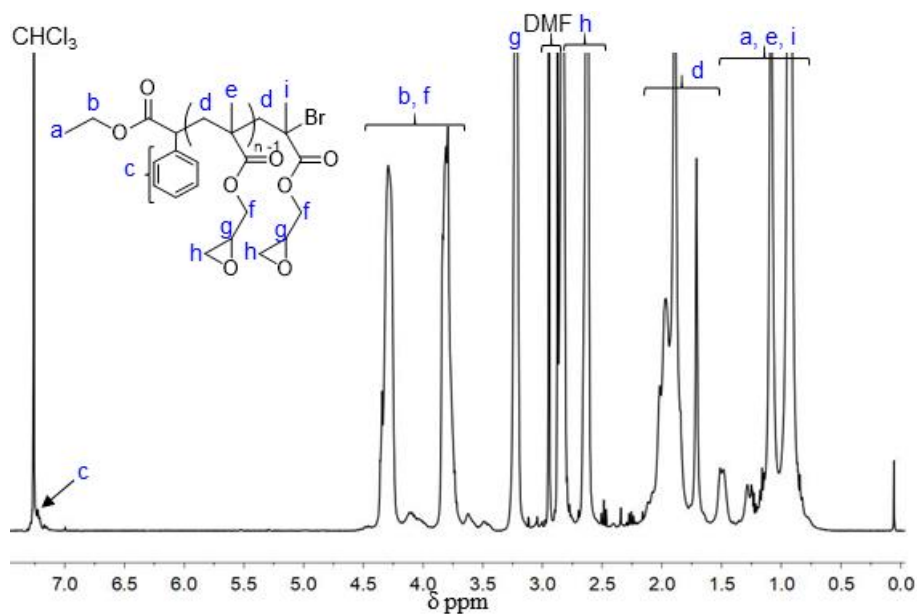


Figure A7. 400 MHz ¹H NMR spectrum, in CHCl₃, of PGMA-Br homopolymer ($M_n^{th} = 22600$, $M_n^{SEC} = 37300$, $M_w/M_n = 1.31$).

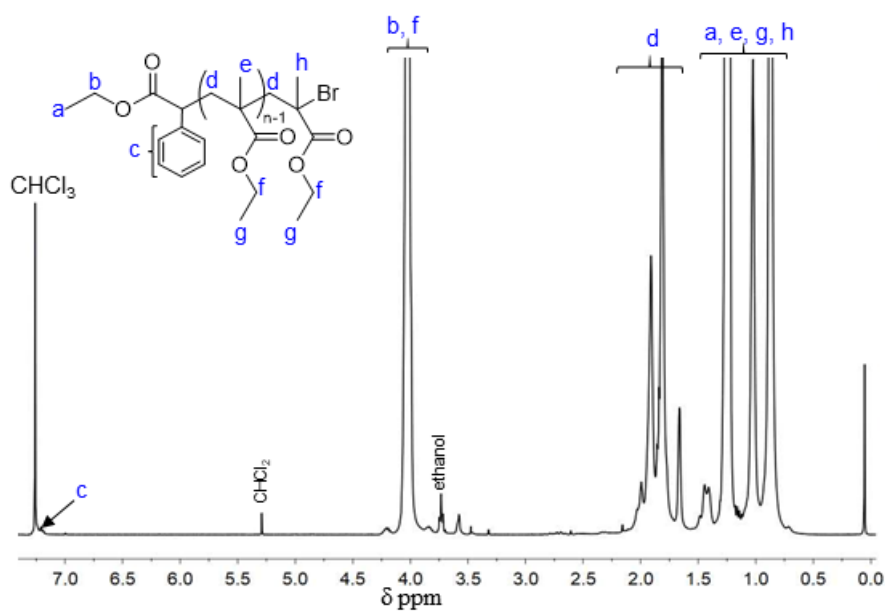


Figure A8. 400 MHz ^1H NMR spectrum, in CHCl_3 , of PEMA-Br homopolymer ($M_n^{\text{th}} = 8340$, $M_n^{\text{SEC}} = 1070$, $M_w/M_n = 1.26$).

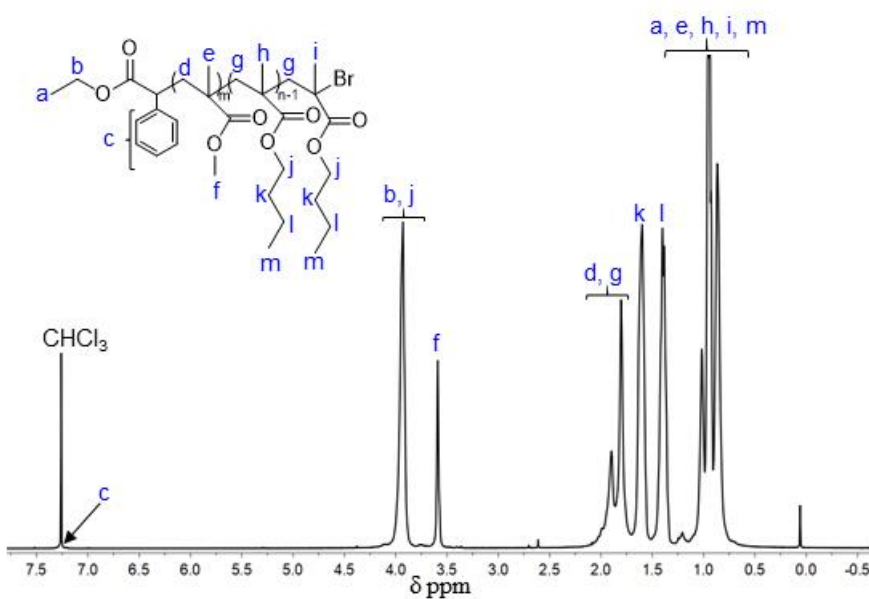


Figure A9. 400 MHz ^1H NMR spectrum in CHCl_3 of PMMA-*b*-PBMA-Br copolymer ($M_n^{\text{th}} = 27900$, $M_n^{\text{SEC}} = 35200$, $M_w/M_n = 1.06$).

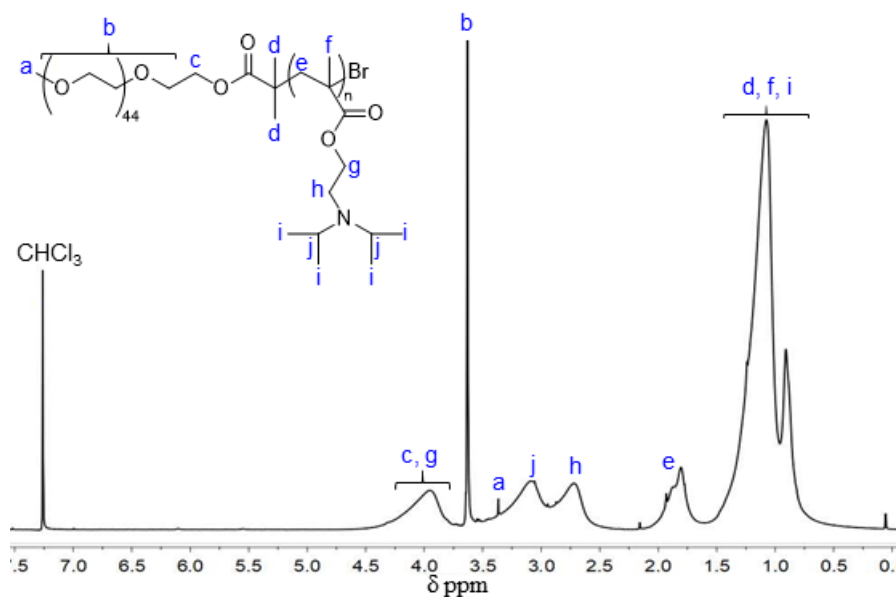


Figure A10. 400 MHz ^1H NMR spectrum in CHCl_3 of PEG-*b*-PDPA-Br block copolymer ($M_n^{\text{th}} = 20100$, $M_n^{\text{SEC}} = 20900$, $M_w/M_n = 1.24$).

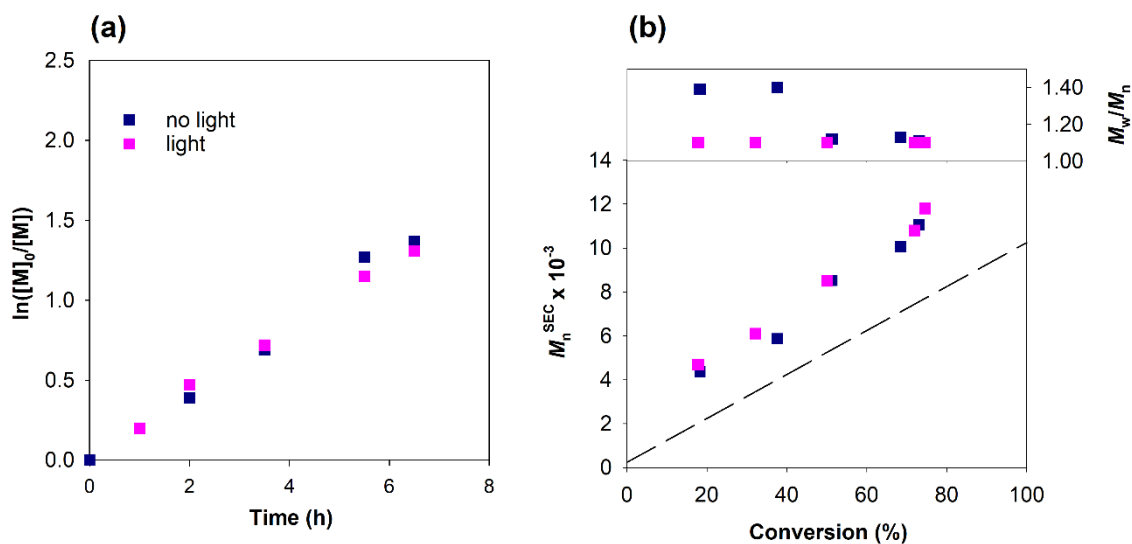


Figure A11. Kinetic plots of (a) $\ln([M]_0/[M])$ vs. time and (b) M_n^{SEC} and M_w/M_n vs. monomer conversion for SARA ATRP of MMA at 30 °C in DMSO in the presence and absence of light. Conditions: $[MMA]_0/[DMSO] = 2/1$ (v/v); $[MMA]_0/[EBPA]_0/[CuBr_2]_0/[TMG]_0 = 100/1/0.1/2$; Cu^0 wire: $l = 5.0$ cm, $d = 1$ mm.

Appendix B

Increasing the antimicrobial activity of amphiphilic cationic copolymers by the facile synthesis of high molecular weight stars by SARA ATRP

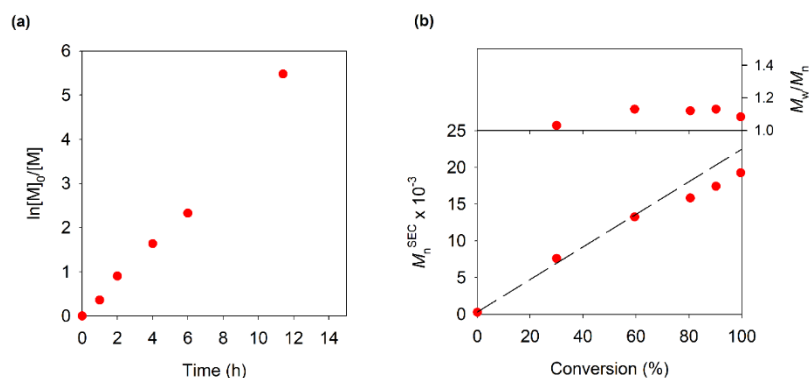


Figure B1. Kinetic plots of (a) $\ln[M]_0/[M]$ vs. time and (b) plot of number-average molecular weights (M_n^{SEC}) and M_w/M_n vs. conversion for the SARA ATRP of AMPTMA in EtOH. $[\text{AMPTMA}]_0/[\text{EBiB}]_0/[\text{CuBr}_2]_0/[\text{Me}_6\text{TREN}]_0/\text{Cu}^0 \text{ wire} = 100/1/0.5/1.0/\text{Cu}^0 \text{ wire}$; $[\text{AMPTMA}]_0 = 2.0 \text{ M}$; $\text{Cu}^0 \text{ wire}$: $l = 5 \text{ cm}$; $d = 1 \text{ mm}$; $V_{\text{solvent}} = 4.8 \text{ mL}$.

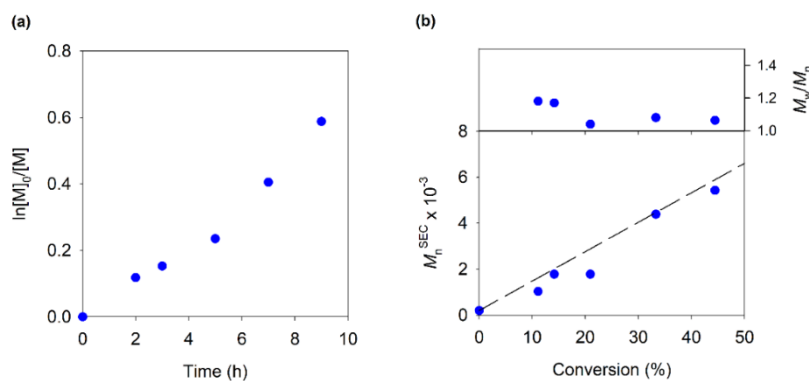


Figure B2. Kinetic plots of (a) $\ln[M]_0/[M]$ vs. time and (b) plot of number-average molecular weights (M_n^{SEC}) and M_w/M_n vs. conversion for the SARA ATRP of *n*-BA in EtOH. $[\textit{n}\text{-BA}]_0/[\text{EBiB}]_0/[\text{CuBr}_2]_0/[\text{Me}_6\text{TREN}]_0/\text{Cu}^0 \text{ wire} = 100/1/0.5/1.0/\text{Cu}(0) \text{ wire}$; $[\textit{n}\text{-BA}]_0 = 6.9 \text{ M}$; $\text{Cu}(0) \text{ wire}$: $l = 5 \text{ cm}$; $d = 1 \text{ mm}$; $V_{\text{solvent}} = 2.0 \text{ mL}$.

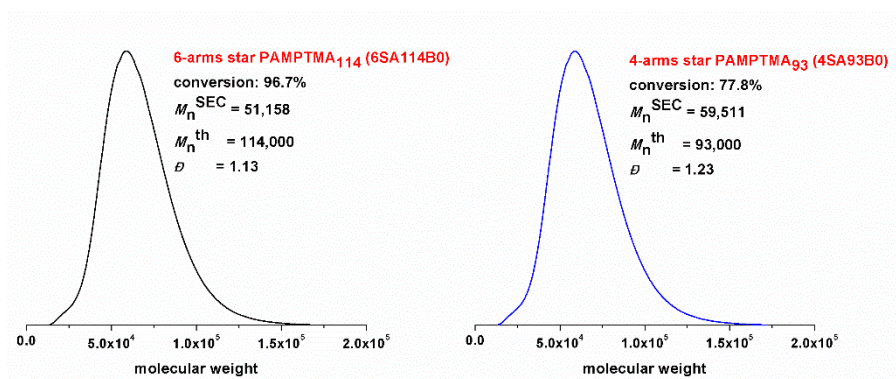


Figure B3. SEC traces of star-shaped (a) 6-arm and (b) 4-arm PAMPTMA homopolymers prepared by SARA ATRP in EtOH.

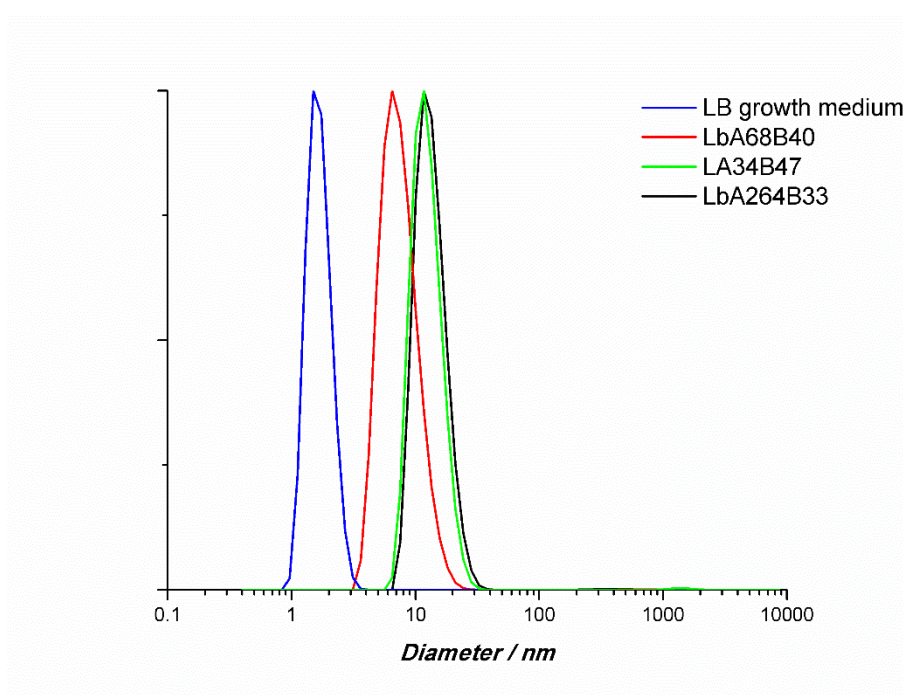


Figure B4. DLS volume distributions of representatives PAMPTMA-*co(b)*-PBA in LB bacterial cell culture media at their respective MIC values (25 °C).

Table B1. Characteristics and of the antimicrobial polymers and the respective MIC values, determined in liquid medium, in weight-based concentration.

Polymer code	% PBA (molar)	$M_n^{\text{th}} \times 10^{-3}$	MIC (mg/mL)				
			<i>S. aureus</i>	<i>B. subtilis</i>	<i>B. cereus</i>	<i>E. coli</i>	<i>P. aeruginosa</i>
6SA114B0	0	142.0	0.36	0.17	1.42	5.68	1.42
6SA69B41	37	117.4	2.35	0.07	>4.69	4.69	1.17
6SA79B24	23	117.3	2.35	0.14	>4.70	>4.70	1.17
6SA22B0	0	28.1	1.12	0.14	0.281	>4.70	>4.70
6SA9B0	0	12.7	>4.7	0.51	>4.7	>4.70	>4.70
4SA93B0	0	77.6	0.19	0.09	0.78	3.10	1.55
4SA84B20	20	80.5	1.61	0.09	>4.7	3.22	3.22
LA38B2	5	8.3	>1.66	0.03	1.66	>1.66	>1.66
LA34B9	20	8.4	>1.67	0.007	1.68	1.68	>1.68
LA23B23	50	8.0	>1.68	0.22	0.9	0.45	>1.66
LA27B33	56	10.0	>1.69	2.00	2.00	1.00	2.00
LA50B4	7	11.0	0.27	0.008	0.55	2.20	2.20
LA45B15	24	11.5	>2.3	0.02	>2.3	2.3	>2.3
LA39B47	55	14.2	2.84	0.09	0.36	2.84	2.84
LA115B0	0	24.0	0.60	0.15	0.300	4.80	4.80
LA98B29	23	24.2	4.84	0.02	4.840	4.84	0.07
LA59B44	42	18.2	>3.64	0.02	>3.64	1.82	1.82
LbA78B63	44	24.4	4.88	1.22	4.88	4.88	4.88
LbA68B40	37	19.4	4.37	0.02	0.55	4.36	2.18
LbA264B33	10	59.0	1.18	0.07	>2.36	>2.36	2.36
LA335B0	0	69.4	0.17	0.08	0.69	0.69	2.78
LA0B49	100	6.4	0	0	0	0	0

Table B2. Characterization of the antimicrobial polymers prepared by SARA ATRP.

Polymer code	Time (h)	Conv. (%) AMPTMA ^a	Conv. (%) <i>n</i> -BA ^a	DP _{AMPTMA} / DP _{<i>n</i>-BA} ^b	% PBA (molar) ^c	$M_n^{\text{th}} \times 10^{-3d}$
6SA114B0	15	96.7	-	114/0	0	142.0
6SA69B41	15	78.5	73.2	69/41	37	117.4
6SA79B24	15	80.6	95.3	79/24	23	117.3
6SA22B0	15	87.2	-	22/0	0	28.1
6SA9B0	15	93.2	-	9/0	0	12.7
4SA93B0	8	77.8	-	93/0	0	77.6
4SA84B20	8	66.3	59.4	84/20	20	80.5
LA38B2	15	95.5	100	38/2	5	8.3
LA34B9	15	97.7	97.5	34/9	20	8.4
LA23B23	15	92.2	96.6	23/23	50	8.0
LA27B33	10	67.4	67.2	27/33	56	10.0
LA50B4	15	88.3	89.4	50/4	7	11.0
LA45B15	20	90.4	92.5	45/15	24	11.5
LA39B47	15	93.6	88.2	39/47	55	14.2
LA115B0	15	97.6	-	115/0	0	24.0
LA98B29	19	81.5	82.2	98/29	23	24.2
LA59B44	10	76.6	91.3	59/44	42	18.2
LbA78B63	18	82.0	52.7	78/63	44	24.4
LbA68B40	14	64.1	39.5	68/40	37	19.4
LbA264B33	18	73.9	30.2	26/33	10	59.0
LA315B0	23	89.5	-	335/0	0	69.4
LA0B49	19	-	80.4	0/49	100	6.4

^a Monomer conversion; ^b Degree of polymerization; ^c Molar percentage of PBA in the copolymer; ^d Theoretical number average molecular weight values were determined by ¹H NMR peak integration analysis.

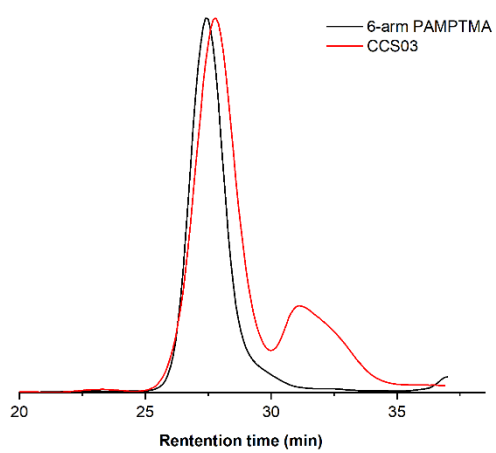


Figure B5. SEC traces of the (black) 6-arm PAMPTMA and (red) CCS03

Appendix C

Antimicrobial photodynamic inactivation

Table C1. Molar ratio and kinetic data of polymers prepared via Cu⁰-mediated SARA ATRP

Entry	[AMPTMA] ₀ /[<i>n</i> -BA] ₀ /	Time (h)	Conv. (%)	Conv. (%)	<i>M</i> _n th × 10 ⁻³
	[I] ₀ /[Me ₆ TREN] ₀ /[CuBr ₂] ₀		AMPTMA	<i>n</i> -BA	
1 ^a	375 / 0 / 1 / 1 / 0.5	24	89	-	67
2 ^b	375 / 0 / 1 / 1 / 0.5	24	44	-	35.4
3 ^b	375 / 0 / 1 / 1 / 0.5	72	50	-	39.8
4 ^b	375 / 0 / 1 / 2 / 1.0	72	62	-	46.2
5 ^b	740 / 0 / 1 / 1 / 0.5	72	31	-	47.4
6 ^b	375 / 37 / 1 / 1 / 0.5	24	19	33	16.3
7 ^b	375 / 37 / 1 / 2 / 1	72	55	69	45.5

^a[I] = EBiB; ^b[I] = Cl.

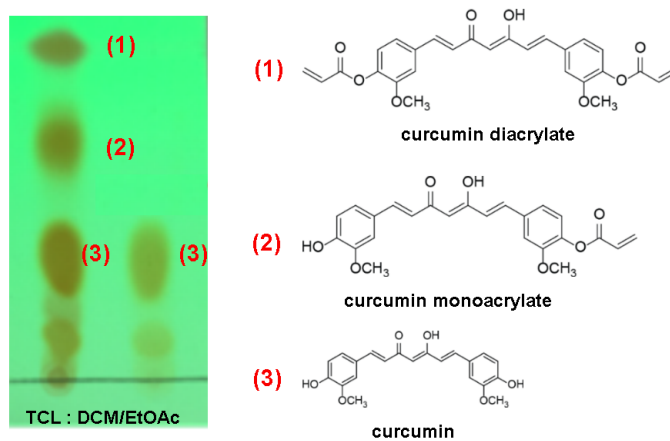


Figure C1. TLC of the curcumin (right stains) and the resulting product of the acetylation reaction (left stains)

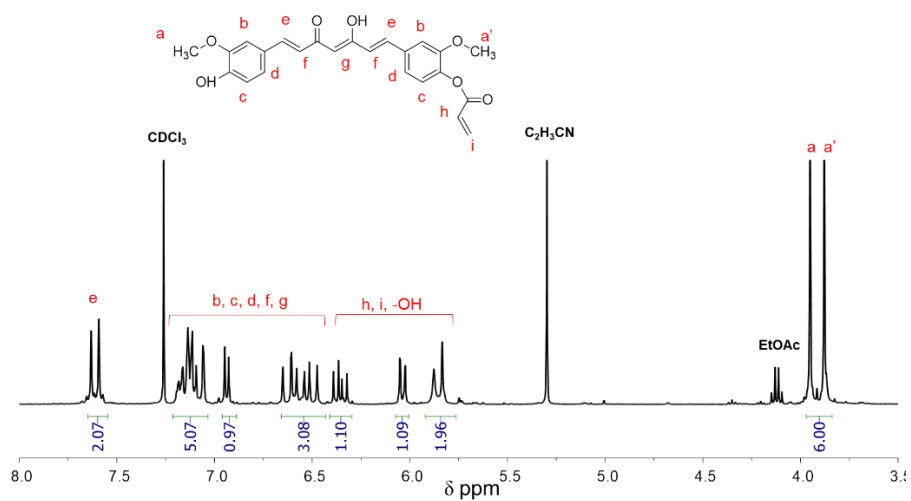


Figure C2. 400 MHz ^1H NMR spectrum 400 Hz, in CDCl_3 , of the curcumin monoacrylate.

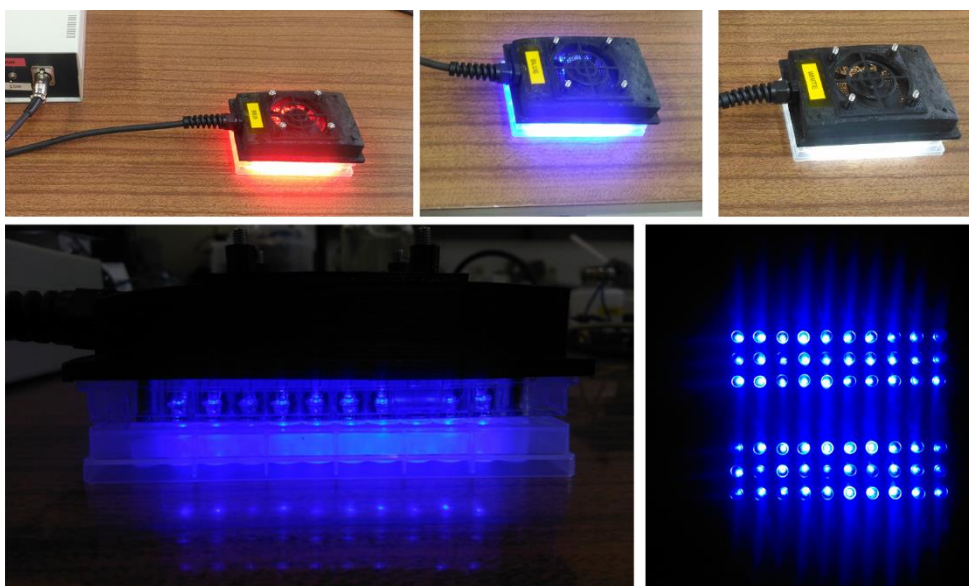


Figure C3. LED systems used for the antimicrobial assays in liquid medium.

References

1. Moad, G.; Solomon, D. H., 2 - Radical Reactions. In *The Chemistry of Radical Polymerization (Second Edition)*, Moad, G.; Solomon, D. H., Eds. Elsevier Science Ltd: Amsterdam, 2005; pp 11-48.
2. Nuyken, O., The Chemistry of Free Radical Polymerization. Von G. Moad und D. H. Solomon. Pergamon-Elsevier Science Ltd., Oxford, 1995. 408 S., geb. 75.00 £.—ISBN 0-08-42078-8. *Angewandte Chemie* **1997**, 109, (10), 1173-1175.
3. Matyjaszewski, K.; Tsarevsky, N. V., Macromolecular Engineering by Atom Transfer Radical Polymerization. *Journal of the American Chemical Society* **2014**, 136, (18), 6513-6533.
4. Nuyken, O., The Chemistry of Free Radical Polymerization. Von G. Moad und D. H. Solomon. Pergamon-Elsevier Science Ltd., Oxford, 1995. 408 S., geb. 75.00 £.—ISBN 0-08-42078-8. *Angewandte Chemie* **1997**, 109, (10), 1173-1175.
5. Scott, N. D.; Walker, J. F.; Hansley, V. L., Sodium Naphthalene. I. A New Method for the Preparation of Addition Compounds of Alkali Metals and Polycyclic Aromatic Hydrocarbons. *Journal of the American Chemical Society* **1936**, 58, (12), 2442-2444.
6. Szwarc, M.; Levy, M.; Milkovich, R., Polymerization initiated by electron transfer to monomer. A new method of formation of block copolymers. *Journal of the American Chemical Society* **1956**, 78, (11), 2656-2657.
7. Storey, R. F., CHAPTER 2 Fundamental Aspects of Living Polymerization. In *Fundamentals of Controlled/Living Radical Polymerization*, The Royal Society of Chemistry: 2013; pp 60-77.
8. Coessens, V. M. C.; Matyjaszewski, K., Fundamentals of Atom Transfer Radical Polymerization. *Journal of Chemical Education* **2010**, 87, (9), 916-919.
9. Abreu, C. M. R.; Fonseca, A. C.; Rocha, N. M. P.; Guthrie, J. T.; Serra, A. C.; Coelho, J. F. J., Poly(vinyl chloride): current status and future perspectives via reversible deactivation radical polymerization methods. *Progress in Polymer Science* **2018**, 87, 34-69.
10. Moad, G.; Rizzardo, E.; Thang, S. H., Radical Addition–Fragmentation Chemistry and RAFT Polymerization. In *Reference Module in Materials Science and Materials Engineering*, Elsevier: 2016.
11. Chong, Y. K.; Ercole, F.; Moad, G.; Rizzardo, E.; Thang, S. H.; Anderson, A. G., Imidazolidinone Nitroxide-Mediated Polymerization. *Macromolecules* **1999**, 32, (21), 6895-6903.

12. Braunecker, W. A.; Matyjaszewski, K., Controlled/living radical polymerization: Features, developments, and perspectives. *Progress in Polymer Science* **2007**, 32, (1), 93-146.
13. Studer, A., Tin-free radical chemistry using the persistent radical effect: alkoxyamine isomerization, addition reactions and polymerizations. *Chemical Society Reviews* **2004**, 033, (5), 267-273.
14. Matyjaszewski, K., General Concepts and History of Living Radical Polymerization. *Handbook of Radical Polymerization* **2002**, 361-406.
15. Matyjaszewski, K., Controlled Radical Polymerization: State of the Art in 2008. In *Controlled/Living Radical Polymerization: Progress in ATRP*, American Chemical Society: 2009; Vol. 1023, pp 3-13.
16. Schué, F., Controlled/living radical polymerization: progress in ATRP, NMP and RAFT: ACS symposium series no 768 Edited by: Krzysztof Matyjaszewski American Chemical Society, Washington, DC, September 2000 pp 484, price \$150.00 ISBN 0-8412-3707-7. *Polymer International* **2002**, 51, (4), 370-370.
17. Zetterlund, P. B.; Thickett, S. C.; Perrier, S.; Bourgeat-Lami, E.; Lansalot, M., Controlled/Living Radical Polymerization in Dispersed Systems: An Update. *Chemical Reviews* **2015**, 115, (18), 9745-9800.
18. Shanmugam, S.; Matyjaszewski, K., Reversible Deactivation Radical Polymerization: State-of-the-Art in 2017. In *Reversible Deactivation Radical Polymerization: Mechanisms and Synthetic Methodologies*, American Chemical Society: 2018; Vol. 1284, pp 1-39.
19. Matyjaszewski, K., Atom Transfer Radical Polymerization (ATRP): Current Status and Future Perspectives. *Macromolecules* **2012**, 45, (10), 4015-4039.
20. Tang, W.; Matyjaszewski, K., Effect of Ligand Structure on Activation Rate Constants in ATRP. *Macromolecules* **2006**, 39, (15), 4953-4959.
21. Tang, W.; Kwak, Y.; Braunecker, W.; Tsarevsky, N. V.; Coote, M. L.; Matyjaszewski, K., Understanding Atom Transfer Radical Polymerization: Effect of Ligand and Initiator Structures on the Equilibrium Constants. *Journal of the American Chemical Society* **2008**, 130, (32), 10702-10713.
22. Matyjaszewski, K.; Paik, H.-j.; Zhou, P.; Diamanti, S. J., Determination of Activation and Deactivation Rate Constants of Model Compounds in Atom Transfer Radical Polymerization. *Macromolecules* **2001**, 34, (15), 5125-5131.

-
23. Matyjaszewski, K.; Xia, J., Atom Transfer Radical Polymerization. *Chemical Reviews* **2001**, 101, (9), 2921-2990.
 24. Matyjaszewski, K., Controlled Radical Polymerization: State-of-the-Art in 2014. In *Controlled Radical Polymerization: Mechanisms*, American Chemical Society: 2015; Vol. 1187, pp 1-17.
 25. Kwak, Y.; Magenau, A. J. D.; Matyjaszewski, K., ARGET ATRP of Methyl Acrylate with Inexpensive Ligands and ppm Concentrations of Catalyst. *Macromolecules* **2011**, 44, (4), 811-819.
 26. Jakubowski, W.; Matyjaszewski, K., Activators Regenerated by Electron Transfer for Atom-Transfer Radical Polymerization of (Meth)acrylates and Related Block Copolymers. *Angewandte Chemie International Edition* **2006**, 45, (27), 4482-4486.
 27. Gnanou, Y.; Hizal, G., Effect of phenol and derivatives on atom transfer radical polymerization in the presence of air. *Journal of Polymer Science Part A: Polymer Chemistry* **2004**, 42, (2), 351-359.
 28. Min, K.; Gao, H.; Matyjaszewski, K., Use of Ascorbic Acid as Reducing Agent for Synthesis of Well-Defined Polymers by ARGET ATRP. *Macromolecules* **2007**, 40, (6), 1789-1791.
 29. Costa, J. R. C.; Góis, J. R.; De Bon, F.; Serra, A. C.; Guliashvili, T.; Isse, A. A.; Gennaro, A.; Coelho, J. F. J., Addressing the role of triphenylphosphine in copper catalyzed ATRP. *Polymer Chemistry* **2018**, 9, (44), 5348-5358.
 30. Konkolewicz, D.; Magenau, A. J. D.; Averick, S. E.; Simakova, A.; He, H.; Matyjaszewski, K., ICAR ATRP with ppm Cu Catalyst in Water. *Macromolecules* **2012**, 45, (11), 4461-4468.
 31. De Bon, F.; Isse, A. A.; Gennaro, A., Electrochemically Mediated Atom Transfer Radical Polymerization of Methyl Methacrylate: The Importance of Catalytic Halogen Exchange. *ChemElectroChem* **2019**, 6, (16), 4257-4265.
 32. Ryan, M. D.; Pearson, R. M.; French, T. A.; Miyake, G. M., Impact of Light Intensity on Control in Photoinduced Organocatalyzed Atom Transfer Radical Polymerization. *Macromolecules* **2017**, 50, (12), 4616-4622.
 33. Cole, J. P.; Federico, C. R.; Lim, C.-H.; Miyake, G. M., Photoinduced Organocatalyzed Atom Transfer Radical Polymerization Using Low ppm Catalyst Loading. *Macromolecules* **2019**, 52, (2), 747-754.

-
34. Pan, X.; Malhotra, N.; Zhang, J.; Matyjaszewski, K., Photoinduced Fe-Based Atom Transfer Radical Polymerization in the Absence of Additional Ligands, Reducing Agents, and Radical Initiators. *Macromolecules* **2015**, 48, (19), 6948-6954.
35. Zhang, Y.; Wang, Y.; Matyjaszewski, K., ATRP of Methyl Acrylate with Metallic Zinc, Magnesium, and Iron as Reducing Agents and Supplemental Activators. *Macromolecules* **2011**, 44, (4), 683-685.
36. Abreu, C. M. R.; Fu, L.; Carmali, S.; Serra, A. C.; Matyjaszewski, K.; Coelho, J. F. J., Aqueous SARA ATRP using inorganic sulfites. *Polymer Chemistry* **2017**, 8, (2), 375-387.
37. Abreu, C. M. R.; Mendonça, P. V.; Serra, A. C.; Popov, A. V.; Matyjaszewski, K.; Guliashvili, T.; Coelho, J. F. J., Inorganic Sulfites: Efficient Reducing Agents and Supplemental Activators for Atom Transfer Radical Polymerization. *ACS Macro Letters* **2012**, 1, (11), 1308-1311.
38. Mendonça, P. V.; Konkolewicz, D.; Averick, S. E.; Serra, A. C.; Popov, A. V.; Guliashvili, T.; Matyjaszewski, K.; Coelho, J. F. J., Synthesis of cationic poly((3-acrylamidopropyl)trimethylammonium chloride) by SARA ATRP in ecofriendly solvent mixtures. *Polym Chem.* **2014**, 5, (19), 5829-5836.
39. Mendonça, P. V.; Lima, M. S.; Guliashvili, T.; Serra, A. C.; Coelho, J. F. J., Deep eutectic solvents (DES): Excellent green solvents for rapid SARA ATRP of biorelevant hydrophilic monomers at ambient temperature. *Polymer* **2017**, 132, 114-121.
40. Mendonça, P. V.; Oliveira, A. S. R.; Ribeiro, J. P. M.; Castilho, A.; Serra, A. C.; Coelho, J. F. J., Pushing the limits of robust and eco-friendly ATRP processes: untreated water as the solvent. *Polymer Chemistry* **2019**, 10, (8), 938-944.
41. De Bon, F.; Isse, A. A.; Gennaro, A., Towards scale-up of electrochemically-mediated atom transfer radical polymerization: Use of a stainless-steel reactor as both cathode and reaction vessel. *Electrochimica Acta* **2019**, 304, 505-512.
42. Bienemann, O.; Haase, R.; Jesser, A.; Beschnitt, T.; Döring, A.; Kuckling, D.; dos Santos Vieira, I.; Flörke, U.; Herres-Pawlis, S., Synthesis and Application of New Guanidine Copper Complexes in Atom Transfer Radical Polymerisation. *European Journal of Inorganic Chemistry* **2011**, 2011, (15), 2367-2379.
43. Herres-Pawlis, S.; Haase, R.; Bienemann, O., Dissecting the role of guanidine copper complexes in atom transfer radical polymerization by density functional theory. *Journal of Cheminformatics* **2011**, 3, (1), P28.
-

-
44. Ren, J. M.; McKenzie, T. G.; Fu, Q.; Wong, E. H. H.; Xu, J.; An, Z.; Shanmugam, S.; Davis, T. P.; Boyer, C.; Qiao, G. G., *Star Polymers. Chemical Reviews* **2016**, 116, (12), 6743-6836.
45. Matyjaszewski, K.; Spanswick, J., *Atom Transfer Radical Polymerization (ATRP). In Reference Module in Materials Science and Materials Engineering*, Elsevier: 2016.
46. Gao, H.; Matyjaszewski, K., Synthesis of Star Polymers by A New “Core-First” Method: Sequential Polymerization of Cross-Linker and Monomer. *Macromolecules* **2008**, 41, (4), 1118-1125.
47. Li, S.; Chung, H. S.; Simakova, A.; Wang, Z.; Park, S.; Fu, L.; Cohen-Karni, D.; Averick, S.; Matyjaszewski, K., Biocompatible Polymeric Analogues of DMSO Prepared by Atom Transfer Radical Polymerization. *Biomacromolecules* **2017**, 18, (2), 475-482.
48. Lyu, J.; Gao, Y.; Zhang, Z.; Greiser, U.; Tai, H.; Wang, W., Can Flory-Stockmayer theory be applied to predict conventional free radical polymerization of multivinyl monomers? A study via Monte Carlo simulations. *Science China Chemistry* **2018**, 61, (3), 319-327.
49. Matsumoto, A.; Kitaguchi, Y.; Sonoda, O., Approach to Ideal Network Formation Governed by Flory–Stockmayer Gelation Theory in Free-Radical Cross-Linking Copolymerization of Styrene with m-Divinylbenzene. *Macromolecules* **1999**, 32, (25), 8336-8339.
50. Tew, G. N.; Clements, D.; Tang, H.; Arnt, L.; Scott, R. W., Antimicrobial activity of an abiotic host defense peptide mimic. *Biochimica et Biophysica Acta (BBA) - Biomembranes* **2006**, 1758, (9), 1387-1392.
51. Ding, H.; Park, S.; Zhong, M.; Pan, X.; Pietrasik, J.; Bettinger, C. J.; Matyjaszewski, K., Facile Arm-First Synthesis of Star Block Copolymers via ARGET ATRP with ppm Amounts of Catalyst. *Macromolecules* **2016**, 49, (18), 6752-6760.
52. McKenzie, T. G.; Wong, E. H. H.; Fu, Q.; Lam, S. J.; Dunstan, D. E.; Qiao, G. G., Highly Efficient and Versatile Formation of Biocompatible Star Polymers in Pure Water and Their Stimuli-Responsive Self-Assembly. *Macromolecules* **2014**, 47, (22), 7869-7877.
53. Mulani, M. S.; Kamble, E. E.; Kumkar, S. N.; Tawre, M. S.; Pardesi, K. R., Emerging Strategies to Combat ESKAPE Pathogens in the Era of Antimicrobial Resistance: A Review. *Frontiers in Microbiology* **2019**, 10, 539.
54. Kouchak, F.; Askarian, M., Nosocomial infections: the definition criteria. *Iran J Med Sci* **2012**, 37, (2), 72-73.
-

-
55. Brumfitt, W.; Percival, A.; Louvois, J. d., The Role of Penicillinase in Determining Natural and Acquired Resistance of Gram -Negative Bacteria to Penicillins. **1963**, 77-89.
56. Witte, W., International dissemination of antibiotic resistant strains of bacterial pathogens. *Infection, Genetics and Evolution* **2004**, 4, (3), 187-191.
57. Pendleton, J. N.; Gorman, S. P.; Gilmore, B. F., Clinical relevance of the ESKAPE pathogens. *Expert Review of Anti-infective Therapy* **2013**, 11, (3), 297-308.
58. Mulani, M. S.; Kamble, E. E.; Kumkar, S. N.; Tawre, M. S.; Pardesi, K. R., Emerging Strategies to Combat ESKAPE Pathogens in the Era of Antimicrobial Resistance: A Review. *Frontiers in microbiology* **2019**, 10, 539-539.
59. Billington, E. O.; Phang, S. H.; Gregson, D. B.; Pitout, J. D. D.; Ross, T.; Church, D. L.; Laupland, K. B.; Parkins, M. D., Incidence, Risk Factors, and Outcomes for Enterococcus spp. Blood Stream Infections: A Population-Based Study. *International Journal of Infectious Diseases* **2014**, 26, 76-82.
60. Markwart, R.; Willrich, N.; Haller, S.; Noll, I.; Koppe, U.; Werner, G.; Eckmanns, T.; Reuss, A., The rise in vancomycin-resistant Enterococcus faecium in Germany: data from the German Antimicrobial Resistance Surveillance (ARS). *Antimicrobial Resistance & Infection Control* **2019**, 8, (1), 147.
61. Rice, L.; xa, B, Progress and Challenges in Implementing the Research on ESKAPE Pathogens. *Infection Control and Hospital Epidemiology* **2010**, 31, (S1), S7-S10.
62. Tommasi, R.; Brown, D. G.; Walkup, G. K.; Manchester, J. I.; Miller, A. A., ESKAPEing the labyrinth of antibacterial discovery. *Nat Rev Drug Discov* **2015**, 14, (8), 529-542.
63. Penchovsky, R.; Traykovska, M., Designing drugs that overcome antibacterial resistance: where do we stand and what should we do? *Expert Opinion on Drug Discovery* **2015**, 10, (6), 631-650.
64. Antimicrobial resistance, Fact sheet N°194.
<http://www.who.int/mediacentre/factsheets/fs194/en/#>
65. Balouiri, M.; Sadiki, M.; Ibnsouda, S. K., Methods for in vitro evaluating antimicrobial activity: A review. *Journal of Pharmaceutical Analysis* **2016**, 6, (2), 71-79.
66. Humphries, R. M.; Ambler, J.; Mitchell, S. L.; Castanheira, M.; Dingle, T.; Hindler, J. A.; Koeth, L.; Sei, K., CLSI Methods Development and Standardization Working Group Best Practices for Evaluation of Antimicrobial Susceptibility Tests. *Journal of Clinical Microbiology* **2018**, 56, (4), e01934-17.
-

-
67. Gautam, V.; Singhal, L.; Arora, S.; Jha, C.; Ray, P., Reliability of Kirby-Bauer disk diffusion method for detecting carbapenem resistance in *Acinetobacter baumannii-calcoaceticus* complex isolates. *Antimicrobial agents and chemotherapy* **2013**, 57, (4), 2003-2004.
68. Reller, L. B.; Weinstein, M.; Jorgensen, J. H.; Ferraro, M. J., Antimicrobial Susceptibility Testing: A Review of General Principles and Contemporary Practices. *Clinical Infectious Diseases* **2009**, 49, (11), 1749-1755.
69. Hacek, D. M.; Dressel, D. C.; Peterson, L. R., Highly reproducible bactericidal activity test results by using a modified National Committee for Clinical Laboratory Standards broth macrodilution technique. *Journal of clinical microbiology* **1999**, 37, (6), 1881-1884.
70. Pfaller, M. A.; Sheehan, D. J.; Rex, J. H., Determination of Fungicidal Activities against Yeasts and Molds: Lessons Learned from Bactericidal Testing and the Need for Standardization. *Clinical Microbiology Reviews* **2004**, 17, (2), 268.
71. Paparella, A., Flow cytometric assessment of the antimicrobial activity of essential oils against *Listeria monocytogenes*. *Food control* **2008**, v. 19, (no. 12), pp. 1174-1182-2008 v.19 no.12.
72. Stiefel, P.; Schmidt-Emrich, S.; Maniura-Weber, K.; Ren, Q., Critical aspects of using bacterial cell viability assays with the fluorophores SYTO9 and propidium iodide. *BMC Microbiology* **2015**, 15, (1), 36.
73. Wong, E. H. H.; Khin, M. M.; Ravikumar, V.; Si, Z.; Rice, S. A.; Chan-Park, M. B., Modulating Antimicrobial Activity and Mammalian Cell Biocompatibility with Glucosamine-Functionalized Star Polymers. *Biomacromolecules* **2016**, 17, (3), 1170-1178.
74. Steiner, H.; Hultmark, D.; Engström, Å.; Bennich, H.; Boman, H. G., Sequence and specificity of two antibacterial proteins involved in insect immunity. *Nature* **1981**, 292, (5820), 246-248.
75. Som, A.; Vemparala, S.; Ivanov, I.; Tew, G. N., Synthetic mimics of antimicrobial peptides. *Peptide Science* **2008**, 90, (2), 83-93.
76. Zhang, Q.; Ma, P.; Xie, J.; Zhang, S.; Xiao, X.; Qiao, Z.; Shao, N.; Zhou, M.; Zhang, W.; Dai, C.; Qian, Y.; Qi, F.; Liu, R., Host defense peptide mimicking poly- α -peptides with fast, potent and broad spectrum antibacterial activities. *Biomaterials Science* **2019**, 7, (5), 2144-2151.
-

-
77. Takahashi, H.; Caputo, G. A.; Vemparala, S.; Kuroda, K., Synthetic Random Copolymers as a Molecular Platform To Mimic Host-Defense Antimicrobial Peptides. *Bioconjugate Chemistry* **2017**, 28, (5), 1340-1350.
78. McCoy, C. P.; O'Neil, E. J.; Cowley, J. F.; Carson, L.; De Baróid, Á. T.; Gdowski, G. T.; Gorman, S. P.; Jones, D. S., Photodynamic Antimicrobial Polymers for Infection Control. *PLOS ONE* **2014**, 9, (9), e108500.
79. Barzic, A. I.; Ioan, S., Antibacterial Drugs — From Basic Concepts to Complex Therapeutic Mechanisms of Polymer Systems. In *Concepts, Compounds and the Alternatives of Antibacterials*, Bobbarala, V., Ed. Science, Technology and Medicine: 2015.
80. Kenawy, E.-R.; Kandil, S., CHAPTER 3 Synthesis, Antimicrobial Activity and Applications of Polymers with Ammonium and Phosphonium Groups. In *Polymeric Materials with Antimicrobial Activity: From Synthesis to Applications*, The Royal Society of Chemistry: 2014; pp 54-74.
81. E. F. Panarin, M. V. S.; Ekzemplyarov, O. N., Synthesis and Antimicrobial Properties of Polymers Containing Quaternary Ammonium Groups. **1972**, 5, (7), 24-26.
82. Ganewatta, M. S.; Tang, C., Controlling macromolecular structures towards effective antimicrobial polymers. *Polymer* **2015**, 63, A1-A29.
83. Jämsä, S.; Mahlberg, R.; Holopainen, U.; Ropponen, J.; Savolainen, A.; Ritschkoff, A. C., Slow release of a biocidal agent from polymeric microcapsules for preventing biodeterioration. *Progress in Organic Coatings* **2013**, 76, (1), 269-276.
84. Li, Y.; Liu, G.; Wang, X.; Hu, J.; Liu, S., Enzyme-Responsive Polymeric Vesicles for Bacterial-Strain-Selective Delivery of Antimicrobial Agents. *Angewandte Chemie International Edition* **2016**, 55, (5), 1760-1764.
85. Brogden, K. A., Antimicrobial peptides: pore formers or metabolic inhibitors in bacteria? *Nature Reviews Microbiology* **2005**, 3, (3), 238-250.
86. Gilbert, P.; Moore, L. E., Cationic antiseptics: diversity of action under a common epithet. *Journal of Applied Microbiology* **2005**, 99, (4), 703-715.
87. Kenawy, E.-R.; Abdel-Hay, F. I.; El-Shanshoury, A. E.-R. R.; El-Newehy, M. H., Biologically active polymers. V. Synthesis and antimicrobial activity of modified poly(glycidyl methacrylate-co-2-hydroxyethyl methacrylate) derivatives with quaternary ammonium and phosphonium salts. *Journal of Polymer Science Part A: Polymer Chemistry* **2002**, 40, (14), 2384-2393.
-

-
88. Schulz, M.; Olubummo, A.; Binder, W. H., Beyond the lipid-bilayer: interaction of polymers and nanoparticles with membranes. *Soft Matter* **2012**, 8, (18), 4849-4864.
89. Palermo, E. F.; Vemparala, S.; Kuroda, K., Cationic Spacer Arm Design Strategy for Control of Antimicrobial Activity and Conformation of Amphiphilic Methacrylate Random Copolymers. *Biomacromolecules* **2012**, 13, (5), 1632-1641.
90. Baul, U.; Kuroda, K.; Vemparala, S., Interaction of multiple biomimetic antimicrobial polymers with model bacterial membranes. *The Journal of Chemical Physics* **2014**, 141, (8), 084902.
91. Tang, H.; Doerksen, R. J.; Jones, T. V.; Klein, M. L.; Tew, G. N., Biomimetic Facially Amphiphilic Antibacterial Oligomers with Conformationally Stiff Backbones. *Chemistry & Biology* **2006**, 13, (4), 427-435.
92. Gabriel, G. J.; Maegerlein, J. A.; Nelson, C. F.; Dabkowski, J. M.; Eren, T.; Nüsslein, K.; Tew, G. N., Comparison of Facially Amphiphilic versus Segregated Monomers in the Design of Antibacterial Copolymers. *Chemistry – A European Journal* **2009**, 15, (2), 433-439.
93. Subbalakshmi, C.; Sitaram, N., Mechanism of antimicrobial action of indolicidin. *FEMS Microbiology Letters* **1998**, 160, (1), 91-96.
94. Salomón, R. A.; Farías, R. N., Microcin 25, a novel antimicrobial peptide produced by *Escherichia coli*. *J Bacteriol* **1992**, 174, (22), 7428.
95. Andreu, D.; Rivas, L., Animal antimicrobial peptides: An overview. *Peptide Science* **1998**, 47, (6), 415-433.
96. Lee, M. W.; Chakraborty, S.; Schmidt, N. W.; Murgai, R.; Gellman, S. H.; Wong, G. C. L., Two interdependent mechanisms of antimicrobial activity allow for efficient killing in nylon-3-based polymeric mimics of innate immunity peptides. *Biochimica et Biophysica Acta (BBA) - Biomembranes* **2014**, 1838, (9), 2269-2279.
97. Chindera, K.; Mahato, M.; Kumar Sharma, A.; Horsley, H.; Kloc-Muniak, K.; Kamaruzzaman, N. F.; Kumar, S.; McFarlane, A.; Stach, J.; Bentin, T.; Good, L., The antimicrobial polymer PHMB enters cells and selectively condenses bacterial chromosomes. *Scientific Reports* **2016**, 6, 23121.
98. Santiago-Morales, J.; Amariei, G.; Letón, P.; Rosal, R., Antimicrobial activity of poly(vinyl alcohol)-poly(acrylic acid) electrospun nanofibers. *Colloids and Surfaces B: Biointerfaces* **2016**, 146, 144-151.
99. Matsuzaki, K., Control of cell selectivity of antimicrobial peptides. *Biochimica et Biophysica Acta (BBA) - Biomembranes* **2009**, 1788, (8), 1687-1692.
-

-
100. Gabriel, G. J.; Som, A.; Madkour, A. E.; Eren, T.; Tew, G. N., Infectious disease: Connecting innate immunity to biocidal polymers. *Materials Science and Engineering: R: Reports* **2007**, *57*, (1), 28-64.
101. Silhavy, T. J.; Kahne, D.; Walker, S., The bacterial cell envelope. *Cold Spring Harbor perspectives in biology* **2010**, *2*, (5), a000414-a000414.
102. Nikaido, H., Molecular basis of bacterial outer membrane permeability revisited. *Microbiol Mol Biol Rev* **2003**, *67*, (4), 593-656.
103. Engler, A. C.; Wiradharma, N.; Ong, Z. Y.; Coady, D. J.; Hedrick, J. L.; Yang, Y.-Y., Emerging trends in macromolecular antimicrobials to fight multi-drug-resistant infections. *Nano Today* **2012**, *7*, (3), 201-222.
104. Rahman, M. A.; Bam, M.; Luat, E.; Jui, M. S.; Ganewatta, M. S.; Shokfai, T.; Nagarkatti, M.; Decho, A. W.; Tang, C., Macromolecular-clustered facial amphiphilic antimicrobials. *Nature Communications* **2018**, *9*, (1), 5231.
105. Mohy Eldin, M. S.; Elazzazy, A. M.; Saleh, T. S.; Mekky, A. E. M.; Al-Bogami, A. S., Development of Novel Amphiphilic Pyrazole-g-PolyGlycidyl methacrylate-Based Polymers with Potential Antimicrobial Activity. *Advances in Polymer Technology* **2018**, *37*, (3), 706-713.
106. Hong, S.; Takahashi, H.; Nadres, E. T.; Mortazavian, H.; Caputo, G. A.; Younger, J. G.; Kuroda, K., A Cationic Amphiphilic Random Copolymer with pH-Responsive Activity against Methicillin-Resistant *Staphylococcus aureus*. *PLOS ONE* **2017**, *12*, (1), e0169262.
107. Locock, K. E. S.; Michl, T. D.; Valentin, J. D. P.; Vasilev, K.; Hayball, J. D.; Qu, Y.; Traven, A.; Griesser, H. J.; Meagher, L.; Haeussler, M., Guanylated Polymethacrylates: A Class of Potent Antimicrobial Polymers with Low Hemolytic Activity. *Biomacromolecules* **2013**, *14*, (11), 4021-4031.
108. Ergene, C.; Yasuhara, K.; Palermo, E. F., Biomimetic antimicrobial polymers: recent advances in molecular design. *Polymer Chemistry* **2018**, *9*, (18), 2407-2427.
109. Locock, K. E. S.; Michl, T. D.; Stevens, N.; Hayball, J. D.; Vasilev, K.; Postma, A.; Griesser, H. J.; Meagher, L.; Haeussler, M., Antimicrobial Polymethacrylates Synthesized as Mimics of Tryptophan-Rich Cationic Peptides. *ACS Macro Letters* **2014**, *3*, (4), 319-323.
110. Mortazavian, H.; Foster, L. L.; Bhat, R.; Patel, S.; Kuroda, K., Decoupling the Functional Roles of Cationic and Hydrophobic Groups in the Antimicrobial and Hemolytic

- Activities of Methacrylate Random Copolymers. *Biomacromolecules* **2018**, 19, (11), 4370-4378.
111. Lei, J.; Sun, L.; Huang, S.; Zhu, C.; Li, P.; He, J.; Mackey, V.; Coy, D. H.; He, Q., The antimicrobial peptides and their potential clinical applications. *Am J Transl Res* **2019**, 11, (7), 3919-3931.
112. Zhang, Q.; Ma, P.; Xie, J.; Zhang, S.; Xiao, X.; Qiao, Z.; Shao, N.; Zhou, M.; Zhang, W.; Dai, C.; Qian, Y.; Qi, F.; Liu, R., Host defense peptide mimicking poly- β -peptides with fast, potent and broad spectrum antibacterial activities. *Biomaterials Science* **2019**, 7, (5), 2144-2151.
113. Klumperman, B., Reversible Deactivation Radical Polymerization. *Encyclopedia of Polymer Science and Technology* **2015**, 1-27.
114. Park, D.; Finlay, J. A.; Ward, R. J.; Weinman, C. J.; Krishnan, S.; Paik, M.; Sohn, K. E.; Callow, M. E.; Callow, J. A.; Handlin, D. L.; Willis, C. L.; Fischer, D. A.; Angert, E. R.; Kramer, E. J.; Ober, C. K., Antimicrobial Behavior of Semifluorinated-Quaternized Triblock Copolymers against Airborne and Marine Microorganisms. *ACS Applied Materials & Interfaces* **2010**, 2, (3), 703-711.
115. Yuan, W.; Wei, J.; Lu, H.; Fan, L.; Du, J., Water-dispersible and biodegradable polymer micelles with good antibacterial efficacy. *Chemical Communications* **2012**, 48, (54), 6857-6859.
116. Guo-Dong, F.; Fang, Y.; Zhigang, L.; Xinsong, L., Solvent-resistant antibacterial microfibers of self-quaternized block copolymers from atom transfer radical polymerization and electrospinning. *Journal of Materials Chemistry* **2008**, 18, (8), 859-867.
117. Oda, Y.; Kanaoka, S.; Sato, T.; Aoshima, S.; Kuroda, K., Block versus Random Amphiphilic Copolymers as Antibacterial Agents. *Biomacromolecules* **2011**, 12, (10), 3581-3591.
118. Wang, Y.; Xu, J.; Zhang, Y.; Yan, H.; Liu, K., Antimicrobial and Hemolytic Activities of Copolymers with Cationic and Hydrophobic Groups: A Comparison of Block and Random Copolymers. *Macromolecular Bioscience* **2011**, 11, (11), 1499-1504.
119. Shirbin, S. J.; Insua, I.; Holden, J. A.; Lenzo, J. C.; Reynolds, E. C.; O'Brien-Simpson, N. M.; Qiao, G. G., Architectural Effects of Star-Shaped α -Structurally Nanoengineered Antimicrobial Peptide Polymers (SNAPPs) on Their Biological Activity. *Advanced Healthcare Materials* **2018**, 7, (21), 1800627.

-
120. Zhao, P.; Mecozzi, F.; Wessel, S.; Fieten, B.; Driesse, M.; Woudstra, W.; Busscher, H. J.; van der Mei, H. C.; Loontjens, T. J. A., Preparation and Evaluation of Antimicrobial Hyperbranched Emulsifiers for Waterborne Coatings. *Langmuir* **2019**, *35*, (17), 5779-5786.
121. Palermo, E. F.; Lienkamp, K.; Gillies, E. R.; Ragogna, P. J., Antibacterial Activity of Polymers: Discussions on the Nature of Amphiphilic Balance. *Angewandte Chemie International Edition* **2019**, *58*, (12), 3690-3693.
122. Kuroda, K.; Caputo, G. à.; DeGrado, W. à., The Role of Hydrophobicity in the Antimicrobial and Hemolytic Activities of Polymethacrylate Derivatives. *Chemistry – A European Journal* **2009**, *15*, (5), 1123-1133.
123. Yang, X.; Hu, K.; Hu, G.; Shi, D.; Jiang, Y.; Hui, L.; Zhu, R.; Xie, Y.; Yang, L., Long Hydrophilic-and-Cationic Polymers: A Different Pathway toward Preferential Activity against Bacterial over Mammalian Membranes. *Biomacromolecules* **2014**, *15*, (9), 3267-3277.
124. Cheng, C.-Y.; Wang, J.-Y.; Kausik, R.; Lee, K. Y. C.; Han, S., Nature of Interactions between PEO-PPO-PEO Triblock Copolymers and Lipid Membranes: (II) Role of Hydration Dynamics Revealed by Dynamic Nuclear Polarization. *Biomacromolecules* **2012**, *13*, (9), 2624-2633.
125. Zhang, H.; Liu, Y.; Luo, T.; Zhao, Q.; Cui, K.; Huang, J.; Jiang, T.; Ma, Z., Synthesis of novel guanidine-based ABA triblock copolymers and their antimicrobial honeycomb films. *Polymer Chemistry* **2018**, *9*, (28), 3922-3930.
126. Chen, Y.; Wilbon, P. A.; Chen, Y. P.; Zhou, J.; Nagarkatti, M.; Wang, C.; Chu, F.; Decho, A. W.; Tang, C., Amphipathic antibacterial agents using cationic methacrylic polymers with natural rosin as pendant group. *RSC Advances* **2012**, *2*, (27), 10275-10282.
127. Hirayama, M., The Antimicrobial Activity, Hydrophobicity and Toxicity of Sulfonium Compounds, and Their Relationship. *Biocontrol Science* **2011**, *16*, (1), 23-31.
128. Liang, J.; Wang, J.; Li, S.; Xu, L.; Wang, R.; Chen, R.; Sun, Y., The size-controllable preparation of chitosan/silver nanoparticle composite microsphere and its antimicrobial performance. *Carbohydrate Polymers* **2019**, *220*, 22-29.
129. Judzewitsch, P. R.; Zhao, L.; Wong, E. H. H.; Boyer, C., High-Throughput Synthesis of Antimicrobial Copolymers and Rapid Evaluation of Their Bioactivity. *Macromolecules* **2019**, *52*, (11), 3975-3986.
-

130. Alahmadi, N. S.; Elshaarawy, R. F. M., Novel aminothiazolyl-functionalized phosphonium ionic liquid as a scavenger for toxic metal ions from aqueous media; mining to useful antibiotic candidates. *Journal of Molecular Liquids* **2019**, 281, 451-460.
131. Loczenski Rose, V.; Mastrotto, F.; Mantovani, G., Phosphonium polymers for gene delivery. *Polymer Chemistry* **2017**, 8, (2), 353-360.
132. Cuthbert, T. J.; Hisey, B.; Harrison, T. D.; Trant, J. F.; Gillies, E. R.; Ragona, P. J., Surprising Antibacterial Activity and Selectivity of Hydrophilic Polyphosphoniums Featuring Sugar and Hydroxy Substituents. *Angewandte Chemie* **2018**, 130, (39), 12889-12892.
133. Inta, O.; Yoksan, R.; Limtrakul, J., Hydrophobically modified chitosan: A bio-based material for antimicrobial active film. *Materials Science and Engineering: C* **2014**, 42, 569-577.
134. Huang, Z.; Xu, H.; Meyers, A. D.; Musani, A. I.; Wang, L.; Tagg, R.; Barqawi, A. B.; Chen, Y. K., Photodynamic therapy for treatment of solid tumors--potential and technical challenges. *Technol Cancer Res Treat* **2008**, 7, (4), 309-320.
135. Patrice, T., Challenges for photodynamic therapy in the treatment of gastrointestinal tumours. *Journal of Photochemistry and Photobiology B: Biology* **1991**, 9, (3), 372-374.
136. Almeida, A.; Faustino, M. A. F.; Tomé, J. P. C., Photodynamic inactivation of bacteria: finding the effective targets. *Future Medicinal Chemistry* **2015**, 7, (10), 1221-1224.
137. Hamblin, M. R.; Hasan, T., Photodynamic therapy: a new antimicrobial approach to infectious disease? *Photochemical & Photobiological Sciences* **2004**, 3, (5), 436-450.
138. Merchat, M.; Bertolini, G.; Giacomini, P.; Villaneuva, A.; Jori, G., Meso-substituted cationic porphyrins as efficient photosensitizers of gram-positive and gram-negative bacteria. *Journal of Photochemistry and Photobiology B: Biology* **1996**, 32, (3), 153-157.
139. Wilson, M.; Burns, T.; Pratten, J.; Pearson, G. J., Bacteria in supragingival plaque samples can be killed by low-power laser light in the presence of a photosensitizer. *Journal of Applied Bacteriology* **1995**, 78, (5), 569-574.
140. Minnock, A.; Vernon, D. I.; Schofield, J.; Griffiths, J.; Howard Parish, J.; Brown, S. B., Photoinactivation of bacteria. Use of a cationic water-soluble zinc phthalocyanine to photoinactivate both Gram-negative and Gram-positive bacteria. *Journal of Photochemistry and Photobiology B: Biology* **1996**, 32, (3), 159-164.

-
141. Friedrich, C. L.; Moyles, D.; Beveridge, T. J.; Hancock, R. E. W., Antibacterial Action of Structurally Diverse Cationic Peptides on Gram-Positive Bacteria. *Antimicrobial Agents and Chemotherapy* **2000**, 44, (8), 2086.
142. Nikaido, H., Prevention of drug access to bacterial targets: permeability barriers and active efflux. *Science* **1994**, 264, (5157), 382.
143. Leive, L., The Barrier function of the Gram-negative envelope. *Annals of the New York Academy of Sciences* **1974**, 235, (1), 109-129.
144. Hamblin, M. R.; Hasan, T., Photodynamic therapy: a new antimicrobial approach to infectious disease? *Photochem Photobiol Sci* **2004**, 3, (5), 436-450.
145. Hamblin, M. R., Antimicrobial photodynamic inactivation: a bright new technique to kill resistant microbes. *Curr Opin Microbiol* **2016**, 33, 67-73.
146. Ochsner, M., Photophysical and photobiological processes in the photodynamic therapy of tumours. *Journal of Photochemistry and Photobiology B: Biology* **1997**, 39, (1), 1-18.
147. Kashef, N.; Huang, Y.-Y.; Hamblin, M. R., Advances in antimicrobial photodynamic inactivation at the nanoscale. *Nanophotonics* **2017**, 6, (5), 853-879.
148. Imlay, J., Oxidative Stress. *EcoSal Plus* **2009**.
149. Anjem, A.; Varghese, S.; Imlay, J. A., Manganese import is a key element of the OxyR response to hydrogen peroxide in Escherichia coli. *Molecular microbiology* **2009**, 72, (4), 844-858.
150. Cadet, J.; Wagner, J. R., DNA Base Damage by Reactive Oxygen Species, Oxidizing Agents, and UV Radiation. *Cold Spring Harb Perspect Biol* **2013**, 5, (2).
151. Cabiscol, E.; Tamarit, J.; Ros, J., Oxidative stress in bacteria and protein damage by reactive oxygen species. *INTERNATL MICROBIOL* **2000**, 3.
152. Slauch, J. M., How does the oxidative burst of macrophages kill bacteria? Still an open question. *Molecular Microbiology* **2011**, 80, (3), 580-583.
153. Yin, H.; Xu, L.; Porter, N. A., Free Radical Lipid Peroxidation: Mechanisms and Analysis. *Chemical Reviews* **2011**, 111, (10), 5944-5972.
154. Dizaj, S. M.; Lotfipour, F.; Barzegar-Jalali, M.; Zarrintan, M. H.; Adibkia, K., Antimicrobial activity of the metals and metal oxide nanoparticles. *Materials Science and Engineering: C* **2014**, 44, 278-284.
155. Xu, Q.; He, C.; Xiao, C.; Chen, X., Reactive Oxygen Species (ROS) Responsive Polymers for Biomedical Applications. *Macromolecular Bioscience* **2016**, 16, (5), 635-646.
-

156. Qi, M.; Li, X.; Sun, X.; Li, C.; Tay, F. R.; Weir, M. D.; Dong, B.; Zhou, Y.; Wang, L.; Xu, H. H. K., Novel nanotechnology and near-infrared photodynamic therapy to kill periodontitis-related biofilm pathogens and protect the periodontium. *Dental Materials* **2019**, 35, (11), 1665-1681.
157. Chen, J.; Yang, L.; Chen, J.; Liu, W.; Zhang, D.; Xu, P.; Dai, T.; Shang, L.; Yang, Y.; Tang, S.; Zhang, Y.; Lin, H.; Chen, Z.; Huang, M., Composite of silver nanoparticles and photosensitizer leads to mutual enhancement of antimicrobial efficacy and promotes wound healing. *Chemical Engineering Journal* **2019**, 374, 1373-1381.
158. Wong, T.-W.; Wang, Y.-Y.; Sheu, H.-M.; Chuang, Y.-C., Bactericidal Effects of Toluidine Blue-Mediated Photodynamic Action on *Vibrio vulnificus*. *Antimicrobial Agents and Chemotherapy* **2005**, 49, (3), 895.
159. Ozkan, E.; Allan, E.; Parkin, I. P., White-Light-Activated Antibacterial Surfaces Generated by Synergy between Zinc Oxide Nanoparticles and Crystal Violet. *ACS Omega* **2018**, 3, (3), 3190-3199.
160. Sobotta, L.; Skupin-Mrugalska, P.; Piskorz, J.; Mielcarek, J., Non-porphyrinoid photosensitizers mediated photodynamic inactivation against bacteria. *Dyes and Pigments* **2019**, 163, 337-355.
161. Neidle, S.; Pearl, L. H.; Herzyk, P.; Berman, H. M., A molecular model for proflavine-DNA intercalation. *Nucleic Acids Res* **1988**, 16, (18), 8999-9016.
162. Fekrazad, R.; Zare, H.; Vand, S. M. S., Photodynamic therapy effect on cell growth inhibition induced by Radachlorin and toluidine blue O on *Staphylococcus aureus* and *Escherichia coli*: An in vitro study. *Photodiagnosis and Photodynamic Therapy* **2016**, 15, 213-217.
163. Rout, B.; Liu, C.-H.; Wu, W.-C., Increased anti-biofilm efficacy of toluidine blue on *Staphylococcus* species after nano-encapsulation. *Photodiagnosis and Photodynamic Therapy* **2018**, 21, 190-200.
164. Vilela, S. F. G.; Junqueira, J. C.; Barbosa, J. O.; Majewski, M.; Munin, E.; Jorge, A. O. C., Photodynamic inactivation of *Staphylococcus aureus* and *Escherichia coli* biofilms by malachite green and phenothiazine dyes: An in vitro study. *Archives of Oral Biology* **2012**, 57, (6), 704-710.
165. Martinez, R.; Chacon-Garcia, L., The Search of DNA-Intercalators as Antitumoral Drugs: What it Worked and What did not Work. *Current Medicinal Chemistry* **2005**, 12, (2), 127-151.

166. Philippe, B.; Johann, B.; Thomas, G.; Martin, T., Acridine and Acridone Derivatives, Anticancer Properties and Synthetic Methods: Where Are We Now? *Anti-Cancer Agents in Medicinal Chemistry* **2007**, 7, (2), 139-169.
167. Lang, X.; Li, L.; Chen, Y.; Sun, Q.; Wu, Q.; Liu, F.; Tan, C.; Liu, H.; Gao, C.; Jiang, Y., Novel synthetic acridine derivatives as potent DNA-binding and apoptosis-inducing antitumor agents. *Bioorganic & Medicinal Chemistry* **2013**, 21, (14), 4170-4177.
168. Mitra, P.; Chakraborty, P. K.; Saha, P.; Ray, P.; Basu, S., Antibacterial efficacy of acridine derivatives conjugated with gold nanoparticles. *International Journal of Pharmaceutics* **2014**, 473, (1), 636-643.
169. Wainwright, M.; Phoenix, D. A.; Marland, J.; Wareing, D. R.; Bolton, F. J., In-vitro photobactericidal activity of aminoacridines. *Journal of Antimicrobial Chemotherapy* **1997**, 40, (4), 587-589.
170. Araújo, T. S. D.; Rodrigues, P. L. F.; Santos, M. S.; de Oliveira, J. M.; Rosa, L. P.; Bagnato, V. S.; Blanco, K. C.; da Silva, F. C., Reduced methicillin-resistant *Staphylococcus aureus* biofilm formation in bone cavities by photodynamic therapy. *Photodiagnosis and Photodynamic Therapy* **2018**, 21, 219-223.
171. Santezi, C.; Reina, B. D.; Dovigo, L. N., Curcumin-mediated Photodynamic Therapy for the treatment of oral infections—A review. *Photodiagnosis and Photodynamic Therapy* **2018**, 21, 409-415.
172. Cusicanqui Méndez, D. A.; Gutierrez, E.; José Dionisio, E.; Afonso Rabelo Buzalaf, M.; Cardoso Oliveira, R.; Andrade Moreira Machado, M. A.; Cruvinel, T., Curcumin-mediated antimicrobial photodynamic therapy reduces the viability and vitality of infected dentin caries microcosms. *Photodiagnosis and Photodynamic Therapy* **2018**, 24, 102-108.
173. Hewlings, J. S.; Kalman, S. D., Curcumin: A Review of Its' Effects on Human Health. *Foods* **2017**, 6, (10).
174. Page, K.; Correia, A.; Wilson, M.; Allan, E.; Parkin, I. P., Light-activated antibacterial screen protectors for mobile telephones and tablet computers. *Journal of Photochemistry and Photobiology A: Chemistry* **2015**, 296, 19-24.
175. Noimark, S.; Dunnill, C. W.; Kay, C. W. M.; Perni, S.; Prokopovich, P.; Ismail, S.; Wilson, M.; Parkin, I. P., Incorporation of methylene blue and nanogold into polyvinyl chloride catheters; a new approach for light-activated disinfection of surfaces. *Journal of Materials Chemistry* **2012**, 22, (30), 15388-15396.

176. Walker, T.; Canales, M.; Noimark, S.; Page, K.; Parkin, I.; Faull, J.; Bhatti, M.; Ciric, L., A Light-Activated Antimicrobial Surface Is Active Against Bacterial, Viral and Fungal Organisms. *Scientific Reports* **2017**, 7, (1), 15298.
177. Dahl, T. A.; Midden, W. R.; Hartman, P. E., Comparison of killing of gram-negative and gram-positive bacteria by pure singlet oxygen. *Journal of bacteriology* **1989**, 171, (4), 2188-2194.
178. Jankova, K.; Chen, X.; Kops, J.; Batsberg, W., Synthesis of Amphiphilic PS-b-PEG-b-PS by Atom Transfer Radical Polymerization. *Macromolecules* **1998**, 31, (2), 538-541.
179. Pandey, S.; Das, P. P.; Singh, A. K.; Mukherjee, R., Cobalt(ii), nickel(ii) and copper(ii) complexes of a hexadentate pyridine amide ligand. Effect of donor atom (ethers vs. thioether) on coordination geometry, spin-state of cobalt and MIII–MII redox potential. *Dalton Transactions* **2011**, 40, (40), 10758-10768.
180. Matyjaszewski, K.; Miller, P. J.; Pyun, J.; Kickelbick, G.; Diamanti, S., Synthesis and Characterization of Star Polymers with Varying Arm Number, Length, and Composition from Organic and Hybrid Inorganic/Organic Multifunctional Initiators. *Macromolecules* **1999**, 32, (20), 6526-6535.
181. Raab, V.; Kipke, J.; Burghaus, O.; Sundermeyer, J., Copper Complexes of Novel Superbasic Peralkylguanidine Derivatives of Tris(2-aminoethyl)amine as Constraint Geometry Ligands. *Inorganic Chemistry* **2001**, 40, (27), 6964-6971.
182. Abreu, C. M. R.; Serra, A. C.; Popov, A. V.; Matyjaszewski, K.; Guliashvili, T.; Coelho, J. F. J., Ambient temperature rapid SARA ATRP of acrylates and methacrylates in alcohol–water solutions mediated by a mixed sulfite/Cu(ii)Br₂ catalytic system. *Polymer Chemistry* **2013**, 4, (23), 5629-5636.
183. Maximiano, P.; Mendes, J. P.; Mendonça, P. V.; Abreu, C. M. R.; Guliashvili, T.; Serra, A. C.; Coelho, J. F. J., Cyclopentyl methyl ether: A new green co-solvent for supplemental activator and reducing agent atom transfer radical polymerization. *Journal of Polymer Science Part A: Polymer Chemistry* **2015**, 53, (23), 2722-2729.
184. Magenau, A. J. D.; Kwak, Y.; Matyjaszewski, K., ATRP of Methacrylates Utilizing Cu(II)X₂/L and Copper Wire. *Macromolecules* **2010**, 43, (23), 9682-9689.
185. Singha, N. K.; Rimmer, S.; Klumperman, B., Mass spectrometry of poly(methyl methacrylate) (PMMA) prepared by atom transfer radical polymerization (ATRP). *Eur. Polym. J.* **2004**, 40, (1), 159-163.

186. Borman, C. D.; Jackson, A. T.; Bunn, A.; Cutter, A. L.; Irvine, D. J., Evidence for the low thermal stability of poly(methyl methacrylate) polymer produced by atom transfer radical polymerisation. *Polymer* **2000**, 41, (15), 6015-6020.
187. Zhou, J.; Wang, J.; Han, J.; He, D.; Yang, D.; Xue, Z.; Liao, Y.; Xie, X., Amide group-containing polar solvents as ligands for iron-catalyzed atom transfer radical polymerization of methyl methacrylate. *RSC Advances* **2015**, 5, (54), 43724-43732.
188. Catalão, F.; Góis, J. R.; Trino, A. S. M.; Serra, A. C.; Coelho, J. F. J., Facile synthesis of well-controlled poly(glycidyl methacrylate) and its block copolymers via SARA ATRP at room temperature. *Polymer Chemistry* **2015**, 6, (10), 1875-1882.
189. Góis, J. R.; Konkolewicz, D.; Popov, A. V.; Guliashvili, T.; Matyjaszewski, K.; Serra, A. C.; Coelho, J. F. J., Improvement of the control over SARA ATRP of 2-(diisopropylamino)ethyl methacrylate by slow and continuous addition of sodium dithionite. *Polymer Chemistry* **2014**, 5, (16), 4617-4626.
190. Stanek, J.; Sackers, N.; Fink, F.; Paul, M.; Peters, L.; Grunzke, R.; Hoffmann, A.; Herres-Pawlis, S., Copper Guanidinoquinoline Complexes as Entatic State Models of Electron-Transfer Proteins. *Chemistry – A European Journal* **2017**, 23, (62), 15738-15745.
191. Konkolewicz, D.; Schröder, K.; Buback, J.; Bernhard, S.; Matyjaszewski, K., Visible Light and Sunlight Photoinduced ATRP with ppm of Cu Catalyst. *ACS Macro Letters* **2012**, 1, (10), 1219-1223.
192. Mosnáček, J.; Ilčíková, M., Photochemically Mediated Atom Transfer Radical Polymerization of Methyl Methacrylate Using ppm Amounts of Catalyst. *Macromolecules* **2012**, 45, (15), 5859-5865.
193. Hoffmann, A.; Bienemann, O.; Vieira, D. I.; Herres-Pawlis, S., New Guanidine-Pyridine Copper Complexes and Their Application in ATRP. *Polymers* **2014**, 6, (4).
194. Wern, M.; Ortmeier, J.; Josephs, P.; Schneider, T.; Neuba, A.; Henkel, G.; Schindler, S., Syntheses, characterization, and reactivity of copper complexes with camphor-like tetramethylguanidine ligands. *Inorganica Chimica Acta* **2018**, 481, 171-175.
195. Rösener, T.; Bienemann, O.; Sigl, K.; Schopp, N.; Schnitter, F.; Flörke, U.; Hoffmann, A.; Döring, A.; Kuckling, D.; Herres-Pawlis, S., A Comprehensive Study of Copper Guanidine Quinoline Complexes: Predicting the Activity of Catalysts in ATRP with DFT. *Chemistry – A European Journal* **2016**, 22, (38), 13550-13562.
196. England, J.; Martinho, M.; Farquhar, E. R.; Frisch, J. R.; Bominaar, E. L.; Münck, E.; Que Jr, L., A Synthetic High-Spin Oxoiron(IV) Complex: Generation, Spectroscopic

- Characterization, and Reactivity. *Angewandte Chemie International Edition* **2009**, 48, (20), 3622-3626.
197. Santos, R. M.; Fonseca, C. A.; Mendonça, V. P.; Branco, R.; Serra, C. A.; Morais, V. P.; Coelho, F. J., Recent Developments in Antimicrobial Polymers: A Review. *Materials* **2016**, 9, (7).
198. Mendonca, P. V.; Moreno, M. J.; Serra, A. C.; Simoes, S.; Coelho, J. F. J., Synthesis of tailor-made bile acid sequestrants by supplemental activator and reducing agent atom transfer radical polymerization. *RSC Advances* **2016**, 6, (57), 52143-52153.
199. Mendonca, P. V.; Konkolewicz, D.; Averick, S. E.; Serra, A. C.; Popov, A. V.; Guliashvili, T.; Matyjaszewski, K.; Coelho, J. F. J., Synthesis of cationic poly((3-acrylamidopropyl)trimethylammonium chloride) by SARA ATRP in ecofriendly solvent mixtures. *Polym. Chem.* **2014**, 5, (19), 5829-5836.
200. Matyjaszewski, K.; Nakagawa, Y.; Jasieczek, C. B., Polymerization of n-Butyl Acrylate by Atom Transfer Radical Polymerization. Remarkable Effect of Ethylene Carbonate and Other Solvents. *Macromolecules* **1998**, 31, (5), 1535-1541.
201. Patrizi, M. L.; Diociaiuti, M.; Capitani, D.; Masci, G., Synthesis and association properties of thermoresponsive and permanently cationic charged block copolymers. *Polymer* **2009**, 50, (2), 467-474.
202. Coelho, J. F. J.; Silva, A. M. F. P.; Popov, A. V.; Percec, V.; Abreu, M. V.; Gonçalves, P. M. O. F.; Gil, M. H., Single electron transfer–degenerative chain transfer living radical polymerization of N-butyl acrylate catalyzed by Na₂S₂O₄ in water media. *Journal of Polymer Science Part A: Polymer Chemistry* **2006**, 44, (9), 2809-2825.
203. Matyjaszewski, K.; Dong, H.; Jakubowski, W.; Pietrasik, J.; Kusumo, A., Grafting from Surfaces for “Everyone”: ARGET ATRP in the Presence of Air. *Langmuir* **2007**, 23, (8), 4528-4531.
204. Pan, X.; Tasdelen, M. A.; Laun, J.; Junkers, T.; Yagci, Y.; Matyjaszewski, K., Photomediated controlled radical polymerization. *Progress in Polymer Science* **2016**, 62, 73-125.
205. Mueller, L.; Jakubowski, W.; Tang, W.; Matyjaszewski, K., Successful Chain Extension of Polyacrylate and Polystyrene Macroinitiators with Methacrylates in an ARGET and ICAR ATRP. *Macromolecules* **2007**, 40, (18), 6464-6472.
206. Chmielarz, P., Synthesis of α -d-glucose-based star polymers through simplified electrochemically mediated ATRP. *Polymer* **2016**, 102, 192-198.

-
207. Wang, Z.; Wang, Z.; Pan, X.; Fu, L.; Lathwal, S.; Olszewski, M.; Yan, J.; Enciso, A. E.; Wang, Z.; Xia, H.; Matyjaszewski, K., Ultrasonication-Induced Aqueous Atom Transfer Radical Polymerization. *ACS Macro Letters* **2018**, 7, (3), 275-280.
208. Rodríguez-Hernández, J., Chapter 5 - Antimicrobial micro/nanostructured functional polymer surfaces A2 - Grumezescu, Alexandru Mihai. In *Nanobiomaterials in Antimicrobial Therapy*, William Andrew Publishing: 2016; pp 153-192.
209. Kuroda, K.; Caputo, G. A.; DeGrado, W. F., The Role of Hydrophobicity in the Antimicrobial and Hemolytic Activities of Polymethacrylate Derivatives. *Chemistry – A European Journal* **2009**, 15, (5), 1123-1133.
210. Hae Cho, C. A.; Liang, C.; Perera, J.; Liu, J.; Varnava, K. G.; Sarojini, V.; Cooney, R. P.; McGillivray, D. J.; Brimble, M. A.; Swift, S.; Jin, J., Molecular Weight and Charge Density Effects of Guanidinylated Biodegradable Polycarbonates on Antimicrobial Activity and Selectivity. *Biomacromolecules* **2017**.
211. Takahashi, H.; Nadres, E. T.; Kuroda, K., Cationic Amphiphilic Polymers with Antimicrobial Activity for Oral Care Applications: Eradication of *S. mutans* Biofilm. *Biomacromolecules* **2017**, 18, (1), 257-265.
212. Lam, S. J.; O'Brien-Simpson, N. M.; Pantarat, N.; Sulistio, A.; Wong, E. H. H.; Chen, Y.-Y.; Lenzo, J. C.; Holden, J. A.; Blencowe, A.; Reynolds, E. C.; Qiao, G. G., Combating multidrug-resistant Gram-negative bacteria with structurally nanoengineered antimicrobial peptide polymers. *Nat. Microbiol.* **2016**, 1, 16162.
213. Kuroda, K.; DeGrado, W. F., Amphiphilic Polymethacrylate Derivatives as Antimicrobial Agents. *Journal of the American Chemical Society* **2005**, 127, (12), 4128-4129.
214. Mowery, B. P.; Lee, S. E.; Kissounko, D. A.; Epanand, R. F.; Epanand, R. M.; Weisblum, B.; Stahl, S. S.; Gellman, S. H., Mimicry of Antimicrobial Host-Defense Peptides by Random Copolymers. *Journal of the American Chemical Society* **2007**, 129, (50), 15474-15476.
215. Ilker, M. F.; Nüsslein, K.; Tew, G. N.; Coughlin, E. B., Tuning the Hemolytic and Antibacterial Activities of Amphiphilic Polynorbornene Derivatives. *Journal of the American Chemical Society* **2004**, 126, (48), 15870-15875.
216. Pan, Y.; Xue, Y.; Snow, J.; Xiao, H., Tailor-Made Antimicrobial/Antiviral Star Polymer via ATRP of Cyclodextrin and Guanidine-Based Macromonomer. *Macromolecular Chemistry and Physics* **2015**, 216, (5), 511-518.
-

217. Chen, C. Z.; Beck-Tan, N. C.; Dhurjati, P.; van Dyk, T. K.; LaRossa, R. A.; Cooper, S. L., Quaternary Ammonium Functionalized Poly(propylene imine) Dendrimers as Effective Antimicrobials: Structure–Activity Studies. *Biomacromolecules* **2000**, 1, (3), 473-480.
218. Liu, L.; Xu, K.; Wang, H.; Jeremy Tan, P. K.; Fan, W.; Venkatraman, S. S.; Li, L.; Yang, Y.-Y., Self-assembled cationic peptide nanoparticles as an efficient antimicrobial agent. *Nature Nanotechnology* **2009**, 4, 457.
219. Chakrabarty, S.; King, A.; Kurt, P.; Zhang, W.; Ohman, D. E.; Wood, L. F.; Lovelace, C.; Rao, R.; Wynne, K. J., Highly Effective, Water-Soluble, Hemocompatible 1,3-Propylene Oxide-Based Antimicrobials: Poly[(3,3-quaternary/PEG)-copolyoxetanes]. *Biomacromolecules* **2011**, 12, (3), 757-769.
220. Sauvet, G.; Fortuniak, W.; Kazmierski, K.; Chojnowski, J., Amphiphilic block and statistical siloxane copolymers with antimicrobial activity. *Journal of Polymer Science Part A: Polymer Chemistry* **2003**, 41, (19), 2939-2948.
221. Zhang, Z.; Bilalis, P.; Zhang, H.; Gnanou, Y.; Hadjichristidis, N., Core Cross-Linked Multiarm Star Polymers with Aggregation-Induced Emission and Temperature Responsive Fluorescence Characteristics. *Macromolecules* **2017**, 50, (11), 4217-4226.
222. Zhang, Q.; Wilson, P.; Li, Z.; McHale, R.; Godfrey, J.; Anastasaki, A.; Waldron, C.; Haddleton, D. M., Aqueous Copper-Mediated Living Polymerization: Exploiting Rapid Disproportionation of CuBr with Me6TREN. *Journal of the American Chemical Society* **2013**, 135, (19), 7355-7363.
223. Barbosa, A. F.; Sangiorgi, B. B.; Galdino, S. L.; Barral-Netto, M.; Pitta, I. R.; Pinheiro, A. L., Photodynamic antimicrobial chemotherapy (PACT) using phenothiazine derivatives as photosensitizers against *Leishmania braziliensis*. *Lasers in Surgery and Medicine* **2012**, 44, (10), 850-855.
224. Dastidar, G. S.; Kristiansen, E. J.; Molnar, J.; Amaral, L., Role of Phenothiazines and Structurally Similar Compounds of Plant Origin in the Fight against Infections by Drug Resistant Bacteria. *Antibiotics* **2013**, 2, (1).
225. Grimsey, E. M.; Piddock, L. J. V., Do phenothiazines possess antimicrobial and efflux inhibitory properties? *FEMS Microbiology Reviews* **2019**.
226. Tseng, S. P.; Teng, L. J.; Chen, C. T.; Lo, T. H.; Hung, W. C.; Chen, H. J.; Hsueh, P. R.; Tsai, J. C., Toluidine blue O photodynamic inactivation on multidrug-resistant *Pseudomonas aeruginosa*. *Lasers in Surgery and Medicine* **2009**, 41, (5), 391-397.

227. Demidova, T. N.; Hamblin, M. R., Photodynamic inactivation of Bacillus spores, mediated by phenothiazinium dyes. *Appl Environ Microbiol* **2005**, *71*, (11), 6918-6925.
228. Zhao, X.; Drlica, K., Reactive oxygen species and the bacterial response to lethal stress. *Current Opinion in Microbiology* **2014**, *21*, 1-6.
229. Tyagi, P.; Singh, M.; Kumari, H.; Kumari, A.; Mukhopadhyay, K., Bactericidal Activity of Curcumin I Is Associated with Damaging of Bacterial Membrane. *PLOS ONE* **2015**, *10*, (3), e0121313.
230. Morão, L. G.; Polaquini, C. R.; Kopacz, M.; Torrezan, G. S.; Ayusso, G. M.; Dilarri, G.; Cavalca, L. B.; Zielińska, A.; Scheffers, D.-J.; Regasini, L. O.; Ferreira, H., A simplified curcumin targets the membrane of Bacillus subtilis. *MicrobiologyOpen* **2019**, *8*, (4), e00683.
231. Fillipin, L. I.; Mauriz, J. L.; Vedovelli, K.; Moreira, A. J.; Zettler, C. G.; Lech, O.; Marroni, N. P.; González-Gallego, J., Low-level laser therapy (LLL) prevents oxidative stress and reduces fibrosis in rat traumatized Achilles tendon. *Lasers in Surgery and Medicine* **2005**, *37*, (4), 293-300.
232. Tong, W.; Xiong, Y.; Duan, S.; Ding, X.; Xu, F.-J., Phthalocyanine functionalized poly(glycidyl methacrylate) nano-assemblies for photodynamic inactivation of bacteria. *Biomaterials Science* **2019**, *7*, (5), 1905-1918.
233. Fila, G.; Kawiak, A.; Grinholc, M. S., Blue light treatment of Pseudomonas aeruginosa: Strong bactericidal activity, synergism with antibiotics and inactivation of virulence factors. *Virulence* **2017**, *8*, (6), 938-958.
234. Tubby, S.; Wilson, M.; Nair, S. P., Inactivation of staphylococcal virulence factors using a light-activated antimicrobial agent. *BMC Microbiology* **2009**, *9*, (1), 211.
235. Amaral, L.; Martins, A.; Spengler, G.; Molnar, J., Efflux pumps of Gram-negative bacteria: what they do, how they do it, with what and how to deal with them. *Front Pharmacol* **2014**, *4*, 168-168.
236. Boluki, E.; Kazemian, H.; Peeridogaheh, H.; Alikhani, M. Y.; Shahabi, S.; Beytollahi, L.; Ghorbanzadeh, R., Antimicrobial activity of photodynamic therapy in combination with colistin against a pan-drug resistant Acinetobacter baumannii isolated from burn patient. *Photodiagnosis and Photodynamic Therapy* **2017**, *18*, 1-5.
237. Pérez-Laguna, V.; Pérez-Artiaga, L.; Lampaya-Pérez, V.; García-Luque, I.; Ballesta, S.; Nonell, S.; Paz-Cristobal, M. P.; Gilaberte, Y.; Rezusta, A., Bactericidal Effect of Photodynamic Therapy, Alone or in Combination with Mupirocin or Linezolid, on Staphylococcus aureus. *Frontiers in Microbiology* **2017**, *8*, 1002.

238. Fiebelkorn, K. R.; Crawford, S. A.; McElmeel, M. L.; Jorgensen, J. H., Practical Disk Diffusion Method for Detection of Inducible Clindamycin Resistance in *Staphylococcus aureus* and Coagulase-Negative Staphylococci. *Journal of Clinical Microbiology* **2003**, 41, (10), 4740.
239. Shih, M.-H.; Huang, F.-C., Effects of Photodynamic Therapy on Rapidly Growing Nontuberculous Mycobacteria Keratitis. *Investigative Ophthalmology & Visual Science* **2011**, 52, (1), 223-229.
240. Mary, C. P. V.; Vijayakumar, S.; Shankar, R., Metal chelating ability and antioxidant properties of Curcumin-metal complexes - A DFT approach. *J Mol Graph Model* **2018**, 79, 1-14.
241. Wanninger, S.; Lorenz, V.; Subhan, A.; Edelman, F. T., Metal complexes of curcumin – synthetic strategies, structures and medicinal applications. *Chemical Society Reviews* **2015**, 44, (15), 4986-5002.
242. Jia, H.-R.; Zhu, Y.-X.; Chen, Z.; Wu, F.-G., Cholesterol-Assisted Bacterial Cell Surface Engineering for Photodynamic Inactivation of Gram-Positive and Gram-Negative Bacteria. *ACS Applied Materials & Interfaces* **2017**, 9, (19), 15943-15951.
243. Salgado, C. D.; Sepkowitz, K. A.; John, J. F.; Cantey, J. R.; Attaway, H. H.; Freeman, K. D.; Sharpe, P. A.; Michels, H. T.; Schmidt, M. G., Copper surfaces reduce the rate of healthcare-acquired infections in the intensive care unit. *Infection control and hospital epidemiology* **2013**, 34, (5), 479-486.
244. He, W.; Zhang, Y.; Li, J.; Gao, Y.; Luo, F.; Tan, H.; Wang, K.; Fu, Q., A Novel Surface Structure Consisting of Contact-active Antibacterial Upper-layer and Antifouling Sub-layer Derived from Gemini Quaternary Ammonium Salt Polyurethanes. *Scientific Reports* **2016**, 6, (1), 32140.
245. McCubbin, P. J.; Forbes, E.; Gow, M. M.; Gorham, S. D., Covalent attachment of quaternary ammonium compounds to a polyethylene surface via a hydrolyzable ester linkage: Basis for a controlled-release system of antiseptics from an inert surface. *Journal of Applied Polymer Science* **2006**, 100, (1), 538-545.
246. Patel, S. K.; Rohan, L. C., On-demand microbicide products: design matters. *Drug Deliv Transl Res* **2017**, 7, (6), 775-795.
247. Esteban-Tejeda, L.; Prado, C.; Cabal, B.; Sanz, J.; Torrecillas, R.; Moya, J. S., Antibacterial and Antifungal Activity of ZnO Containing Glasses. *PLOS ONE* **2015**, 10, (7), e0132709.

248. Noimark, S.; Allan, E.; Parkin, I. P., Light-activated antimicrobial surfaces with enhanced efficacy induced by a dark-activated mechanism. *Chemical Science* **2014**, *5*, (6), 2216-2223.
249. Ozkan, E.; Allan, E.; Parkin, I. P., The antibacterial properties of light-activated polydimethylsiloxane containing crystal violet. *RSC Advances* **2014**, *4*, (93), 51711-51715.
250. Huang, S.-T.; Wu, C.-Y.; Lee, N. Y.; Cheng, C.-W.; Yang, M.-J.; Hung, Y.-A.; Wong, T.-W.; Liang, J.-Y., Effects of 462 nm Light-Emitting Diode on the Inactivation of *Escherichia coli* and a Multidrug-Resistant by Tetracycline Photoreaction. *Journal of Clinical Medicine* **2018**, *7*, (9).
251. Lubart, R.; Lipovski, A.; Nitzan, Y.; Friedmann, H., A possible mechanism for the bactericidal effect of visible light. *Laser therapy* **2011**, *20*, (1), 17-22.